Role of low density lipoprotein - cholesterol in focal adhesion assembly and migration of cancer cells

Inauguraldissertation
zur Erlangung des Grades eines Doktors der Medizin
des Fachbereichs Medizin
der Justus-Liebig-Universität Gießen

vorgelegt von Engel, Johanna Marie
aus Gießen

Gießen 2024

Aus dem Fachbereich Medizin der Justus-Liebig-Universität Gießen

Molekulare Onkologie solider Tumore
Klinik für Innere Medizin
Medizinisches Forschungszentrum Seltersberg

Gutachter: Prof. Dr. Andre Menke

Gutachter: Prof. Dr. Attila Németh

Tag der Disputation: 12.12.2024

Contents

1 Introduction **1**
1.1 Cholesterol homeostasis in cancer cells . . . 2
1.1.1 Cellular cholesterol supply . . . 2
LDL receptor-mediated endocytosis . . . 3
1.1.2 Cellular cholesterol efflux . . . 5
1.1.3 Cellular cholesterol transport . . . 6
1.1.4 The mevalonate pathway and cell signalling in cancer . . . 7
1.2 LDL-cholesterol and cancer cell migration . . . 9
1.2.1 Focal adhesion formation and turnover . . . 10
1.2.2 The role of cholesterol for focal adhesion formation . . . 12
1.3 The role of Annexin A6 in cholesterol transport, focal adhesion formation, and cell migration . . . 15
1.4 Aims . . . 19

2 Methods **21**
2.1 Tissue culture . . . 21
2.1.1 Cell cultivation . . . 21
Cell passaging . . . 21
Cell storage . . . 21
Cell plating . . . 22
Transient transfection . . . 22
Cell lysis . . . 22
2.2 Biochemical methods . . . 23
2.2.1 Protein quantification - Lowry assay . . . 23
2.2.2 Gel electrophoresis and western blotting . . . 23
Gel electrophoresis . . . 23
Western blotting . . . 24
2.2.3 DNA preparation . . . 25
LB agar plate preparation . . . 25
Bacterial transformation . . . 25
Plasmid purification . . . 26

2.3 Microscopy . . . 26
2.3.1 Biochemical methods for slide preparation . . . 26
Slide preparation . . . 26
Cell fixation, immunostaining and slide mounting . . . 26
2.3.2 Microscopy imaging and image analysis . . . 27
Focal adhesion counting . . . 27
Colocalisation analysis . . . 28
Focal adhesion size analysis . . . 28
2.4 Statistical analysis . . . 28
2.4.1 Statistical analysis of focal adhesion characteristics . . . 29
2.4.2 Statistical analysis of western blot signals . . . 29

3 Results **30**
3.1 Characterisation of proteins involved in cholesterol homeostasis and focal adhesion assembly in CHO cells lacking NPC1 only or both NPC1 and AnxA6 . . . 30
3.1.1 Comparison of lipoprotein receptors, regulatory endocytic proteins and enzymes involved in cholesterol homeostasis . . . 31
3.1.2 Comparison of expression patterns in serum-stimulated CHO WT, M12 and M12-A6ko cells . . . 32
3.1.3 Western blot analysis of signalling proteins mediating cell adhesion and migration . . . 34
3.1.4 Serum-stimulated activation of FAK and Src kinase in NPC1 mutant cells . . . 36
3.1.5 Expression of late endosomal proteins in migrating cells . . . 37
3.1.6 Src and FAK activation in migrating NPC1 mutant cells . . . 39
3.1.7 Expression of late endosomal proteins in cells after incubation with lipoprotein-deficient, cholesterol-depleted media . . . 42
3.1.8 Src and FAK activation after incubation with lipoprotein-deficient, cholesterol-depleted media . . . 43
3.1.9 Expression of late endosomal proteins in serum-activated cells after incubation with LPDS-statin media . . . 45
3.1.10 Src and FAK activation in serum-activated cells after incubation with LPDS-statin media . . . 47
3.1.11 Summary of western blot analyses . . . 49
3.2 Characterisation of focal adhesion assembly in CHO cells lacking NPC1 only or both NPC1 and AnxA6 . . . 50

3.2.1 Focal adhesion assembly in steady state and serum-stimulated CHO WT, M12 and M12-A6ko cells 50
3.2.2 Focal adhesion assembly in LDL-stimulated CHO WT, M12 and M12-A6ko cells 54
3.2.3 Focal adhesion assembly in CHO cells ectopically expressing the focal adhesion markers vinculin and paxillin 56
Focal adhesion assembly in GFP-vinculin-overexpressing CHO WT, M12 and M12-A6ko cells 56
Focal adhesion assembly in GFP-paxillin-overexpressing CHO WT, M12 and M12-A6ko cells 60
Cholesterol associates with focal adhesions in paxillin- and vinculin-overexpressing cells 63
3.2.4 Focal adhesion assembly in CHO cells overexpressing wild type and oncogenic Src kinase 67

4 Discussion **73**

4.1 Characterisation of proteins involved in cholesterol homeostasis and focal adhesion assembly in CHO cells lacking NPC1 only or both NPC1 and AnxA6 74
4.1.1 The role of NPC1 loss of function on the expression of enzymes involved in cholesterol homeostasis and focal adhesion assembly . 74
4.1.2 The role of NPC1 and AnxA6 loss of function on the expression of enzymes involved in cholesterol homeostasis and focal adhesion assembly 77
4.1.3 Autophagy in CHO cells lacking NPC1 and AnxA6 78
4.1.4 Characterisation of focal adhesion formation in CHO cells lacking NPC1 and AnxA6 79
4.2 Focal adhesion dynamics depend on cholesterol balance 80
4.2.1 Intracellular cholesterol distribution can regulate focal adhesion dynamics 81
4.2.2 Focal adhesion turnover requires Src kinase activity 83
4.3 The role of AnxA6 in focal adhesion formation 84
4.3.1 AnxA6 and cell migration 84
4.4 Evaluation of the methodological approach 86
4.4.1 Experimental models and methods for the investigation of the role of cholesterol on focal adhesion formation and cell migration . . . 86

5 Conclusion **92**

6 Abstract **94**

Abbreviations **96**

List of Figures **100**

List of Tables **103**

Bibliography **105**

Appendix A Supplements **133**

Appendix B Material **141**

List of Publications **153**

Eidesstattliche Erklärung **154**

Danksagung **155**

Chapter 1

Introduction

Cell migration in response to environmental signals is a fascinating and fundamental part of many biological processes. However, improper surroundings triggering abnormal cell migration can result in life-threatening scenarios, such as immunosuppression, defective wound repair, or the spread of cancer cells to other sites in the body (metastasis). Over the last years the role of cholesterol in cell motility, which determines metastatic potential and behaviour, has gained increased attention (*18*, *77*, *88*, *163*, *165*, *186*). Cell growth, proliferation and migration are well-known features of neoplasms, requiring cholesterol for rapid membrane expansion, focal adhesion (FA) formation, proper functioning of organelles, and membrane-anchoring of signalling factors such as the prenylation of small GTPases (guanosine triphosphate (GTP) hydrolising enzymes). To meet the energy demands required to support these processes in cancer, metabolic adaptions are needed (*165*, *196*). These metabolic changes are now well recognised as additional hallmarks of cancer, and commonly involve an increased demand for lipids. This includes cholesterol, a unique molecule essential for membrane organisation, growth and development, but also cell migration (*37*, *125*).

There is growing evidence that dysregulation of cholesterol metabolism is linked to the development and progression of cancer, e.g. breast, prostate and colon cancer (*162*, *218*). Yet, where this cholesterol is coming from and how it contributes to cell motility is not well understood. As a structural element of the plasma membrane (PM), cholesterol is enriched in particular at specialised microdomains called lipid rafts, playing a crucial role in regulating the response to environmental signals and coordinating cell adhesion and migration (*162*). Studying the effect of diet-induced hypercholesterolemia on prostate cancer, Moon and co-workers showed elevated cholesterol levels to trigger prostate cancer cell migration (*160*). In transgenic mouse models for breast cancer, hypercholesterolaemia induced tumour growth and metastasis (*7*, *141*). Zhuang and colleagues found the cholesterol content of lipid rafts and raft-dependent signalling in prostate cancer cells to be altered by cholesterol levels *in vivo* and *in vitro*. Moreover, inhibition of choles-

terol synthesis using simvastatin strongly decreased cholesterol levels in lipid rafts and inhibited signalling of Akt1 serine-threonine kinase/ protein kinase B (Akt/PKB), causing cell apoptosis. These effects were reversed by cholesterol replenishment (*273*). While a lipid-rich environment, including elevated cholesterol, is generally considered to favour tumour growth and aggressiveness, the role of statins in tumour progression is still not fully understood, as in some cases, such as breast, bladder or non-melanoma skin cancers, statin-mediated inhibition of *de novo* cholesterol synthesis has also been associated with tumour progression and risk (*87*, *187*). Hence, the exact mechanisms by which cholesterol influences cancerogenesis have not been fully understood (*196*).

However, as outlined further below, studies have indicated a stimulatory role of cholesterol on cell migration, potentially by affecting lipid raft signalling as well as many intracellular transport mechanisms required for the proper functioning of cell surface molecules involved in migratory and invasive cell behaviour (*77*, *104*, *109*, *231*, *251*).

1.1 Cholesterol homeostasis in cancer cells

1.1.1 Cellular cholesterol supply

As a precursor of steroid hormones, vitamins, and bile acids and as a structural component of cell membranes, cholesterol plays an important role in cellular homeostasis. By maintaining membrane fluidity and organisation in cholesterol-rich microdomains such as lipid rafts, as well as FA, cholesterol preserves membrane integrity and enables signalling and endo- and exocytic transport across the PM (*80*, *88*, *196*). Cell growth, proliferation and migration are well-known features of neoplasms, that require cholesterol for rapid membrane expansion, FA formation, intracellular vesicle transport, organelle homeostasis, such as mitochondrial well-being, and membrane-anchoring of signalling factors such as the prenylation of small GTPases of the Ras superfamily (Ras, Rac/Rho, Rab) (*161*). Hence, cholesterol availability is critical for proper cellular functioning, and cells either cover cholesterol demands through *de novo* biosynthesis or uptake of dietary cholesterol from plasma (*196*).

The energetically expensive *de novo* cholesterol biosynthesis is based on the mevalonate pathway, which is regulated by three crucial actors: the rate-limiting enzymes β-methylglutaryl-coenzyme A reductase (HMGCR) and squalene monooxygenase (SQLE) and the transcription factor sterol-regulatory-element-binding protein 2 (SREBP2) (*146*). An early step in the mevalonate pathway is the conversion of β-hydroxy β-methylglutaryl-coenzyme A (HMG-CoA) to mevalonate by HMGCR (*80*). This step is inhibited by high

cellular cholesterol levels, hence providing an effective feedback mechanism to control energy-consuming cholesterol biosynthesis. In addition, besides elevated sterol levels, HMGCR activity is also regulated by cellular energy levels; and lack of an adenosine triphosphate (ATP) reserves are associated with HMGCR downregulation (*33*, *213*). The second rate-limiting enzyme in the mevalonate pathway is SQLE, which alike HMGCR, can be upregulated at the transcriptional level when cholesterol levels are low via SREBP2 (*64*, *91*). The transcription factor SREBP2 is the key regulator of genes involved in cholesterol homeostasis. When cellular cholesterol levels are low, SREBP2 is cleaved and released from the endoplasmic reticulum (ER) by the SREBP-cleavage activating protein (SCAP). This triggers relocation of SREBP2 to the Golgi, processing to its mature form (*184*) and ultimately SREBP2 translocation into the nucleus. Once in the nucleus, activated SREBP2 binds to sterol-regulatory-elements (SRE) within promoter regions of cholesterol-regulated genes and activates their transcription. This includes HMG-CoA synthase, HMGCR, SQLE, low-density lipoprotein (LDL) receptor (LDLR) and many other cholesterologenic enzymes (*91*). Once cellular cholesterol levels have reached higher levels, SREBP-mediated activation of gene expression is downregulated. Yet, SREBP2 activity not only depends on cellular cholesterol levels and in order to properly manage energy supplies under starvation, SREBP2-mediated transcription and SREBP2 gene expression itself are downregulated (*90*, *232*, *244*).

Another mechanism for meeting the increasing demand for cholesterol is to increase the influx of cholesterol from circulating dietary cholesterol pools. After the absorption of cholesterol from dietary lipids in the intestine, cholesterol enters the blood as cholesteryl esters in triglyceride-rich lipoproteins, chylomicrons (*227*). Chylomicrons are processed by lipoprotein lipase to remnants and then delivered to the liver, where cholesteryl esters are incorporated into very low-density lipoproteins (VLDL). VLDL particles are released from the liver for distribution in the body, and once in the blood, lipoprotein lipase-mediated removal of fatty acids from VLDL generates cholesteryl ester-rich LDL particles. LDL delivers cholesterol to peripheral tissues and elevated LDL levels can be normalised by hepatic uptake and clearance via LDL receptor-mediated endocytosis. On the other hand, cholesteryl ester-rich high-density lipoprotein (HDL) particles are formed in extrahepatic tissues and through scavenger receptor class B type I (SRB1), can be internalised into liver and secreted as bile acids (*227*).

LDL receptor-mediated endocytosis

In order for cells to internalise dietary cholesterol, expression of LDLR at the cell surface enables binding and internalisation of LDL by receptor-mediated endocytosis (*67*) (FIGURE

1.1). Subsequently, cholesteryl ester-containing LDL particles are trafficked to early and then late endosomes (LE)/multivesicular bodies (MVB). The acidic pH in the LE compartment leads to the dissociation of LDL from the LDLR, which is recycled to the cell surface for another round of internalisation. LE/MVB then fuse with lysosomes (Lys), where cholesteryl esters are hydrolysed by lysosomal acid lipase (*68*). To exit the LE, cholesterol first binds to the soluble Niemann-Pick C2 protein (NPC2) before passing to the membrane-bound Niemann-Pick C1 protein (NPC1) (*127*). The free intracellular cholesterol is then transported to the PM, ER, the trans-Golgi network (TGN) or other membranous organelles (*96*, *165*). Besides NPC1, several other cholesterol transporters in the LE/Lys compartment exist, including members of the steroidogenic acute regulatory-related lipid transfer domain (StARD) and oxysterol-binding protein (OSBP) families. However, while NPC1 is considered the main cholesterol transporter in LE/Lys, the role and function of these other cholesterol transporters are still not fully understood (*96*, *165*).

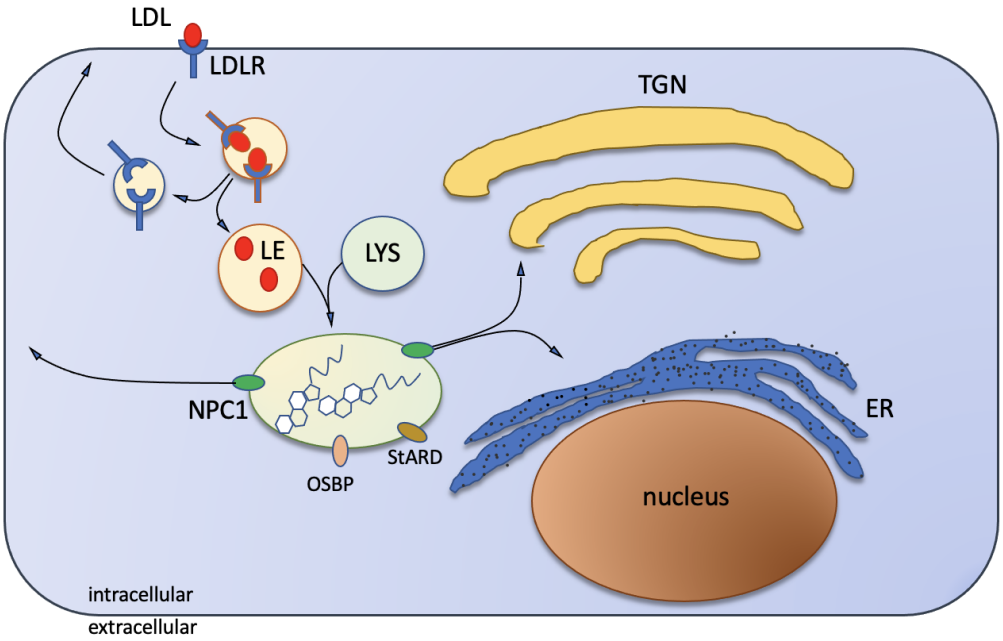

FIGURE 1.1: **LDL receptor (LDLR) mediated LDL-cholesterol uptake and intracellular trafficking.** After receptor-mediated endocytosis of LDLR-bound LDL-cholesterol, LDL particles traffic to early and then late endosomes (LE). While LDLR gets recycled to the plasma membrane (PM), the LDL-cholesteryl esters are hydrolysed upon LE/lysosome (Lys) fusion. In order to be distributed to the PM, endoplasmic reticulum (ER), the trans-Golgi network (TGN) or other membranous organelles, free cholesterol exits the LE/Lys compartment predominantly by the Niemann-Pick C1 protein (NPC1). However other cholesterol transporters such as members of the steroidogenic acute regulatory-related lipid transfer domain (StARD) and oxysterol-binding protein (OSBP) families may also play a role (*96*, *165*).

A key regulator enabling cells to internalise dietary cholesterol is the LDLR. In normal cells, feedback control mediated by transcriptional regulation via SREBP2 ensures LDLR

upregulation when cellular cholesterol levels are low. In addition, cell surface LDLR levels are regulated by proprotein convertase subtilisin/kexin type 9 (PCSK9) (*72*, *146*). Circulating extracellular PCSK9 can bind LDLR at the cell surface and promote LDLR degradation (*236*). Besides PCSK9, cell surface LDLR levels are influenced by the E3 ubiquitin ligase IDOL (inducible degrader of the LDL receptor), which binds the cytoplasmic region of LDLR and targets LDLR for lysosomal degradation. IDOL promotes polyubiquitylation of the intracellular domain of LDLR, initiating LDLR internalisation and subsequent lysosomal degradation (*267*). While PCSK9 expression is regulated by SREBP2, the accumulation of sterols activates the transcription factor liver X receptor (LXR), which upregulates the expression of IDOL, indicating complex networks that coordinate the activity of LDLR. Most relevant for cancer settings, these regulatory circuits are often dysregulated and increased expression of LDLR at the cell surface has been demonstrated in several cancer types including breast cancer, prostate cancer, colorectal cancer and glioblastoma (*31*, *58*, *165*, *242*, *246*).

Besides LDLR, the receptors VLDL receptor (VLDLR) and SRB1, which can internalise VLDL and HDL, respectively, may also play a role in SREBP-regulated cholesterol uptake in cancer (*196*). The inverse correlation of low HDL and cholesterol-filled PM in malignant cells has caught increasing attention for the role of HDL in cancer. A negative correlation between HDL-cholesterol and cancer risk has been established (*37*). However, Danilo *et al.* showed uptake of HDL-cholesteryl esters to trigger cell migration via the phosphoinositide 3-kinase (PI3K)/Akt kinase pathway in breast cancer (*40*). The ability of cancer cells to upregulate the uptake of dietary cholesterol may also contribute to statin resistance in some cancers, as statin-mediated inhibition of cholesterol synthesis ultimately elevates LDLR levels, thus promoting LDL uptake by cancer cells (*52*, *196*).

1.1.2 Cellular cholesterol efflux

Since excess amounts of cellular cholesterol are toxic, cholesterol must be stored as cholesteryl esters in lipid droplets or exported (*146*). In particular the increased storage of cholesterol via esterification through acetyl-CoA acetyltransferase (ACAT1) (*146*) is often upregulated in cancers (*58*, *185*). In many cell types, ATP-binding cassette (ABC) transporters A1 and G1 (ABCA1, ABCG1) promote cholesterol and phospholipid efflux by ABCA1 first lipidating lipid-free apolipoprotein A-I, resulting in a pre-HDL particle that is also compatible with ABCG1 (*62*). In macrophages, sterol excess upregulates ABCA1 and ABCG1 expression via LXR/retinoid X receptor (RXR)-mediated transcription (*36*, *113*). Elevated ABC transporter expression has been observed in cancers and might contribute to increase HDL availability to cancer cells (*153*, *175*). Yet, as ABC transporters may also

efflux other ligands, such as anticancer drugs, they might contribute to drug resistance and aggressiveness in manners unrelated to cholesterol homeostasis (*153*, *175*).

1.1.3 Cellular cholesterol transport

The transport of cholesterol within membranous vesicles occurs along cytoskeletal filaments and is regulated by members of the Rab GTPase family (*209*). Besides the numerous intracellular vesicle trafficking routes (FIGURE 1.2), this also includes receptor-mediated endocytic uptake of LDL, which is regulated by Rab5, Rab7 and several other regulatory proteins along the endocytic pathway. The transport routes of LDL-derived cholesterol exiting LE/Lys are complex and still not fully understood (*50*, *51*). NPC1 is considered the most important cholesterol transporter exporting cholesterol from LE/Lys. However, several other cholesterol transporters in LE/Lys exist, including members of the StARD and OSBP families, yet their roles in cholesterol homeostasis remain to be fully clarified (*165*). It is generally believed that NPC1 delivers the majority of LDL-derived cholesterol to the PM, which could occur along exocytic vesicular transport routes or non-vesicular routes that might include sterol transport through the cytoplasm or cholesterol transfer across membrane contact sites (MCS) (*97*, *166*). Earlier reports described LDL-cholesterol transport from LE/Lys to the ER, followed by its delivery to the trans-Golgi network (TGN), involving Rab9 (*32*, *96*, *237*). Alternatively, LDL-cholesterol might be transported from LE/Lys to the PM and then be delivered back to the ER to regulate cholesterol homeostasis. Grewal and colleagues recently demonstrated that the GTPase Rab7 is required for LDL-cholesterol transfer across MCS to the ER, followed by cholesterol esterification and storage in lipid droplets (*155*). On the route to the cell surface, NPC1 might deliver LDL-derived cholesterol from LE/Lys to recycling endosomes. Indeed, NPC1-dependent recruitment of Rab8a to peripheral endosomes containing LDL-derived cholesterol was followed by Rab8a - myosin-5b (Myo5b) interaction to enable transport of LDL-cholesterol-loaded organelles along cytoskeletal elements towards the cell periphery (*109*). Besides delivering cholesterol to the cell surface, this Rab8-mediated transport route might also connect to cholesterol efflux mediated by ABCA1 (*136*).

Other cholesterol transporters, some of those considered to promote non-vesicular transport include the above mentioned StARD proteins, OSBP and OSBP-related proteins (ORP) (*132*). Like shuttles, these sterol transporters often seem to transport cholesterol across MCS of adjacent organelles (*147*). The endosomal membrane proteins ORP1L and StARD3, for example, promote cholesterol transfer between LE and the ER, by using vesicle-associated membrane protein-associated protein A (VAP-A) as a binding partner at the ER membrane (*155*, *271*). ORP2 is involved in FAK/integrin recycling to the PM by regulating cholesterol-loading to RE (*231*).

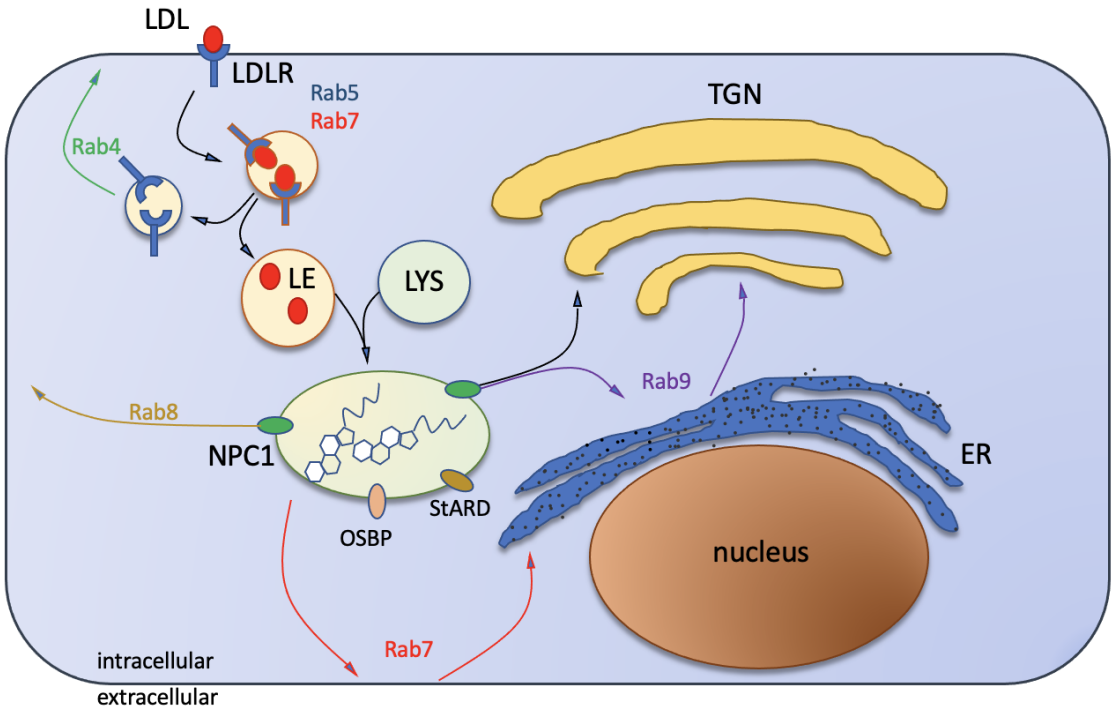

FIGURE 1.2: **Rab protein-regulated cholesterol transport.** Rab proteins control the directional intracellular vesicle transport along the cytoskeleton in an organelle-specific manner. For the LE/Lys compartment, Rab7 is a critical regulator of cholesterol homeostasis by working with Rab5 to control LDL transport to the LE/Lys compartment and coordinating egress and distribution to other organelles. Rab9 has been shown to control cholesterol from LE/Lys to the endoplasmic reticulum (ER) and further to the trans-Golgi network (TGN). While Rab4 plays an important role in membrane recycling, Rab8 promotes the transport of NPC1-ejected LDL-cholesterol vesicles to the plasma membrane by interacting with myosin-5b (Myo5b) (*165*). LDL: low density lipoprotein, LDLR: LDL receptor, OSBP: oxysterol-binding protein, StARD: steroidogenic acute regulatory-related lipid transfer domain.

1.1.4 The mevalonate pathway and cell signalling in cancer

In line with a critical role in cancer cell metabolism, the mevalonate pathway is modulated by several oncogenic and tumour suppressive signalling pathways. These include the PI3K/Akt kinase signalling pathway, mammalian target of rapamycin (mTOR) complex 1 (mTORC1) and the adenosine monophosphate-activated protein kinase (AMPK) signalling pathway as well as the tumour suppressors p53 and retinoblastoma protein (RB) (*161*).

Upon stimulation of growth factors such as insulin, platelet-derived growth factor (PDGF), and vascular-endothelial growth factor (VEGF), upregulation of the PI3K/Akt pathway stimulates cell proliferation and survival. These findings correlate with PI3K/Akt-mediated increase of SREBP1/2 expression (*161*). Hence, enhanced PI3K/Akt signalling

leading to an increase in cellular lipid and cholesterol levels through upregulated *de novo* synthesis has been linked to tumourigenesis (*27*, *192*).

mTORC1 is a nutrient- and growth signal-sensitive regulator of cell growth downstream of the PI3K/Akt pathway (*161*). In hepatocellular carcinoma cells, mTORC1 can promote SREBP2 activation and cholesterogenic transcription by activation of ribosomal S6 kinase 1 (S6K1) (*245*). Moreover, mTORC1 may affect SREBP through phosphorylation of lipin 1, which when unphosphorylated inhibits SREBP-mediated transcription (*177*).

As a counterpart of mTORC1, AMPK downregulates *de novo* cholesterol biosynthesis by phosphorylation of HMGCR under ATP deficiency and inhibits cell growth through additional phosphorylation of mTORC1 (*205*, *214*). AMPK is a direct substrate of ATP-sensitive liver kinase B1 (LKB1), a known tumour suppressor whose inactivation is associated with carcinogenesis. Thus, the LKB1–AMPK–mTORC1 axis is considered an important checkpoint for cell growth (*214*).

Furthermore, a cellular cholesterol imbalance has been linked to the gain-of-function mutations R273H and R280K in the tumour suppressor gene TP53, which allow interaction between p53 and SREBP and activation of SREBP-mediated transcription (*56*). Wild type (WT) p53, in contrast, downregulates SREBP-mediated transcription through lipin 1 under glucose starvation (*177*).

In addition, activation of the proliferative and anti-apoptotic transcription factors yes-associated protein (YAP) and transcriptional coactivator with PDZ-binding motif (TAZ) depends on geranylgeranyl diphosphate, a metabolite originating from the mevalonate pathway. Geranylgeranylation of Rho-GTPases is a prerequisite for the prevention of YAP/TAZ phosphorylation to allow translocation into the nucleus (*226*). In cancer, mutant p53-mediated activation of the SREBP/mevalonate pathway and consequent stimulation of YAP/TAZ activity by increased mevalonic acid has been reported (*226*).

In summary, multiple signalling pathways that are commonly deregulated in cancer settings target activation of SREBP1/2 and other transcription factors (e.g. LXR) that control the expression of enzymes involved in the synthesis of cholesterol and other lipids. These oncogenic alterations in signalling networks appear as major underlying mechanisms that ensure cancer cells a sufficient supply with cholesterol and other lipids for cell growth and aggressiveness. It would go beyond the scope of this thesis to outline in more detail the numerous signaling events that modulate SREBP activity and other transcription factors in cancer settings, therefore reference is made to detailed articles for further reading (*65*, *134*, *161*, *261*). Alternatively, cancer cells can utilise dietary cholesterol to promote

aggressiveness, which will be described in more detail in the following.

1.2 LDL-cholesterol and cancer cell migration

In several cancer models, increased uptake of LDL-cholesterol as well as elevated LDL levels in plasma have been linked to cancer cell migration and metastasis (*88*, *162*, *165*, *218*). These findings indicate that LDL-cholesterol can serve to promote cancer cell motility and it is generally believed that LDL supplies cholesterol to the cell surface. At this location, besides being a structural component of lipid rafts, which can serve as signalling platforms that drive oncogenic behaviour, cholesterol is also critical for the functioning of FA, which represent specialised and dynamic microdomains at the cell surface that determine cell spreading and motility (*162*).

Cellular locomotion depends on the transfer of intracellular mechanical tension to the extracellular environment. Thus, cells create specialised contact sites called integrin adhesion complexes that connect an extracellular anchor, integrins, which represent cell adhesion receptors composed of α and β subunits that bind to extracellular matrix (ECM), to the intracellular cytoskeleton. The best investigated integrin adhesion complexes are FA (FIGURE 1.3A), which link integrins to intracellular actin filaments (*157*). Migration is a cyclic progress involving protrusive and retractive membrane dynamics (FIGURE 1.3B). In the direction of migration, the leading edge is formed by polymerisation of actin filaments and anchorage of the resulting protrusion in the ECM or to adjacent cells. While the adhesion sites in the front allow forward traction, cell detachment is prepared by FA dissolution at the rear (*194*).

A growing number of studies has demonstrated the importance of cholesterol for cell migration (*88*, *109*, *189*, *231*, *251*). At the cell surface, LDL-derived cholesterol from LE/Lys feeds into the pool of cholesterol found in FA. As outlined above, at the leading edge, these structures continuously undergo assembly and disassembly to promote cell migration. For cells to move forward, coordinated delivery of integrins, and recruitment of signalling proteins such as Src and FAK to FA is essential (*28*). Increased integrin cell surface expression, ECM and metalloprotease secretion, and elevated Src and FAK activity significantly contribute to tumour progression (*4*, *28*). Unphysiological cholesterol depletion studies that disrupted the functional integrity of cholesterol-rich cell surface microdomains supported cholesterol being essential for FA assembly, recruitment and signalling (*47*, *60*, *71*, *186*, *251*).

For instance, lipid raft disruption through methyl-β cyclodextrin (MβCD)-mediated cholesterol depletion led to morphogenic changes and a significantly reduced migration capacity. In contrast to the cell spreading and the formation of lamellipodial extensions

in the controls, MβCD-treated cells were rather irregularly shaped and smaller (*251*). Moreover, LDL-cholesterol-containing vesicles emanating from LE/Lys were delivered in the vicinity of FA at the cell surface (*104*, *109*). In these and other studies, LDL stimulated FA numbers, dynamics and migration, enabling aggressive behavior characterised by enhanced integrin recycling (*9*, *56*, *104*, *109*).

Along these lines, Grewal and co-workers and other researchers showed LDL to stimulate migration, an effect that vanished when LDL-cholesterol liberation from the endosome was inhibited (*104*, *109*). Upon LDL treatment, FA numbers and FA turnover increased and a cell size extension by 2.5-fold was determined. Consistently, LDL-cholesterol-containing vesicles were directed to FA sites at the PM (*109*). In follow-up studies, Takahashi *et al.* demonstrated that the LDL-mediated increase in FA assembly and turnover required FAK signalling (*231*). Nevertheless, besides the involvement of NPC1, the cholesterol transporters in LE/Lys, Rab-GTPases and possibly other regulatory proteins that coordinate LDL-derived cholesterol delivery to the migratory machinery at the cell surface remain yet to be fully characterised.

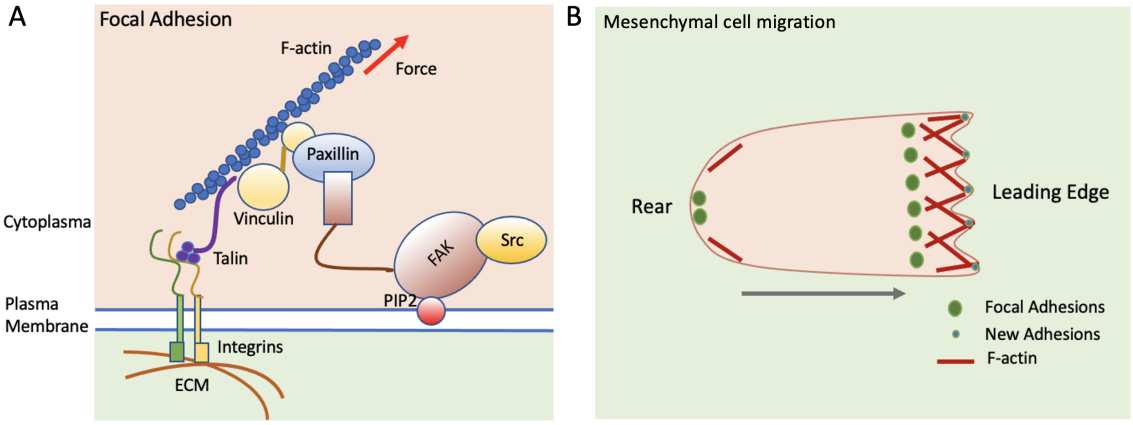

FIGURE 1.3: **Focal adhesion dynamics in cell migration.** (A) Focal adhesions (FA) are integrin adhesion complexes that link integrins to the cytoskeleton which enables the cell to generate traction forces required for cell spreading and migration. FA are dynamic complexes of multiple signalling molecules such as talin, vinculin, paxillin, focal adhesion kinase (FAK), and Src kinase (*157*). (B) For directed forward motion, mesenchymal cells create protrusions of polymerising actin filaments and new adhesion sites at the leading edge, while cell detachement at the rear is characterised by FA disassembly (*194*). F-actin: filamentous actin, ECM: extracellular matrix, PIP2: phosphatidylinositol (4,5)-bisphosphate.

1.2.1 Focal adhesion formation and turnover

FA are dynamic multiprotein complexes that undergo assembly, disassembly or maturation upon mechanical stress through actin polymerisation at the leading edge (FIGURE 1.3). Based on proteomic analyses of integrin adhesion complexes Horten *et al.* identified a

'consensus adhesome' of 60 proteins (*89*). While the lipid microenvironment, in particular cholesterol, for proper FA functioning was highlighted in the previous section, here the focus shall be on three main pathways of the 'core cell adhesion machinery': talin–vinculin, FAK–paxillin, and α-actinin–zyxin–vasodilator stimulated phosphoprotein (VASP).

The talin-vinculin axis forms the linkage of ECM-anchored integrins and the intracellular actin cytoskeleton. Talin is prerequisite for cells to maintain spreading (*269*), as the N-terminal talin head binds integrins, phosphatidylinositol 4,5-bisphosphate (PIP2) and F-actin (actin-binding site 1; ABS1) and the talin rod at the C-terminus can bind Rap1-interactive adaptor molecule (RIAM), vinculin, integrins and F-actin (ABS2 and ABS3) (*13*). Vinculin binding to talin and F-actin can stabilise the linkage, a mechanism which is promoted by activation of vinculin or mechanical tension along the talin-ABS3 - F-actin bond (*13*). In vinculin-deficient mouse embryo fibroblasts, Saunders *et al.* showed a decrease in FA size and number and an increase in FA turnover, indicating vinculin to play a role in FA growth and stabilisation (*206*). In platelets, Zhang and colleagues described Src-mediated vinculin phosphorylation at tyrosine residues Y100 and Y1065 to provoke a conformational change that promoted cell spreading (*270*). Vinculin phosphorylation may lead to vinculin activation or modulate binding to actin and PIP2 (*69*). Furthermore, actin-cytoskeletal tension-induced myosin-2 (Myo2)- FAK/Src - paxillin signalling recruits vinculin to the FA site and promotes the association of vinculin and paxillin (*174*). In mouse F9 embryonal carcinoma cells, Subauste and colleagues showed vinculin-paxillin interaction to downregulate cell migration by reducing FAK-mediated phosphorylation of paxillin and subsequent activation of extracellular signal-regulated kinases (ERK) 1/2. In contrast, cells depleted of vinculin were highly motile and metastatic (*229*). Upon LDL treatment, migrating cancer cells increased the number and size of vinculin-immunostained FA (*109*). MβCD-mediated cholesterol depletion from the PM was linked to an increase of centrally located vinculin signals overlapping with the end of stress fibres. Furthermore, under these conditions, FA increased in number and size, forming rather longer FA (*251*).

FAK is a key mediator of FA signalling. Upon integrin clustering, FAK is recruited to FA where its N-terminal FERM (4.1 protein, ezrin, radixin, moesin) domain builds a 'basic patch' with the membrane phospholipid PIP2 (*172*). Subsequent FAK autophosphorylation of Y397 creates a docking site for Src family kinases, such as Src and Fyn, via their Src Homology 2 (SH2) domain which promotes further phosphorylation and mutual activation (*207*). Among the downstream targets of the FAK-Src complex are paxillin and p130Cas (Crk-associated substrate) (*208*, *243*). At the C-terminus, the focal adhesion targeting (FAT) domain has been shown necessary and sufficient to direct FAK to adhe-

sion complexes (*86*). The FAT sequence comprises binding sites for paxillin, vinculin, p130Cas, α-catenin and other adhesion proteins (*11*).

Paxillin serves as an adaptor protein and comprises four LIM (Lin-11, Isl-1, MEC-3) domains at its C-terminus, two of which promote FA targeting dependent on their phosphorylation status (*21*). At the N-terminus, paxillin has binding sites for vinculin, FAK and Src (*20*, *256*). Moreover, as a key regulator of Rho GTPases such as RhoA, Cdc42, and Rac1, paxillin plays a pivotal role in actin cytoskeleton and actin-associated adhesion dynamics in the context of cell migration (*19*). In detail, RhoA promotes F-actin polymerisation and cell contraction, Cdc42 controls microtubule network polarisation and filopodial, whereas Rac1, controls lamellipodial expansion of actin-rich projections (*193*). The FAK-Src-paxillin-p130Cas-ERK-myosin light-chain kinase (MLCK) axis is a critical regulator of adhesion turnover. Fibroblasts with loss of function of paxillin, p130Cas, mitogen-activated protein kinase (MAPK)/ ERK or MLCK showed reduced FAK or paxillin turnover (*254*). Using green fluorescent protein (GFP)-paxillin expressing cell lines, an increase in FAK-dependent FA formation and disassembly upon LDL treatment was demonstrated (*231*). Cholesterol depletion by MβCD, moreover, led to centralisation of paxillin-stained FA (*186*).

As the intracellular mechanical tension increases, α-actinin is attracted to the nascent FA and competes with talin for the integrin-actin linkage. Through the takeover by α-actinin, FA maturation is triggered (*198*). The α-actinin binding partner zyxin is recruited to mature but not nascent adhesions in a force-dependent manner when the leading edge stops moving forward (*131*, *133*, *266*). Zyxin localises at the termini of F-actin where it can regulate actin polymerisation (*55*) and additionally, directs Ena/VASP family members to the FA site (*46*). Zyxin-VASP interaction was shown to enhance actin fibre formation at specific sites, e.g. during cell spreading (*45*), however, zyxin did not colocalise with the ectopically expressed and fluorescently-tagged VASP in lamellipodial tips of mouse melanoma cells. Consequently, zyxin may not be involved in lamellipodial protrusion, there might be other proteins involved in VASP targeting (*199*). Cholesterol content has been shown to regulate F-actin polymerisation (*252*), but no evidence was found for how the α-actinin-zyxin-VASP axis is affected by cholesterol.

1.2.2 The role of cholesterol for focal adhesion formation

The composition and order of cell membranes can be modified by the cholesterol content which may promote changes in cell adhesion and motility. Cell membranes consist of

dynamic lipid-protein layers that harbour the fluctuating assembly of sphingolipids, cholesterol and glycosylphosphatidylinositol (GPI)-anchored proteins into specialised membrane domains called lipid rafts. These nanoscale platforms serve as functional sites promoting cellular functions such as signalling and trafficking events (*137*). The inner leaflet of rafts is host to the lipid messengers PIP2 and phosphatidylinositol (3,4,5)-triphosphate (PIP3), which play an important role in the temporal and spatial regulation of signal transduction at the membrane–cytosol interface (*44*, *249*). Other proteins with binding affinity for raft domains involve members of the Src kinase family and heterotrimeric G proteins (*219*). From the Golgi, where the cholesterol-sphingolipid rafts assemble, they are delivered to the PM and incorporated or endocytosed as required (*219*). This membrane subcompartmentalisation is a prerequisite for the coordination of several signalling pathways including T-cell antigen receptor, immunglobulin E, H-Ras, and integrin signalling (*137*, *219*). Ligand-mediated receptor acitvation within lipid rafts may recruit proteins to the activated site and initiate signalling pathways by local kinase or phosphatase activity.

Disruption of lipid rafts by cholesterol depletion consequently impairs translocation of proteins to the PM and regulation of FA and cytoskeletal dynamics. In non-small cell lung cancer (NSCLC) cells, MβCD-induced raft cholesterol depletion inhibited cell migration. The authors demonstrated a decrease in epidermal growth factor (EGF)-mediated phosphorylation of EGF receptor (EGFR), FAK, Src, Akt, and p44/42 as well as translocation of Src from the cell membrane into the cytoplasm (*101*). After MβCD treatment of human melanoma cells, Wang *et al.* showed the formation of robust stress fibres extending through the cell body and the accumulation of large FA at the end of the stress fibres in the cell centre (*251*). They proposed the cytoplasmatic translocation of Src, which is a negative regulator of RhoA, to trigger RhoA-ROCK-mediated F-actin polymerisation. Raft cholesterol depletion was associated with increased phosphorylation of vinculin and paxillin, and with decreased internalisation of β3 integrins (*251*). This is in line with findings of Webb *et al.* who described reduced FA disassembly rates in FAK- or Src-deficient fibroblasts and chinese hamster ovary (CHO) cells (*254*). FA disassembly has been linked to dephosphorylation of FA proteins (*118*, *129*), a process which can be catalysed by protein tyrosine phosphatases (PTP). Accordingly, lack of function of the cytoplasmic tyrosine phosphatase Shp-2 or the PTP-PEST were associated with an increase of FA and stress fibres (*8*, *264*). In addition, Shp-2 and PTP-PEST localisation was related to lipid rafts (*10*, *115*). Consequently, lipid raft disruption may inhibit FA protein dephosphorylation by preventing PTP association with rafts. In neuroepithelial cells, β1 integrin distribution colocalises with lipid rafts and β1 integrin-fibronectin (FN)-mediated cell adhesion depends on lipid rafts (*262*). Consistently, in migrating colonic epithelial cells, colocalisation of the lipid raft marker cholera toxin and β1 integrin in

cytosolic vesicles at the leading edge was demonstrated (*239*). Redistribution of cytosolic β1 integrin into lipid rafts can be promoted by Rab1a. Accordingly, Rab1a knockout or lipid raft disruption by cholesterol depletion diminished colocalisation of β1 integrin with lipid rafts (*247*). Thus, cholesterol-dependent lipid raft formation plays an important role in the temporal and spatial coordination of FA dynamics by creating a subcompartment for specific signal transduction and vesicular transport.

Not to be neglected, the cholesterol content has a major impact on membrane rigidity. At the leading edge of migrating cells an increased membrane microviscosity is required to promote lamellipodial extension. In MβCD-treated endothelial cells, the membrane microviscosity gradient was disrupted and cell migration reduced. Since the authors did not find abnormal actin filament formation, they explained the antimigratory effect by altered membrane microviscosity (*238*). However, some studies have described intense formation of stress fibres after MβCD treatment (*126*, *251*), so changes in actin filament formation may have gone undetected.

PM cholesterol may affect cell migration by influencing integrin recycling. Ramprasad and colleagues showed MβCD-induced cholesterol depletion from the cell membrane to impair cell spreading, adhesion and motility in L27 cells (derived from the mouse S180 sarcoma cell line) especially on FN (*186*). This effect was mediated by the FN-specific integrin α5β1 (*186*). Specifically, in CHO cells, the integrin α5β1 was shown to play an important role in cell motility rather than cell adhesion (*212*). In line with this, Coppolino and colleagues demonstrated integrin α5β1 sequestration in Rab11-positive compartments by inhibition of the soluble N-ethylmaleimide-sensitive-factor attachment receptor (SNARE) protein vesicle-associated membrane protein 3 (VAMP3) to impair cell migration but not adhesion (*220*, *233*).

Integrin recycling depends on LDL-cholesterol-controlled TGN localisation of the t-SNARE syntaxin 6 (Stx6). Since cell migration is characterised by high rate FA turnover, integrin recycling plays an important role. Integrin recycling to the cell membrane is regulated by Stx6 in a cholesterol-dependent manner. During integrin recycling, Riggs *et al.* suggested integrins to be transferred from Rab11-positive recycling endosomes to the TGN through vesicle fusion, a process dependent on complex formation between the recycling endosomal v-SNARE protein VAMP3 and the TGN-associated t-SNARE Stx6 (*195*). Using NPC1 mutant cell lines, in which cholesterol egress from the LE is impaired and LDL-cholesterol levels at the TGN consequently are depleted, Reverter *et al.* showed hampered integrin recycling by translocation of the t-SNARE protein Stx6 from the TGN to recycling endosomes (*189*). TGN - recycling endosome translocation of Stx6 is promoted towards the organelle with higher cholesterol content, since cholesterol enrichment of recycling endosomes led to a Stx6 distribution comparable to the NPC1

phenotype (*189*). Stx6 may act as a cholesterol sensor by binding directly to cholesterol or through response to general membrane adaptations mediated by cholesterol (*189*).

FAK/integrin delivery to the PM depends on ORP2-induced cholesterol loading into recycling endosomes. Takahashi *et al.* showed LDL-cholesterol translocation from LE to FAK/integrin-loaded recycling endosomes to depend on the lipid transporter ORP2 and FAK activity. FAK - type I phosphatidylinositol phosphate kinaseγ (PIPKIγ) signalling was shown to increase PIP2 in endosomal membranes (*164*). ORP2 can regulate cholesterol delivery to the PM and modulate PM lipid levels by exchanging cholesterol for PIP2, which shifts PIP2 to subcellular membranes (*231*, *248*). By the same counter current transport, ORP2 was proposed to promote LDL-cholesterol transfer from LE to recycling endosomes. Since colocalisation of ORP2 with FAK/integrin-loaded vesicles outperformed colocalisation with NPC1-positive organelles and ORP2 silencing reduced cell adhesion, it was proposed that ORP2 promotes FAK/integrin recycling while regulating cholesterol distribution into the PM at the level of LE-recycling endosome interaction (*231*). Consistently, overexpression of GFP-ORP2, but not the PIP2 binding-deficient mutant (ORP2-mHHK), led to colocalisation with NPC1-mCherry and intensified anti-PIP2 signals (*231*). In addition to reduced cell adhesion, ORP2 depletion was linked to diminished FAK membrane association and phosphorylation. Binding to membranous PIP2 is a known mechanism of FAK activation, thus ORP2-mediated exchange of cholesterol for PIP2 does not seem an obvious activator of FAK. However, by imaging the association of fluorescently labeled FERM (PIP2 binding site of FAK) and PIP2-containing giant unilamellar vesicles, Takahashi and colleagues suggested cholesterol to enhance PIP2-induced activation of FAK (*70*, *231*).

Taken together, cholesterol is a critical regulator of FA formation by controlling cell membrane order, raft-associated signalling, including FA and cytoskeletal turnover, and intracellular recycling and transport mechanisms.

1.3 The role of Annexin A6 in cholesterol transport, focal adhesion formation, and cell migration

Over the last decade, Annexin A6 (AnxA6), a Ca^{2+}-dependent membrane-binding protein, has gained increasing attention as a regulator of endocytic and exocytic pathways including cholesterol transport (*49*).

AnxA6 binding to late endosomal membranes is influenced by the cholesterol content and thereby regulates the Tre-2/Bub2/Cdc16 domain family member 15 (TBC1D15)/Rab7/StARD3 axis (Figure 1.4). In CHO cells, about 75% of the AnxA6-membrane associations are Ca^{2+}-dependent, 25% are Ca^{2+}-independent and found in endosomal membranes.

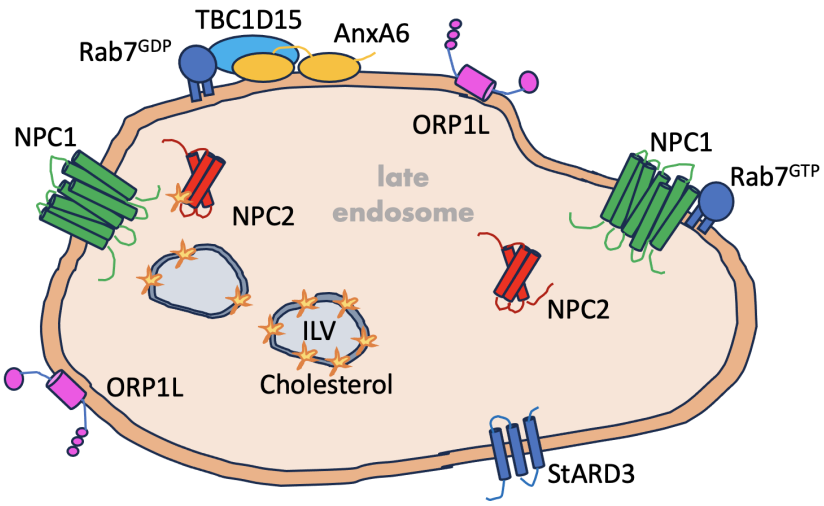

FIGURE 1.4: **Late endosomal cholesterol transporters and co-proteins associated with cholesterol egress.** ILV: intraluminal vesicles, NPC1/2: Niemann–Pick Type C1/2, AnxA6: Annexin A6, TBC1D15: Tre-2/Bub2/Cdc16 domain family member 15, ORP1L: OSBP-related protein 1L, StARD3: Steroidogenic acute regulatory (StAR)-related lipid transfer domain containing 3. Image was adapted from (*165*).

Ca^{2+}-independent association of AnxA6 with LE decreased by digitonin-mediated cholesterol depletion and increased by LDL-cholesterol loading showing its sensitivity to cholesterol levels (*42*). Cubells *et al.* demonstrated overexpression of AnxA6 to be associated with cholesterol accumulation in LE and concomitant depletion of cholesterol at the PM and Golgi, reminiscent of the NPC1 mutant phenotype (*38*). This was explained by the finding that LE-associated AnxA6 triggers the recruitment of TBC1D15, a Rab7 GTPase activator, which acts as a negative regulator of Rab7 signalling (*155*). Rab7 is critical for endocytic structure/Lys fusion and the formation of MCS (membrane contact sites) to enable non-vesicular lipid transport between endosomes, the ER, and the Golgi (*23*, *32*, *155*). Consistently, in NPC1 mutants, Choudhury *et al.* showed overexpression of Rab7 to restore cholesterol delivery to the Golgi and to reduce cholesterol accumulation in LE/Lys (*32*). As cholesterol-controlled AnxA6 binding to LE seems to prevent cholesterol transfer to the Golgi by downregulation of Rab7 activity, Meneses *et al.* hypothesised restored cholesterol distribution upon AnxA6 depletion and consequent upregulation of Rab7 in NPC1 mutant cells (*155*). Consistent with this, they showed that cholesterol egress and peripheral distribution of LE were rescued in a Rab7-StARD3-dependent manner (*155*). Respectively, MCS were reduced in NPC1-deficient CHO M12 cells but increased with additional AnxA6 knockout (CHO M12-A6ko) (*155*). However, membrane bridging and cholesterol transport at the MCS seem to be two different mechanisms (*155*). The endo-

somal membrane protein StARD3 can build a complex with its ER-based binding partner VAP-A which enables efficient cholesterol transport between the ER and endosomes (*258*). In CHO M12-A6ko cells, StARD3 lack of function inhibited the rescuing effect of AnxA6 depletion, although the number of MCS remained stable (*155*). Another known cholesterol transfer route between the ER and LE involves ORP1L - VAP-A interaction, however, ORP1L requires NPC1 function and the CHO cells used in the study lacked ORP1L expression (*155*, *271*). Thus, AnxA6 depletion can rescue cholesterol accumulation in NPC1 mutant cells by promoting Rab7-StARD3-mediated formation of MCS and cholesterol transfer.

AnxA6 alters the intracellular distribution of cholesterol which affects cell migration by inhibiting intracellular vesicular trafficking. While AnxA6 overexpression causes cholesterol accumulation in LE/Lys, other compartments such as the PM or Golgi are reduced in their cholesterol content (*38*). Studying CHOanx6 cells, a CHO cell line overexpressing AnxA6, Cubells *et al.* reported cholesterol sequestration to be accompanied by caveolin-1 (Cav-1) and caveolin-3 (Cav-3) accumulation in the Golgi (*38*). Caveolins are structure proteins of caveolae at the cell surface and travel between the Golgi and PM in a cholesterol-dependent manner (*179*). Caveolae are cell membrane pits characterised by a lipid raft-like higher-order structure and their major membrane proteins the caveolins. Caveolae can undergo endocytosis and fuse with endosomal vesicles, they later can be recycled to the cell surface or ubiquitylated for degradation. The coordination of caveolae dynamics is modulated by the actin- and microtubule-cytoskeleton and plays an important role in mechanotransduction (*173*). Cav-1 has been shown to regulate FA turnover and promote cell migration via Src- and ROCK-dependent signalling (*105*). To examine whether direct AnxA6 - caveolin interaction may cause caveolin retention in the Golgi, Cubells *et al.* searched for colocalisation of AnxA6 and Cav-1 using an immunoprecipitation and colocalisation assay, of which both were negative (*38*). Cav-1 accumulation was also seen in AnxA6-depleted A431 cells upon treatment with the NPC1 inhibitor U18666A while cholesterol treatment of CHOanx6 could reduce Cav-1 accumulation in the Golgi (*38*). Intracellular cholesterol distribution appeared to be the predominant factor regulating the exit of caveolin from the Golgi. Consistent with the sequestration of caveolin in the Golgi, AnxA6-overexpressing cells had fewer caveolae on the cell surface. Comparing CHO WT to CHOanx6, a reduction in caveolae of 61% was determined (*38*).

Export from the Golgi is promoted by cytoplasmic phospholipase A2 ($cPLA_2$)-mediated Golgi vesiculation in a cholesterol-dependent manner. With increasing cholesterol levels in the Golgi, $cPLA_2$ is recruited to the Golgi membrane and generates lysophospholipids and arachidonic acid (AA) that are required to create a membrane bulge to enable later vesiculation and dispersal (*49*). Consistently, in CHOanx6 cells, $cPLA_2$ association

with the Golgi as well as $cPLA_2$ activity were reduced (*38*). However, since some members of the annexin family such as AnxA1 and AnxA5 have been shown to inhibit $cPLA_2$ activity (*24*, *117*), AnxA6 might also act as a direct effector of the Golgi transport system. Moreover, AA has been indicated as a positive regulator of SNARE complex formation (*34*, *191*), which is a prerequisite for membrane fusion and consequently for vesicular trafficking. In CHO cells overexpressing AnxA6, the SNARE proteins synaptosome-associated protein 23 (SNAP23) and Stx4 accumulated in Golgi membranes with enhanced colocalisation to caveolin, which they are thought to be responsible for transporting (*181*). Anx6-induced accumulation of SNAP23 and Stx4 was linked to impaired exocytic secretion, e.g. of FN (*190*).

AnxA6-induced depletion of Golgi cholesterol impairs integrin recycling by interfering with Stx6 localisation to the Golgi. The tSNARE Stx6 plays an import role in integrin recycling and cholesterol trafficking between LE and the Golgi (*189*, *195*). Upon AnxA6 overexpression, Stx6 was displaced from the TGN to scattered cytoplasmic vesicles, which was accompanied by reduced integrin molecules at the cell surface of CHOanx6 cells as determined by flow cytometry (*59*). This was mimicked by depletion of Stx6 in CHO WT cells (*59*). Since increased colocalisation of Stx6 with the recycling endosome markers Rab11 and VAMP3 but decreased formation of Stx6-VAMP4 (TGN marker) complexes were observed in CHOanx6 cells, the authors concluded an association deficit between Stx6 and Golgi membranes (*59*).

AnxA6 can regulate migration by downregulation of EGFR/Ras signalling and direct F-actin interaction. Like the other annexins, AnxA6 can bind to cellular membranes in a Ca^{2+}-dependent manner, moreover its protein structure contains binding sites for the Ras inhibitor GTPase-activating protein (GAP) p120GAP and F-actin (*75*). The EGFR/Ras/MAPK pathway plays an important role in cancer development and dysregulation of oncogene Ras has been linked to multiple cancer types, e.g. breast cancer, melanoma, and lung cancer (*151*). p120GAP catalyses the hydrolysation of GTP, by which it downregulates Ras activity, and is the only known EGFR-associated GAP (*103*, *150*, *253*). Several cancer studies have linked AnxA6 loss of function to increased EGFR/Ras activity, suggesting AnxA6 to modulate EGFR/Ras signalling by promoting p120GAP recruitment to the cell surface (*74*, *241*). EGFR localisation within lipid rafts and caveolae has been discussed controversially since results are inconsistent (*73*). However, as AnxA6 can impact the formation of these membranous microdomains by cholesterol sequestration, this might be another mechanism by which AnxA6 can influence EGFR/Ras signalling (*73*).

Furthermore, AnxA6 may regulate migration by direct interaction with the actin-cytoskeleton. With increasing intracellular Ca^{2+} levels, AnxA6 is targeted to the cell

surface where it can form a membrane-F-actin complex. In human embryonic kidney cells, the interaction between membrane-targeted AnxA6 and F-actin led to cytoskeletal rearrangments including the formation of cortical actin and to a F-actin-dependent decrease of store-operated Ca^{2+} entry (SOCE) (*159*). In cardiomyocytes, AnxA6-mediated reduction of Ca^{2+} entry negatively affected cardiomyocyte contractility (*81*).

AnxA6 is a positive regulator of autophagy, which in turn can promote FA degradation and cell migration. Grewal and colleagues proposed AnxA6 to play a role in autophagosome biogenesis (*48*). Accordingly, in HeLa cells, AnxA6 is upregulated in starvation-induced autophagy and the latter is impaired by AnxA6 loss of function (*230*). While starvation-induced autophagy is rather unselective in the uptake of cellular components, FA disassembly requires high selectivity for FA sites (*112*). This is achieved by autophagy cargo receptor proteins which bind the substrate and also interact with microtubule-associated protein 1A/1B light chain 3 (LC3) on the autophagosomal membrane (*112*, *228*). During autophagosome formation, cytoplasmic LC3-I is converted to membrane-bound LC3-II, which localises specifically to autophagosome membranes and correlates with the rate of autophagy (*106*). In cervical cancer, Sun and colleagues correlated the expression of AnxA6 and LC3, and showed AnxA6-induced autophagy to suppress tumour growth (*230*). Morever, in head and neck squamous cell carcinoma, AnxA6-induced autophagy by inhibtion of Akt and mTOR phosphorylation was linked to metastasis and invasion (*250*).

1.4 Aims

The mechanisms by which cholesterol influences tumour growth and metastasis are not fully understood. This work aims to investigate the role of LDL-cholesterol in FA formation and cancer cell migration. Building on recent findings by Grewal and colleagues, it was hypothesised that LDL-cholesterol released from LE in AnxA6-depleted CHO M12 cells could be delivered to the PM and support the formation and function of specialised structures such as FA, which are required to promote cell migration. Aiming to elucidate the regulatory circuits linking intracellular LDL-cholesterol trafficking with the machinery that drives migratory cell behaviour, the protein levels of enzymes involved in intracellular cholesterol dynamics and the number, (co-)localisation and size of FA components visualised by immunofluorescence-labelled FA markers will be analysed using the CHO cell models CHO wild type (WT), CHO M12 and CHO M12-A6ko.

Since cholesterol trafficking is critical for FA dynamics and cell migration behaviour, a loss of serum-induced migration in CHO M12 and a restoration of this cellular behaviour

in AnxA6-depleted CHO M12 cells was hypothesised. Starvation is a known trigger of autophagy and AnxA6 has been suggested to play a role in autophagosome biogenesis (*48*, *85*, *100*, *230*). Therefore, different levels of autophagic activity are expected between the CHO cell lines and will be determined by analysing the endosomal proteins and autophagic markers LC3-I/II, ATGL and Rab7.

Previous studies used MβCD, an unphysiological method to deplete cholesterol at the PM, which impaired FA function, in order to demonstrate a role for cholesterol in FA distribution and assembly (*71*, *251*). These studies did not visualise cholesterol at the cell surface. To study the distribution of cholesterol under more physiological conditions, mCherry-labelled D4H, a biosensor for membrane-bound cholesterol in organelles and at the PM (*148*), will be used comparing CHO WT and NPC1 mutant cells. It is speculated that cholesterol release upon depletion of AnxA6 in M12 cells could improve cholesterol delivery to the periphery to support FA formation at the cell edge. To assess the ability of a cell to form FA, differences in the number, distribution and size of FA and cell size as a marker of cell attachment must be identified. Also, problems with FA assembly in cholesterol-depleted cells are hypothesised, suggesting reduced colocalisation of key FA markers such as FAK, vinculin and paxillin, and also reduced colocalisation of FA markers with cholesterol, since cholesterol depletion from the PM has been associated with impaired FA function (*71*, *251*). As above, a rescueing effect of additional AnxA6 knockout in CHO M12 is suggested.

Chapter 2

Methods

2.1 Tissue culture

2.1.1 Cell cultivation

To investigate the role of LDL-cholesterol in FA assembly and cell migration of cancer cells, the wild type Chinese hamster ovary (CHO) cell line K1 (WT) (*182*) and two Niemann-Pick type C1 (NPC1) mutant CHO cell lines were used: CHO M12, in which the locus for the cholesterol transporter NPC1 was deleted (*156*) and CHO M12-A6ko, which are CHO M12 cells with a stable annexin A6 (AnxA6) knockdown generated using CRISPR/CAS technology (*155*). Cultivation was executed in 75cm^2 flasks at 37°C, 95% relative air moisture and 5% CO_2. Cells were grown in Ham's nutrient mixture F12, containing 1.0mM L-glutamin, supplemented with 10% fetal bovine serum (FBS) and 1% Pen-Strep (100 Units/ml penicillin, 100μg/ml streptomycin).

Cell passaging

For cell passaging, cells were washed with 3-5ml phosphate buffered saline (PBS) and detached by a 2-minute incubation in 0.05% trypsin-ethylenediaminetetraacetic acid (EDTA) at 37°C. Subsequently, trypsinisation was stopped with 8ml growth media. In the splitting step, cell aliquots were taken and diluted 1/10 in fresh growth media.

Cell storage

For long-term storage, cells were transferred into dimethyl sulfoxide (DMSO)-containing freezing media and shelved at -80°C. In detail, cells were washed with 3-5ml PBS, detached by 0.05% trypsin-EDTA, diluted in up to 10ml growth media and transferred into a 15ml centrifuge tube. Then, tubes were centrifuged at 1,500rpm (~180 x g) for 5min, resuspended in 5ml PBS and again centrifuged as above. Finally, cells were resuspended in 1.5ml media (10% FBS) followed by addition of 1.5ml freezing media (40% FBS, 20%

DMSO). Aliquots of 750μl were taken and instantly incubated on ice for one hour before being transferred to -80°C.

To recover frozen cells, cryo tubes were quickly thawed in a 37°C heated waterbath and suspended in 5ml growth media. After 5min centrifugation at 1,500rpm (~180 x g), resuspension in 5ml PBS and another 5min of centrifugation, cells were diluted in 5ml growth media and grown in a 25cm^2 flask.

Cell plating

For the execution of experiments, cells were grown on 6-well plates. Therefore, cells were detached, diluted in growth media up to 10ml, centrifuged as described above and resuspended in 5ml growth media. To ensure comparable confluency across all cell lines within one experiment as well as over a number of experiments, the procedure was performed as follows: cells were trypsinised (see Chapter 2.1.1), counted using a hemocytometer, and $1.5x10^5$ cells/well for microscopy, $2x10^5$ cells/well for western blotting and $5x10^5$ cells/well for scratch assays were plated.

Transient transfection

A common method for microscopy-based localisation studies is the transfection of expression vectors expressing fluorescently labelled recombinant proteins. For DNA uptake, the transfection reagent Lipofectamine® LTX (Invitrogen) was used following the manufacturers' instructions. Prior to the transfection step, the transfection reagent was prepared for a 6-well plate as follows: For each well 1.5μg DNA and 4μl Lipofectamine® were separately diluted in 250μl Opti-MEM™ media. After allowing the Lipofectamine® to form liposomes for 5min, both solutions were mixed and incubated for 20min. In the meanwhile, cells were washed with 1ml PBS and covered with serum-free media. Then, 500μl Lipofectamin®-DNA solution was added to each well. Cells were incubated for 5h before replacing the DNA-media mix with normal growth media (F12 + 10% FBS).

Cell lysis

Cell lysis was carried out as described by Grewal and co-workers using 20mM Tris-HCl (pH 7.5), 2mM EDTA, 100mM NaCl, 5mM $MgCl_2$, 1% (v/v) Triton X-100, 5mM NaF, 10% (v/v) glycerol, 0.5% (v/v) 2-mercaptoethanol, 0.1mM Na_3VO_4, and protease inhibitors (*79*) (see Appendix B.16 & B.17). For each well, 100μl ice-cold lysis buffer was applied, cells were subsequently scraped and transferred to an reaction tube. After 20min incubation on ice, samples were centrifuged at 14,000rpm (~20,900 x g) and 4°C for 5min. The pellet was discarded and the supernatant collected for further processing.

2.2 Biochemical methods

2.2.1 Protein quantification - Lowry assay

To determine the protein concentration of cell lysates the Lowry method was used (*144*). Therefore, a standard curve for bovine serum albumin (BSA) (1mg/ml) was prepared as shown in TABLE 2.1. Further, 5μl of each lysate was diluted in 395μl H_2O.

TABLE 2.1: BSA Standard Curve

No.	**BSA** [μl]	**H_2O** [μl]
1	0	400
2	2.5	397.5
3	5	395
4	7.5	392.5
5	10	390
6	15	385
7	25	375
8	50	350

TABLE 2.2: Lowry Solution

	for 10ml [ml]
Solution A	9.7
Solution B	0.15
Solution C	0.15

In the next step, Lowry solution consisting of solution A, B and, C (TABLE B.10, B.11, B.12) was freshly prepared as shown in TABLE 2.2 and 1ml added to each sample. While incubating the Lowry mix for 10min, folin solution was prepared (1:3 folin reagent in H_2O) and 0.125ml added. After 30min incubation, the absorbance at 750nm was measured. To limit pipetting errors, all samples were prepared as duplicates and the standard curve calculated by regression analysis estimating the relation of protein concentration and absorbance. Then, the protein concentrations of samples were determined by applying the obtained function on the mean absorbance values.

2.2.2 Gel electrophoresis and western blotting

Gel electrophoresis

Aiming to analyse single proteins, the components within a sample must be separated. Therefore, sodium dodecyl sulfate (SDS) polyacrylamide gel electrophoresis, a method filtering molecules by size (*224*), was applied using 0.75mm mini-gels. The compounds as shown in TABLE 2.3 and 2.4 were prepared. The sample solution was composed of 30μg protein, 4μl 5x Laemmli sample buffer (LSB, TABLE B.15) and destilled H_2O (dH_2O). For protein denaturation, the solution was incubated at 95°C for 5min, then placed on ice

for 5min followed by another 5min centrifugation at 14,000rpm (~20,900 x g) to remove precipitated debris. As protein size marker, 4μl Precision Plus Protein™ Dual Color Standards were loaded. Gel electrophoresis proceeded in 1x running buffer (TABLE B.5) at 200V for approximately 1h. Detailed buffer compositions can be found in Appendix B.

TABLE 2.3: 12% Resolving Gel

12% Resolving Gel	**1 Gel**
Aqua dest.	3.4ml
40% Acrylamide/N,N'-Methylenebisacrylamide (37.5:1)	2.4ml
1.5M TrisHCl pH 8.8	2ml
10%(w/v) SDS	80μl
10% APS	80μl
TEMED	8μl

TABLE 2.4: 4% Stacking Gel

4% Stacking Gel	**1 Gel**
Aqua dest.	2.9ml
40% Acrylamide/N,N'-Methylenebisacrylamide (37.5:1)	0.75ml
0.5M TrisHCl pH 8.8	1.25ml
10%(w/v) SDS	50μl
10% APS	50μl
TEMED	5μl

Western blotting

After gel electrophoresis, the separated proteins were transferred to a polyvinylidene difluoride (PVDF) membrane by performing a wet transfer, a technique first published in 1979 (*188*). Therefore, the membrane was activated for 30sec in methanol, washed for 1min in dH_2O and 5min moistened in 1x transfer buffer (TABLE B.7). Two tissue pads and six filter paper were moistened, too. Then, gel and membrane were trapped between three filter paper at each side and an outer layer of tissue pads. The sandwich was placed in a transfer tank filled with 1x transfer buffer and the transfer was run for 1h at 100V. More detailed instruction are given by Mahmood and co-workers (*149*).

To reduce unspecific binding, the membrane was blocked by incubating either with 5% skim milk diluted in Tris-buffered saline, 0.1% Tween (TBS-T, TABLE B.9) or in 5% BSA, when analysing phosphorylated proteins, for 1h. After blocking, the primary antibody, diluted 1:1000, was applied on the membrane in small drops, a technique as described by Pan and co-workers (*169*), and left overnight at 4°C. Then the membrane was washed in three steps, first for 15min then twice for 5min. The secondary antibody, diluted 1:2000, was applied equally to the first but left for 1h at room temperature. After incubation, the three-step-washing was repeated.

For visualisation the ChemiDoc Touch Imaging System by BioRad with the Image Lab™ Touch Software was utilised. To do so, Clarity™ Western ECL (enhanced chemiluminescence) substrates by BioRad were mixed 1:1 and distributed on the membrane's surface just before imaging. Densitometric analysis was performed using ImageJ (version 1.52a) software.

To correct unequal loading, the signal intensities were normalised to an internal loading control, in case of phosphoproteins, to the western blot signal obtained for the total protein. All antibodies used can be found in TABLE B.18.

To reuse PVDF membranes, antibodies were stripped off the membrane by washing twice for 10min with mild stripping buffer (TABLE B.14), twice for 10min with PBS and twice for 5min before restarting the blocking process. This method was executed following the protocol provided by Abcam (https://www.abcam.com/protocols/western-blot-membrane-stripping-for-restaining-protocol).

2.2.3 DNA preparation

The expression of fluorescently tagged cDNA using plasmid DNA is a well-established method for microscopy-based protein localisation studies. Common fluorescent proteins used as protein tags are the green fluorescent protein (GFP) (*217*) or the red fluorescent mCherry (*215*). To obtain a sufficient quantity of plasmid DNA, the DNA of interest was multiplied and extracted from bacteria.

LB agar plate preparation

For the preparation of 10 plates, 500ml LB (lysogeny broth) agar was assembled as listed in TABLE B.24. After autoclaving, the solution was left to cool down to 50°C, then kanamycin was added up to a final concentration of 50μg/ml. The liquid media was promptly poured into Petri dishes. Hardened LB agar plates were incubated at 37°C overnight, afterwards stored at 4°C, in an inverted position and air-sealed.

Bacterial transformation

Starting the transformation following the manufacturers' instructions, 5ng plasmid DNA was added to 30μl competent *E. coli* HB101 cells ($> 10^8 cfu/\mu$g) and incubated on ice for 30min. The samples were heated up for 30sec at 42°C and subsequently placed onto ice for 2min. Then, 500μl LB media, without antibiotics, was added and the tubes tucked in a shaking incubator at 37°C for 1h. In the next step, 400μl sample was spread evenly on kanamycin (50μg/ml) containing LB agar plates. LB agar plates with plated bacteria

were incubated upside down at 37°C overnight. The following day, single colonies were picked using sterile 200μl pipette tips. Tips were dropped into 3ml LB media (50μg/ml kanamycin) and tubes placed into the 37°C-heated shaking incubator. After 2-3 days, bacterial cultures had reached an OD_{600}[1] $\geq$ 1-2 and DNA was ready for extraction.

Plasmid purification

For plasmid harvest, the DNA was isolated using the QIAprep® Spin Miniprep Kit from Qiagen®. In the first step, following the protocol provided by Qiagen® (*183*), the bacterial cultures were centrifuged at $>$ 8000rpm (~ 6800 x g) for 3min and the pellets resolved in 250μl resuspension buffer P1, containing EDTA and RNase A. To continue, samples were transferred to 1.5ml reaction tubes. After cell lysis with NaOH and SDS by incubation with 250μl buffer P2 for 5min. Lysis was stopped with 350μl buffer N3 and samples were centrifuged for 10min at 13,000rpm (~17,900 x g). The supernatant was then applied to a QIAprep® spin column and centrifuged 30sec with the same settings. Next, the columns were washed first with 500μl buffer PB, repeating the 30sec-centrifugation, then with 750μl buffer PE and again centrifuged for 30min as above. To remove residual buffer, tubes were centrifuged for 60sec. For DNA elution, columns were placed into a clean tube and treated wit 60μl buffer EB. After 1min incubation, columns were centrifuged for 1min. The eluate was collected and DNA concentration was determined.

2.3 Microscopy

2.3.1 Biochemical methods for slide preparation

Slide preparation

For microscopy-based methods, cells were grown on coverslips with a diameter of 15mm and 1mm thickness. Each 6-well-plate well was equipped with two in ethanol stored coverslips, left to dry for 20min under UV light and washed extensively with PBS before plating $1.5x10^5$ cells. The next day, the transfection of plasmid DNA was performed as described in Chapter 2.1.1.

Cell fixation, immunostaining and slide mounting

48h after transfection, cells were fixed with 4% formaldehyde for 20min and then washed four times for 5min with PBS. Next, cells were permeabilised applying 0.3% Triton-X for 10min. If proteins of interest were meant to be visualised by immunostaining, cells were

[1]Optical density at 600nm

blocked with 1% BSA diluted in 0.3% Triton-X. Otherwise, cells were washed in PBS, stained with light-sensitive 6-diamidino-2-phenylindole (DAPI, 1:1000) for 10min and mounted onto microscope slides. For immunostaining, blocked cells were incubated for 60min with 1:500 diluted primary antibody, washed three times for 5min with PBS, and stained with an Alexa Fluor® fluorescent secondary antibody, diluted 1:300, for 45min, protected from light. Subsequently, cells were incubated 10min in 1:1000 DAPI-PBS solution and three times for 5min washed with PBS. To mount coverslips onto microscope slides, coverslips were dipped into dH_2O, carefully dried and mounted using $10\mu l$ Mowiol each. Approximately 1-2 days after mounting, cover slips were sealed using nail polish and stored light-protected at 4°C.

2.3.2 Microscopy imaging and image analysis

Fluorescent microscopy was performed using a Leica DM5500 microscope equipped with a Leica HCX PL Fluotar $63x1.25$ NA oil objective. Images were taken with a Leica DFC395 FX digital camera. The microscope was equipped with an EL6000 metal halide light source and the following laser settings were used for imaging: To detect DAPI staining a laser with an excitation between 340-380nm, a 400nm beam splitter and an emission between 450-490nm was used. For GFP and Alexa Fluor®488 detection, the excitation was between 460-500nm, the beam splitter 505nm and the emission between 512-542nm. For mCherry, near-infrared fluorescent protein (iRFP) and Alexa Fluor®594 visualisation, the laser was set up with an excitation between 540-552nm, a beam splitter of 565nm and emission between 580-620nm. The white light laser excited waves between 590-620nm, had a beam splitter of 660nm and an emission of 662-738nm. For imaging, the computer software Leica LAS X v.1.1.0.12420 was used. Further image processing was done with the software FIJI (ImageJ 2.0.0-rc-68/1.52h). The images were not manually spatially calibrated, but scaled to 6.1833 pixels/micron on the basis of the image information. The unit pixel (px) was therefore used where suitable.

Focal adhesion counting

For the detection and quantification of focal adhesions (FA) using FIJI (see above), the experimental approach was modified based on the method of Horzum and co-workers (*92*). Images were initially background subtracted with a 50.0-pixel rolling ball radius and adapted in brightness. Then, the mathematical function 'Exp' was run and the plugin 'Mexican Hut Filter' applied. A region of interest (ROI) was chosen and the threshold adjusted using the 'B&W' setting with ticked 'Stack histogram'. As the upper threshold the maximum of 65535 was set, the lower limit was selected by eye, depending on the image quality. Fluorescent signals with an approximate size of $> 0.25\mu m^2$ were selected

for counting. To count the structures within the ROI, the function 'Analyze Particles...' was run.

Colocalisation analysis

Aiming to quantify the colocalisation of structures given by two stainings it was proceded as described by Vadim and Olga Zinchuk (*276*). Using FIJI, images were background subtracted and adapted in brightness before analysing the overlap with 'Coloc2'. To quantify a rough impression of colocalisation, Pearson's R value (no threshold) was used, disregarding p-values or warnings.

In a second approach, the intensities of two stains measured along a defined straight line through the cell body or along the cell surface were analysed. The images were background subtracted with a 50.0 pixel rolling sphere radius and brightness adjusted. A straight line was drawn through the area of interest and the 'Plot Profile' function was run separately for each stain. The coordinates (distance vs. intensity) were downloaded and an overlay of both intensity profiles was generated using the programming language R (version 4.0.0).

Focal adhesion size analysis

To determine the area occupied by a FA, images were background subtracted and adapted in brightness. In contrast to Chapter 2.3.2, no further mathematical processing was applied. An ROI was chosen and the threshold adjusted as described in Chapter 2.3.2. Before analysing particles, measurement settings were adapted to display the particle area. Fluorescent signals with an approximate size of > $0.25\mu m^2$ were selected for counting.

2.4 Statistical analysis

To investigate the role of LDL-cholesterol in FA formation a multi-group design with three test groups was used (TABLE 2.5). Statistical calculations and graphics were performed using the programming language R. The statistical parameters *mean* (EQUATION 2.1), *standard deviation* (SD, EQUATION 2.3), and *mean absolute deviation* (MAD, EQUATION 2.4) were used to describe the data. For the exact definition, see the formulas below, with x_1, x_2, ..., x_n being the data sample, μ the expected value and p the probability of a random variable x.

$$Mean : \overline{x} = \frac{1}{n}\sum_{i=1}^{n} x_i = \frac{x_1 + x_2 + ... + x_n}{n} \tag{2.1}$$

$$Variance : \sigma^2 = \sum_{i \geq 1} (x_i - \mu)^2 p_i \tag{2.2}$$

$$Standard\ deviation : \sigma = \sqrt{\sigma^2} = \sqrt{\sum_{i \geq 1} (x_i - \mu)^2 p_i} \tag{2.3}$$

$$Mean\ absolute\ deviation : \overline{d}_{0.5} = \frac{1}{n} \sum_{i=1}^{n} |x_i - \overline{x}| \tag{2.4}$$

TABLE 2.5: Test Groups

Group	Cell line	Characteristics
1	CHO WT	Control
2	CHO M12	NPC1 locus deletion, late endosomal LDL-cholesterol sequestration
3	CHO M12-A6ko	NPC1 locus deletion with additional AnxA6 knockout, LDL-cholesterol release

2.4.1 Statistical analysis of focal adhesion characteristics

At steady state, groups were compared using the one-way ANOVA statistical test, when analysing the effect of a treatment, two-way ANOVA was used. Statistical tests within a single experiment were corrected using the Tukey's post hoc test. However, as the focus was on identifying differences between groups, it was not corrected for multiple testing across all experiments, as small effects might have gone undetected.

2.4.2 Statistical analysis of western blot signals

Densitometric WB results were presented in bar plots, each showing data from a single experiment (n = 1). Samples were blotted as singlet or doublet, for the latter, the mean and MAD were calculated. WB results were normalised to the WB signal of a stably expressed protein in all three cell lines, such as actin or TBC1D15. All results of a tested protein were set in relation to the WT control, which corresponds to 100% (1.0). Thus, the relative values or relative means (RM) in the case of singlets or doublets, respectively, were displayed in the bar plot. For doublets, the relative normalised MAD was shown as an error bar. No statistical tests were performed on the WB densitometric data due to the small sample size.

Chapter 3

Results

Intracellular cholesterol supply is a crucial regulator of cell migration. The Grewal group recently demonstrated that cholesterol accumulation in late endosomes (LE) of Niemann-Pick type C1 (NPC1) mutant cells (CHO M12) and annexin A6 (AnxA6) overexpressing CHO cells, which are characterised by an NPC1-mutant like phenotype, inhibits cell migration and invasion (*59*, *189*). In follow-up studies, Grewal and co-workers then identified that AnxA6 depletion restored cholesterol export from LE in NPC1 mutant cells (CHO M12-A6ko) (*155*). It has therefore been speculated that cholesterol pools released from LE in AnxA6-depleted CHO M12 cells could be delivered to the cell surface and support the formation and functioning of cholesterol-enriched and specialised structures (focal adhesions, FA) required to promote cell migration. Therefore, to gain insight into the regulatory circuits linking the uptake, transport and metabolism of LDL-derived cholesterol with the machinery driving migratory cell behaviour in the above-mentioned CHO cell models (CHO WT, M12 and M12-A6ko), the relative protein levels of cholesterol-modifying enzymes were compared, the number, location and size of FA were analysed using immunofluorescence-labelled FA markers, and the distribution and colocalisation of FA components were assessed in the CHO WT, M12 and M12-A6ko cell lines.

3.1 Characterisation of proteins involved in cholesterol homeostasis and focal adhesion assembly in CHO cells lacking NPC1 only or both NPC1 and AnxA6

The relative protein levels of cholesterol-modifying enzymes and FA signalling molecules were analysed to confirm the expression or depletion of the proteins in the cell lines and to get an impression of the differential protein levels between the cell lines. Based on densitometric analysis, results were marked as increased if they were more than 1.5 times the western blot (WB) signal of the WT control and as decreased if they were less than

0.75 times the WB signal of the WT control. The bar plots show the result of single experiments (n = 1).

3.1.1 Comparison of lipoprotein receptors, regulatory endocytic proteins and enzymes involved in cholesterol homeostasis

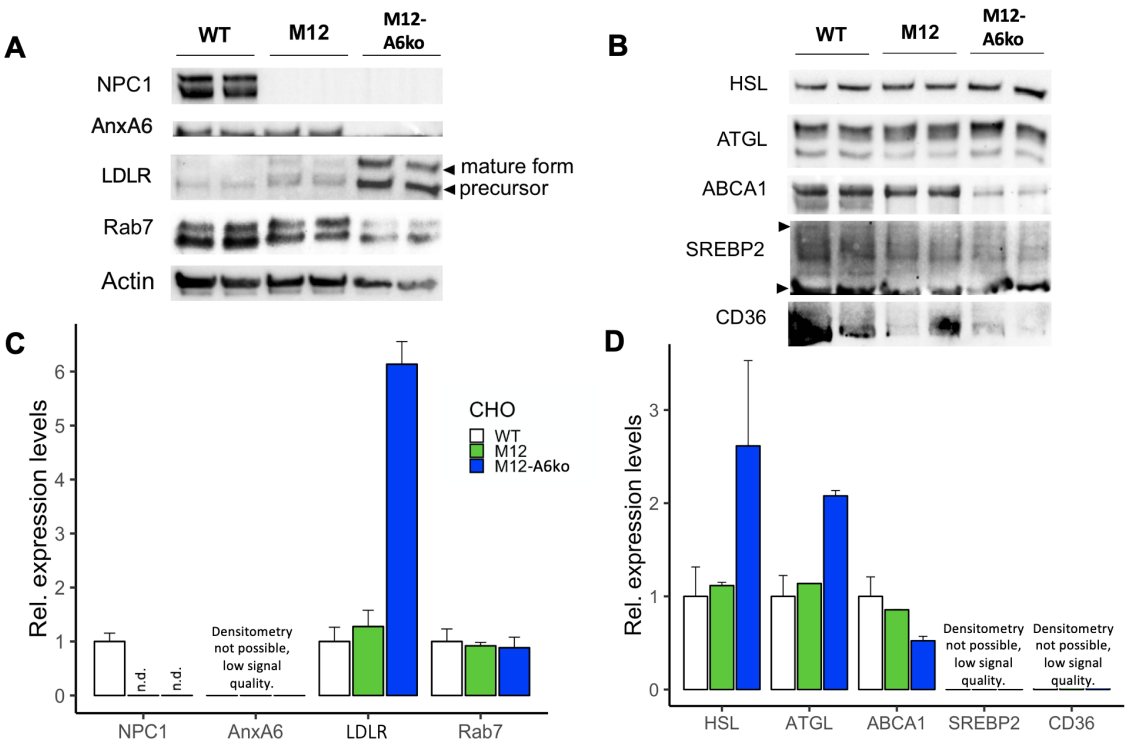

FIGURE 3.1: **Western blot analysis of proteins involved in cholesterol homeostasis and focal adhesion assembly in CHO WT, M12 and M12-A6ko.** (A-B) Cell lysates from CHO WT, CHO M12 and CHO M12-A6ko grown in 10% FBS containing media were prepared and analysed by western blotting (WB) as described in Methods (Chapter 2.2.2). The left panels show the WB analysis of Niemann-Pick type C1 (NPC1), annexin A6 (AnxA6), low density lipoprotein receptor (LDLR), Rab7 and β-actin (actin). The right panels show WB signals obtained for hormone-sensitive lipase (HSL), adipose triglyceride lipase (ATGL), ABC transporter A1 (ABCA1), sterol regulatory element-binding protein 2 (SREBP2) and CD36. Arrowheads indicate the mature form and precursor of LDLR and the premature (upper) and mature (lower) form of SREBP2, respectively. (C-D) The protein levels were quantified using ImageJ and normalised to the β-actin signal (n.d.: not detected). Results of a tested protein were set in relation to the WT signal, which corresponds to 100% (1.0). The relative mean (RM) of doublets and the relative mean absolute deviation (MAD) are given.

Initially the expression patterns of lipoprotein receptors, regulatory endocytic proteins, and enzymes involved in cholesterol homeostasis were compared using WB. Whole cell lysates from WT, M12 and M12-A6ko cells grown in full serum (10% FBS) were prepared and duplicates of the same sample from each cell line were separated by SDS-PAGE

electrophoresis, followed by transfer onto PVDF membranes. Then membranes were immunoblotted for NPC1, AnxA6, LDLR, Rab7, HSL, ATGL, ABCA1, SREBP2 and CD36 (FIGURE 3.1A-B). All WB signals were quantified using ImageJ and normalised to the β-actin signal (FIGURE 3.1C-D).

The WB analysis confirmed the lack of NPC1 expression in CHO M12 and M12-A6ko cells and the AnxA6 knockout in CHO M12-A6ko cells. LDLR protein levels, which often appear as a mature and precursor form in WB, were highly elevated in M12-A6ko cells (relative mean (RM) = 6.14), this might indicate AnxA6 affecting the feedback loop that controls LDLR expression. The relative protein levels of Rab7, a GTPase in LE, were comparable in all three cell lines. To examine whether cholesterol exit from LE by AnxA6 depletion might impact on enzymes capable of hydrolysing cholesteryl esters in lipid droplets, the protein levels of HSL and ATGL were determined. HSL and ATGL quantities were increased in AnxA6-depleted CHO M12 cells (HSL: RM = 2.62, ATGL: RM = 2.08). This could indicate that an increased ability of M12-A6ko cells to store cholesteryl esters may alter HSL and ATGL levels and function. Furthermore, the protein level of the ABCA1 transporter was reduced in CHO M12-A6ko (RM = 0.52) compared to CHO WT cells. The WB signalling quality of SREBP2 and CD36 was unsuitable for densitometric analysis, but both appear to be expressed in all three cell lines.

Taken together, AnxA6 depletion in NPC1 mutant cells could be associated with significant changes in the protein levels of lipoprotein and cholesterol transporters (LDLR, ABCA1), and lipid storage-modifying enzymes (HSL, ATGL), which might lead to changes in cholesterol homeostasis and cholesterol-dependent cellular functions.

3.1.2 Comparison of expression patterns in serum-stimulated CHO WT, M12 and M12-A6ko cells

Based on the hypothesis that LDL-cholesterol transport to the cell surface can stimulate cell migration, protein levels were next compared upon activation with 20% FBS, a common stimulus to promote cell migration (*265*). Therefore, cells were starved in serum-depleted media overnight, followed by an incubation with or without 20% FBS for 45min. Then duplicates of cell lysates were prepared, separated by SDS-PAGE and the protein levels of NPC1, AnxA6, Rab7, light chain 3 (LC3), TBC1D15 and LDLR, all with roles in LDL endocytosis and cholesterol transport (see Chapter 1), were analysed by WB (FIGURE 3.2).

NPC1 levels of WT control and 20% FBS-treated samples were comparable. The relative protein level of AnxA6 appeared to decrease in FBS-treated WT (RM = 0.66) and

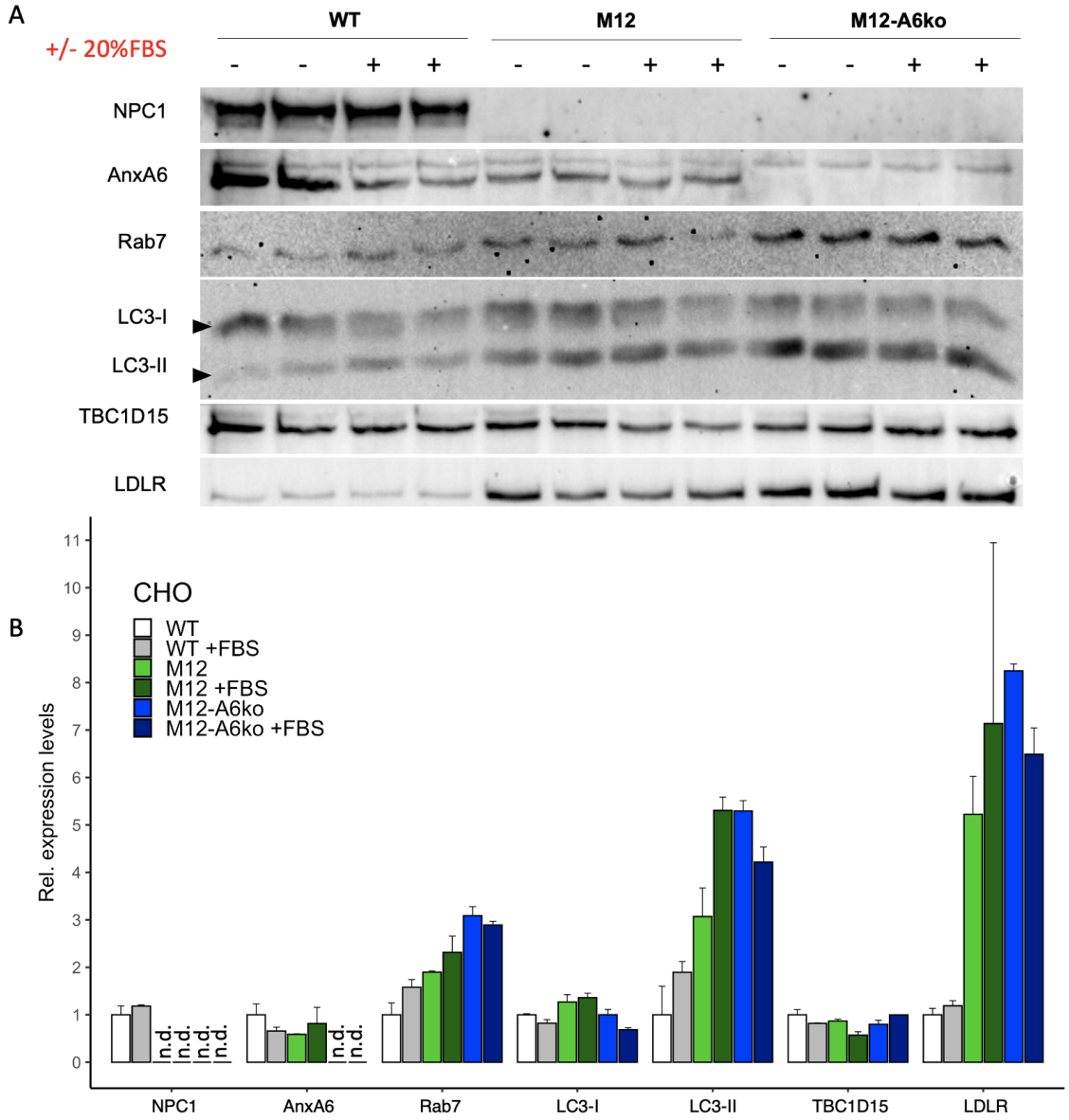

FIGURE 3.2: **Western blot analysis of proteins involved in cholesterol homeostasis and focal adhesion assembly in serum-stimulated CHO WT, M12 and M12-A6ko cells.** (A) Cell lysates from CHO WT, CHO M12 and CHO M12-A6ko were starved in serum-free media overnight, and incubated with 20% FBS for 45min. Duplicate samples were prepared and analysed by western blotting (WB) as described in Methods (Chapter 2.2.2). Shown are the protein levels of Niemann-Pick type C1 (NPC1), annexin A6 (AnxA6), Rab7, light chain 3 (LC3)-I (upper), LC3-II (lower), Tre-2/Bub2/Cdc16 1 domain family member 15 (TBC1D15), and low density lipoprotein receptor (LDLR) as indicated. (B) The relative expression levels were quantified using ImageJ (n.d.: not detected). The WB signals of NPC1, AnxA6, Rab7, LC3-I/II, and LDLR were normalised to TBC1D15. Results of a tested protein were set in relation to the WT signal, which corresponds to 100% (1.0). The relative mean (RM) of doublets and the relative mean absolute deviation (MAD) are given.

also in M12 control cells (RM = 0.59). The CRISPR/Cas-generated AnxA6 knockdown in M12-A6ko cells was also not affected after serum activation. The minor increase

displayed for FBS-treated M12 cells is due to a decrease in TBC1D15, to which the signal was normalised. M12-A6ko cells showed highest Rab7 protein levels in the presence or absence of serum (control: RM = 3.09, treated: RM = 2.89). At first sight, these findings seem to contradict findings from the previous chapter, but it should be noted these experiments were performed in either full serum (FIGURE 3.1) or after overnight starvation (FIGURE 3.2), which could impact on the level of Rab7 and other proteins. In addition, TBC1D15 protein levels, a Rab7-GAP, remained relatively unchanged in the presence or absence of serum besides the drop in FBS-treated M12 cells (RM = 0.57). To address if overnight starvation impacted differently on the CHO cell lines, the protein levels of the autophagy marker LC3-I/II were also determined. Herein, LC3-I levels were relatively comparable besides the decrease in FBS-treated M12-A6ko cells (RM = 0.69), LC3-II was strongly increased in M12 (control: RM = 3.07, treated: RM = 5.30) and M12-A6ko cells (control: RM = 5.29, treated: RM = 4.21), possibly indicating intensified LC3 processing in cells lacking NPC1. LDLR expression levels were increased in M12 (control: RM = 5.22, treated: RM = 7.14) and M12-A6ko cells (control: RM = 8.25, treated: RM = 6.49), which could indicate that starvation-induced cholesterol depletion in cells carrying the NPC1 mutation, but not WT cells, may lead to a significant increase in LDLR levels. Exposure of these cells to serum for 45min, which contains large amounts of LDL-like particles, seemed not sufficient to downregulate LDLR levels in these cells.

Comparing the overall protein level profiles, a comparable pattern was recognised for Rab7, LC3-II and LDLR. In fact, overall protein levels of all three proteins were increased in M12 and M12-A6ko compared to WT cells. Serum stimulation further appeared to increase Rab7 and LC3-II in WT, the latter also in M12, but not in M12-A6ko cells. Based on these findings, a possible role for AnxA6 in mediating the cell response to an activating stimulus under lipoprotein starvation could be suspected.

3.1.3 Western blot analysis of signalling proteins mediating cell adhesion and migration

To study the role of LDL-cholesterol on FA assembly, the activation status of FAK, Src and p130Cas was monitored, as judged by the phosphorylation of FAK (pY861, pY397), Src (pY416), and p130Cas (pY410). Cell lysates from CHO WT, CHO M12 and CHO M12-A6ko grown in serum-containing media were prepared and duplicates of the same sample were analysed by WB as described (Chapter 2.2.2). Signals were quantified as described above (Chapter 3.1.1).

Strikingly, all three cell lines expressed substantial amounts of FAK and Src kinase (see total FAK and total Src in FIGURE 3.3A and C), yet, pY861 FAK (M12: RM =

0.12, M12-A6ko: RM = 0.26) and pY416 Src (M12: RM = 0.39, M12-A6ko: RM = 0.15) phosphorylation were almost completely abolished in M12 and M12-A6ko cells, indicating that FAK and Src activation could be severely compromised in cells lacking NPC1. On the other hand, pY397 FAK phosphorylation was detectable in all three cell lines, suggesting that FAK autophosphorylation can occur, even in the absence of NPC1 and AnxA6. In line with compromised FAK and Src activation in M12 and M12-A6ko cells, p130Cas phosphorylation was reduced in these cell lines (M12: RM = 0.72, M12-A6ko: RM = 0.57).

Taken together, loss of NPC1-dependent LDL-cholesterol export routes could interfere with the activation status of key signalling proteins of the cellular migration machinery. Despite the ability of AnxA6 depletion to restore cholesterol export from NPC1 mutant cells, the presence of these AnxA6-dependent alternative cholesterol transport routes do not appear to reinstate basal levels of FAK and Src activity.

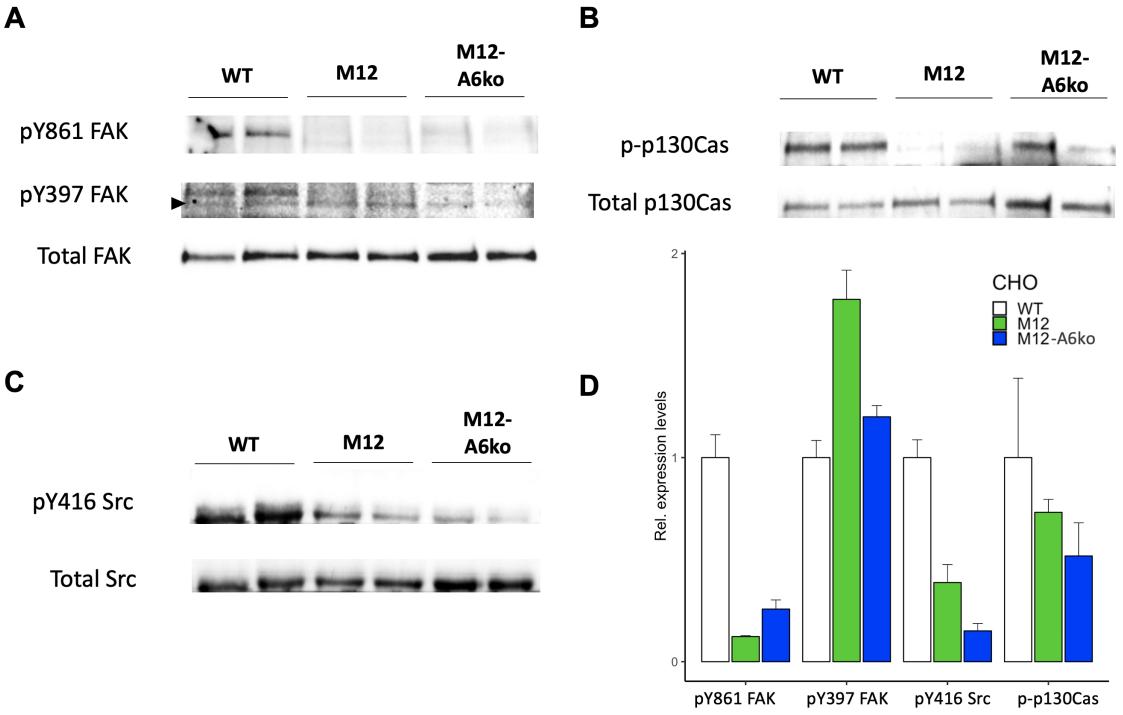

FIGURE 3.3: **Western blot analysis of signalling proteins mediating cell adhesion and migration in CHO WT, M12 and M12-A6ko cells.** (A-C) Cell lysates from CHO WT, CHO M12 and CHO M12-A6ko grown in full serum (10% FBS) containing media were prepared and analysed by western blotting (WB) for phosphorylated and total focal adhesion kinase (pY861 FAK, pY397 FAK) in (A), phosphorylated and total p130Cas in (B) and phosphorylated (pY416 Src) and total Src in (C) as described in Methods (Chapter 2.2.2). (D) The relative protein levels were quantified using ImageJ and normalised to the corresponding total protein signal. Results of a tested protein were set in relation to the WT signal, which corresponds to 100% (1.0). The relative mean (RM) of doublets and the relative mean absolute deviation (MAD) are given.

3.1.4 Serum-stimulated activation of FAK and Src kinase in NPC1 mutant cells

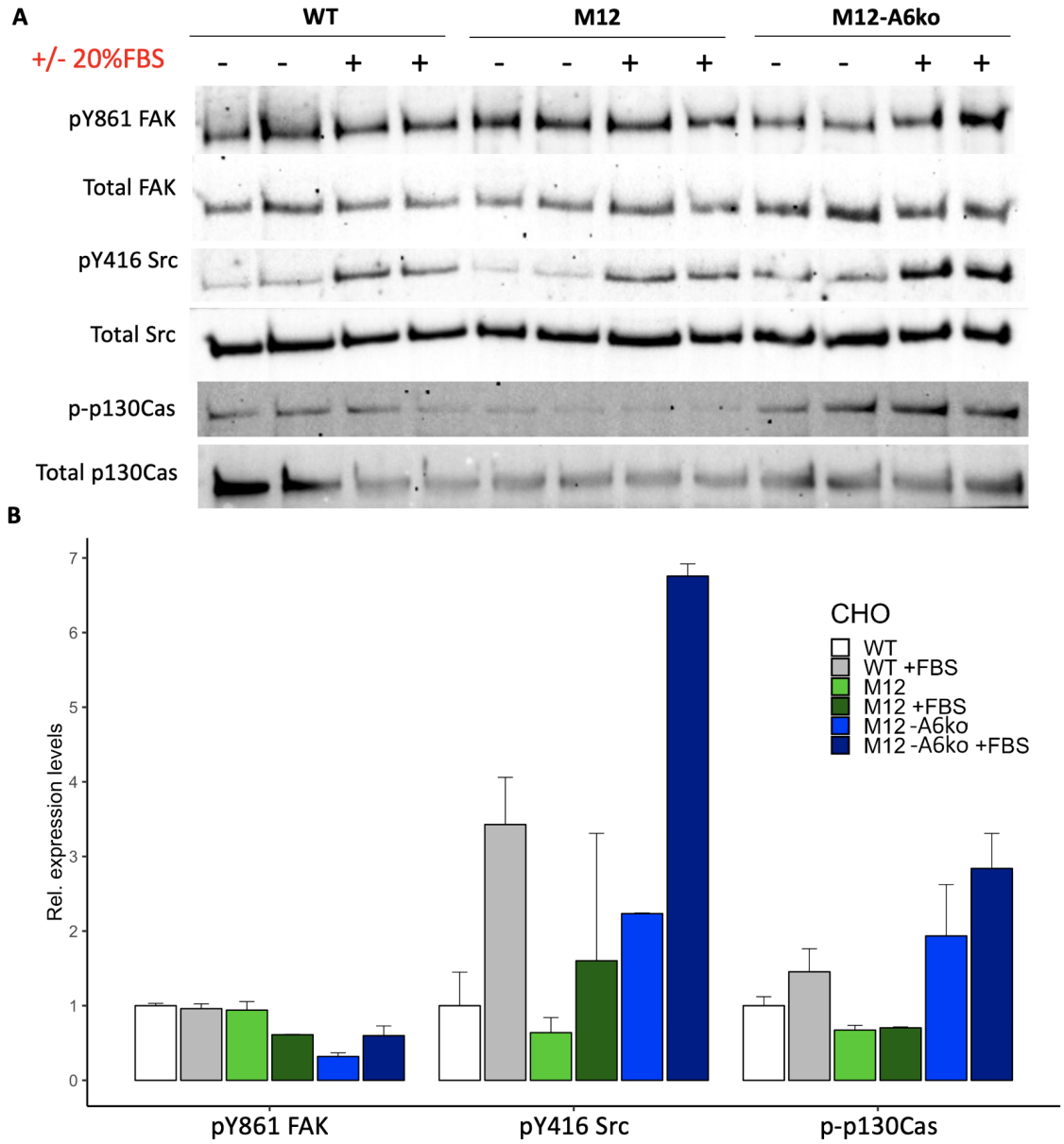

FIGURE 3.4: **Western blot analysis of FAK and Src kinase activation in serum-stimulated CHO WT, M12 and M12-A6ko cells.** CHO WT, CHO M12 and CHO M12-A6ko were starved in serum-free media overnight, and incubated with or without 20% FBS for 45min. Cell lysates from duplicate samples were prepared and analysed by western blotting (WB) (described in Chapter 2.2.2) for pY861 focal adhesion kinase (FAK), total FAK, pY416 Src, total Src, p-p130Cas and total p130Cas. (B) The relative protein levels were quantified using ImageJ and were normalised to the corresponding total protein signal. Results of a tested protein were set in relation to the WT signal, which corresponds to 100% (1.0). The relative mean (RM) of doublets and the relative mean absolute deviation (MAD) are given.

The strongly reduced phosphorylation of FAK, Src kinase and p130Cas at steady-state in NPC1 mutant M12 and AnxA6-depleted M12 cells (FIGURE 3.3) may indicate a role for late endosomal cholesterol in signalling events required for FA formation. To assess the ability of cells lacking NPC1 and/or AnxA6 to activate FAK and Src kinase, CHO WT, M12 and M12-A6ko were serum-starved overnight, and then stimulated with or without 20% FBS for 45min (FIGURE 3.4). Duplicates of the same sample for each condition were prepared and analysed by WB for phosphorylated and total FAK, Src and p130Cas as described above (FIGURE 3.3).

Alike under steady-state conditions (FIGURE 3.3), serum starvation and/or activation upon incubation with 20% serum for 45min did not alter total FAK and Src protein levels in any of the three cell lines. PY861 FAK activation was apparent in all three cell lines with and without serum activation, this could indicate that overnight serum starvation, which also reduces cellular cholesterol levels, may already lead to FAK activation, even in cells lacking NPC1 and/or AnxA6. On the other hand, pY416 Src phosphorylation was stimulated upon serum stimulation in all three cell lines, in particular in the M12-A6ko cell line (WT: control: RM = 1.0, treated: RM = 3.42; M12: control: RM = 0.64, treated: RM = 1.60; M12-A6ko: control: RM = 2.23, treated: RM = 6.76). These findings could suggest that all regulatory mechanisms that are required to activate Src kinase are still in place in M12 and M12-A6ko cells. Although the WB analysis of this experiment showed downregulated total and p-p130Cas levels in samples run in the centre of the gel, these results should not be overinterpreted as this could be due to limiting amounts of primary or secondary antibodies in this experiment.

Taken together, serum starvation appears to induce FAK activation independently of NPC1 and AnxA6 expression. Moreover, Src activation upon serum stimulation was evident in CHO WT, M12 and M12-A6ko, this could indicate that compromised cholesterol transport in NPC1 mutants or restoration of cholesterol homeostasis in AnxA6-depleted M12 cells may not alter the cell's capacity to upregulate Src kinase activity.

3.1.5 Expression of late endosomal proteins in migrating cells

To investigate relative protein levels of endosomal proteins involved in cholesterol homeostasis during migration, a dual stimulus of 20% FBS and multiple scratching through the cell layer was used. The multiscratch assays were performed as described in the literature (*59*, *234*), thereby enabling the preparation of protein lysates enriched within migrating cells. Therefore, CHO WT, M12 and M12-A6ko were starved in serum-free media overnight, activated for 30min with or without 20% FBS and then five longitudinal scratches per 6-well were performed. Cell lysates were prepared and WB analysis and

immunoblotting of NPC1, AnxA6, Rab7, LC3, TBC1D15, and LDLR (FIGURE 3.5) was performed as described above (Chapter 2.2.2).

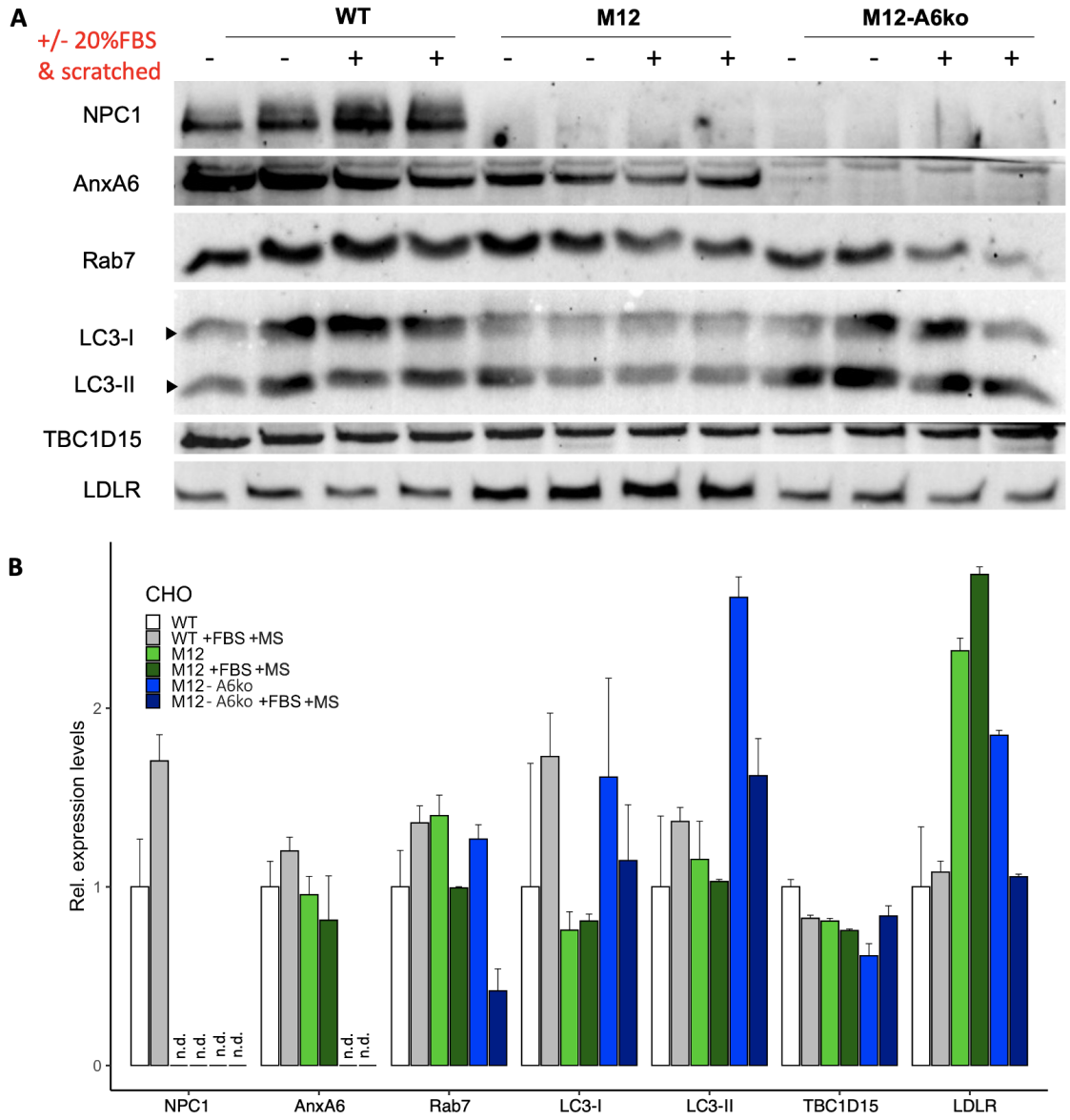

FIGURE 3.5: **Western blot analysis of late endosomal proteins in migrating CHO WT, M12 and M12-A6ko cells.** (A) CHO WT, CHO M12 and CHO M12-A6ko were starved in serum-free media overnight, scratched and incubated with 20% FBS for 30min. Multiple (5x) scratches per well were performed as described in the literature (*59*, *234*). Lysates were prepared and analysed by western blotting (WB) as described in Methods (Chapter 2.2.2) for Niemann-Pick type C1 (NPC1), annexin A6 (AnxA6), Rab7, light chain 3 (LC3)-I (upper), LC3-II (lower), Tre-2/Bub2/Cdc16 1 domain family member 15 (TBC1D15), and low density lipoprotein receptor (LDLR). (B) The relative protein levels were quantified using ImageJ (n.d.: not detected). The WB signals of NPC1, AnxA6, Rab7, LC3 I/II, and LDLR were normalised to TBC1D15. Results of a tested protein were set in relation to the WT signal, which corresponds to 100% (1.0). The relative mean (RM) of doublets and the relative mean absolute deviation (MAD) are given.

As expected, NPC1 was detectable in WT, but not in M12 and M12-A6ko cells, and

slightly increased in serum-stimulated migrating cells (RM = 1.70). AnxA6 expression was unaffected by dual stimulation in WT and M12 cells. Rab7 levels were comparable in starved CHO WT, M12 (RM = 1.40) and M12-A6ko (RM = 1.27) cells (controls), but upon dual stimulation decreased by approximately 30% and 66% in CHO M12 and M12-A6ko, respectively. TBC1D15 protein levels were similar in all three cell lines except for a decrease in the CHO M12-A6ko control (RM = 0.61), which was not seen in stimulated M12-A6ko cells. LC3-I/II were comparable in starved WT and M12 cells (LC3-I: M12 control: RM = 0.76, LC3-II: M12 control: RM = 1.15) though increased in CHO M12-A6ko cells (LC3-I: M12-A6ko control: RM = 1.61, LC3-II: M12-A6ko control: RM = 2.62). With dual activation, LC3-I levels increased in WT (RM = 1.73), remained unaffected in M12 cells, and decreased in M12-A6ko cells by about 30%. LC3-II levels were unchanged in WT and M12 cells, but also decreased in M12-A6ko cells by aproximately 40% upon stimulation. However, the blot appeared to be subject to technical artefacts, so that conclusions should only be drawn with caution. LDLR levels were elevated in M12 cells (control: RM = 2.32), while in M12-A6ko cells (control: RM = 1.85), the increase was less pronounced. The dual stimulus was associated with a 43% reduction in LDLR in M12-A6ko cells, while there was no effect in WT or M12 cells.

In summary, the dual migratory stimulus did not significantly alter the expression of LDLR and the Rab7/TBC1D15/AnxA6 complex in WT and M12 cells. However, the reduction of Rab7 and LDLR in M12-A6ko cells requires confirmation. Similarly, the increase in autophagy markers LC3-I/II in M12-A6ko cells needs to be confirmed before any conclusions can be drawn.

3.1.6 Src and FAK activation in migrating NPC1 mutant cells

The activation of Src and FAK kinases was then analysed in lysates from multiscratched and serum-stimulated CHO WT, M12 and M12-A6ko cells (Figure 3.6). As described above, cells were plated in 6-wells, starved in serum-free media overnight, and then activated with 20% FBS for 30min after performing five longitudinal scratches per 6-well. Lysates were prepared and WB analysis was performed as described earlier.

For better comparison of the activation status of Src and FAK kinases in the three cell lines treated with either the double stimulus or control, SDS-PAGE of control samples (Figure 3.6A) and stimulated samples was performed separately (Figure 3.6B). Shown are duplicates of the same sample. In the controls, the relative levels of pY861 FAK (M12: RM = 0.61, M12-A6ko: RM = 0.52) and pY416 Src (M12: RM = 0.73, M12-A6ko: RM = 0.70) were decreased in CHO M12 and M12-A6ko cells compared to WT (Figure 3.6A).

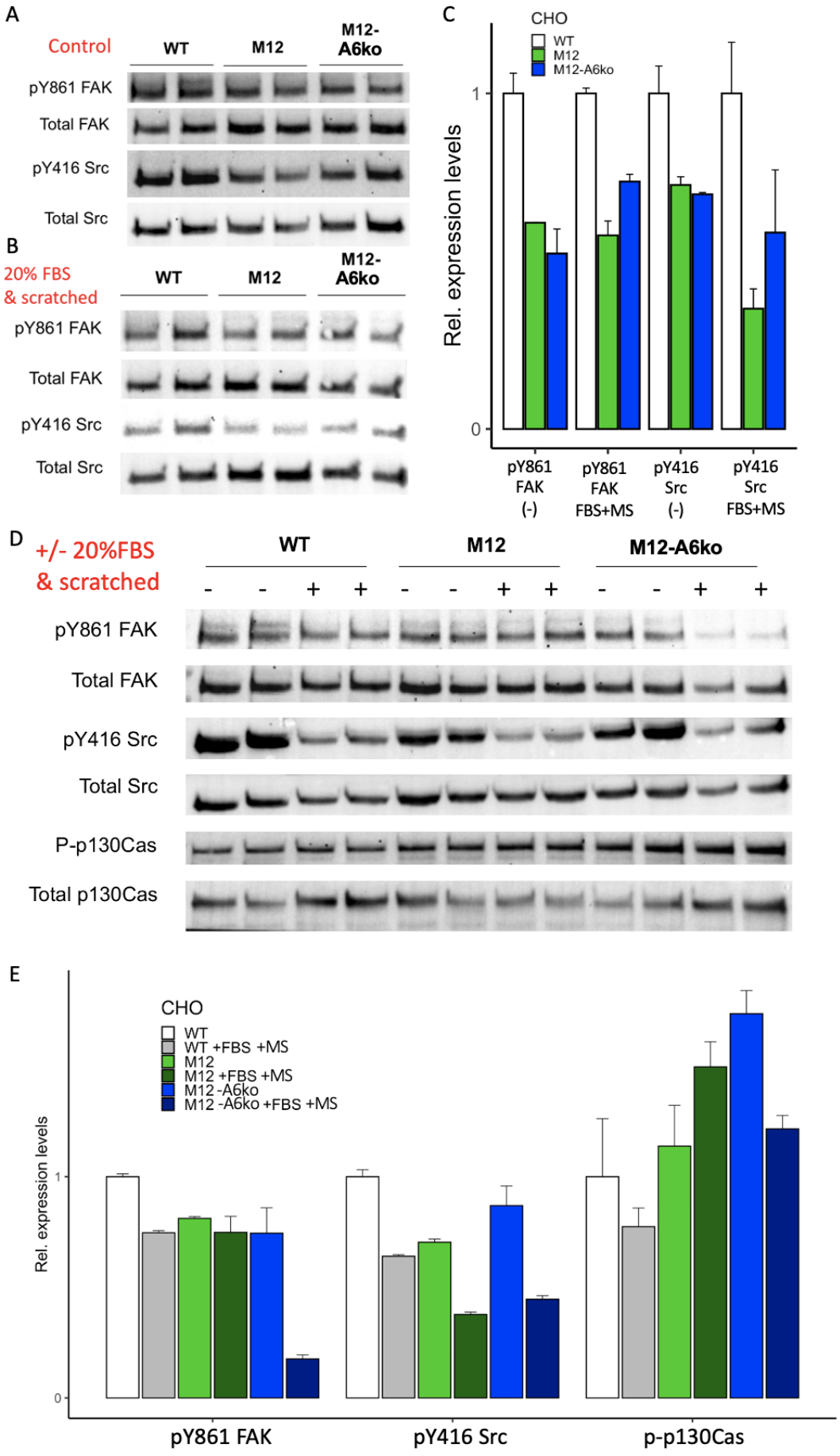
A
Control
WT
M12
M12-A6ko
pY861 FAK
Total FAK
pY416 Src
Total Src
B
20% FBS & scratched
WT
M12
M12-A6ko
pY861 FAK
Total FAK
pY416 Src
Total Src
C
CHO
WT
M12
M12-A6ko
Rel. expression levels
1
0
pY861 FAK (-)
pY861 FAK FBS+MS
pY416 Src (-)
pY416 Src FBS+MS
D
+/- 20%FBS & scratched
WT
M12
M12-A6ko
- - + + - - + + - - + +
pY861 FAK
Total FAK
pY416 Src
Total Src
P-p130Cas
Total p130Cas
E
CHO
WT
WT +FBS +MS
M12
M12 +FBS +MS
M12 -A6ko
M12 -A6ko +FBS +MS
Rel. expression levels
1
0
pY861 FAK
pY416 Src
p-p130Cas

FIGURE 3.6: **Western blot analysis of Src and FAK activation in serum-stimulated and multi-scratched CHO WT, M12 and M12-A6ko cells.** CHO WT, CHO M12 and CHO M12-A6ko were starved in serum-free media overnight, scratched (>5/well) and subsequently incubated with or without 20% FBS for 30min. Lysates were prepared and analysed by western blotting (WB) as described in Methods (Chapter 2.2.2). Panel (A) shows pY861 focal adhesion kinase (FAK), total FAK, pY416 Src, and total Src that were starved overnight but not stimulated by 20% FBS nor scratched. Panel (B) shows pY861 FAK, total FAK, pY416 Src, and total Src that were starved overnight, serum-activated (20% FBS) and scratched (>5). (C) The relative protein levels of signals displayed in (A-B) were quantified using ImageJ and were normalised to the corresponding total protein signal. The mean relative expression of duplicate samples and mean absolute deviation (MAD) is given. Panel (D) shows pY861 FAK, total FAK, pY416 Src, total Src, p-p130Cas, and total p130Cas of the same experiment. The presence or absence of serum is indicated. (E) The relative protein levels of signals displayed in (D) were quantified using ImageJ and were normalised to the corresponding total protein signal. The mean relative expression of duplicate samples of the same experiment and MAD are given.

Likewise, in double stimulated CHO M12 and M12-A6ko cells, pY861 FAK (M12: RM = 0.58, M12-A6ko: RM = 0.74) and pY416 Src (M12: RM = 0.36, M12-A6ko: RM = 0.59) levels dropped.

To analyse the effect of the migration stimulus within the cell lines, a second loading order was chosen (FIGURE 3.6D). Herein, upon double treatment, pY861 FAK levels decreased in CHO WT and M12-A6ko cells by 25% and 76%, respectively, but remained unchanged in M12 cells. This could indicate defects in FAK signalling in CHO-M12 cells when cholesterol accumulates in LE and reduces cholesterol levels at the PM, which may impair FAK regulation. In addition, restoration of cholesterol homeostasis in M12-A6ko cells correlated with drastically altered FAK activation patterns. PY416 Src levels decreased in double stimulated samples for all cell lines by 36-49%. These patterns also were seen in scratched CHO cells upon serum stimulation (FIGURE A.6E). The relative p-p130Cas levels were comparable in untreated and treated WT (control: RM = 1.0, treated: RM = 0.77) and M12 (control: RM = 1.14, treated: RM = 1.496) cells. In untreated M12-A6ko cells, p-p130Cas levels increased (RM = 1.74), which did not correlate with the dynamics seen for phosphorylated Src and FAK, though alike the latters, p-p130Cas levels decreased upon dual stimulation by 30%.

Taken together, despite the major defects in cholesterol distribution in NPC1 mutant cells, this does not seem to lead to a complete loss of Src, FAK and p130Cas phosphorylation, suggesting that the regulatory mechanisms governing the activity of these kinases in cell migration are still functional. However, further confirmation is required to suggest comparable dynamics in WT and M12-A6ko cells after dual stimulation, especially for pY861 FAK and p-p130Cas.

3.1.7 Expression of late endosomal proteins in cells after incubation with lipoprotein-deficient, cholesterol-depleted media

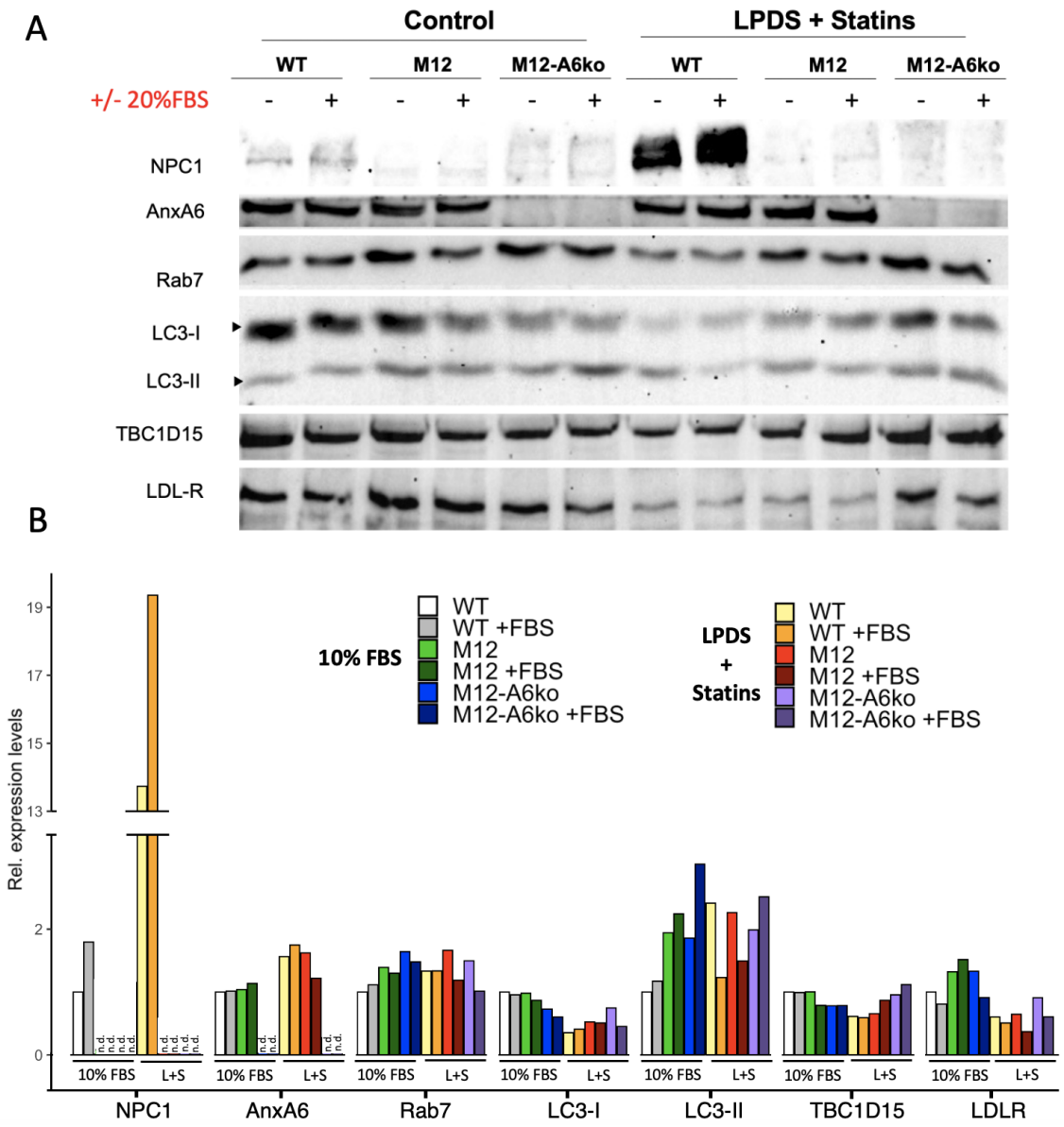

FIGURE 3.7: **Western blot analysis of late endosomal proteins in CHO WT, M12 and M12-A6ko cells after incubation with LPDS-statin media.** (A) Cell lysates from CHO WT, CHO M12 and CHO M12-A6ko grown in 10% FBS containing media were incubated in 10%-LPDS-5mg/ml-mevastatin media (Appendix B.25) or were left in growth media (10% FBS) for 48h. Then, cells were starved in serum-free media for 2h and activated by 20% FBS for 30min. Subsequently, samples were analysed by western blotting (WB) as described in Methods (Chapter 2.2.2). Shown are the protein levels of Niemann-Pick type C1 (NPC1), annexin A6 (AnxA6), Rab7, light chain 3 (LC3)-I (upper), LC3-II (lower), Tre-2/Bub2/Cdc16 1 domain family member 15 (TBC1D15), and low density lipoprotein receptor (LDLR). (B) The relative expression levels were quantified using ImageJ (n.d.: not detected). The WB signals of NPC1, AnxA6, Rab7, LC3-I/II, and LDLR were normalised to TBC1D15. Results of a tested protein were set in relation to the WT signal, which corresponds to 100% (1.0). The relative value of a singlet is displayed.

Comparing protein levels of enzymes that are involved in cholesterol trafficking in CHO WT, M12 and M12-A6ko cells that were triggered to migrate, differences in the cell response have been determined. To further differentiate the role of LDL-cholesterol on these findings, the following experiments were performed under lipoprotein-deficient, cholesterol-depleted conditions. CHO WT, M12 and M12-A6ko cells were incubated in a media containing 10% LPDS and 5mg/ml mevastatin or were left in growth media (10% FBS) for 48h. Then, cells were starved in serum-free media for 2h and activated by 20% FBS for 30min. The relative expression level of NPC1, AnxA6, Rab7, LC3-I/II, TBC1D15 and LDLR were determined as described earlier.

NPC1 protein levels were strongly increased in delipidated CHO WT (control: relative value (RV) = 13.74, treated: RV = 19.35). However, the difference in intensity between control and delipidated samples should not be over-interpreted, as controlling for the hyperintensity in delipidated CHO cells may let the control signal appear falsely weak. AnxA6 protein levels were slightly increased in WT samples (control: RV = 1.56, treated: RV = 1.75) and M12 control (RV = 1.62) incubated in LPDS-statin media. Relative protein levels of Rab7 increased in AnxA6-depleted CHO M12 cells that were grown in regular growth media (M12-A6ko control: RV = 1.64) which matches findings from Chapter 3.1.2. Serum stimulation had no effect on Rab7 levels grown in 10% FBS. On delipidating media, Rab7 levels of starved M12 and M12-A6ko cells were comparable to that of WT cells, and decreased in both NPC1 mutants by 30-40% upon serum stimulation. LC3-I, which is converted to LC3-II in the context of autophagy, decreased in M12-A6ko control (RV = 0.35). In contrast, LC3-II increased in both NPC1 mutants, thereby indicating an elevated conversion rate of LC3-I to LC3-II. In delipidated samples, LC3-I levels dropped in WT and M12 (WT control: RV = 0.35, M12 control: RV = 0.53), whereas LC3-II was overall increased. The relative protein levels of TBC1D15, were comparable across samples incubated in growth media but decreased in delipidated CHO WT and M12 (WT control: RV = 0.61, M12 control: RV = 0.66). The unexpected decrease of LDLR in WT (control RV = 0.60, treated RV = 0.51) and M12 (control RV = 0.65, treated RV = 0.37) that were grown on delipidated media might be the consequence of insufficient antibody.

3.1.8 Src and FAK activation after incubation with lipoprotein-deficient, cholesterol-depleted media

To analyse the effect of lipoprotein and cholesterol deficiency on the activation of FAK, Src and the downstream target p130Cas, CHO WT, M12 and M12-A6ko were incubated in a lipoprotein-deficient, cholesterol-depleted media containing 10% LPDS and 5mg/ml mevastatin or were left in growth media (10% FBS) for 48h. Then, cells were starved in

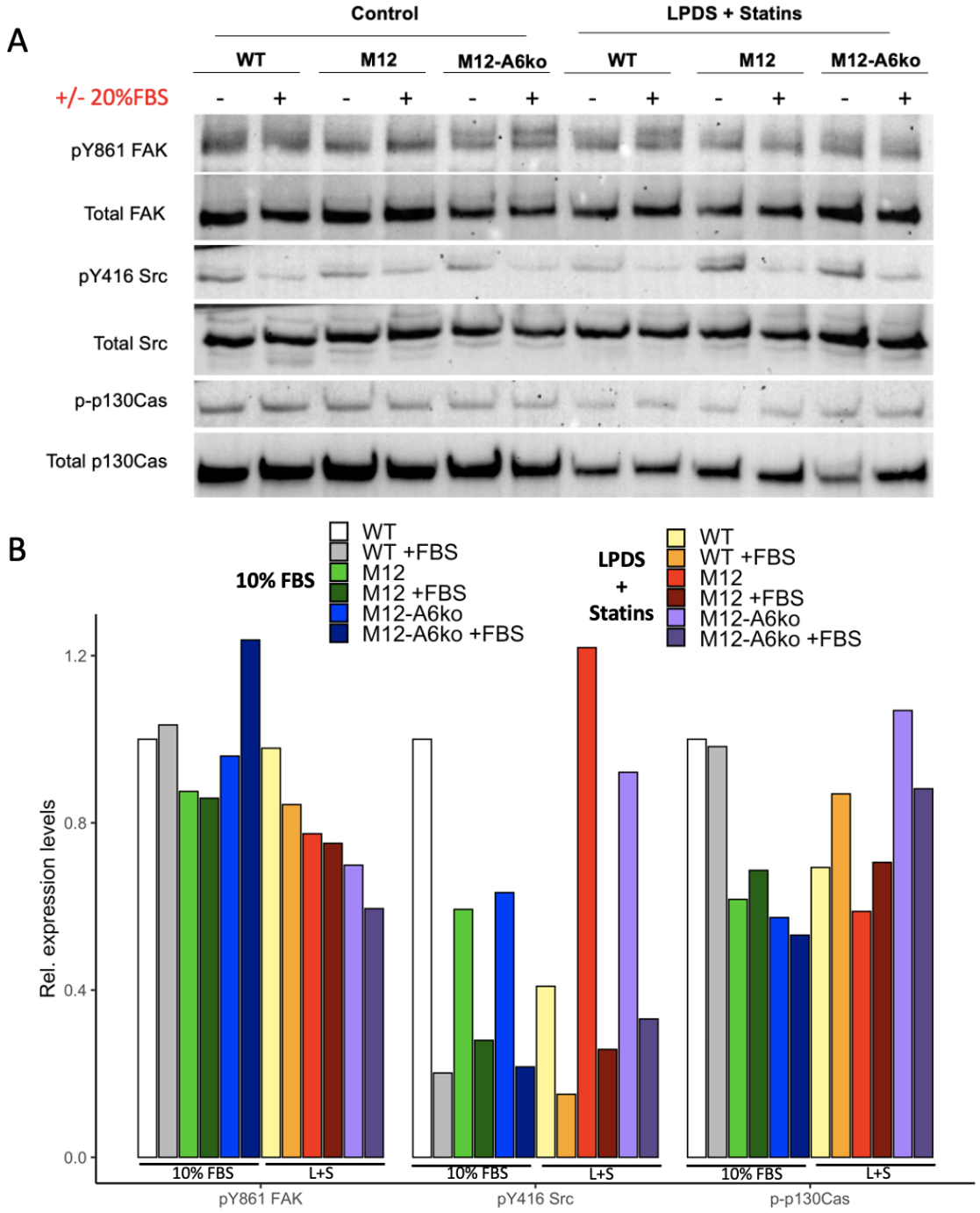

FIGURE 3.8: **Western blot analysis of Src and FAK activation in CHO WT, M12 and M12-A6ko cells after incubation with LPDS-statin media.** (A) Cell lysates from CHO WT, CHO M12 and CHO M12-A6ko grown in 10% FBS containing media were incubated in 10%-LPDS-5mg/ml-mevastatin media (Appendix B.25) or were left in growth media (10% FBS) for 48h. Then, cells were starved in serum-free media for 2h and activated by 20% FBS for 30min. Subsequently, samples were analysed by western blotting (WB) as described in Methods (Chapter 2.2.2). Shown are the relative protein levels of pY861 focal adhesion kinase (FAK), total FAK, pY416 Src, total Src, p-p130Cas, and p130Cas. (B) The relative protein levels of signals displayed in (A) were quantified using ImageJ and were normalised to the corresponding total protein signal. Results of a tested protein were set in relation to the WT signal, which corresponds to 100% (1.0). The relative value of a singlet is displayed.

serum-free media for 2h and activated by 20% FBS for 30min. The relative protein levels of pY861 FAK, pY416 Src, and p-p130Cas were determined by WB as described earlier.

In 10% FBS-incubated samples, Y861 FAK levels were comparable across all cell lines. In LPDS-statin-grown cells, the phosphorylated FAK portion decreased in M12-A6ko (control: RV = 0.70, treated: RV = 0.59). FBS stimulation did not appear to have an effect on Y861-FAK levels in any of the constellations. The relative amount of pY416 Src in 10% FBS-grown samples decreased by approximately 40% in both NPC1 mutants (M12 control: RV = 0.59, M12-A6ko control: RV = 0.63), whereas in the LPDS-Statin group, pY416 Src dropped in WT (control: RV = 0.41) though recovered in the mutants (M12 control: RV = 1.22, M12-A6ko control: RV = 0.92). Interestingly, in all samples, cell activation with 20% FBS appeared to cause a drastic decrease in the phosphorylated Src fraction. For p130Cas, the phosphorylated portion was lowered in M12 (control: RV = 0.62, treated: RV = 0.69) and M12-A6ko (control: RV = 0.57, treated: RV = 0.53) cells when incubated in 10% FBS media. In LPDS-statin-grown samples, p-p130Cas was reduced in WT (control: RV = 0.69) and M12 (control: RV = 0.59) cells but recovered in M12-A6ko (control: RV = 1.07). No effect was seen for stimulation with 20% FBS. P130Cas is a known downstream target of pY416 Src signalling. While in cells on growth medium (10% FBS) the protein levels of both pY416 Src and p-p130Cas decreased in the NPC1 mutants, in delipidated M12 cells the dynamics of p-p130Cas did not follow the relative increase in pY416 Src. The effect of 20% FBS on pY416 Src levels was also not reflected in the p-p130Cas fraction. However, before conclusions can be drawn, the results require confirmation.

3.1.9 Expression of late endosomal proteins in serum-activated cells after incubation with LPDS-statin media

To analyse the effect of cholesterol sequestration by NPC1 loss of function and the role of additional AnxA6 knockout under cholesterol-depleted, lipoprotein-deficient conditions on the protein level of endosomal proteins, CHO WT, M12 and M12-A6ko cells were incubated in LPDS-statin media for 48h, starved for 2h in serum-free media, before half of the samples were activated with 30min 20% FBS, as it was done in Chapter 3.1.7. The WB signals of NPC1, AnxA6, Rab7, LC3-I/II, TBC1D15 and LDLR were examined as described earlier.

In CHO WT cells incubated in delipidated media, NPC1 levels were comparable in control and serum treated samples (treated: RM = 1.46). Likewise, AnxA6 levels were unchanged in WT and M12. Rab7 decreased in M12-A6ko cells by 60% (control: RM

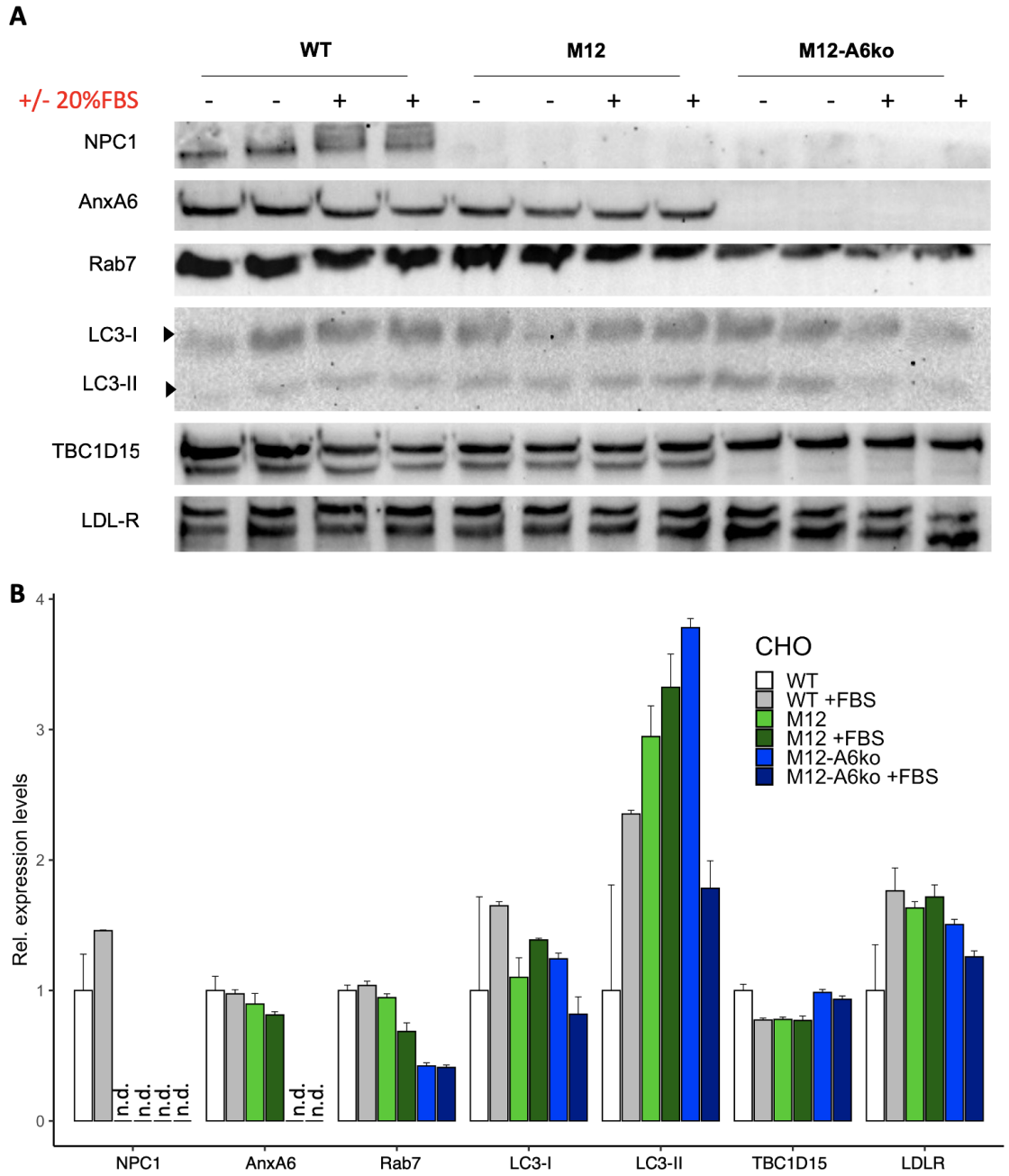

FIGURE 3.9: **Western blot analysis of late endosomal proteins in serum-activated CHO WT, M12 and M12-A6ko cells after incubation with LPDS-statin media.** (A) Cell lysates from CHO WT, CHO M12 and CHO M12-A6ko cells grown in 10% FBS containing media were incubated in 10%-LPDS-5mg/ml-mevastatin media (Appendix B.25) for 48h. Then, cells were starved in serum-free media for 2h and activated by 20% FBS for 30min. Subsequently, samples were analysed by western blotting (WB) as described in Methods (Chapter 2.2.2). Shown are the protein expression levels of Niemann-Pick Type type C1 (NPC1), annexin A6 (AnxA6), Rab7, light chain 3 (LC3)-I (upper), LC3-II (lower), Tre-2/Bub2/Cdc16 1 domain family member 15 (TBC1D15), and low density lipoprotein receptor (LDLR). (B) The relative protein levels were quantified using ImageJ (n.d.: not detected). The WB signals of NPC1, AnxA6, Rab7 LC3-I/II, and LDLR were normalised to TBC1D15. Results of a tested protein were set in relation to the WT signal, which corresponds to 100% (1.0). The relative mean (RM) of doublets and the relative mean absolute deviation (MAD) are given.

= 0.42, treated: RM = 0.41), however, the WB signal was cut and may not be suitable for densitometric analysis. LC3-I was comparable between controls of WT, M12 and M12-A6ko cells. After serum stimulation, LC3-I increased by 65% in WT and decreased by 35% in M12-A6ko cells. LC3-II strongly increased in the NPC1 mutants (M12 control: RM = 2.95, M12-A6ko: RM = 3.78). While LC3-II was raised by 135% in WT following serum stimulation, it declined in M12-A6ko by 53%. TBC1D15 levels (upper signal) were stable across all samples. The lower band in WT and M12 cells appears to be a cross-reaction with AnxA6, which has a slightly lower molecular weight and is absent in M12-A6ko cells. For LDLR, the densitometric analysis showed increased protein levels in both NPC1 mutants (M12 control: RM = 1.63, M12-A6ko control: RM = 1.51). However, the relatively low value of the WT control may be partly due to a relatively strong TBC1D15 signal to which it was normalised. Nevertheless, an increase in the autophagy marker LC3-II and the lipoprotein receptor LDLR is consistent with previous findings analysing cells starved overnight or at steady state (Figures 3.7, 3.2).

The experiment modified by cellular activation with LDL for 30 minutes gave comparable results (Figure A.3).

3.1.10 Src and FAK activation in serum-activated cells after incubation with LPDS-statin media

The experimental procedure from Chapter 3.1.9 was applied to analyse the relative phosphoprotein levels of pY861 FAK, pY416 Src, and p-p130Cas after incubation with LPDS-statin media.

For FAK and Src kinases, serum stimulation was associated with a decrease in the phosphorylated portion in WT by 48% and 56% and in M12 cells by 77% and 47%, respectively. In M12-A6ko cells, the relative level of pY861 FAK was reduced in control (RM = 0.15) and serum-treated (RM = 0.19) samples, similarly, pY416 Src levels were decreased in control (RM = 0.44) and treated (RM = 0.42) samples. Alike the drop of pY861 FAK and pY416 Src, the phosphorylated level of p130Cas, the downstream target of FAK and Src signalling, was reduced in serum-treated WT cells (RM = 0.62). Also in M12-A6ko control samples, p-p130Cas was decreased (RM = 0.54), although serum-treated samples were comparable to the WT control.

Compromised FAK and Src activation in cells lacking NPC1 had prior been seen in CHO cells in growth media or after starvation in serum-free media (Figure 3.3, 3.4, 3.6), however, incubation in delipidated media seemed to reduce especially the portion of pY861 FAK in the NPC1 mutants (vs Figure 3.4, 3.6). In M12-A6ko cells, total and phosphorylated protein levels were altered, suggesting that AnxA6 may affect FA dynamics under delipidated conditions.

The experiment altered by cellular activation with LDL for 30min provided comparable results (FIGURE A.4).

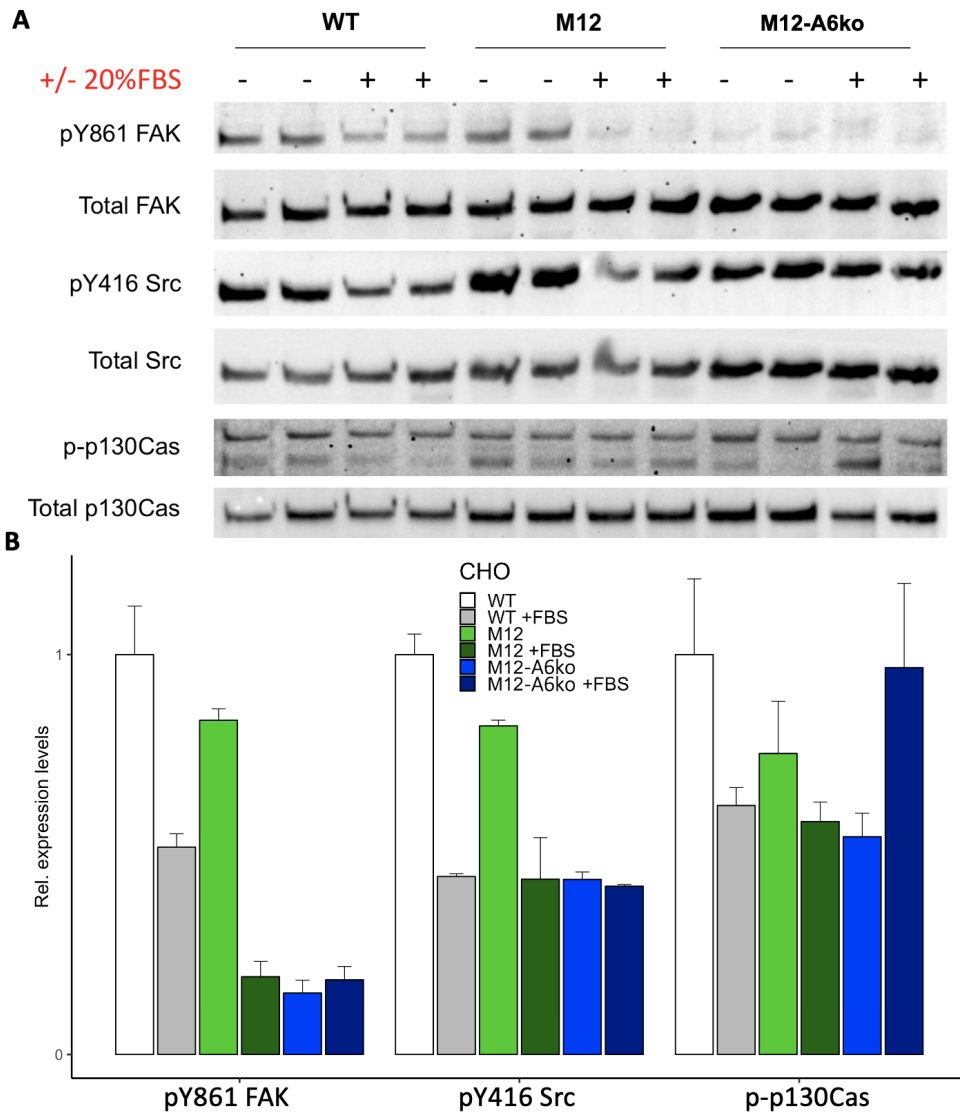

FIGURE 3.10: **Western blot analysis of Src and FAK activation in serum-activated CHO WT, M12 and M12-A6ko cells after incubation with LPDS-statin media.** (A) Cell lysates from CHO WT, CHO M12 and CHO M12-A6ko cells grown in 10% FBS containing media were incubated in 10%-LPDS-5mg/ml-mevastatin media (Appendix B.25) for 48h. Then, cells were starved in serum-free media for 2h and activated by 20% FBS for 30min. Subsequently, samples were analysed by western blotting (WB) as described in Methods (Chapter 2.2.2). Shown are the relative protein levels of pY861 focal adhesion kinase (FAK), total FAK, pY416 Src, total Src, p-p130Cas, and p130Cas. (B) The relative protein levels of signals displayed in (A) were quantified using ImageJ and were normalised to the corresponding total protein signal. Results of a tested protein were set in relation to the WT signal, which corresponds to 100% (1.0). The relative mean (RM) of doublets and the relative mean absolute deviation (MAD) are given.

3.1.11 Summary of western blot analyses

In summary, loss of NPC1-dependent LDL-cholesterol export routes seem to interfere with the activation status of key signalling proteins of the cellular migration machinery, such as FAK and Src. However, this does not lead to a complete loss of Src, FAK and p130Cas phosphorylation, despite the major defects in cholesterol distribution in NPC1 mutant cells. Consequently, the regulatory mechanisms that govern the activity of these kinases in cell migration are still functional in these cells. AnxA6 depletion in NPC1 mutant cells is associated with significant changes in the expression levels of lipoprotein, cholesterol transporters and lipid storage-modifying enzymes. Despite the ability of AnxA6 depletion to restore cholesterol export from NPC1 mutant cells, these alternative cholesterol transport routes do not seem to reinstate basal levels of FAK and Src activity.

3.2 Characterisation of focal adhesion assembly in CHO cells lacking NPC1 only or both NPC1 and AnxA6

The accumulation of cholesterol in LE of NPC1 mutants has been associated with reduced migratory behaviour (see Chapter 1.3), but the underlying mechanism how LDL-derived cholesterol from LE could stimulate cell migration remain unclear. Since AnxA6 depletion in NPC1 mutant cells restored LE-cholesterol export and abolished LDL-cholesterol sequestration, it was hypothesised that loss of AnxA6 could also restore the migratory behaviour of CHO M12 cells. FA are multiprotein complexes that anchor cells within the ECM, that are enriched with cholesterol and/or often embedded in cholesterol-rich membrane domains. These structures contain many signalling proteins, facilitating signal and transmembrane force transduction (see Chapter 1.2). It has therefore been speculated that LDL-derived cholesterol from LE could reach the cell surface to support the formation of these specialised adhesion structures. To gain initial insights into this hypothesis and to evaluate FA assembly in CHO WT, M12 and M12-A6ko cells, the total number of FA, their spatial distribution and density, the size of FA and cell size as well as the distribution of FA markers and cholesterol were analysed and compared by immunofluorescence microscopy.

3.2.1 Focal adhesion assembly in steady state and serum-stimulated CHO WT, M12 and M12-A6ko cells

To investigate differences in FA assembly in CHO cells lacking NPC1 and AnxA6, the total number of FA, their relative distribution at the PM (FA at cell edges versus cell body), and FA size and cell size were analysed using the FA marker pY861 FAK. For the examination of FA dynamics at steady state, CHO WT, M12 and M12-A6ko cells were plated at $1.5 * 10^5$ cells/well of a 6-well plate and incubated for 48h in full serum (10% FBS). In the run-up, after cell fixation, immunostaining of FA was tested using anti-FAK or anti-pY861 FAK, each in a dilution of 1:200 and 1:500, followed by secondary antibodies coupled to Alexa Fluor® 488. Immunolabelling with anti-pY861 FAK, diluted 1:500, was found to be superior to anti-FAK due to better delineation of FA and less unspecific background staining, particularly in the perinuclear region (FIGURE A.1). Consequently, FA were quantified based on anti-pY861 FAK staining using the image processing program FIJI (ImageJ) (Chapter 2.3.2). The method was validated by manual counting. To analyse the distribution of FA within the cell, FA at the cell edges were compared with those at the cell body (see FIGURE A.2).

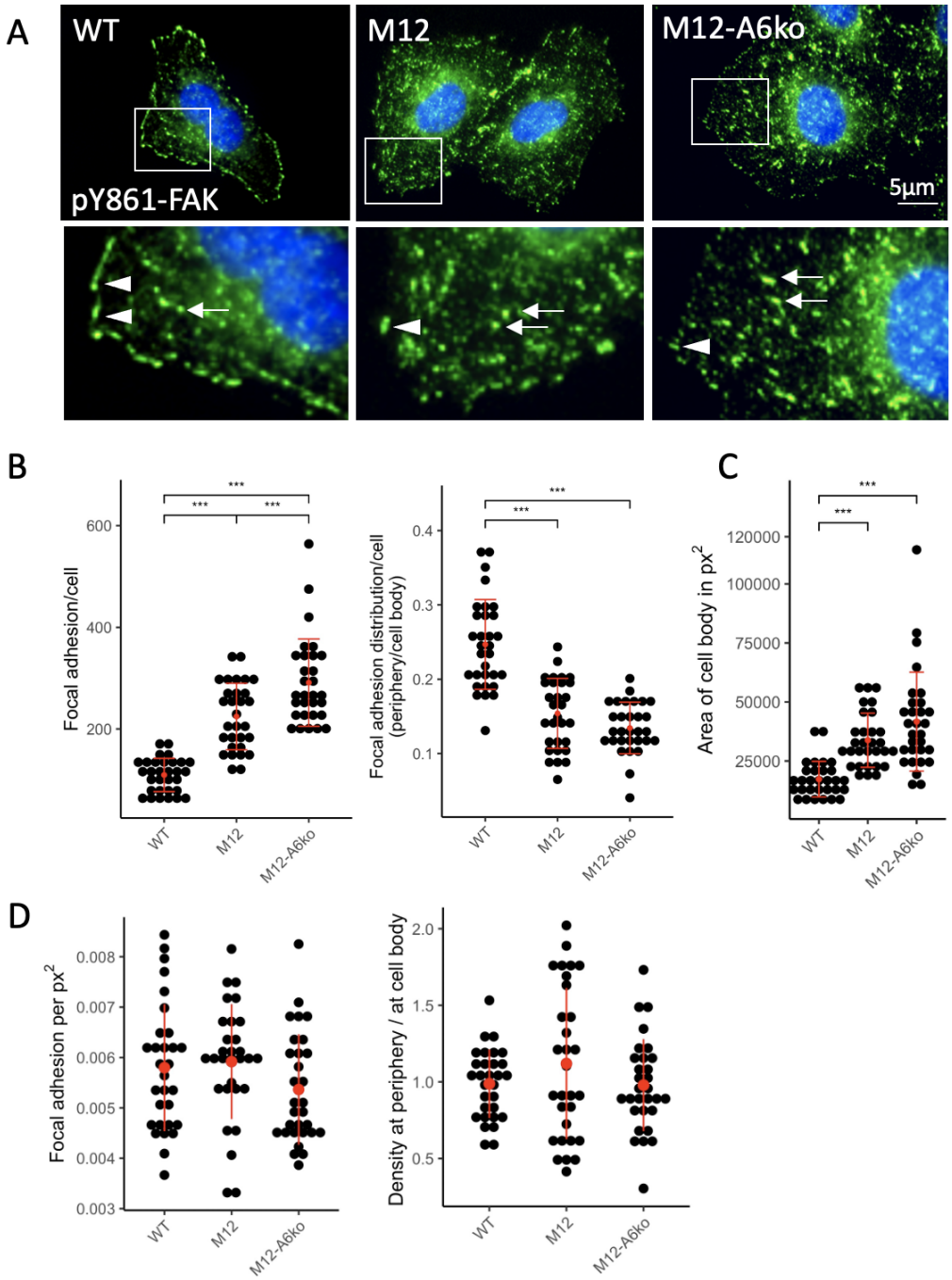

FIGURE 3.11: **Focal adhesion distribution and numbers in CHO WT, M12 and M12-A6ko cells at steady state (10% FBS).** Cells were plated at $1.5 * 10^5$ cells/well of a 6-well plate and grown for 48h in full serum (10% FBS). (A) Cells were stained for pY861 FAK (green) and DAPI (blue, nucleus). In M12 cells, the proportion of peripheral focal adhesions (FA, arrowhead) decreased, while the number of central FA (arrow) increased. In AnxA6-depleted M12, peripheral FA appeared to be partially restored. (B) The total number of FA (> $0.25\mu m^2$) per cell (n = 30-31 per cell line from two independent experiments) and their spatial distribution, the ratio of FA at the cell periphery vs. the cell body were quantified with FIJI using pY861 FAK as FA marker. (C) The cell size of CHO WT, M12 and M12-A6ko cells (n = 30 per cell line) was determined as area in pixel $(px)^2$ using FIJI. (D) The spatial density of FA was calculated by dividing the FA number of a cell by the cell area measured in px^2 (n = 30 per cell line) and the density distribution, cell edge vs. cell body, was determined. The mean ± SD is given. *p < 0.05, **p < 0.01, ***p < 0.001; one-way ANOVA with Tukey's post-hoc test.

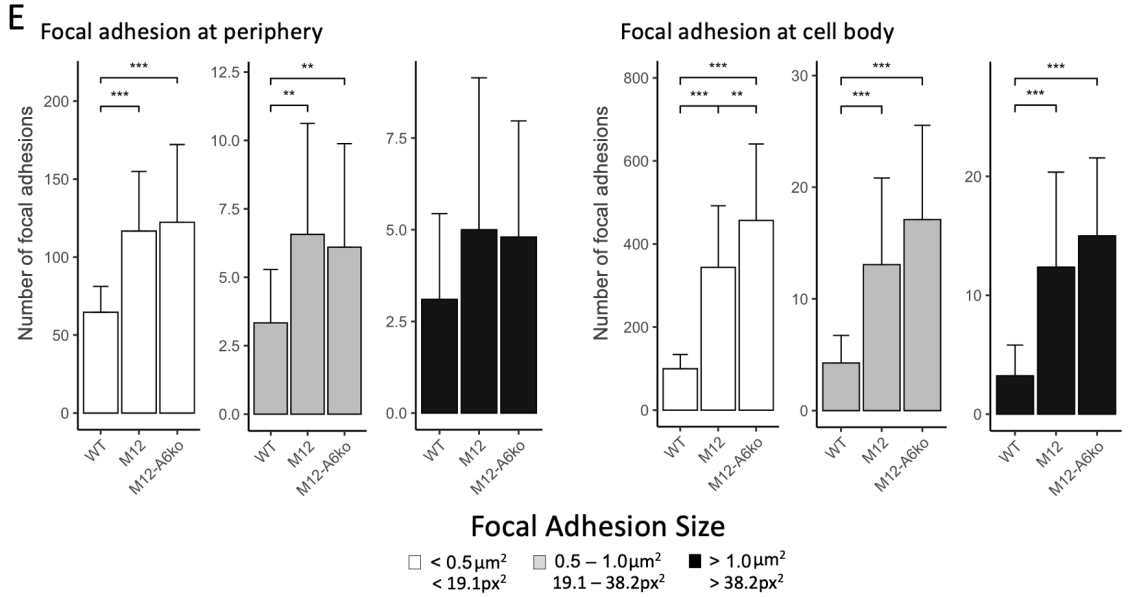

FIGURE 3.11: (E) The focal adhesion (FA) size at the cell edge and throughout the cell body of CHO WT, M12 and M12-A6ko cells (n = 30 per cell line from two independent experiments) was determined using FIJI. Cells were plated at $1.5 * 10^5$ cells/well of a 6-well plate and grown for 48h in full serum (10% FBS). Then cells were fixed and stained for pY861 FAK, which was used as FA marker for counting. The mean ± SD is given. *p < 0.05, **p < 0.01, ***p < 0.001; one-way ANOVA with Tukey's post-hoc test.

In CHO WT cells, enlarged pFAK-labelled FA marked the cell border, while in M12 cells this peripheral FA staining was much less prominent and an increase in centrally located FA was observed (FIGURE 3.11A). In AnxA6-depleted M12 cells, a discrete FA staining at the cell edge reappeared, but the increase of FA numbers in the cell body persisted. At steady state, the total number of FA increased in NPC1 mutants, and M12-A6ko cells had significantly more FA compared to M12 cells (FIGURE 3.11B). In contrast to CHO WT cells, the NPC1 mutants accumulated relatively more FA in the cell body and less at the cell edge (FIGURE 3.11B), which confirmed the visual impression described above. Since differences in FA size and cell size were found in the microscopic examinations, we quantified these parameters using FIJI. FA were divided into three size categories; size 1: < $0.5\mu m^2$ (< 19.1px^2), size 2: 0.5 - $1.0\mu m^2$ (19.1 - 38.2px^2) and size 3: > $1.0\mu m^2$ (> 38.2px^2) and scored according to location (cell edge or cell body).

NPC mutant M12 and AnxA6-depleted M12 cells showed increased FA numbers at the cell edge and cell body across all size groups (FIGURE 3.11E). This is consistent with the increased total number of FA described previously (FIGURE 3.11A-B). At the cell periphery, the amount of FA in the NPC1 mutants was increased by 80-90% in size groups 1 and 2 and by 50-60% in group 3. At the cell body, the increase in FA numbers in M12 and M12-A6ko cells was 250% and 360% in size 1, 210% and 300% in size 2, 280% and 360% in size 3. Thus, there was a strong increase in the number of centrally

localised FA, especially for small and large FA. The cell size of M12 and M12-A6ko cells significantly exceeded that of WT cells (FIGURE 3.11C). As there were no significant differences in spatial FA density (FIGURE 3.11D), the number of FA correlated positively with cell spreading. Overall, the NPC1 mutants in the steady state were characterised by an increase in FA numbers, especially in the cell body, which could not be attributed to a specific FA size and was accompanied by cell spreading.

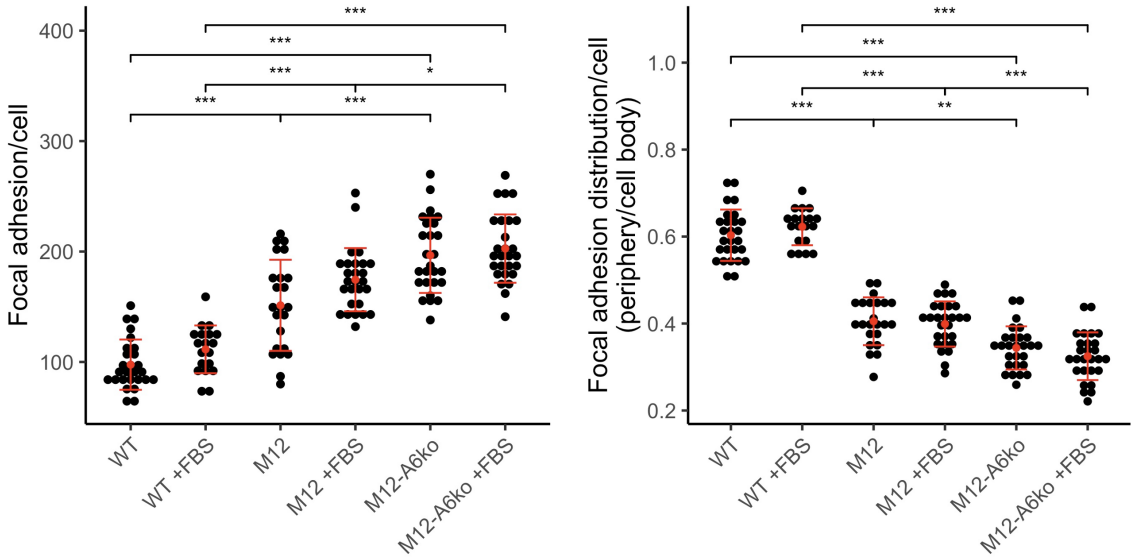

FIGURE 3.12: **Focal adhesion number and distribution in serum-stimulated CHO WT, M12 and M12-A6ko cells.** The total number of FA (> 0.25μm^2) per cell (n = 19-27 per cell line from one experiment) and their spatial distribution and the ratio of FA at the cell periphery vs. the cell body, were quantified with FIJI using pY861 FAK as FA marker. Cells were plated at $1.5 * 10^5$ cells/well of a 6-well plate and grown for 48h in full serum (10% FBS). Then, cells were starved for 2h in serum-free media and stimulated with 20% FBS for 45min. After cell fixation, cells were stained for pY861 FAK, which was used as FA marker for counting. The mean ± SD is given. *p < 0.05, **p < 0.01, ***p < 0.001; two-way ANOVA with Tukey's post-hoc test.

To analyse FA assembly in response to an extracellular stimulus, CHO WT, M12 and M12-A6ko cells were starved in serum-free media for 2h and then treated with 20% FBS for 45min. After serum stimulation, FA numbers tended to increase slightly, but not significantly, in all three cell lines (WT: mean = 97.56, WT +FBS: mean = 111.42, M12: mean = 151.30, M12 +FBS: mean = 174.52, M12-A6ko: mean = 196.56, M12-A6ko +FBS: mean = 202.67) (FIGURE 3.12).

Overall, loss of NPC1 function was associated with an increase in total FA numbers and a shift in spatial FA distribution towards the cell body. Despite restoration of cholesterol release from LE in M12-A6ko cells, these trends were further enhanced by AnxA6 depletion. This suggests that AnxA6 plays a role in FA (dis)assembly that may go beyond cholesterol delivery from LE to FA.

3.2.2 Focal adhesion assembly in LDL-stimulated CHO WT, M12 and M12-A6ko cells

Based on the ability of AnxA6 depletion to restore LDL-inducible cell migration in cells lacking NPC1, the role of LDL in FA formation in CHO WT, M12 and M12-A6ko cells was next investigated. Cells were plated at $1.5 * 10^5$ cells/well of a 6-well plate and then, to reduce cellular cholesterol levels, cells were grown for 48 hours in media supplemented with lipoprotein-deficient serum (10% LPDS) and mevastatin (1μM) (see Appendix B.25), an inhibitor of cholesterol synthesis. Then cells were starved 2h and stimulated ± LDL (50μg/ml) for 4h. Immunostaining with anti-pY861 FAK was performed as described above.

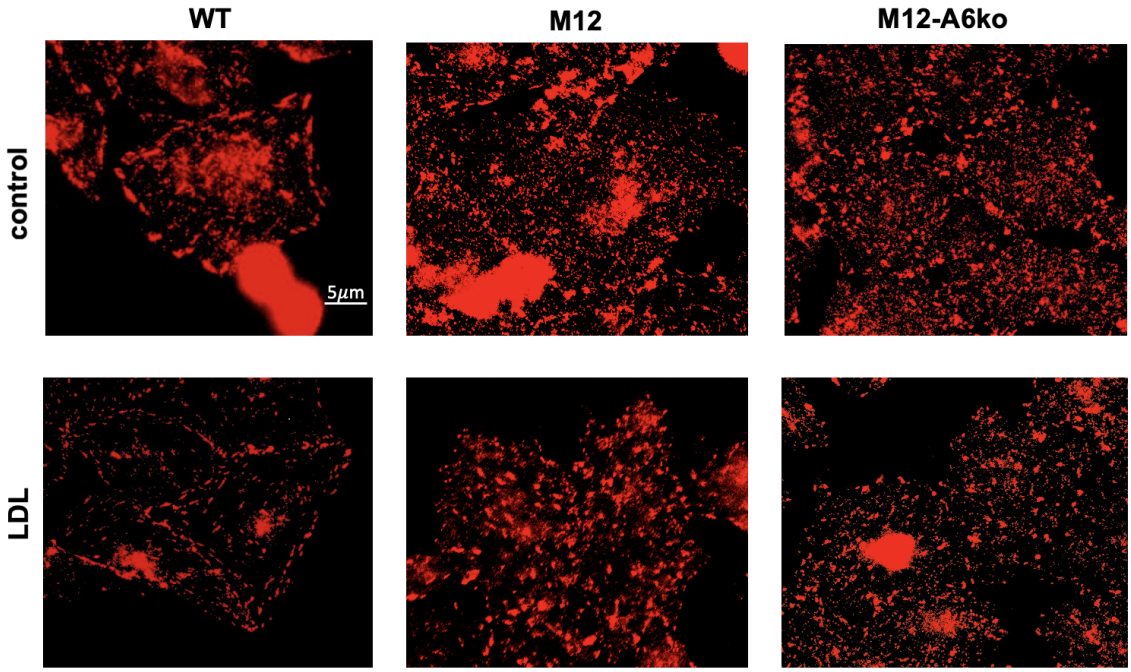

FIGURE 3.13: **LDL stimulation of CHO WT, M12 and M12-A6ko cells.** CHO WT, M12 and M12-A6ko cells were plated at $1.5 * 10^5$ cells/well of a 6-well plate and grown for 48h in media supplemented with lipoprotein-deficient serum (10% LPDS) and mevastatin (1μM) (see Appendix B.25). Cells were starved for 2h and stimulated ± LDL (50μg/ml) for 4h. Afterwards cells were fixed and stained for pY861 FAK (red). Bar is 5μm.

To analyse FA formation, the number, distribution, and size of FA as well as the cell size were quantified (FIGURE 3.14). In NPC1-deficient CHO M12 cells grown in LPDS, FA numbers were significantly increased, even more so in M12-A6ko, compared to WT cells (FIGURE 3.14A). The spatial distribution of FA shifted significantly towards the cell body in M12 and M12-A6ko cells. Although LDL did not increase the total number of FA

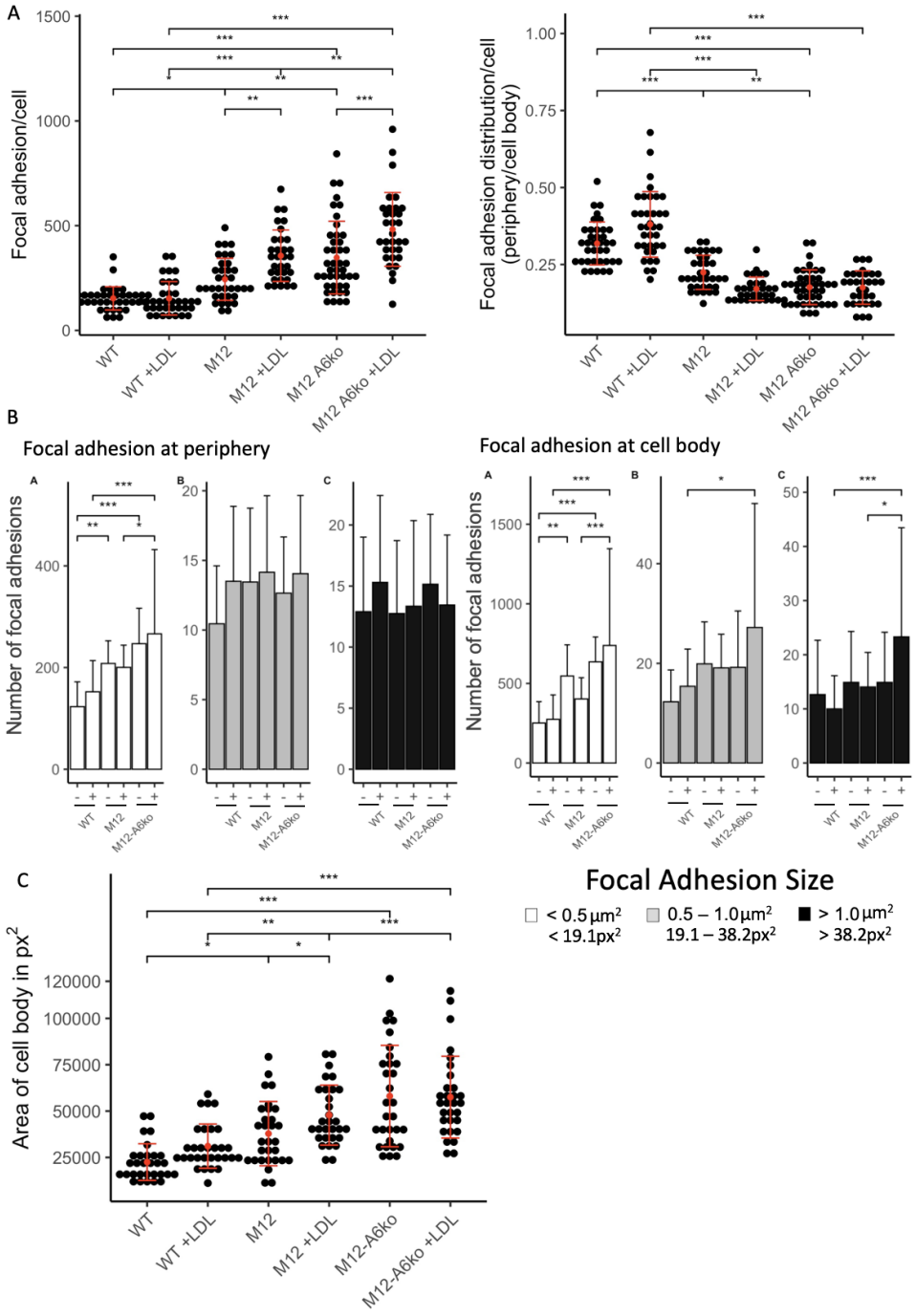

FIGURE 3.14: **Focal adhesion assembly in LDL-stimulated CHO WT, M12 and M12-A6ko cells.** (A) The total number of focal adhesions (FA) (> 0.25 μm^2) per cell (n = 35-43 per cell line from two independent experiments) and their spatial distribution, the ratio of FA at the cell periphery vs. the cell body, were quantified with FIJI using the anti-pY861 FAK signal as FA marker. (B) FA were classified by three size categories, size 1: < $0.5\mu m^2$ (< $19.1px^2$), size 2: 0.5 - $1.0\mu m^2$ (19.1 - $38.2px^2$) and size 3: > $1.0\mu m^2$ (> $38.2px^2$) (n = 20 per cell line from two independent experiments). (C) The cell size of CHO WT, M12 and M12-A6ko (n = 30 per cell line from two independent experiments) was determined as area in pixel $(px)^2$ using FIJI. Cells were plated at $1.5 * 10^5$ cells/well of a 6-well plate and grown for 48h in media supplemented with lipoprotein-deficient serum (10% LPDS) and mevastatin ($1\mu M$) (Appendix B.25). Cells were starved 2h and stimulated ± LDL ($50\mu g$/ml) for 4h. Then, cells were fixed and stained for pY861 FAK. The mean ± SD is given. *p < 0.05, **p < 0.01, ***p < 0.001; two-way ANOVA with Tukey's post-hoc test.

in WT, but in NPC1-deficient cell lines, the proportion of peripheral FA tended to increase slightly, not significantly, in CHO WT cells upon LDL stimulation. Accordingly, LDL treatment was associated with a not significant trend towards increased intermediate and large FA at the cell edge of CHO WT and the cell body of M12-A6ko cells. Alike the increased number of FA in NPC1-depleted CHO M12 cells, the cell size was significantly increased in M12 and M12-A6ko cells.

This could suggest that LDL may promote FA turnover in the cell body of CHO WT cells, allowing increased FA formation at the cell edge. However, in NPC1 mutant cell lines, LDL treatment tended to enhance the mutant phenotype. Although the microscopic images (FIGURE 3.13) suggested a reappearance of the prominent edge in M12-A6ko cells, especially after LDL treatment, the data do not allow a conclusion to be drawn.

3.2.3 Focal adhesion assembly in CHO cells ectopically expressing the focal adhesion markers vinculin and paxillin

To validate the findings obtained from pY861 FAK stainings, it was aimed to analyse and compare the cellular distribution of the well-established FA markers vinculin and paxillin in CHO WT, M12 and M12-A6ko cells. In order to study vinculin and paxillin distribution and their role on FA dynamics, CHO WT, M12 and M12-A6ko cells were plated at $1.5 * 10^5$ cells/well of a 6-well plate, transfected with GFP-vinculin or GFP-paxillin (Chapter 2.1.1) and grown in full serum (10% FBS) for 48h. Then cells were starved overnight and serum-stimulated with 20% FBS for 45min. After fixation, cells were co-stained with anti-pY861 FAK.

Focal adhesion assembly in GFP-vinculin-overexpressing CHO WT, M12 and M12-A6ko cells

In support of previous findings, at the cell edge of CHO WT cells, GFP-vinculin signals frequently overlapped with pY861 FAK staining in enlarged FA complexes (FIGURE 3.15). In M12 and M12-A6ko cells, colocalisation of GFP-vinculin and pY861 FAK signals decreased compared to WT cells. This was confirmed by a decreased mean Pearson's R value at the cell body and cell edge of M12 and M12-A6ko cells (FIGURE 3.15C). This indicated an altered FA composition in NPC1-deficient CHO cells.

In serum-stimulated cells, the overlap slightly tended to decrease in all three cell lines, but mostly not significantly. This could indicate that despite a different FA composition, all three cell lines were capable to respond to extracellular growth factors. However, the results should be treated with caution as Pearson's R values were used here regardless of their significance level. As measured by the GFP-vinculin staining, the total number of

FA and their proportion at the cell body increased in M12 and even more in M12-A6ko cells (FIGURE 3.16A), a finding that was comparable to the results obtained for pY861 FAK signals in Chapter 3.2.1. In particular, the number of centrally located small FA increased in NPC1-deficient cells (FIGURE 3.17). Furthermore, an increased cell size of M12 and M12-A6ko cells was noted (FIGURE 3.16B). Analysis of the FA size showed that the ratio between small, media and large FA was comparable in non-transfected and vinculin-transfected cells suggesting that the FA size did not increase beyond size thresholds due to vinculin overexpression.

Overall, NPC1 deficiency was associated with altered FA number, distribution as well as molecular composition and depletion of AnxA6 appeared to influence these factors.

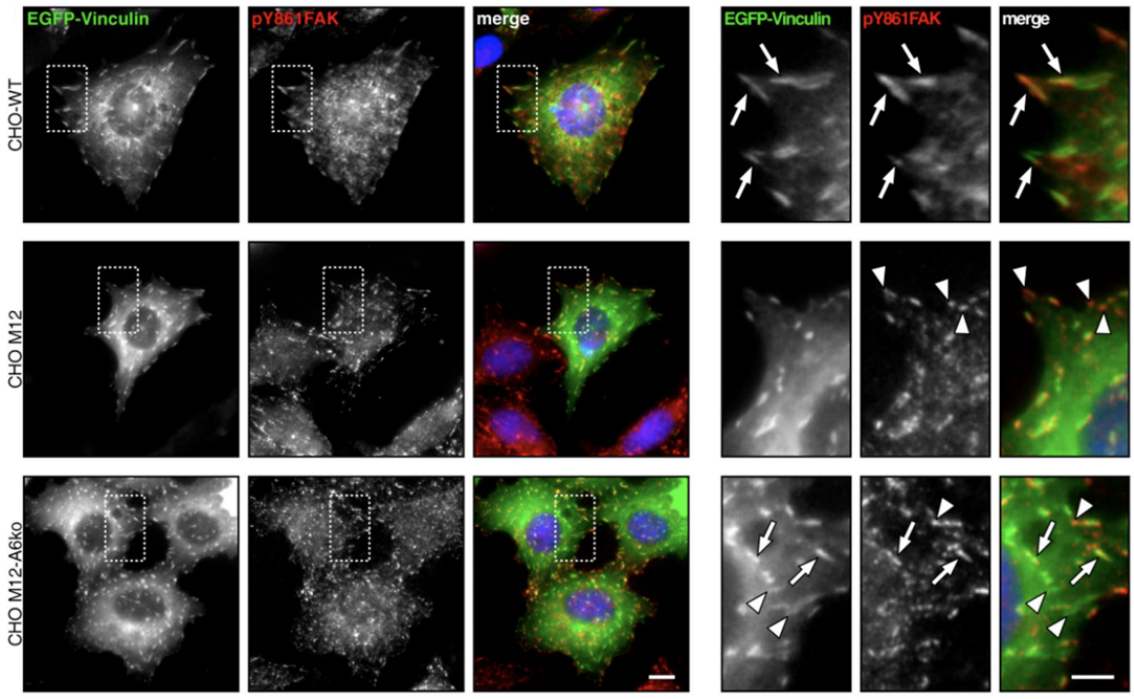

FIGURE 3.15: **Spatial distribution and colocalisation of the FA markers vinculin and pY861 FAK in CHO WT, M12 and M12-A6ko cells.** Cells were plated at $1.5 * 10^5$ cells/well of a 6-well plate, transfected with GFP-vinculin (Chapter 2.1.1) and grown in full serum (10% FBS) for 48h. Then cells were starved overnight and serum-stimulated with 20% FBS for 45min or remained unstimulated. Here, unstimulated cells are shown. Cells were fixed and co-stained for anti-pY861 FAK (red) and DAPI (blue). In the enlarged regions, arrows point at colocalisation of GFP-vinculin (green) and pY861 FAK signals in WT and M12-A6ko cells, while arrowheads mark lack of overlap of pY861 FAK or GFP-vinculin in CHO M12 or M12-A6ko cells. Bar is 5μm. (Results were published in (*104*))

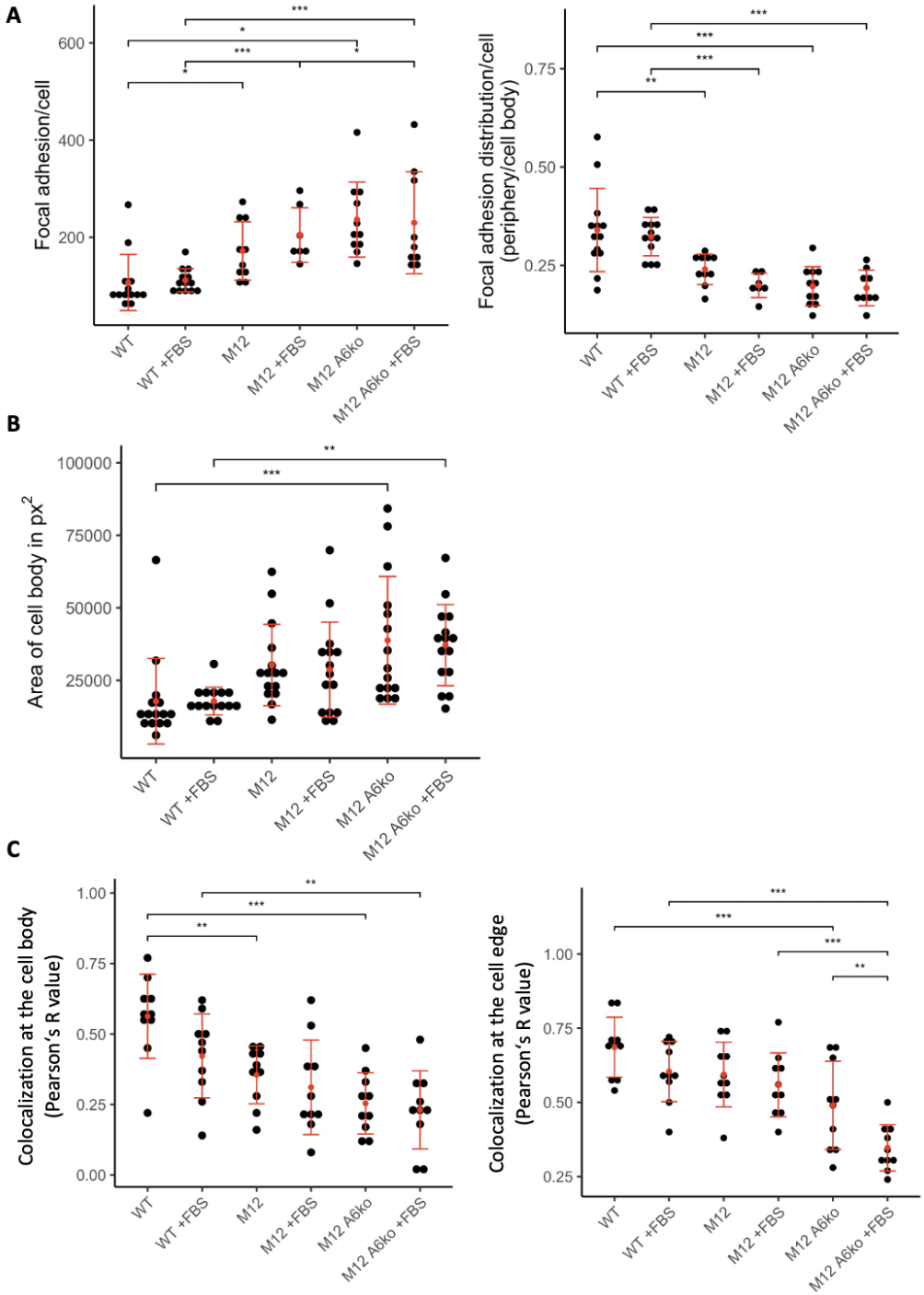

FIGURE 3.16: **Focal adhesion assembly of GFP-vinculin overexpressing CHO WT, M12 and M12-A6ko cells.** Cells were plated at $1.5 * 10^5$ cells/well of a 6-well plate, transfected with GFP-vinculin (Chapter 2.1.1) and grown in full serum (10% FBS) for 48h. Then cells were starved for 2h and serum-stimulated with 20% FBS for 45min. After fixation, cells were stained for pY861 FAK and analysed using FIJI. (A) Focal adhesion (FA) number and their spatial distribution, cell edge vs. cell body, were analysed using the GFP-vinculin signal as FA marker (n = 7-13 per cell line from one experiment). (B) Cell size as area in pixel $(px)^2$ (n = 15 per cell line from one experiment). (C) Colocalisation of GFP-vinculin and pY861 FAK at the cell body and cell edge were quantified (Pearson's R value, n = 10 per cell line from one experiment). The mean ± SD is given. *p < 0.05, **p < 0.01, ***p < 0.001; two-way ANOVA with Tukey's post-hoc test.

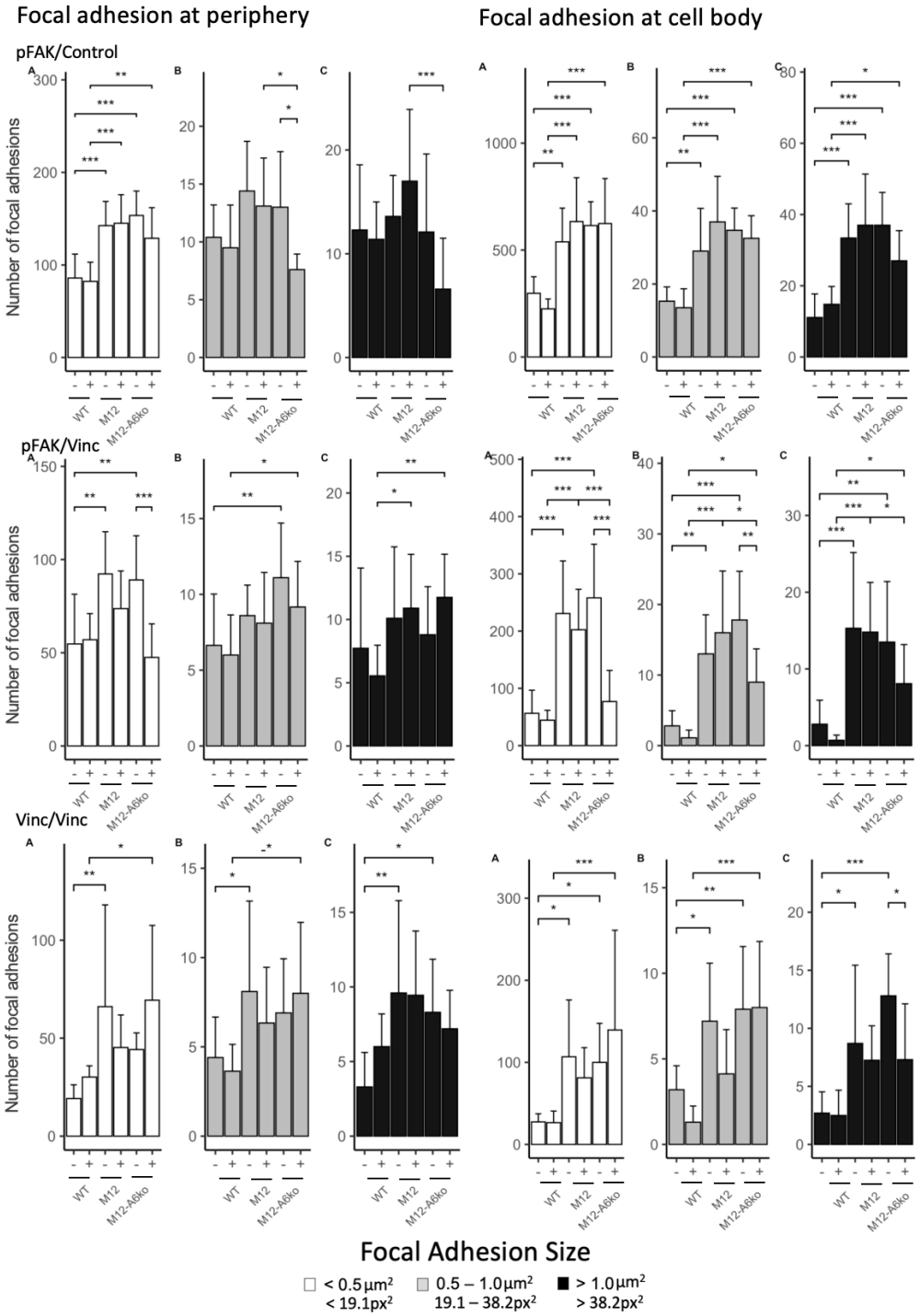

FIGURE 3.17: **Focal adhesion size in GFP-vinculin overexpressing CHO WT, M12 and M12-A6ko cells.** Cells were plated at $1.5 * 10^5$ cells/well of a 6-well plate and transfected with GFP-vinculin (Chapter 2.1.1). Cells were grown for 48h in full serum (10% FBS), starved in serum-free media for 2h and stimulated for 45min with 20% FBS. After fixation, cells were stained for pY861 FAK and analysed using FIJI. FA size was measured using the GFP-vinculin (Vinc/Vinc: Vinc signal for analysis/in Vinc overexpressing cells) and pFAK (pFAK/Vinc) signals as FA markers (each n = 10-11 per cell line from one experiment). FA were grouped into three size categories, size 1: $< 0.5\mu m^2$ (< 19.1px^2), size 2: 0.5 - $1.0\mu m^2$ (19.1 - 38.2px^2) and size 3: $> 1.0\mu m^2$ (> 38.2px^2) and the quantity of each size category was evaluated according to location (cell edge or cell body). The mean ± SD is given. *p < 0.05, **p < 0.01, ***p < 0.001; two-way ANOVA with Tukey's post-hoc test.

Focal adhesion assembly in GFP-paxillin-overexpressing CHO WT, M12 and M12-A6ko cells

In paxillin-overexpressing CHO WT, GFP-paxillin signals often overlapped with pY861 FAK staining at the cell edges, whereas in M12 and M12-A6ko cells, a substantial number of GFP-paxillin and pY861 FAK stainings did not overlap (FIGURE 3.18). At the cell edge, this finding was supported by a significantly reduced Pearson's R value in M12-A6ko cells, but in M12 cells, colocalisation remained comparable to WT (FIGURE 3.19C). At the cell body, colocalisation was comparable in CHO WT, M12 and M12-A6ko cells and increased upon stimulation in WT and M12 cells. FA numbers tended to increase in CHO M12 and M12-A6ko (FIGURE 3.19A), but the slope was less pronounced compared to non-transfected (FIGURE 3.11B) and vinculin-overexpressing CHO cells (FIGURE 3.16A). The cell size tended to increase (not significantly) in the NPC1 mutants (FIGURE 3.19B) and was in the same range as in vinculin-overexpressing CHO cells (FIGURE 3.11B). Due to an increased background signal of GFP-paxillin and pY861 FAK, FA size analysis with FIJI was difficult and results were inconsistent within cell lines (FIGURE 3.20).

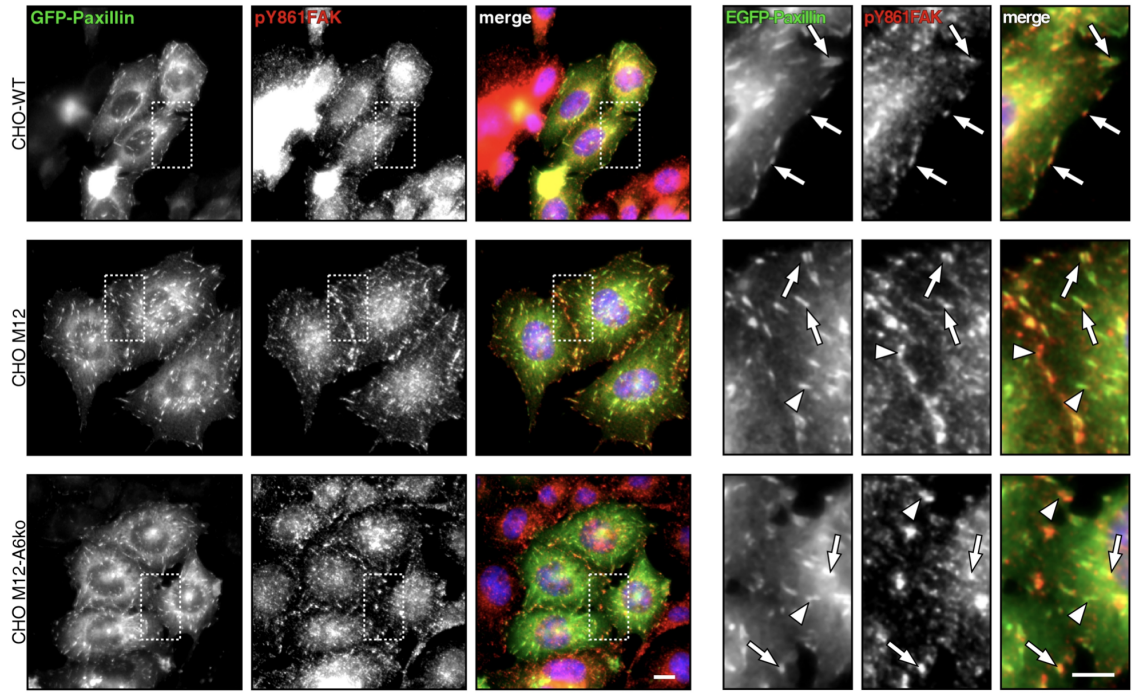

FIGURE 3.18: **Spatial distribution and colocalisation of the FA markers paxillin and pY861 FAK in CHO WT, M12 and M12-A6ko.** Cells were plated at $1.5 * 10^5$ cells/well of a 6-well plate, transfected with GFP-paxillin (green, Chapter 2.1.1) and grown in full serum (10% FBS) for 48h. Then, cells were starved 2h and serum-stimulated with 20% FBS for 45min or remained unstimulated. Here, unstimulated cells are shown. Cells were fixed and stained for pY861 FAK (red) and DAPI (blue). In the enlarged regions, arrows point at colocalising GFP-paxillin and pY861 FAK signals, while arrowheads mark not colocalising signals. Bar is 5μm. (Results were published in (*104*)).

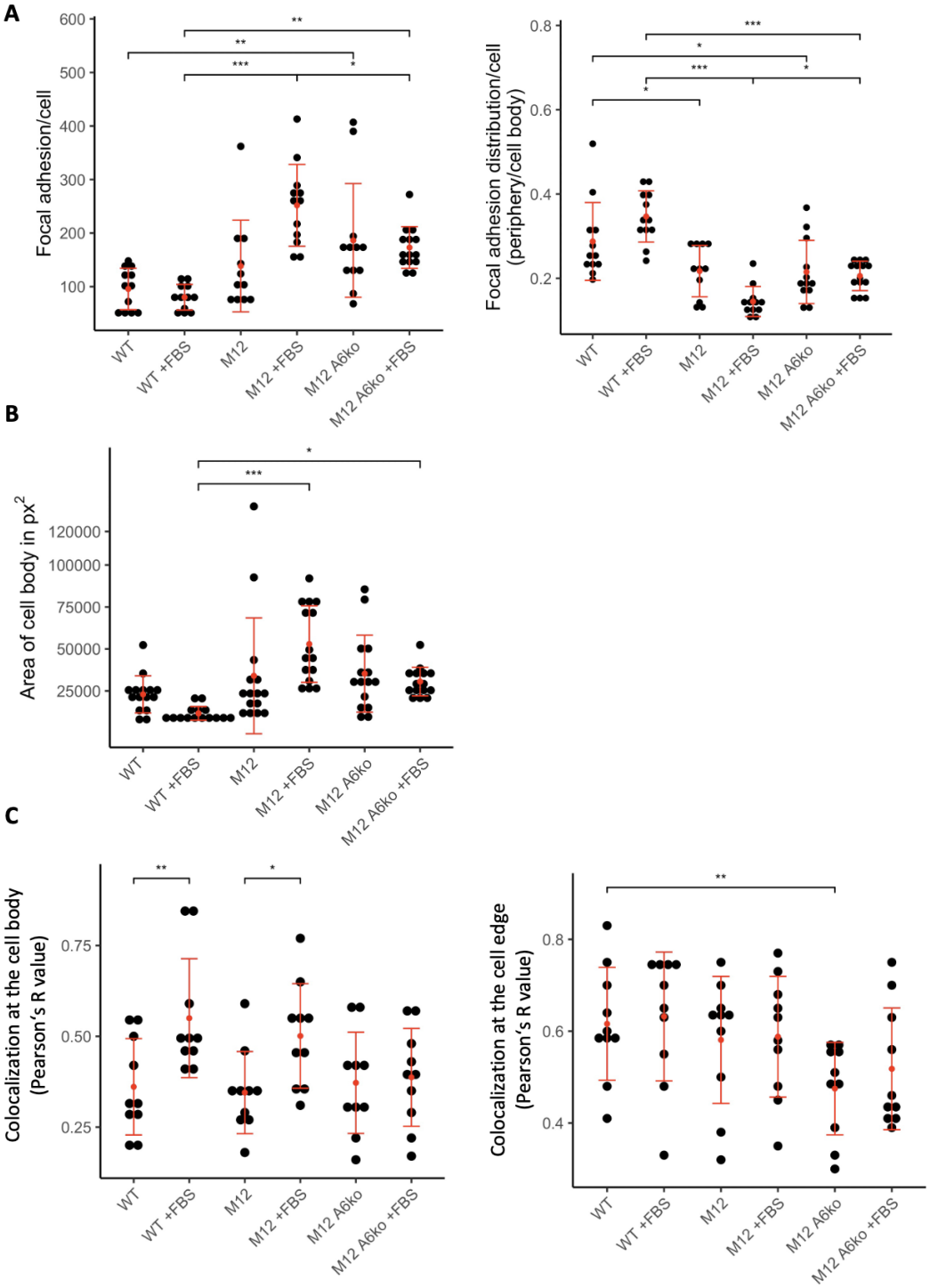

FIGURE 3.19: **Focal adhesion assembly in GFP-paxillin-overexpressing CHO WT, M12 and M12-A6ko cells.** Cells were plated at $1.5 * 10^5$ cells/well of a 6-well plate, transfected with GFP-paxillin (Chapter 2.1.1) and grown in full serum (10% FBS) for 48h. Then cells were starved over 2h and serum-stimulated with 20% FBS for 45min. After fixation, cells were stained for pY861 FAK and analysed using FIJI. (A) Focal adhesion (FA) number and their spatial distribution, cell edge vs. cell body, were analysed using the GFP-paxillin signal as FA marker (n = 11-14 per cell line from one experiment). (B) Cell size as area in pixel $(px)^2$ (n = 15 per cell line from one experiment). (C) Colocalisation of GFP-paxillin and pY861 FAK signals at the cell body and cell edge (Pearson's R value, n = 10 per cell line from one experiment). The mean ± SD is given. *p < 0.05, **p < 0.01, ***p < 0.001; two-way ANOVA with Tukey's post-hoc test.

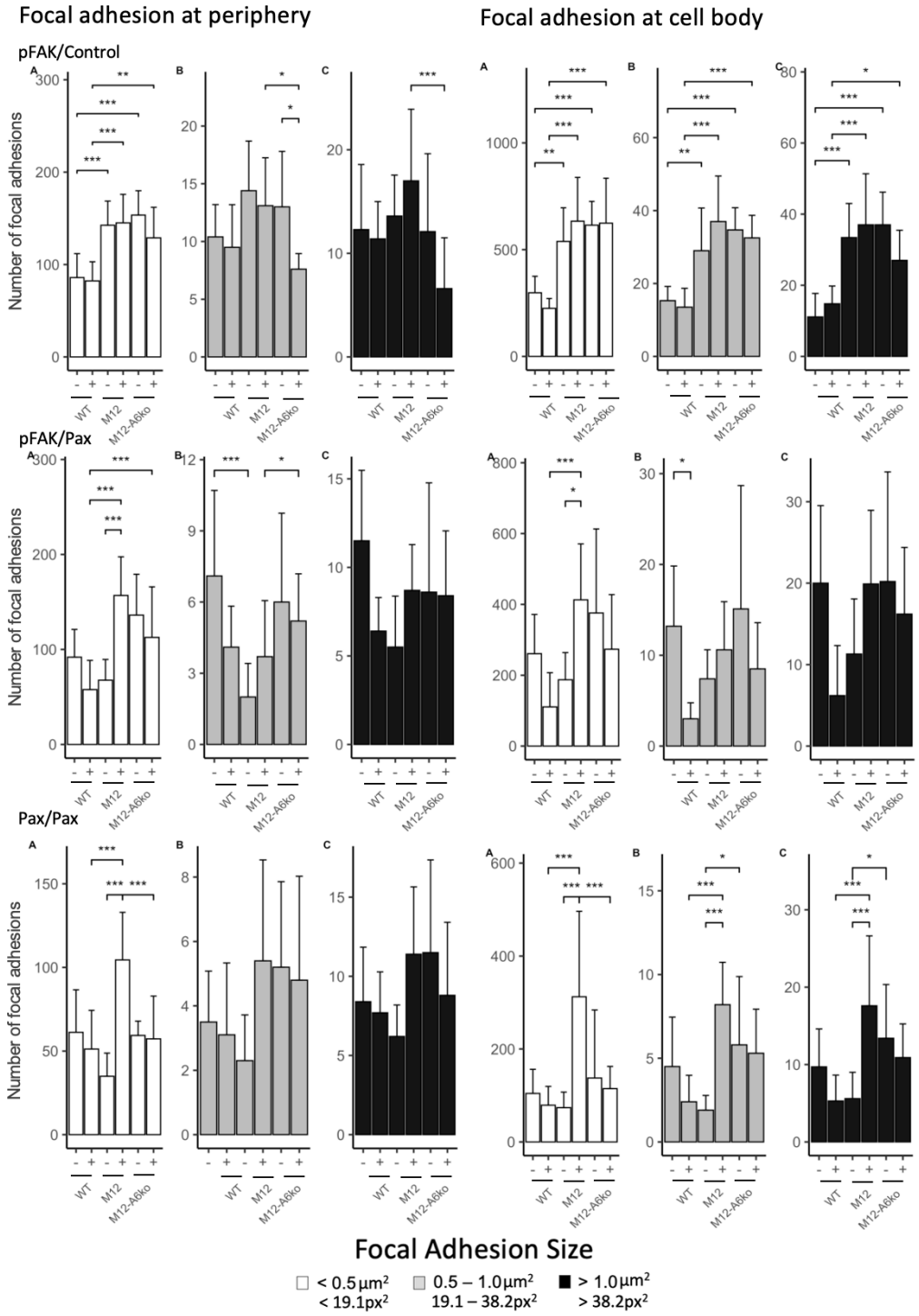

FIGURE 3.20: **Focal adhesion size in GFP-paxillin-overexpressing CHO WT, M12 and M12-A6ko cells.** Cells were plated at $1.5 * 10^5$ cells/well of a 6-well plate and transfected with GFP-paxillin (Chapter 2.1.1). Cells were grown for 48h in full serum (10%FBS), starved in serum-free media for 2h and stimulated for 45min with 20% FBS. After fixation, cells were stained for pY861 FAK and analysed using FIJI. FA size was measured using the GFP-paxillin (Pax/Pax: Pax signal for analysis/in Pax overexpressing cells) and pFAK (pFAK/Pax) signals as FA markers (each n = 10 per cell line from one experiment). FA were grouped into three size categories, size 1: < $0.5\mu m^2$ (< $19.1px^2$), size 2: 0.5 - $1.0\mu m^2$ (19.1 - $38.2px^2$) and size 3: > $1.0\mu m^2$ (> $38.2px^2$) and the quantity of each size category was evaluated according to location (cell edge or cell body). The mean ± SD is given. *p < 0.05, **p < 0.01, ***p < 0.001; two-way ANOVA with Tukey's post-hoc test.

Overall, altered intracellular LDL-cholesterol transport in M12 and M12-A6ko cells was associated with changes in the distribution of pY861 FAK, vinculin and paxillin, resulting in decreased colocalisation of pY861 FAK with the FA markers vinculin and paxillin, which was not reversed in AnxA6-depleted M12 cells despite restored cholesterol efflux from the LE.

Cholesterol associates with focal adhesions in paxillin- and vinculin-overexpressing cells

It was speculated that cholesterol release upon AnxA6 depletion in M12 cells could improve cholesterol delivery to the periphery to support FA formation at the cell edge. To test this hypothesis and investigate the role of cholesterol in FA formation, colocalisation of mCherry-D4H with the adaptor proteins vinculin and paxillin and with the signalling molecule pY861 FAK was analysed in CHO WT, M12 and M12-A6ko cells.

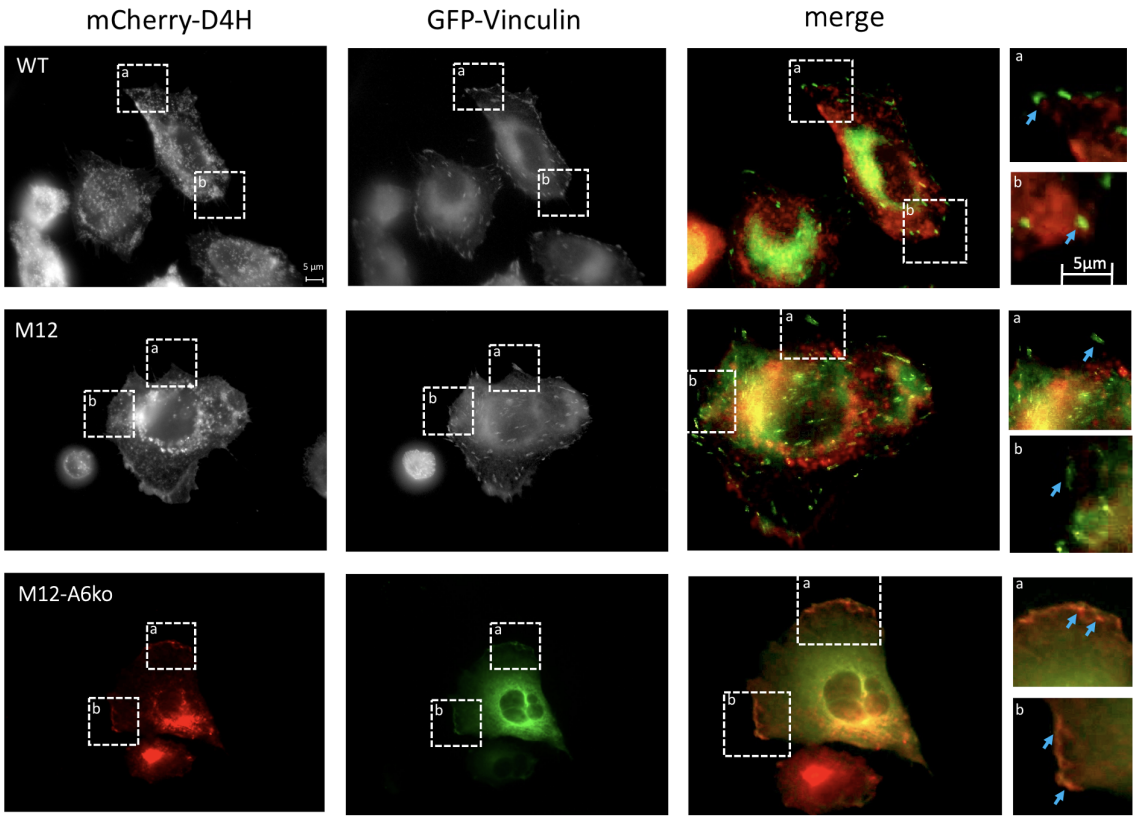

FIGURE 3.21: **Spatial association of cholesterol and vinculin in CHO WT, M12 and M12-A6ko cells.** Cells were plated at $1.5 * 10^5$ cells/well of a 6-well plate, transfected with GFP-vinculin (green, Chapter 2.1.1) and mCherry-D4H (red), a biosensor for membrane-bound cholesterol, and grown for 48h in full serum (10% FBS). Bar is 5μm.

To investigate the spatial relationship between cholesterol and vinculin, CHO WT, M12 and M12-A6ko were plated at a density of $1.5 * 10^5$ cells/well of a 6-well plate, transfected with GFP-vinculin (green) and mCherry-D4H (red) and grown for 48 hours in full serum (10% FBS). The cells were analysed with FIJI.

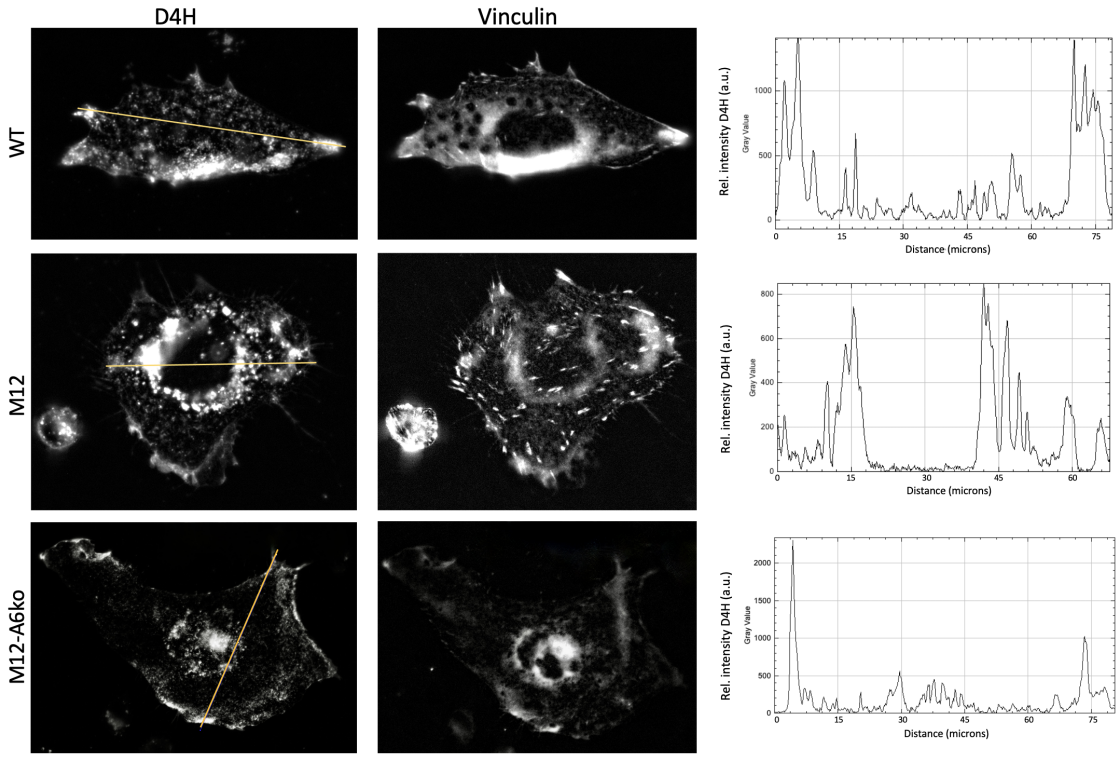

FIGURE 3.22: **Spatial distribution of cholesterol in CHO WT, M12 and M12-A6ko cells.** Cells were plated at $1.5 * 10^5$ cells/well of a 6-well plate, transfected with GFP-vinculin (green, Chapter 2.1.1) and mCherry-D4H (red), a biosensor for membrane-bound cholesterol, and grown for 48h in full serum (10%FBS). Cells were fixed and analysed by microscopy as described (see Methods). The line profiles (approx. 70-80μm) of fluorescence intensities (a.u.: arbitrary unit) of mCherry-D4H in CHO WT, M12 and M12-A6ko cells are shown.

In WT, the D4H signal was scattered within the cell, with single enlarged spots at the cell edge (FIGURE 3.21). In M12, cholesterol accumulation in LE/Lys compartments was confirmed by strong mCherry-D4H signals in close proximity to the nucleus (FIGURE 3.21 and 3.22). As hypothesised, AnxA6-depleted M12 had increased cholesterol staining at the cell edge (FIGURE 3.21 and 3.22), indicating restoration of LE-cholesterol export to the cell surface. However, residual cholesterol accumulation remained near the nucleus, suggesting that CHO M12-A6ko cells still contain detectable amounts of LDL-derived cholesterol in LE. In vinculin-overexpressing WT cells, vinculin-labelled FA were predominantly at the cell edge and in close proximity to D4H-labelled cholesterol. In contrast, the number of centrally located FA increased in M12, but there was less colocalisation

with cholesterol. In AnxA6-deficient M12 cells, adhesion complexes were concentrated on the peripheral PM, where vinculin often colocalised with cholesterol.

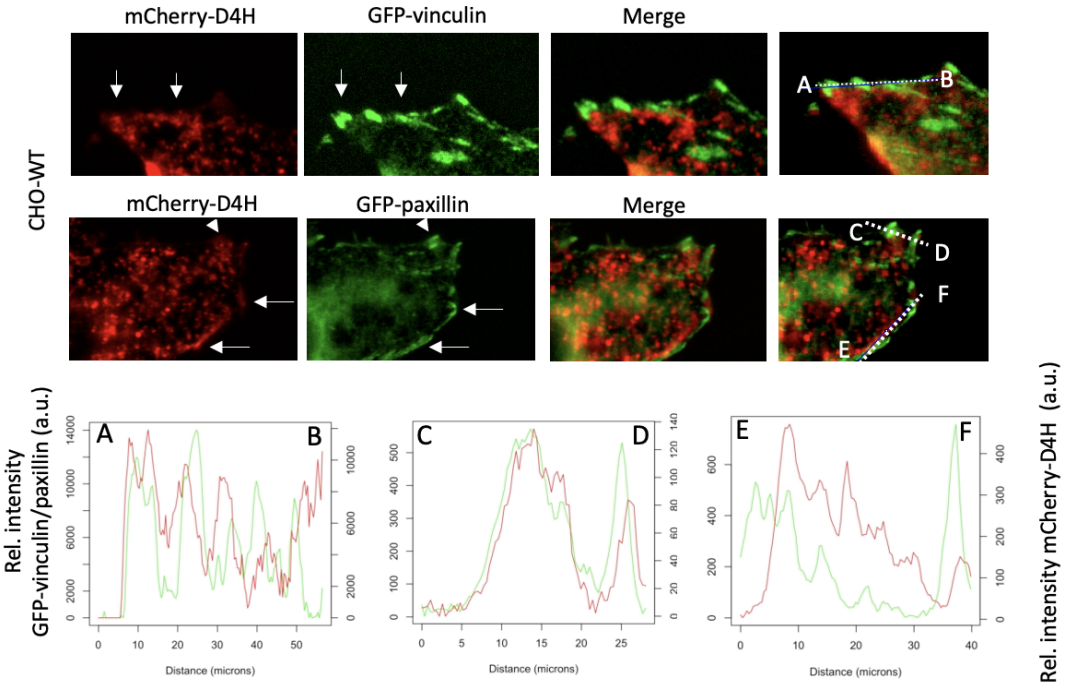

FIGURE 3.23: **Colocalisation of cholesterol and vinculin or paxillin in CHO WT cells.** Cells were plated at $1.5 * 10^5$ cells/well of a 6-well plate, transfected with GFP-vinculin or GFP-paxillin together with mCherry-D4H (red, Chapter 2.1.1), a cholesterol binding biosensor, and grown for 48h in full serum (10% FBS). Arrows and an arrowhead (lower panel) indicate colocalisation. The line profiles of fluorescence intensities (a.u.: arbitrary unit) of GFP-vinculin/paxillin (green) and mCherry–D4H (red) (A-B, C-D and E-F; 0–50, 0-30 and 0-40 μm, respectively) are shown.

To further analyse the association of cholesterol with FA, the colocalisation of mCherry-D4H with GFP-vinculin, GFP-paxillin and anti-pY861 FAK immunofluorescence signals was quantified (FIGURE 3.23). In WT, D4H-stained cholesterol was closely associated with GFP-paxillin and GFP-vinculin at the cell edge. In M12 and AnxA6-deficient M12 cells transfected with mCherry-D4H and immunostained for pY861 FAK, the centrally located D4H signals, particularly in M12, confirmed LE-cholesterol accumulation as observed for the NPC1 mutant phenotype (FIGURE 3.24). While M12 cells lacked peripheral cholesterol, the PM at the cell edges in M12-A6ko cells clearly contained D4H signals. When analysing the colocalisation of cholesterol with pY861 FAK, there was little overlap in M12 cells (FIGURE 3.24, see G-H, I-J, K-L), in contrast to AnxA6-depleted M12 cells, in which D4H and pY861 FAK signals often colocalised strongly (FIGURE 3.24, see A-B, C-D, E-F).

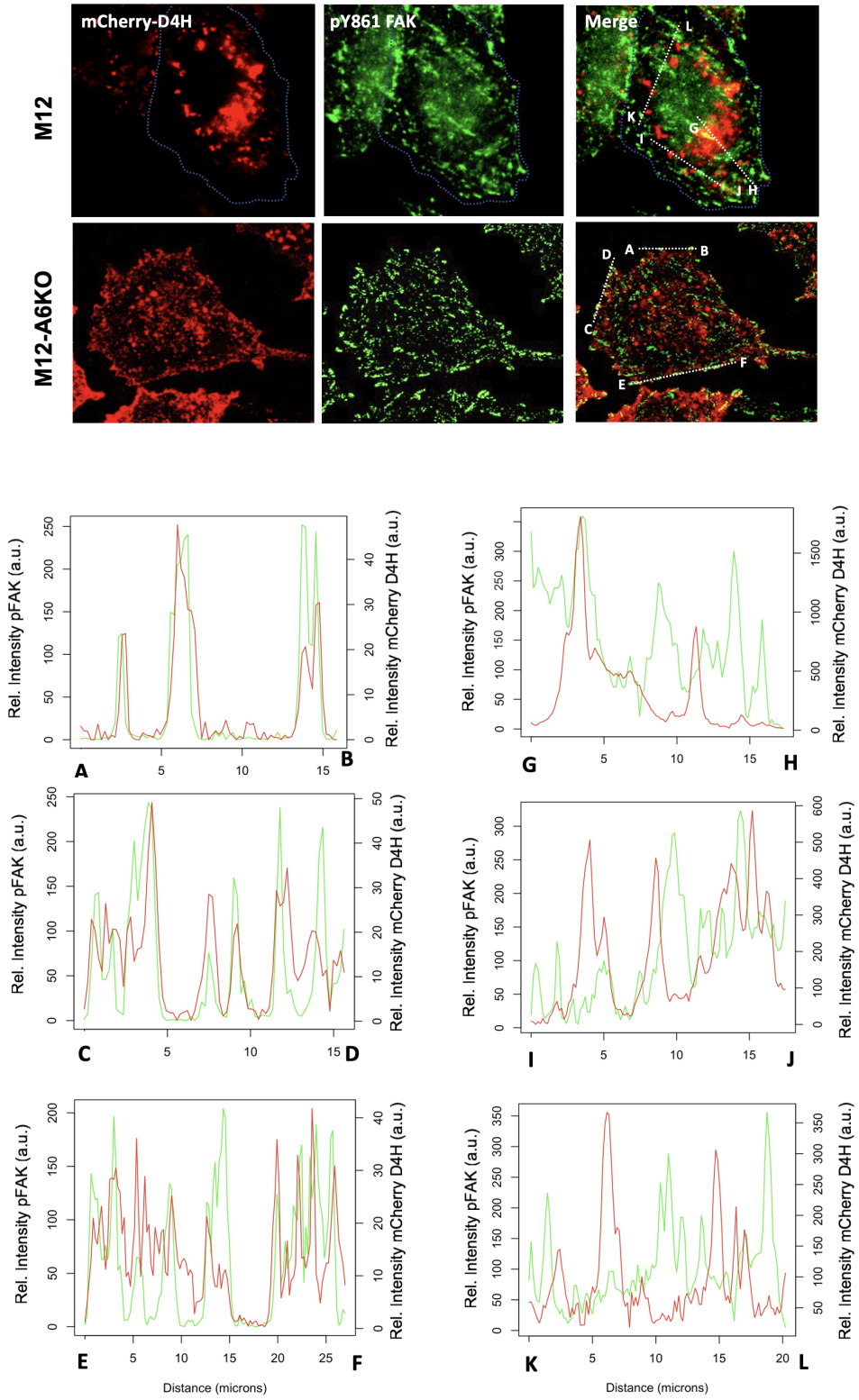

FIGURE 3.24: **Colocalisation of cholesterol and pY861 FAK in CHO M12 and M12-A6ko cells.** Cells were plated at $1.5 * 10^5$ cells/well of a 6-well plate, transfected with mCherry-D4H (red, Chapter 2.1.1), a cholesterol marker, and grown for 48h in full serum (10% FBS). Cells were fixed and stained for pY861 FAK (green) as described above. The line profiles of fluorescence intensities (a.u.: arbitrary unit) of pY861 FAK (green) and mCherry–D4H (red) (A-B, C-D and E-F in lower panel; G-H, I-J, K-L in top panel; 0–15, 0-20 or 0-25μm, respectively) are shown.

Taken together, these results suggest that depletion of AnxA6 in M12 cells restores cholesterol transport to the cell edge, allowing spatial association of cholesterol derived from LE with FA structures.

3.2.4 Focal adhesion assembly in CHO cells overexpressing wild type and oncogenic Src kinase

To investigate the role of Src kinase in FA distribution, CHO WT, M12 and M12-A6ko cells were transfected with GFP-Src and the constitutively active oncogenic mutant pEGFP-Src Y527F. Cells were plated at $1.5 * 10^5$ cells/well of a 6-well plate and transfected with GFP-Src or pEGFP-Src Y527F (Chapter 2.1.1). Cells were grown in media that was supplemented with lipoprotein-deficient serum (10% LPDS) and mevastatin (1μM) (see Appendix B.25) for 48h. Then, cells were starved for 2h and stimulated ± LDL (50 μg/ml) for 4h. Immunostaining with anti-pY861 FAK was performed as described in Chapter 2.3.1. To analyse FA dynamics in Src- and Src Y527F-overexpressing cells, FA number, distribution, size, as well as cell size and Src-pFAK colocalisation was determined.

In WT Src-overexpressing WT cells, the cell edge contained very large complexes of colocalising anti-pY861 FAK and GFP-Src signals, while in the cell body rather small FA were found (Figure 3.25). Similarly, in Src Y527F-overexpressing WT cells, a strong staining of large FA complexes at the cell periphery, but not throughout the cell body, was observed by colocalising EGFP-Src Y527F and anti-pFAK signals. Thus, in CHO WT cells, overexpression of WT Src and oncogenic Src kinase can promote the formation of large FA complexes at the cell edge. In WT Src-overexpressing NPC1 mutants, however, the number of FA complexes in the cell body increased. This coincided with reduced colocalisation of pY861 FAK and Src signals, suggesting that the cholesterol imbalance caused by NPC1 loss of function may affect Src activation. In contrast, overexpression of Src Y527F reversed the NPC1 mutant phenotype and restored the prominent cell edge pattern consistent of huge FA complexes of overlapping pFAK and Src signals in M12 and M12-A6ko cells. This could indicate that NPC1 mutants lack the ability to activate Src, presumably due to dysregulated cholesterol-sensitive signalling.

Examining FA numbers (Figure 3.26), alike untransfected CHO cells, WT Src-overexpressing NPC1 mutants formed significantly more FA compared to WT. However, the overall FA count dropped by >18% in all three cell lines when overexpressing WT Src. In NPC1 mutants, this was accompanied by a partial FA redistribution towards the cell edge. In Src Y527F-overexpressing WT and M12-A6ko cells, the FA number decreased by >24% compared to untransfected cells. In contrast, in M12 cells, the total FA amount remained unchanged. When overexpressing Src Y527F, the spatial distribution of FA

towards the cell edge increased by the factors 1.53, 1.32, and 1.72 in CHO WT, M12, and M12-A6ko cells, respectively, compared to controls. Upon LDL stimulation, FA levels significantly increased in untransfected CHO M12 and M12-A6ko cells, an effect that in CHO M12 cells was accompanied by an increase of the centrally located FA portion. Although, there was no significant effect of LDL stimulation in WT Src- or Src Y527F-overexpressing cells, ectopic Src Y527F expression was associated with a slight decrease in FA number and limited shift towards the peripheral FA portion in CHO M12 cells.

Taken together, ectopic expression of Src kinase, in particular constitutively active mutant Src Y527F, was associated with a decrease of total FA numbers and a shift towards FA at the cell edge in all three cell lines, indicating increased FA turnover. Furthermore, overexpression of Src Y527F seemed to partially restore LDL-inducible FA turnover in M12 cells (not significant).

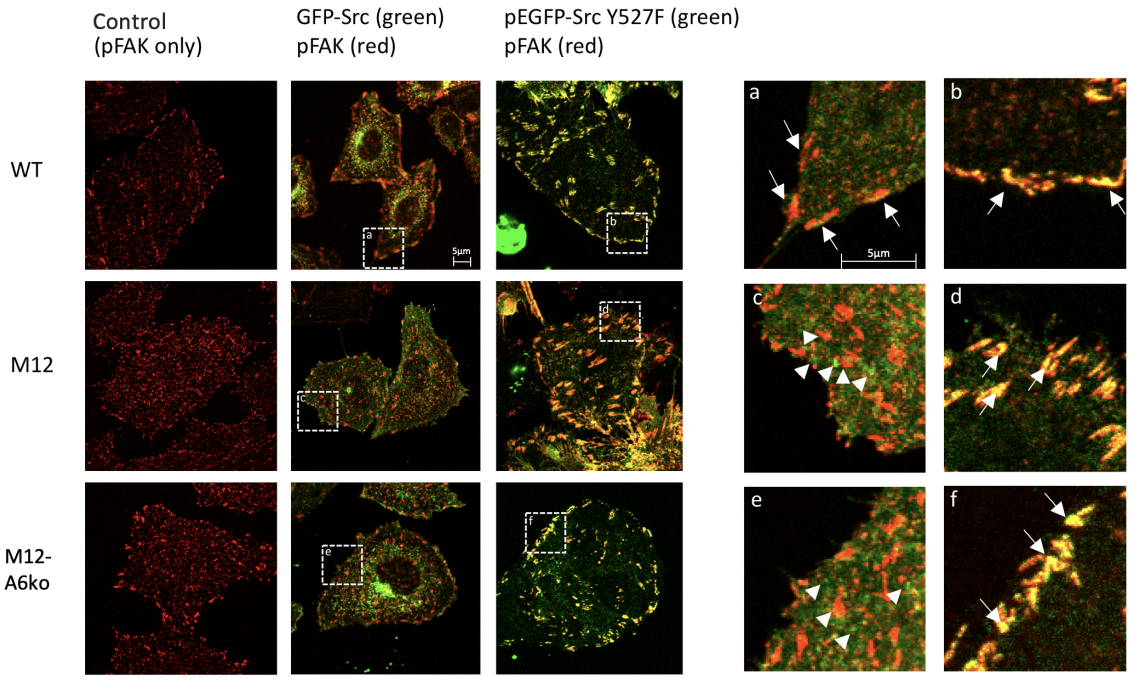

FIGURE 3.25: **Src- and Src Y527F-overexpressing CHO WT, M12 and M12-A6ko cells.** Cells were plated at $1.5 * 10^5$ cells/well of a 6-well plate and transfected with GFP-Src (green, Chapter 2.1.1) or pEGFP-Src Y527F (green). Untransfected cells served as control (control). Cells were grown for 48h in media supplemented with lipoprotein-deficient serum (10% LPDS) and mevastatin (1μM) (see Appendix B.25). Cells were starved for 2h and stimulated ± LDL (50 μg/ml) for 4h. Only untreated samples are shown in this figure (to analyse the effect of LDL stimulation in this setting, see next figure). Cells were fixed and stained for pY861 FAK (red). Colocalisation of pY861 FAK and wild type or oncogenic Src signals are indicated by arrows, not colocalising signals are indicated by arrowheads. Bar is 5μm.

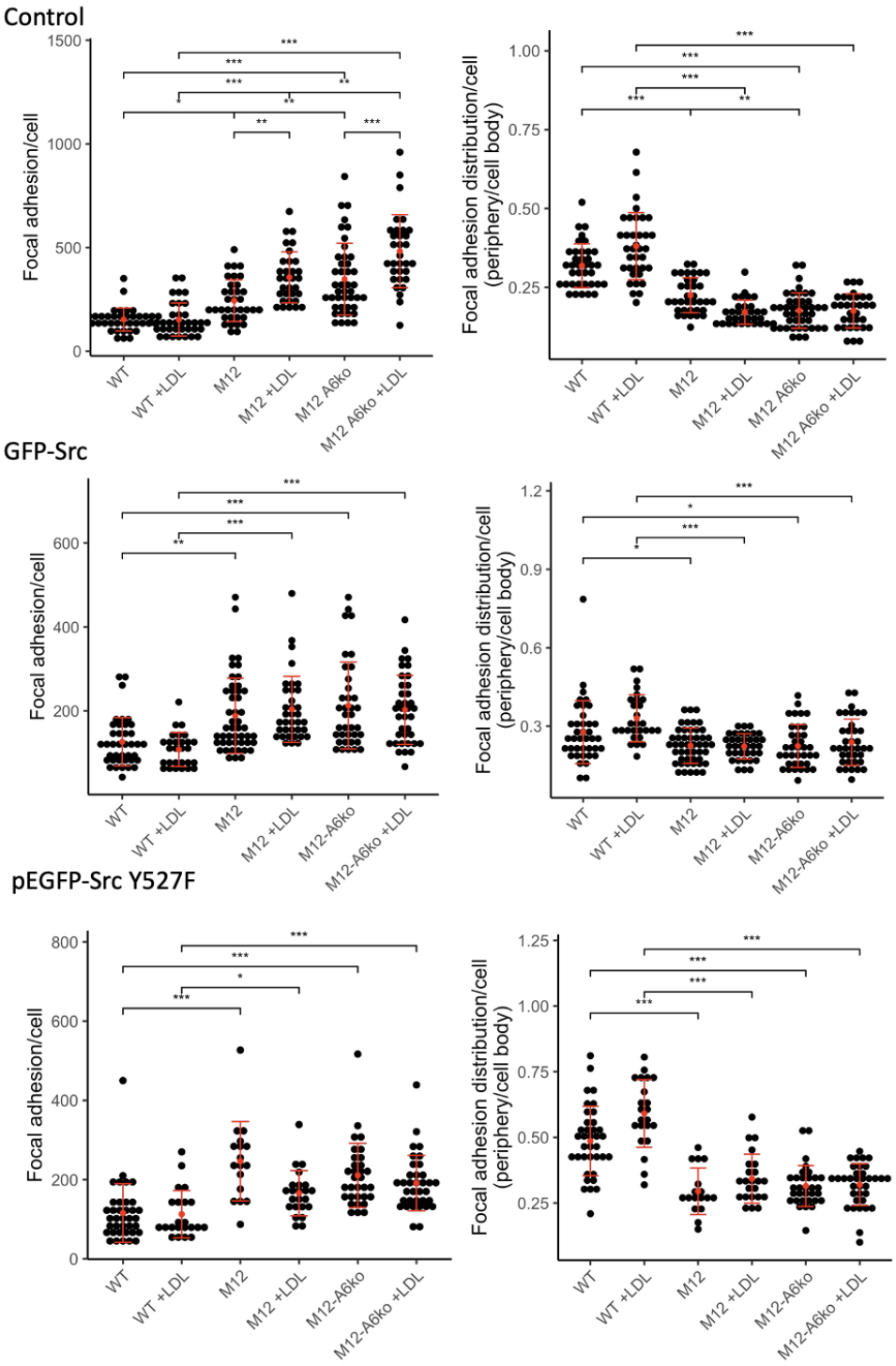

FIGURE 3.26: **Focal adhesion number and distribution in Src- and Src Y527F-overexpressing CHO WT, M12 and M12-A6ko cells.** The total number of FA (> 0.25 μm^2) per cell (WT: n = 35-43, M12: n = 28-48, M12-A6ko: n = 18-37 per cell line of two independent experiments) and their spatial distribution, the ratio of FA at the cell periphery vs. the cell body, were quantified with FIJI using pY861 FAK as FA marker. Cells were plated at $1.5 * 10^5$ cells/well of a 6-well plate and transfected with GFP-Src (Chapter 2.1.1), pEGFP-Src Y527F or remained untransfected (control). Cells were grown for 48h in media supplemented with lipoprotein-deficient serum (10% LPDS) and mevastatin (1μM) (Appendix B.25), starved for 2h and stimulated ± LDL (50 μg/ml) for 4h. Cells were fixed, stained for pY861 FAK and analysed by microscopy (Chapter 2.3.2). The mean ± SD is given. *p < 0.05, **p < 0.01, ***p < 0.001; two-way ANOVA with Tukey's post-hoc test.

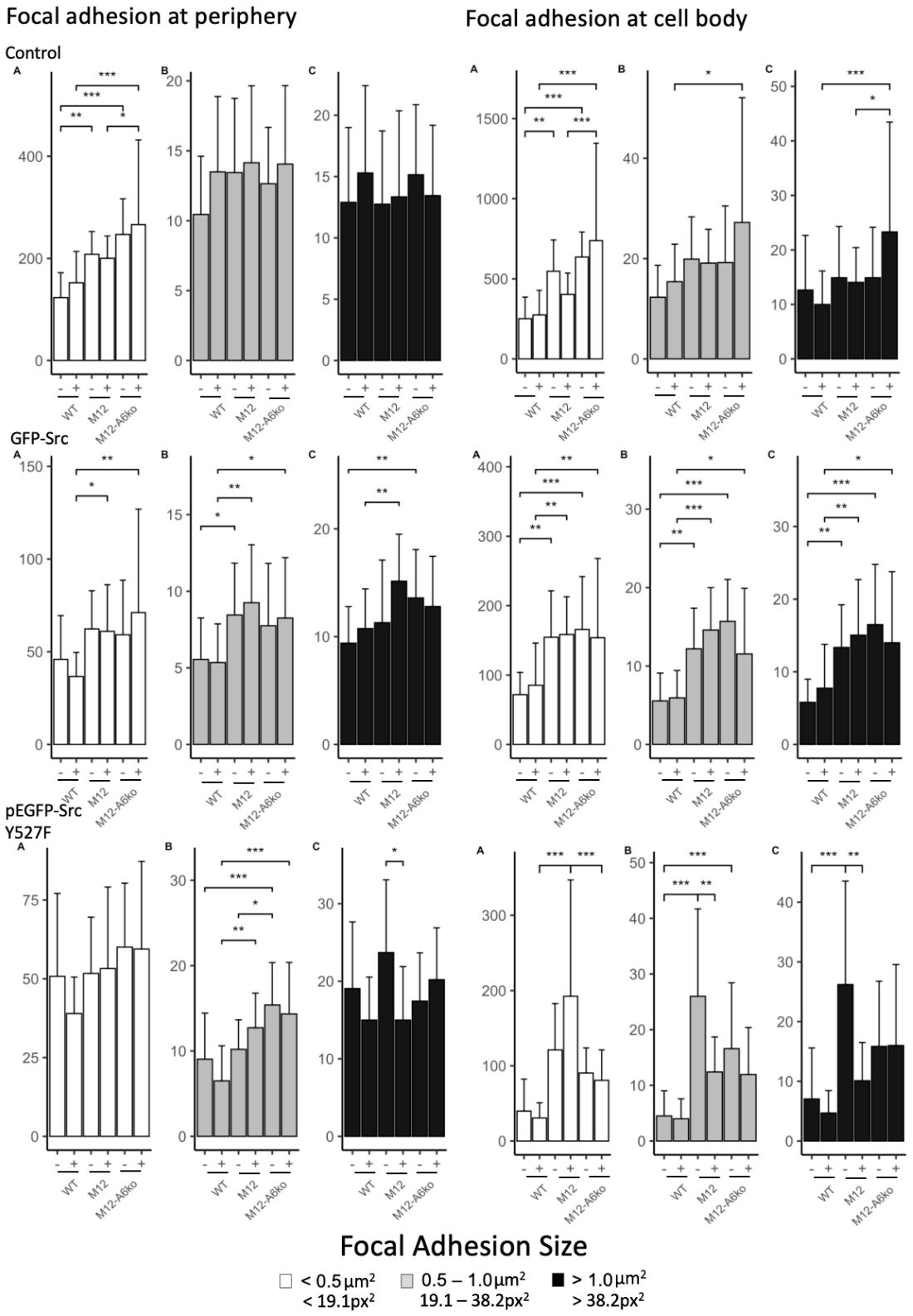

FIGURE 3.27: **Focal adhesion size in Src- and Src Y527F-overexpressing CHO WT, M12 and M12-A6ko.** The focal adhesion (FA) size at the cell edge and cell body of CHO WT, M12 and M12-A6ko (n = 30-31 per cell line of two independent experiments) was determined using FIJI. Cells were plated at $1.5 * 10^5$ cells/well of a 6-well plate and grown for 48h in full serum (10% FBS). Cells were fixed and stained for pY861 FAK and analysed by microscopy (Chapter 2.3.2), which was used as FA marker for counting. The mean ± SD is given. *p < 0.05, **p < 0.01, ***p < 0.001; two-way ANOVA with Tukey's post-hoc test.

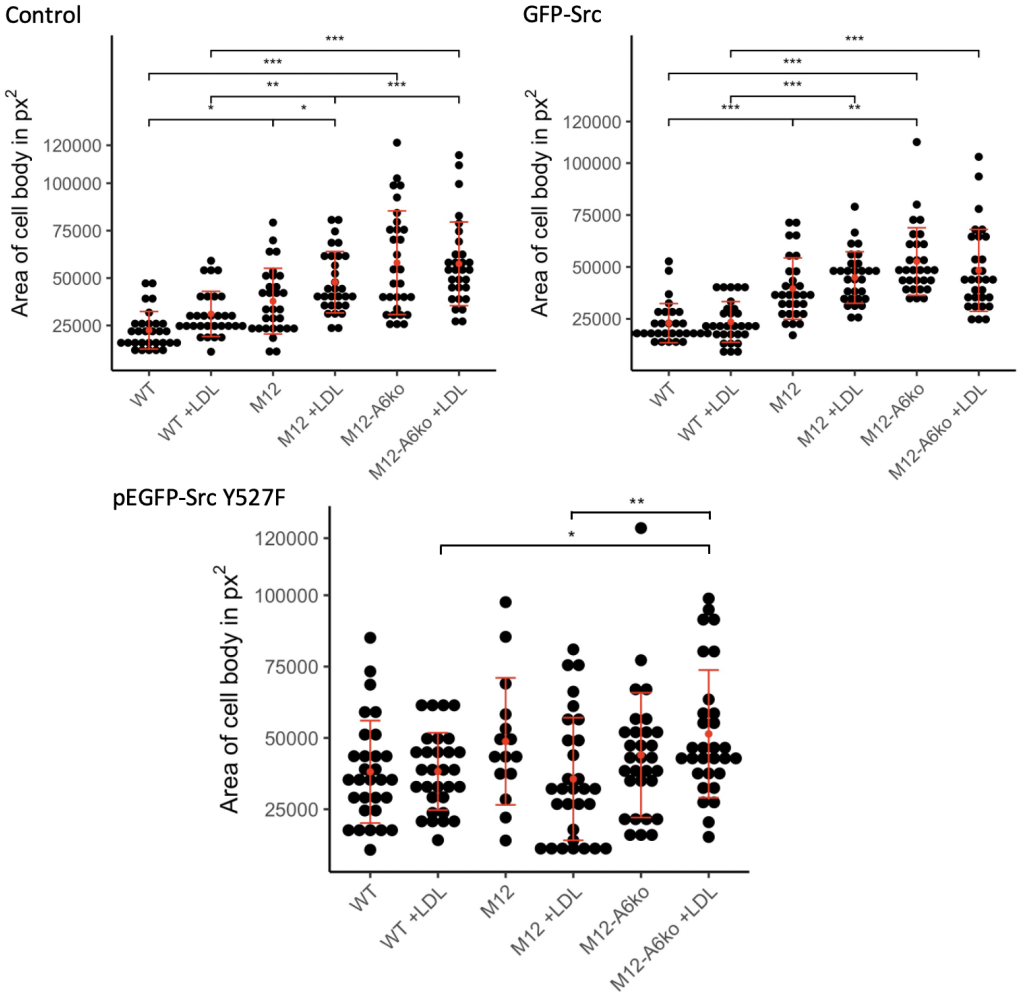

FIGURE 3.28: **Cell size of Src- and Src Y527F-overexpressing CHO WT, M12 and M12-A6ko cells.** The cell size of CHO WT, M12 and M12-A6ko (n = 30 per cell line of two independent experiments) was determined as area in pixel $(px)^2$ using FIJI. Cells were plated at $1.5 * 10^5$ cells/well of a 6-well plate and transfected with GFP-Src (Chapter 2.1.1), pEGFP-Src Y527F or remained untransfected (control). Cells were grown for 48h in media supplemented with lipoprotein-deficient serum (10% LPDS) and mevastatin (1μM) (Appendix B.25). Cells were starved for 2h and stimulated ± LDL (50μg/ml) for 4h. Cells were fixed and stained for pY861 FAK and analysed by microscopy (Chapter 2.3.2). The mean ± SD is given. *p < 0.05, **p < 0.01, ***p < 0.001; two-way ANOVA with Tukey's post-hoc test.

The decrease of total FA numbers in Src- and Src Y527F-overexpressing cells was linked to a reduction of small FA at the cell body and the cell edge (FIGURE 3.27). Ectopic expression of Src Y527F, moreover, increased the number of intermediate to large FA at the cell edge in all three cell lines.

Finally, the FA number was determined in relation to cell size. Although CHO WT, M12 and M12-A6ko cells differed in FA numbers, the spatial FA density, measured as FA number per px^2, and the spatial distribution of FA density were comparable across all cell lines, transfection-, and treatment-groups (FIGURE A.7). Src Y527F overexpression

also had a phenotype-reversing effect on the cell size (FIGURE 3.28). While in control and Src-overexpressing cells, the cell size significantly increased from WT to M12 to M12-A6ko cells, in Src Y527F-overexpressing M12 and M12-A6ko cells, size levels were comparable to WT cells. Stimulation with LDL had no effect on the cell size in any of the three cell lines analysed.

Overall, overexpression of Src and Src Y527F was associated with a decrease in the total number of FA, especially small FA in the cell body of M12 and M12-A6ko cells. While constitutive activation of Src was able to reverse the increased cell size observed in the NPC1 mutants and increase the rate of large FA at the cell edges, overexpression of WT Src was associated with a decrease in small, centrally located FA, but did not reverse the increased cell size observed in M12 and M12-A6ko cells. Furthermore, ectopic expression of Src Y527F rescued LDL-induced alterations in FA distribution in M12 but not in M12-A6ko cells, suggesting a potential inhibitory effect of AnxA6 depletion on LDL regulatory pathways involving Src signalling.

Chapter 4

Discussion

Cell growth, proliferation and migration are well-known features of neoplasms. These involve multiple cholesterol-dependent steps such as focal adhesion (FA) formation, rapid membrane expansion, and modification of signalling factors among others. As a structural element of the plasma membrane, especially of microdomains called lipid rafts, and other intracellular membranes, cholesterol plays a crucial role in regulating cell membrane-associated signalling and coordinating cell adhesion and migration (*162*).

The cellular cholesterol pool is fed either by *de novo* synthesis, or by dietary intake through receptor-mediated uptake of lipoproteins such as LDL and HDL. However, in tumour cells, oncogenic processes can upregulate cholesterol synthesis to meet the increased need for cholesterol and its metabolites for cancer cell proliferation and progression (*218*). Another mechanism for increasing intracellular cholesterol supply is the upregulation of LDL endocytosis. Studies have linked hypocholesterolaemia to increased LDL receptor (LDLR) activity in acute leukaemia, urinary bladder cancer and breast cancer (*176*). In MDA-MB-231 cells, an oestrogen receptor-negative breast cancer cell line that often serves as a model for aggressive cell behaviour, LDLR mRNA levels were twelvefold higher than in non-tumourigenic mammary epithelial cells (*9*). Migration of MDA-MB-231 cells decreased when grown under lipoprotein-depleted conditions and could be restored by LDL treatment in an acetyl-coenzyme A acetyltransferase (ACAT)-dependent manner. Thus, storing LDL-derived cholesterol as cholesteryl esters in lipid droplets for usage in cancer-related molecular events might provide an energetic adventage in cancer cell migration (*9*). ACAT is localised in the endoplasmatic reticulum (ER), pointing at the transfer of LDL-derived cholesterol from the late endosome (LE)/lysosome (Lys) compartment to the ER being associated with increased cancer cell migration. Although LDL-cholesterol transport routes were not investigated, these findings are consistent with studies that implicated LDL to stimulate cell migration. For instance, in the prostate cancer cell line PC-3, Moon and co-workers showed that diet-induced hypercholesterolaemia correlates with increased cell migration (*160*). Likewise, in transgenic mouse models of breast cancer, hypercholesterolaemia triggers tumour growth and metastasis (*7*, *141*). However, other

findings implicate cholesterol to have a limiting role on tumorigenesis. The cholesterol metabolite dendrogenin A was shown to inhibit breast cancer through cell redifferentiation (*43*). Also, hepatocellular carcinoma agressiveness was restricted by high levels of cholesterol, which was explained by impaired CD44-ezrin interaction due to CD44 translocation into lipid rafts (*263*). This suggests that cholesterol has a multifactorial effect on cells in the context of cancer.

The Grewal group has shown that the accumulation of cholesterol in LE of Niemann Pick type C1 (NPC1) mutant cells (CHO M12) and annexin A6 (AnxA6)-overexpressing CHO cells can impair cell migration and invasion (*59*, *189*). These findings highlight the role of exporting LDL-derived cholesterol to other organelles in order to promote cell motility. In follow-up studies, they found that depletion of AnxA6 restored cholesterol export from LE in mutant NPC1 cells (CHO M12-A6ko) (*155*).

Despite a role of LDL-cholesterol in cancer progression, the underlying mechanisms by which cholesterol affects cell migration remain to be clarified. It was speculated that restored cholesterol export from LE/Lys in AnxA6-depleted M12 cells could reverse the NPC1-mutated phenotype and restore the abilty of these cells to promote cell migration upon LDL exposure. Cell motility and invasiveness require dynamic coordination of FA assembly and disassembly. While the leading edge of cells is characterised by FA formation, FA degradation predominates at the rear end of cells. To investigate the role of cholesterol in FA (dis)assembly, the relative protein level of molecules involved in cholesterol homeostasis and FA dynamics was analysed by western blotting (WB) and FA formation was examined by microscopy, determining the number, distribution, size and colocalisation of FA markers in CHO wild type (WT), NPC1 mutant cells (CHO M12) and AnxA6-depleted CHO M12 cells (CHO M12-A6ko).

4.1 Characterisation of proteins involved in cholesterol homeostasis and focal adhesion assembly in CHO cells lacking NPC1 only or both NPC1 and AnxA6

4.1.1 The role of NPC1 loss of function on the expression of enzymes involved in cholesterol homeostasis and focal adhesion assembly

It was shown that loss of NPC1-dependent LDL cholesterol export pathways affects protein levels of cholesterol-modifying enzymes and the activation status of key signalling proteins of the cellular migration machinery.

The lipoprotein and cholesterol transporters (LDLR, ATP-binding cassette transporter A1 (ABCA1), CD36) are important regulators of the intracellular cholesterol content. LDLR protein levels are tightly regulated in a cholesterol-sensitive manner. LDLR increased in NPC-like mutants (CHO M87) (*57*) and LDL-induced downregulation was delayed in NPC mutants (*139*). In line with this, LDLR increased in CHO M12 and exposure of these cells to serum, which contains large amounts of LDL-like particles, was not sufficient to downregulate LDLR levels (FIGURE 3.2, 3.5). The unexpected decrease in LDLR levels in WT and M12 cells grown on delipidated media (FIGURE 3.7) may have been the result of insufficient antibody. ABCA1 mediates the key step of HDL particle formation triggered by lipid-free apoprotein A-I binding. ABCA1 expression can be regulated by cholesterol via liver X receptor (LXR)/ retinoid X receptor (RXR) signalling (*167*). In accordance with our results (FIGURE 3.1), in NPC1-depleted human fibroblasts, the protein level of ABCA1, which can efflux cholesterol from the PM, but also from LE (*30*), was reduced (*17*). CD36, also known as scavenger receptor class B member 3 that binds and internalises fatty acids, as well as cholesterol-rich lipoproteins (*171*), was increased in NPC1 mutant mice liver (*240*). The Nicholson group, however, showed that CD36, unlike LDLR, is upregulated by cellular cholesterol (*83*). Herein, the CD36 signal was not suitable for densitometric analysis.

The maturation of sterol-regulatory-element-binding protein 2 (SREBP2) is widely known to be sensitive to cholesterol delivery from LE (*22*, *142*). When cholesterol levels are low, SREBP2 is processed to its mature form (*91*). In the literature, NPC1-lacking CHO cells showed delayed suppression of SREBP2 maturation upon LDL incubation during the first 24h (*123*, *155*). However, in this work the SREBP2 signals were not suitable for densitometric analysis (FIGURE 3.1).

Rab7 (small RAS-related GTP-binding protein) and Tre-2/Bub2/Cdc16 1 domain family member 15 (TBC1D15) play an important role in LE/Lys structure and function including the formation of membrane contact sites (MCS) to enable non-vesicular lipid transport (*23*, *32*, *155*). Alike published data (*154*, *155*), Rab7 was stably expressed at steady state (FIGURE 3.1) and TBC1D15 throughout the experiments in all cell lines (FIGURE 3.2, 3.2, 3.5, 3.9, A.5). However, in NPC1 mutants grown in 10% FBS (growth media) and starved (± 20% FBS), Rab7 increased (FIGURE 3.2, 3.7), but when grown in delipidated media and starved (± 20% FBS) Rab7 decreased in CHO M12-A6ko cells (FIGURE 3.9). In double-stimulated CHO cells, Rab7 levels were inconclusive (FIGURE 3.9) and in migrating cells (scratched ± 20% FBS) comparable across cell lines (FIGURE A.5). In the liver and artery, cholesterol-loading was linked to an up-regulation of Rab7 (*116*). Assuming such an effect, it is unclear why the NPC1 mutants, but not WT cells, are sensitive to changes in cholesterol levels. To confirm a role of LDL-cholesterol and AnxA6 on differential Rab7

expression, more data is required.

The lipases hormone-sensitive lipase (HSL) and adipose triglyceride lipase (ATGL) are capable of mobilising stored cholesterol by hydrolysing cholesteryl esters in lipid droplets (*6*, *275*). Under high-fat conditions, ATGL expression is downregulated by increased mammalian target of rapamycin complex 1 (mTORC1) activity (*29*), while HSL expression is stimulated (*15*). Herein, HSL and ATGL both were comparable in WT and M12 cells at steady state (FIGURE 3.1), thus their regulation may not be dependent on NPC1-mediated LDL-cholesterol trafficking. Moreover, in contrast to HSL, ATGL has only low substrate affinity for cholesteryl esters (*275*).

Phosphorylation of focal adhesion kinase (FAK), Src kinase and p130 crk-associated substrate (p130Cas) are key regulatory mechanisms in FA dynamics. FAK activation by autophosphorylation at tyrosine residue 397 (pY397) creates a docking site for Src kinase which when binding to it, triggers autophosphorylation of Src kinase at position Y416 (pY416). An Y416-phosphorylated Src then is able to phosphorylate Y861 FAK (pY861) (*26*, *135*, *272*), while phosphorylation of p130Cas is one of the many downstream targets of Src and FAK signalling (*135*). The Grewal group recently demonstrated that cholesterol accumulation in LE through loss of NPC1 function (CHO M12) inhibits cell migration and invasion (*59*, *189*). At steady state (FIGURE 3.3), in overnight starved and double-stimulated cells (FIGURE 3.6), pY861 FAK and pY416 Src levels dropped in CHO M12 and M12-A6ko cells, indicating reduced FA dynamics in NPC1 mutants. Interestingly, it appeared as overnight starvation may already lead to FAK activation independent of serum stimulation, as there was pronounced pY861 FAK levels in all cell lines independent of stimulation (FIGURE 3.6A+E). Moreover, Src activation upon serum stimulation was evident in CHO WT, M12 and M12-A6ko cells that were grown in 10% FBS and starved overnight (FIGURE 3.4), but not after starvation for 2h only (FIGURE 3.8), where pY416 Src levels decreased upon stimulation. It is generally believed that serum activation and induction of wound closure results in Src activation, but unexpectedly, pY416 Src levels decreased in scratched and serum-treated samples for all cell lines by 30-50% (FIGURE 3.6). This was also seen under starved and delipidated conditions. Since the decrease in pY416 Src levels has been repeatedly observed (FIGURE 3.6, 3.8, 3.10, A.4), one cannot rule out yet unkown alternative mechanism that regulate Src activity in NPC1- and AnxA6-depleted cells. However, the observation could be due to Src downregulation upon prolonged exposure to a stimulus (20% FBS), or redistribution of activated Src into specialised microdomains (lipid rafts) (*101*, *251*) that do not dissolve well in Triton-containing lysis buffers. Another approach to explaining the reduced amounts of phosphorylated pY416 Src may lie in the cell detachment that triggers the displacement and degradation of phosphorylated Src in autophagosomes (*210*). However, the decrease observed for pY416 Src

levels was not reflected in the increase of LC3-II, which would have indicated increased autophagy in externally stimulated CHO cells. Although p130Cas is regulated by Src and FAK signalling (*135*), the WB analysis showed little correlation between the phosphorylation patterns of p130Cas, Src and FAK in our experiments (FIGURE 3.6, 3.8). Regardless of the Src phosphorylation status, pY861 FAK levels were elevated in all cell lines, whether stimulated by serum or not, indicating that starvation could trigger Y861 FAK activation by mechanisms other than Src signalling. Another member of the Src kinase family that has been linked to FAK is Fyn (*16*). Baillat and colleagues demonstrated colocalisation of Fyn and FAK in early adhesion complexes of colorectal cancer cells. Since Fyn is palmitoylated in contrast to myristyolated Src (*16*), it might show a different distribution behaviour along the cell membrane in the absence of raft cholesterol. Furthermore, recruitment of Fyn rather than Src to the leading edge was associated with rigidity-induced cell spreading, which was dependent on palmitoylation of Fyn (*121*). The authors showed Fyn-mediated phosphorylation of p130Cas, supporting the hypothesis that in NPC1 mutant cells, cell spreading and phosphorylation of Y861 FAK and p130Cas may be due to other Src family members such as Fyn. However, more data is needed to draw conclusions.

4.1.2 The role of NPC1 and AnxA6 loss of function on the expression of enzymes involved in cholesterol homeostasis and focal adhesion assembly

Despite the ability of AnxA6 depletion to restore cholesterol export from NPC1 mutant cells, these alternative cholesterol transport routes do not seem to simply reinstate protein levels of endosomal enzymes and phosphoproteins involved in FA dynamics.

Although LDLR can be regulated by the intracellular cholesterol content (*139*), LDLR levels were unexpectedly high in M12-A6ko cells and not reversible by serum (FIGURE 3.2), suggesting that AnxA6 does not re-establish the feedback loop that controls LDLR expression in NPC1 mutant cells. Interestingly, in double-stimulated, migrating CHO M12-A6ko cells, LDLR levels returned to a protein level comparable to that of WT cells (FIGURE 3.5), suggesting AnxA6-independent regulatory mechanisms during migration. Lacking restoration of ABCA1 in CHO M12-A6ko cells to protein levels observed in WT (FIGURE 3.1) cells may indicate impaired post-endosomal cholesterol distribution in the absence of AnxA6 or a direct role of AnxA6 in the regulation of lipoprotein and cholesterol transporters. Unexpectedly, HSL and ATGL increased in AnxA6-depleted CHO M12 cells (FIGURE 3.1). This opposes results derived from adipose tissue from Grewal and collegues, which showed unaltered ATGL and slightly reduced but insulin-inducible HSL expression

in AnxA6-depleted adipocytes (*122*). At steady state, AnxA6 depletion did not restore pY861 FAK or pY416 Src levels (FIGURE 3.3), however, in overnight starved CHO cells, there was pronounced pY861 FAK activation in all three CHO cell lines (FIGURE 3.4). This suggests that starvation may already lead to FAK phosphorylation despite lack of NPC1 and AnxA6. Moreover, serum-inducible Src activation was present in starved CHO M12-A6ko cells (FIGURE 3.4).

4.1.3 Autophagy in CHO cells lacking NPC1 and AnxA6

Loss of AnxA6 function was linked to increased autophagic processes in NPC1 mutants. The transformation of cytosolic LC3-I to the membrane-bound form LC3-II has been established as a marker of autophagy, a process inducible by starvation and linked to cholesterol storage in lipid droplets (*100*). Alike Ishibashi and co-workers (*100*), an increase in LC3-II levels was observed in the NPC1 mutant cell lines, particularly in AnxA6-depleted CHO M12 cells (FIGURE 3.2, 3.5, 3.9, A.3, A.5). This is in contrast to findings from Sun and colleagues who showed impaired starvation-induced autophagy in the absence of AnxA6 (*230*). The increase of LC3-II levels in AnxA6-depleted CHO M12 cells may indicate a cellular functional state in which cholesterol homeostasis cannot be maintained by autoregulation. In cardiomyocytes, starvation-induced autophagy was associated with increased Rab7 expression mediated by the sirtuin 1 (Sirt1)- forkhead box protein O1 (FoxO1) pathway (*85*).

The increased Rab7 levels observed in overnight-starved and serum-stimulated CHO M12 and M12-A6ko cells, together with the increase in LC3-II expression (FIGURE 3.2), may therefore indicate a limited resistance of these cells to starvation. Furthermore, the downregulation of Rab7 in starved and double-stimulated NPC1 mutants, especially in CHO M12-A6ko cells, could be interpreted as a decrease of autophagic processes upon the dual stimulation, which was also reflected in the lowering of LC3-II levels. Stimulation of migrating (scratched) cells with FBS only, though, did not decrease LC3-II levels in CHO M12-A6ko cells (FIGURE A.5), suggesting a role of the intensified migration stimulus to overcome autophagy. However, results require confirmation before further conclusions can be drawn. Comparing CHO cells grown on 10% FBS to cells on cholesterol-depleted media (LPDS-statin media) (FIGURE 3.7), the 2-hour starvation period was associated with a similar increase in LC3-II in CHO WT and NPC1 mutant cells grown on LPDS. When grown on regular growth media, this rise was only seen in NPC1 mutants, supporting the hypothesis of higher susceptibility to starvation under regular growth conditions.

At steady state, increased ATGL in CHO M12-A6ko cells, could have been an early indicator of autophagosome formation, while Rab7 levels were unchanged. ATGL plays an important role in autophagy-mediated lipid mobilisation from lipid droplets (*204*).

Sathyanarayan and colleagues showed ATGL to induce autophagy and lipophagy, alike Rab7, via Sirt1 activation in hepatocytes (*204*).

It should be noted that some expression patterns observed in these multiscratched lysates are slightly different to the expression profiles observed in cells that were not migrating into a wound, but also stimulated with serum. Besides expression changes that may occur when comparing migrating versus non-migrating cells, it also cannot be excluded that the wound-making for the multiscratch assays induced a redistribution of proteins inside cells, rendering them less soluble in the Triton-containing lysis buffer. Indeed, activation of cell migration has been associated with the redistribution of proteins into Triton-insoluble, cholesterol-rich fractions, so called lipid rafts (*101*, *152*).

Taken together, cholesterol sequestration by loss of NPC1 function was shown to affect the level of proteins involved in cholesterol homeostasis and also the activation status of FA markers. Although loss of AnxA6 function may induce cholesterol exit from the LE/Lys compartment, the additional AnxA6 knockdown in CHO M12 rarely reversed the effect of NPC1 deficiency. This suggests a role of AnxA6 in post-LE/Lys cholesterol distribution. The cholesterol imbalance in NPC1 mutant cells, however, does not lead to a complete loss of Src, FAK and p130Cas phosphorylation, thus cholesterol- and AnxA6-dependent signalling pathways need further characterisation. Moreover, NPC1 mutants showed an increase of autophagic markers especially in AnxA6-depleted CHO M12 cells, despite the loss of the AnxA6-induced pro-autophagic effect. However, experimental replication is needed to confirm these findings.

4.1.4 Characterisation of focal adhesion formation in CHO cells lacking NPC1 and AnxA6

It was speculated that cholesterol release upon AnxA6 depletion in M12 cells could improve cholesterol delivery to the periphery to support FA formation at the cell edge. In line with findings from Grewal and co-workers (*155*), the restoration of cholesterol transport to the cell edge in AnxA6-depleted M12 cells was shown (Figure 3.21, 3.22, 3.23).

However, the NPC1 mutant phenotype was not fully rescued. Loss of NPC1 function was associated with an increase in total FA numbers and a shift in spatial FA distribution towards the cell body (Figure 3.11, 3.12). Reminiscent of the latter phenotype, in fibroblast-like cells, FAK deficiency has been associated with increased FA formation and decreased cell motility (*99*). Despite restoration of cholesterol release from LE in

M12-A6ko cells, these trends persisted. This suggests that AnxA6 plays a role in FA (dis)assembly that may go beyond cholesterol trafficking.

Nervertheless, loss of AnxA6 function in CHO M12 partially restored colocalisation of FA markers and cholesterol (FIGURE 3.21, 3.22, 3.23). In WT cells, vinculin- and paxillin-labelled FA were predominantly at the cell edge and in close proximity to D4H-labelled cholesterol. In contrast, the number of centrally located FA increased in M12, but there was less colocalisation with cholesterol. In AnxA6-deficient M12 cells, the increased number of central FA remained but more adhesion complexes were concentrated on the peripheral PM, where vinculin and paxillin often colocalised with cholesterol, as judged by the microscopic impression. It was speculated that delivery of LE-derived cholesterol to recycling endosomes might explain the often scattered peripheral D4H staining. Taken together, these results suggest that depletion of AnxA6 in M12 cells restores cholesterol transport to the cell edge, allowing spatial association of cholesterol derived from LE with FA structures.

Interestingly, constitutive activation of Src was associated with a decrease in the total number of FA and the cell size as well as with an increase of large FA at the cell edge (FIGURE 3.25, 3.26, 3.27). Overexpression of EGFP-Src Y527F greatly reduced the central blurry signal seen in CHO M12 and M12-A6ko cells, also that of anti-pY861 FAK. Src transport and activation from the perinuclear compartment to the PM has been linked to Rab11-positive endosomal transport (*201*) and the spatial pattern of recycling endosomes, as judged by Rab11 visualisation (*66*, *203*), is similar to the distribution of the blurry signal described in here. As pFAK also is transported by recycling endosomes in a cholesterol-sensitive manner (*231*), it could be speculated that overexpression of the constitutively active Src mutant might reduce the localisation of Src and pFAK in perinuclear recycling endosomes.

As part of the FAK-Src-paxillin-p130Cas-ERK-MLCK axis, Src is an important regulator of adhesion turnover (*130*, *254*). This suggests that constitutive activation of Src overcomes a failure of FAK activation in NPC1 mutants. Furthermore, ectopic expression of Src Y527F partially restored LDL-inducible alterations in FA distribution in M12 but not in M12-A6ko cells, indicating a potential inhibitory effect of AnxA6 depletion on LDL-regulatory pathways affecting Src signalling.

4.2 Focal adhesion dynamics depend on cholesterol balance

FA assembly is a complex and multi-step process that requires signalling events controlled by Src and FAK kinases, among others. Substantial amounts of Src are located in LE/Lys,

and upon activation, Src translocates to the cell surface where it binds to autophosphorylated pY397 FAK. The trafficking of Src from LE/Lys to the cell surface is regulated by SNARE proteins, several of those operating in a cholesterol-sensitive manner (*51*, *88*, *111*, *221*, *259*). Src binding to activated FAK then mediates the phosphorylation of FAK at Y861 and the formation of the dual kinase complex FAK-Src, which interacts with downstream signalling factors such as PI3K, p130Cas or paxillin (*130*, *158*, *221*). FA are associated with cholesterol-containing microdomains (lipid rafts) and require cholesterol for proper functioning (*88*). Moreover, upon cholesterol depletion, studies showed differential regulation of FAK and Src activity (*101*, *170*, *251*), thus indicating that the communication of Src and FAK in FA could occur in a cholesterol-sensitive manner. While recent findings from the Ikonen group coupled delivery of LDL-cholesterol to FAK activation in recycling endosomes (*231*), the roles of NPC1 and AnxA6 and its consequence for FA assembly and distribution remain unknown.

4.2.1 Intracellular cholesterol distribution can regulate focal adhesion dynamics

It was demonstrated that loss of the NPC1-dependent LDL-cholesterol export pathways appear to affect the activation status of important signalling proteins of the cellular migration machinery. Nevertheless, pY397 FAK phosphorylation was observed in all three cell lines (FIGURE 3.3), suggesting that FAK phosphorylation also occurs even when NPC1-dependent cholesterol export routes from LE/Lys to other cellular sites are compromised. FAK autophosphorylation at Y397 is an established marker for cell migration and invasiveness (*98*, *128*), however, despite FAK being phosphorylated at this tyrosine residue, studies showed decreased migratory behaviour in CHO M12 cells (*59*, *189*). Similar findings, i.e. the presence of pY397 FAK and a simultaneous reduction of pY416 Src and pY861 FAK levels were also found in cells in which cholesterol-sensitive endosomal recycling was defective (*51*, *221*). Expression of the dominant-negative (E329Q) N-ethylmaleimide-sensitive fusion protein (NSF), whose inhibition prevents the disassembly of SNARE complexes and thus membrane trafficking, or truncated SNAP23 (SN23C49) impaired Src redistribution from the perinuclear Rab11-containing compartment to the cell edge. This was accompanied by a reduction of Y416 Src and Src-dependent FAK phosphorylation, though did not affect pY397 FAK levels. Confirming the importance of cholesterol-sensitive Src redistribution to the periphery, overexpression of the membrane-targeted Src mutant Src-CAAX but not overexpression of Src WT restored FAK - Src signalling (*221*).

FA dynamics include the recycling of FA components from rear cell to establish new adhesion contacts at the leading edge, a process which is coordinated by cholesterol-

sensitive soluble N-ethylmaleimide-sensitive-factor attachment receptor (SNARE) proteins. Several SNARE proteins, including vesicle-associated membrane protein (VAMP) 2/3, syntaxin (Stx) 3/4/6 and synaptosome-associated protein 23 (SNAP23), are critical regulators of membrane transport along exocytic routes and involved in β1 integrin recycling (*195*). In particular VAMP3 and Stx6 were important for $\alpha 5\beta 1$ integrin and of FAK localisation at the PM (*235*). When cholesterol levels in the trans-Golgi network (TGN) were low, Stx6 mislocalised to recycling endosomes, compromising Stx6-dependent integrin recycling (*189*). Src delivery to the leading edge depends on the SNARE proteins Stx12 and SNAP23 (*259*). To form invadopodia Src and receptor tyrosine kinases, such as epidermal growth factor receptor (EGFR), need to translocate to the target membrane for β1 integrin-induced SNARE protein activation, membrane fusion, and phosphorylation of the Src-EGFR complex (*259*).

Other studies also support cholesterol-related regulatory circuits for Src and FAK activation at the cell surface. Jeon and co-workers studied the role of raft cholesterol depletion on non-small cell lung cancer (NSCLC) cell migration (*101*). In agreement with the results in here, they showed a loss of pY416 Src levels in cells treated with MβCD and lovastatin. Since the interactions between FAK - Src, FAK - paxillin and FAK - vinculin were not affected by the depletion of cholesterol from the lipid rafts, the authors suggested that the reduced phosphorylation of Y416 Src was associated with the displacement of the FA complex from the raft (*101*).

Moreover, the spatial distribution of FA complexes determined by anti-pY861 FAK, GFP-paxillin, GFP-vinculin and GFP-Src staining was analysed (Figure 3.11, 3.16, 3.19, 3.26). Reminiscent of raft cholesterol depletion studies disrupting FA complex formation (*251*), FA assembly decreased at the cell edge of NPC1-depleted CHO cells (CHO M12) and AnxA6-depleted M12 cells (CHO M12-A6ko). However, increased FA levels in the cell body were observed in these NPC1-depleted cell lines, suggesting that loss of NPC1 does not completely block FA formation. Thus, in the absence of NPC1, alternative cholesterol transport pathways or FA signalling pathways may dominate, resulting in a different spatial pattern of FA within cells. Alike the results herein, Wang *et al.* observed an increase in the average FA number when A375 cells were treated with MβCD for 3h (*251*).

The cholesterol imbalance in NPC1 mutants was accompanied by marked cell spreading, which may reflect the upregulation of FA numbers within the cell body, facilitating increased cell adhesion (Figure 3.11, 3.16, 3.19, 3.28). This is in contrast to other studies in which cholesterol depletion by MβCD or inhibition of cholesterol-sensitive exocytic transport was associated with reduced cell spreading (*51*, *221*, *251*). However, Ilić and

colleagues reported cell spreading and an increase in centrally located and total FA in FAK-deficient cells (*99*).

Notably, AnxA6 knockout in NPC1 mutant CHO M12 cells, which was linked to a (partial) restoration of cholesterol release (FIGURE 3.22, 3.21, 3.18), failed to restore Src and FAK phosphorylation patterns as well as FA dynamics observed in WT cells. This could indicate insufficient cholesterol exit from the LE/Lys compartment or a separate role for AnxA6 in regulating post-endosomal cholesterol transport or recycling pathways.

4.2.2 Focal adhesion turnover requires Src kinase activity

Herein, ectopic expression of constitutively active Y527F Src, but not WT Src, reversed the number, distribution and cell size of FA in CHO M12 and M12-A6ko cells (FIGURE 3.26, 3.28). In addition, LDL inducibility was partially restored in CHO M12 cells. Skalski and colleagues showed that overexpression of PM-targeted Src overcomes SNARE-defective Src maintenance in the Rab11-containing recycling compartment (*221*). However, overexpression of WT Src or C-terminal truncated constitutively active Src, in contrast to constitutively active Y527F Src in here, were unable to restore FA turnover (*221*). Underlining the importance of PM association, defective Src myristoylation was associated with inhibition of Src-mediated cell transformation (*25*) and the formation of "intracellular" FA (*54*). The latter also was seen for kinase-inactive Src mutants (*54*). Since Y527F Src though not C-terminal truncated constitutively active Src seems able to restore FA turnover, it remains to be clarified whether both depend on cholesterol-sensitive and SNARE-mediated transport to the cell membrane. One could envisage that Y527F Src may not locate in the same compartments as WT Src. However, the mutant Y527F Src does not depend on dephosphorylation of Y527 by the transmembrane protein tyrosine phosphatase (PTP) α to enable autophosphorylation of Y416 Src (*84*), so that membrane association might not be a prerequisite for kinase activity.

The potential underlying mechanism by which Src could control FA turnover is by negatively regulating the RhoA/ROCK axis. During lipid raft disruption Src dislocates from rafts causing excessive F-actin formation by increased RhoA/ROCK signalling which counteracts FA disassembly (*251*). In human melanoma cells treated with MβCD, Wang *et al.* observed an increase in average FA number and a change in spatial distribution, resulting in colocalisation with prominent F-actin fibres in the cell body. The underlying mechanism by which Src controls FA turnover is by negatively regulating the RhoA/ROCK axis (*251*).

Taken together, the localisation of Src at the cell membrane and its kinase activity play a crucial role in coordinating FA turnover. The restoration of cholesterol export from LE/Lys to other cellular sites, such as the ER, lipid droplets and most likely the cell surface,

by depletion of AnxA6 in NPC1 mutants, did not appear to be correlated with changes in Src translocation or its activation at the cell membrane.

4.3 The role of AnxA6 in focal adhesion formation

AnxA6 knockdown has been shown to enable cholesterol exit from the LE/Lys compartment of NPC1 mutant cells (*155*). Since cholesterol sequestration resulted in reduced cell migration, it was speculated that restored cholesterol transport to the cell edge could rescue cell migration. In support of this hypothesis, AnxA6-depleted M12 cells showed increased amounts of cholesterol at the cell edge, as measured by mCherry-D4H signals, and increased colocalisation with pY861 FAK and GFP-vinculin compared to M12 cells (FIGURE 3.21, 3.22, 3.23, 3.24). Moreover, in a migration (scratch) assay, the Grewal group showed increased migratory activity of CHO M12-A6ko cells compared to M12 cells (*104*). Despite the cholesterol release in AnxA6-depleted NPC1 mutants, the total number of FA, spatial distribution and cell size were reminiscent of the phenotype of NPC1 mutants (FIGURE 3.11). At steady-state, levels of pY416 Src and its substrate pY861 FAK were decreased in CHO M12 and M12-A6ko cells, and the amount of p-p130Cas was also reduced in both mutant cell lines (FIGURE 3.3). This suggests that cholesterol delivery to the cell periphery and association with FA is (partially) restored, but that FA signalling and turnover, as indicated by the FA pattern, is still pending. Since there was no complete restoration, AnxA6-knockout-induced cholesterol exit may be insufficient or there might be further functions of AnxA6 in cell migration-associated signalling.

4.3.1 AnxA6 and cell migration

AnxA6 is a Ca^{2+}-sensitive scaffolding protein that when overexpressed, inhibits cell migration and invasiveness. In contrast, AnxA6 depletion was linked to increased cell motility (*59*). The inhibitory effect on cell migration is mainly attributed to AnxA6-induced cholesterol sequestration in the Lys/LE compartment, which impairs the cholesterol-promoting coordination of SNARE proteins and the exocytic transport of membrane and FA proteins to the cell surface (*77*). However, the regulatory role of AnxA6 in cell migration appears more complex and other AnxA6-related features should also be considered.

AnxA6 plays a crucial role in membrane microdomain organisation through Ca^{2+}-dependent binding to phospholipids, association with cholesterol-rich membranes, direct interaction with the actin cytoskeleton, and coordination of the recruitment and transport of other lipids and proteins to the surface (*14*, *38*, *49*). As binding partners of F-actin and membrane-associated phospholipids, annexins have been suggested to play a role in

receptor-mediated endocytosis and cell migration (*35*). Through interaction with spectrin and recruitment of the protease calpain I, AnxA6 is involved in LDLR endocytosis by promoting the detachment of clathrin-coated vesicles from the cell surface (*78*), and also in the transport of LDL from the pre-lysosomal compartment to lysosomes for degradation (*180*). Thus, impaired LDLR recycling due to loss of AnxA6 function could lead to a compensatory upregulation of LDLR levels, as observed in CHO M12-A6ko cells (FIGURE 3.1, 3.2).

As a scaffold protein, AnxA6 plays a role in the spatiotemporal regulation of membrane receptor signalling. Grewal and co-workers showed that AnxA6 modulates EGFR, platelet-derived growth factor (PDGF) receptor (PDGFR) and scavenger receptor B1 (SRB1) signalling, e.g. by interacting with the GTPase-activating protein p120GAP, which inhibits Ras, i.e. in EGFR/Ras/mitogen-activated protein kinase (MAPK) signalling, or by mediating protein kinase C (PKC) α-mediated threonine phosphorylation and inactivation of EGFR, both of which have proliferation inhibitory effects (*35*). In cancer, these AnxA6-related aspects may also modulate tumour metastasis and invasiveness via these signalling partners, as downstream of EGFR, Ras and p120GAP signalling, several pathways, including p190Rho-GAP, FAK, and integrin signalling, play a role in cell migration. The AnxA6/p120GAP complex, thus, could play a role in regulating cell polarity, FA turnover, and actin-cytoskeletal dynamics (*77*). Morever, AnxA6 may regulate cell migration by association with several members of the Src kinase family (*77*). The lack of FA turnover in AnxA6-depleted CHO M12 cells, which could be overcome by overexpression of constitutively active Src, could therefore be a consequence of the latter features.

As a positive regulator of autophagy, AnxA6 may play a role in autophagy-mediated FA degradation, which is critical for migration speed. In head and neck squamous cell carcinoma, AnxA6-induced autophagy by inhibtion of Akt and mTOR phosphorylation was linked to metastasis and invasion (*250*). Thus, AnxA6 depletion could impair autophagy-mediated FA degradation and therefore limit the rate of FA turnover. However, elevated LC3-II levels in CHO M12-A6ko indicate that autophagy is still upregulated in the absence of AnxA6.

Overall, AnxA6 plays an important role in coordinating membrane organisation and spatiotemporal regulation of cell surface receptor signalling. As a direct binding protein of F-actin and the cell membrane, AnxA6 coordinates receptor-mediated endocytosis and cell migration. Regarding its role in cholesterol homeostasis, depletion of AnxA6 has been associated with increased cell migration (*59*). However, in oesophageal squamous cell

carcinoma, depletion of AnxA6 resulted in decreased cell motility (*53*), so downstream signalling of AnxA6 appears to be differentially regulated. As described above, in AnxA6-depleted NPC1-deficient CHO cells, redistribution of cholesterol and restored FA assembly at the cell periphery was shown, although an increase in centrally localised FA was maintained, reminiscent of the NPC1 mutant phenotype. Accordingly, pY416 Src and its substrate pY861 FAK were reduced at steady-state. In light of these results, it could be hypothesised that AnxA6 knockout did not fully restore cholesterol balance or its depletion blocks AnxA6-dependent actin-cytoskeletal dynamics required for FA turnover. As a regulator of intracellular Ca^{2+} homeostasis (*159*), AnxA6 knockout-induced Ca^{2+} imbalance could interfere with Ca^{2+}-sensitive cytoskeletal rearrangements.

4.4 Evaluation of the methodological approach

4.4.1 Experimental models and methods for the investigation of the role of cholesterol on focal adhesion formation and cell migration

To investigate the role of cholesterol in FA and cell migration, a cell model of CHO cells lacking the cholesterol transporter NPC1 was chosen (CHO M12). The loss of NPC1 function results in cholesterol accumulating in the Lys/LE compartment and not being transported to the ER, Golgi, recycling endosomes and the cell surface (*38*, *189*, *190*). The PM contains approximately 80% of cellular cholesterol, and to investigate the role of cholesterol in this location on cellular functions, previous studies have used MβCD to disrupt the PM structure via cholesterol depletion. However, MβCD treatment also affects cholesterol levels and distribution in endomembranes and may also alter the membrane distribution of other lipids, such as phospho- and sphingholipids (*274*). Thus, loss of NPC1 function appears to promote membranous cholesterol depletion in a more physiological way.

The most common methods for loss of NPC1 function include the use of NPC1 inhibitors (U18666A) (*145*), itraconazole (*143*), stable expression of NPC1 mutants (*39*, *168*) or knockout of NPC1 (*156*), the latter being the most reliable condition for loss of NPC1 function. Accordingly, overexpression of AnxA6 leads to a cholesterol phenotype similar to that of NPC1 mutants (*38*), yet other AnxA6-related activities upon overexpression (see Chapter 1.3) may not have provided a suitable cell model. On the other hand, depletion of AnxA6 restored cholesterol export in NPC1 mutant cells. To test whether this observation could have an impact on FA formation, an AnxA6-depleted CHO M12 cell line (CHO M12-A6ko) was used. However, in line with the multitude of AnxA6 functions

(*75*), AnxA6 depletion in CHO M12 cells did not simply reverse the full NPC1 mutant phenotype. While the studies shown here have focused on cholesterol transport exiting LE/Lys in NPC1 mutant cells, it should be noted that NPC1 also regulates the transport of sphingomyelin and glycosphingolipids (*138*). Thus, the retention of other lipids can directly or indirectly influence cell migration, which must be taken into account when interpreting the results.

Two approaches were used to study FA dynamics under different conditions: First, membrane-bound cholesterol and FA were directly visualised using fluorescence microscopy, allowing the number, distribution and size of FA, as well as cell size, to be determined and compared in cells incubated under different conditions. In addition, protein levels of receptors, transporter enzymes and kinases involved in cholesterol homeostasis and FA signalling were compared by WB, which may provide additional insight into the ability of cells to assemble FA under cholesterol-rich or cholesterol-deficient conditions.

Visualisation and analysis of intracellular cholesterol trafficking under physiological conditions have been technically challenging. Different approaches to visualise cholesterol include the use of sterol-binding biomolecules such as filipin, fluorescent cholesterol analogues such as BODIPY-labelled LDL-cholesterol or cholesterol-binding bacterial toxins, such as perfringolysin O (PFO) (*211*).

Filipin is an intrinsically fluorescent polyene macrolide antibiotic and can bind to unesterified cholesterol (*124*, *257*). Because it is able to detect free cholesterol, but not that esterified cholesterol in lipid droplets, it has been successfully used to study NPC1 disease (*211*). Although filipin labelling also has a low affinity for some other lipids such as the ganglioside GM1 (*12*), it is a well-established and recognised tool to detect cholesterol accumulation in NPC1 mutant cells. Given that the visualisation of filipin requires UV activation, 'bleaching' of filipin-stained cells is a limitation when aiming to quantify filipin staining intensities. This issue has now been overcome by the utilisation of glutathione S-transferase (GST)-PFO fusion proteins, which allow the immunodetection of PFO staining using GST antibodies, which is not prone to bleach while under microscopic examination (see below). In addition, it can induce cell lysis by damaging the membrane bilayer, which limits its use to fixed cells (*197*).

Another technique for visualising cholesterol is the use of fluorescent cholesterol analogues such as dehydroergosterol or the 1000-fold brighter BODIPY cholesterol (BChol) (*260*). Ikonen and colleagues used LDL labelled with BODIPY-cholesteryl linoleate and studied the transport of LDL-cholesterol from Lys/LE to the cell surface in live human A431 squamous cell carcinoma cells (*109*). However, the studies showed variations in

cholesterol esterification, cholesterol transporter binding and lipid droplet association, so analyses of cholesterol transport based on BChol require cautious interpretation (*211*). Cholesterol-dependent cytolysins derived from pathogenic bacteria and fungi also have come into application targeting cholesterol. A well-known member of this group is PFO, which binds to cell membranes that have molar cholesterol concentrations of more than 35-40 mol% of total membrane lipids (*41*).

Endomembranes appear to have a lower threshold probably through phospholipids supporting PFO-cholesterol binding (*225*). To circumvent the cytolytic effects of PFO, researchers isolated the PFO domain responsible for cholesterol binding (PFO-D4) (*61*, *216*). PFO-D4, however, cannot pass the cell membrane, thus, in-cell expression of fluorescence-labeled PFO-D4 has been established (*1*). To solve the problem of high cholesterol concentration, the D4 mutant D4H was developed, which now starts to bind at a molar cholesterol concentration of 1 mol% of total membrane lipids (*102*, *140*).

In here, in-cell expression of mCherry-tagged D4H was used to study the spatial distribution and colocalisation of cholesterol with the FA marker signal of GFP-vinculin, GFP-paxillin, and anti-pY861 FAK. By this technique, no unphysiological treatment, which may affect the membrane composition, was required for cholesterol visualisation. However, it has not been conclusively clarified whether D4/D4H may modulate cholesterol homeostasis (*211*). In addition, levels of the ectopically expressed D4H plasmid may vary between different cells upon transient transfection and therefore impact on D4H staining patterns.

The number, distribution and size of FA, as well as cell behaviour can reflect the cell's mode of migration by providing information about cell polarity and FA turnover. Fluorescent FA markers are needed to determine these factors. In the literature, the FA proteins paxillin, vinculin and (pY861, pY397) FAK have been widely used (*93*, *99*, *107*).

In here, anti-pY861 FAK was used as the FA marker for quantification. In the run-up, the localisation of anti-FAK to anti-pY861 FAK signals in CHO WT and M12 cells was compared (Figure A.1). While anti-pY861 FAK appeared as adhesion-like, well-defined condensations with a particular focus on the cell edge in WT cells, the anti-FAK signal showed a perinuclear accumulation, an increased diffuse background signal and a less defined cell edge.

FAK interaction with Src, as central signalling mechanism in FA dynamics, requires FAK autophosphorlyation at Y397 to create a docking site for Src family kinases (*207*). However, pY397 FAK was observed to also colocalise with β1 integrins on early and recycling endosomes (*5*, *231*), so it may not be possible to distinguish FA from endosomes based on anti-pY397 FAK staining. Since pY861 FAK is a major phosphorylation site of

Src (*26*) and it has been linked to oncogenic transformation, especially with cell migration and metastasis (*2*, *135*, *222*), it was chosen as FA marker herein. However, given the increased fuzzy anti-pY861 FAK signal in M12 cells, it does not appear to be completely FA specific either. The central spatial distribution of pY861 FAK was similar to that of the recycling endosome marker Rab11 (*63*, *66*, *268*). When analysing GFP-vinculin or GFP-paxillin/anti-pY861 FAK stained cells, the number of pY861 FAK labelled FA exceeded that of vinculin or paxillin labelled FA, especially in M12 and M12-A6ko cells. However, the distribution between cell lines remained unchanged for the different FA markers (data not shown). When the cell bottom was explicitly imaged by confocal microscopy, the pY861 FAK signal was reduced to more defined complexes. Consequently, pY861 FAK-based quantifications of FA number, spatial distribution and size could be confounded by the localisation of pY861 FAK in recycling endosomes. However, despite the deficits, immunostaining was less prone to problems, as cell transfection was associated with an increased rate of cell death, especially in WT cells. And, as the distribution of measurements between cell lines was comparable to results obtained from analyses based on GFP-vinculin, -paxillin, -Src and EGFP-Src-Y527F signals, the conclusions should not be affected.

For simplicity, anti-pY861 FAK also was used to determine FA size. However, in order to analyse FA size, it is important to differentiate between 2D and 3D FA markers. While integrins along the PM serve as FA markers of a 2D plane, adaptor proteins such as vinculin and paxillin can build up to a 3D FA aggregate (*255*). Using light microscopy, only a 2D plane, missing the FA depth, can be resolved (*108*). Thus, the area of the pY861 FAK signal probably is not representative for the FA size. A more accurate approach would be the use of the migration related $\alpha V\beta 3$ integrin (*94*, *255*). Since FA dynamics are a spatiotemporally regulated sequence of protein interactions, with FAK assembly preceding paxillin recruitment at the leading edge (*93*), the paxillin-less pFAK signal could reflect FA initiation, or, since paxillin also promotes FA disassembly, it could be related to the lack of FA turnover, particularly in M12 and M12-A6ko cells. To validate the dynamic interactions in FA in terms of assembly and turnover, FA characterisation requires a parallel analysis of 2D and 3D markers (*255*). An alternative method to investigate the role of cholesterol in FA reconstruction could be the analysis of fluorescence recovery after photobleaching (FRAP). Bleaching by a laser pulse leads to FA degradation, followed by FA recycling and reconstruction. However, the temporal and spatial distribution of FA recycling may reflect cellular regulatory mechanisms (*255*). Analysis of the spatiotemporal behaviour of different FA markers in CHO M12 and M12-A6ko cells may help to decipher the role of cholesterol and AnxA6 in cell migration.

To quantify cell spreading as a marker of cell behaviour and the cell's ability to establish adhesion, the cell size was analysed. The cell size increased in CHO M12, and even more so in CHO M12-A6ko cells, although depletion of AnxA6 was shown to rescue migration in CHO M12 (*104*). Kim and Wirtz suggested that FA size, not shape, is a positive predictor of cell spreading and that both cell size and FA size are biphasically related to the rate of cell migration. Thus, when a certain size was exceeded, the speed of the cells decreased (*114*). Consequently, the comparison of cell size may visualise a mode of behaviour, though its meaning for migration is inconclusive.

As ImageJ was not manually spatially calibrated, though scaled to 6.1833 pixels/micron based on the image information, areas were measured predominantly in pixel $(px)^2$. The aim was to visualise differences between cell lines rather than to determine absolute numbers. Therefore, the figures do not lose their informative value due to the lack of exact calibration.

To characterise the cell lines CHO WT, M12 and M12-A6ko, the relative protein levels of proteins involved in cholesterol homeostasis and phosphoproteins regulating FA dynamics were analysed by WB. This technique involves the separation of proteins according to their molecular weight by gel electrophoresis and subsequent transfer to a PVDF membrane for immunostaining. For phosphoproteins, in particular, this allows sequential staining and quantification of total and phosphorylated proteins on the same probe. Given the limited amount of phosphorylated proteins within a cell, the detection of phosphoproteins, as well as proteins in low concentrations, can be challenging. When analysing >10 samples per WB, equal sample loading, followed by identical transfer and immunoblotting conditions across the entire membrane are vital. Multiple replications of the experiment and WB analysis are required to control for technical error and to ensure validity and reproducibility. A distinction can be made between technical replicates, a replication of the same sample, similar to the duplicates mostly used herein, and biological replicates of independent samples (*178*). Individual biological replicates can be found along the series of experiments, but a systematic replication of the experiments should be added in the future to increase the value of the information.

As displayed earlier, some WB signals showed issues of hyper- and hypointensity. This may be a common issue of enhanced chemiluminescence (ECL), which uses horseradish peroxidase (HRP) conjugated to secondary antibodies that produces photons of light in the presence of luminol-based substrates (*178*). Substrate distribution is a dynamic process influenced by the spatial availability of the secondary antibody and the membrane surface. Strong bands with a high density of HRP reporter can rapidly consume the substrate, even depleting it, resulting in loss of signal. The detection of very high and low intensity

bands at the same time may be challenging due to the loss of linearity (*178*). Although chemiluminescence is widely used, fluorescent WB methods, that use fluorophore-labeled secondary antibodies, are considered the more accurate and robust technique with a broader linear range (*178*).

Common causes of non-linearity are overloading of the sample protein, leading to membrane saturation and consequent loss of abundant protein, and signal saturation beyond the capacity of the detection system. Since linearity between the sample loading and the signal intensity is the foundation of quantitative WB analysis a combined linear range for both the target protein and the loading protein, also referred to as internal loading control should be determined (*178*). In this work, it was possible to rely on the Grewal group's many years of experience with the method and the antibodies used. For densitometry using ImageJ, images were background corrected and contrasts were adjusted, which may also have affected the optical density analysis. Furthermore, membrane stripping for re-use may have had an impact on membrane quality. In light of these difficulties, results from WB analysis are often supported by other approaches, such as microscopy or as outlined below, mass spectroscopy (MS).

Over the last two decades, the latter technology has revolutionised the field of proteomics. However, while in WB the specificity of the antibody used to label the protein of interest is a key factor for the result, MS depends on several parameters that increase complexity and cost (*3*). Although the quality of data obtained with MS surpasses that of WB, the abundance of information obtained in the past, together with features such as lower cost and lower complexity, are still an argument for using WB today (*3*). Moreover, when aiming to address expression levels of a limited number of proteins in a highly complex protein mixture in whole cell lysates, the WB method is generally the preferred and most cost-effective approach. WB analysis is an established methodology in the Grewal laboratory, and the many years of experience with the protocol, providing critical insight into oncogenic signalling events (*76*, *82*, *119*, *241*) and the excellent performance of antibodies used in this study speak for the use of WB in the context of this question.

Chapter 5

Conclusion

LDL-cholesterol sequestration in the late endosomal/lysosomal (LE/Lys) compartment of Niemann-Pick type C1 (NPC1)-depleted Chinese hamster ovary cells (CHO M12) has been linked to impaired cell migration and invasion. It was hypothesised that cholesterol exit from LE in CHO M12 cells lacking annexin A6 (AnxA6, CHO M12-A6ko) could be delivered to the cell surface and peripheral recycling endosomes to support the formation and function of focal adhesion (FA) required to promote cell migration.

Western blot (WB) analysis showed that NPC1 deficiency affected the activation status of focal adhesion kinase (FAK) and Src kinase, key signalling proteins regulating FA dynamics. Phosphorylation of Y861 FAK, Y416 Src and p130Cas was greatly reduced in CHO M12 and AnxA6-depleted CHO M12 cells (CHO M12-A6ko) at steady state. To analyse FA formation and function in NPC1 mutant cells, the cellular distribution of key FA signalling proteins, such as activated FAK (pY397 FAK, pY861 FAK), and structural FA markers such as vinculin and paxillin were quantified by fluorescent microscopy. While control cells showed a prominant FA distribution at the cell periphery, NPC1 mutants displayed an increased FA amount within the cell body. The latter was accompanied by an inability to increase FA numbers at the cell periphery upon LDL treatment. Furthermore, in CHO M12-A6ko cells, an increased colocalisation of the cholesterol biosensor D4H with pY861 FAK and vinculin was observed. These findings indicate restoration of cholesterol transport from LE to the cell edge in CHO M12-A6ko cells. Nevertheless, peripheral FA distribution in CHO M12-A6ko cells remained much lower as compared to control cells, indicating that rescue mechanism upon AnxA6 depletion cannot fully overcome loss of NPC1 function. Interestingly, the NPC1 phenotype could be rescued by ectopic expression of constitutively active Y527F Src but not WT Src. It was speculated that the altered activation status of FAK and Src coincides with their cholesterol-sensitive and improper translocation to the cell surface. Indeed, exocytic transport of membrane and associated FA proteins requires the coordinated action of cholesterol-sensitive SNARE proteins. Since Y527F Src expression restored FA distribution in NPC1 mutant cells, it appears that oncogenic Src can overcome dysregulated cholesterol distribution in these cells to coordinate FA dynamics. As AnxA6 depletion could partially restore cholesterol transport to the cell periphery but did not fully reverse the phenotype, AnxA6 may have

further functions in cell migration-associated signalling.

Chapter 6

Abstract

In cells lacking the Niemann-Pick type C1 (NPC1) cholesterol transporter, cholesterol accumulation in late endosomes (LE) and an inability to distribute cholesterol from LE to other cell compartments causes impaired cell migration. It was speculated that cholesterol released from LE in NPC1 mutant Chinese hamster ovary (CHO) cells by annexin A6 (AnxA6) depletion could be delivered to the cell surface and support the focal adhesion (FA) dynamics required for migration. Cells obtain cholesterol through low-density lipoprotein (LDL) uptake, which is then delivered to LE and distributed to other sites. To study regulatory circuits that link LDL-cholesterol trafficking with the migratory machinery in CHO wild type (WT), NPC1 mutant CHO M12 and AnxA6-depleted CHO M12 cells (M12-A6ko), the relative expression levels of proteins involved in cholesterol homeostasis were compared. Furthermore, the number, location, and size of FA were analysed and the distribution and colocalisation of FA components assessed by immunofluorescence microscopy. Western blot analysis revealed that cholesterol sequestration in CHO M12 appears to affect the activation status of key migration signalling proteins. Phosphorylation of focal adhesion kinase (Y861 FAK), Src (Y416 Src) and p130Cas was greatly reduced in CHO M12 and M12-A6ko at steady state. It was speculated that this coincides with improper translocation of Src kinase and FAK to the cell surface to regulate FA (dis)assembly. Underlying mechanisms likely include the dysregulation of cholesterol-sensitive SNARE proteins, which regulate exocytic transport of membrane and FA proteins to the cell surface. Microscope-based quantification of the distribution of activated FAK (pY397 FAK, pY861 FAK), vinculin and paxillin in NPC1 mutants revealed an increased number and size of FA in the cell body, while the typical peripheral FA distribution observed in WT cells was absent. Interestingly, ectopic expression of constitutively active Y527F Src but not WT Src, appeared to restore FA distribution in NPC1 mutants, indicating that oncogenic Src can overcome dysregulated cholesterol distribution in these cells to coordinate FA dynamics. Strikingly, normalisation of cholesterol homeostasis in M12-A6ko cells correlated with restoration of cholesterol transport to the cell edge, as measured by the increased colocalisation of the cholesterol biosensor D4H with pY861 FAK and vinculin. Hence, AnxA6-regulated transport routes seem to contribute to cholesterol delivery to FA structures, thereby improving NPC1 mutant cell migratory behaviour.

Abstrakt

Das Fehlen des Cholesteroltransporters Niemann-Pick Typ C1 (NPC1) führt zur Akkumulation von Low-Density-Lipoprotein (LDL) - Cholesterol in späten Endosomen (LE) und zu einer defizitäre Umverteilung aus LE in andere Zellkompartimente. In Folge kommt es zu einer Beeinträchtigung der Zellmigration, welche sich durch die Deletion von Annexin A6 (AnxA6) und Aktivierung alternativer Cholesterolexportwege teilweise umkehren lässt. Eine zugrundeliegende Hypothese dieser Arbeit ist, dass durch AnxA6-Knockout freigesetztes Cholesterol aus NPC1-mutanten Chinese Hamster Ovary (CHO) Zellen an die Zelloberfläche gelangen und migrationsrelevante Dynamiken der Fokalkontakte (FA) unterstützen kann. Um die Regelkreise zu untersuchen, die den Transport von LDL-Cholesterol mit der Migrationsmaschinerie in CHO Wildtyp (WT), NPC1-mutanten CHO-M12 und AnxA6-depletierten CHO-M12 Zellen (M12-A6ko) verbinden, wurden Proteinlevels an der Cholesterolhomöostase beteiligter Proteine analysiert. Darüberhinaus wurde die Anzahl, Lage und Größe der FA untersucht und die Verteilung und Kolokalisierung der FA-Komponenten mittels Immunfluoreszenzmikroskopie bewertet. Western Blot-Analysen zeigten, dass die Cholesterolsequestrierung in NPC1-mutanten Zellen den Aktivierungsstatus wichtiger Signalproteine der Zellmigration beeinflusst. Die Phosphorylierung von Focal Adhesion Kinase (Y681 FAK), Src (Y416 Src) und p130Cas war in CHO M12 und M12-A6ko Zellen im Ausgangszustand stark reduziert. Basierend auf Ergebnissen der Grewal Gruppe wurde angenommen, dass dies mit einer fehlerhaften Verlagerung von Src-Kinase und FAK an die Zelloberfläche zur Regulation von FA-Dynamiken zusammenhängt. Zu den zugrundeliegenden Mechanismen gehört vermutlich die Dysregulation der cholesterolsensitiven SNARE-Proteine, die den exozytischen Transport von Membran- und FA-Proteinen zur Zelloberfläche regulieren. Die mikroskopische Quantifizierung der Verteilung von aktiviertem FAK (pY397 FAK, pY861 FAK), Vinculin und Paxillin in NPC1-mutanten Zellen zeigte eine erhöhte Anzahl und Größe von FA im Zellkörper, während die typische periphere FA-Verteilung in WT-Zellen fehlte. Die ektope Expression von konstitutiv aktivem Y527F Src, nicht aber von WT-Src, schien die FA-Verteilung in NPC1-Mutanten wiederherzustellen. Dies deutet darauf hin, dass onkogenes Src die gestörte Cholesterolverteilung in diesen Zellen überwinden und die FA-Dynamik koordinieren kann. Darüberhinaus schien die Normalisierung der Cholesterolhomöostase in A6ko-defizienten CHO-M12 Zellen mit der Wiederherstellung des Cholesteroltransports zum Zellrand zu korrelieren, was durch die verstärkte Kolokalisierung des Cholesterol-Biosensors D4H mit pY861 FAK und Vinculin gemessen wurde. AnxA6-regulierte Transportwege tragen demnach dazu bei, Cholesterol zu FA-Strukturen zu transportieren und so das Migrationsverhalten NPC1-mutanter Zellen zu verbessern.

List of Abbreviations

a.u.	**a**rbitrary **u**nit
AA	**A**rachidonic **A**cid
ABC (-A1, -G1)	**A**TP-**B**inding **C**assette transporter **(-A1, -G1)**
ABS (-1, -2, -3)	**A**ctin **B**inding **S**ite **(-1, -2, -3)**
ACAT1	**A**cetyl-**C**oA-**A**cetyl**t**ransferase **1**
AMPK	**A**denosine **M**ono**p**hosphate-activated **K**inase
Anx (-A5, -A6)	**An**nex**i**n **(-A5, -A6)**
APS	**A**mmonium **P**er**s**ulfate
ATGL	**A**dipose **T**ri**g**lyceride **L**ipase
ATP	**A**denosine **T**ri**p**hosphate
BChol	**B**ODIPY **Chol**esterol
BODIPY	4,4-Difluoro-1,3,5,7,8-Pentamethyl-4-Bora-3a,4a-Diaza-s-Indacene
BSA	**B**ovine **S**erum **A**lbumin
Cav (-1, -3)	**Cav**eolin**(-1, -3)**
CD36	**C**luster of **D**ifferentiation 36
CHO	**C**hinese **H**amster **O**vary
cPLA$_2$	**c**ytoplasmic **P**hospho**l**ipase **A2**
DAPI	6-**D**i**a**midino-2-**P**heny**l**indole
dH$_2$O	**d**estilled **H$_2$O**
DHC	7-**D**e**h**ydro**c**holesterol
DMSO	**Dim**ethyl **S**ulf**o**xide
DNA	**D**esoxyribo**n**ucleic **A**cid
ECL	**E**nhanced **C**hemi**l**uminescence
ECM	**E**xtra**c**ellular **M**atrix
EDTA	**E**thylene**d**iamine**t**etraacetic **A**cid
EGF	**E**pidermal **G**rowth **F**actor
EGFR	**E**pidermal **G**rowth **F**actor **R**eceptor
ER	**E**ndoplasmatic **R**eticulum
ERK	**E**xtracellular Signal-**R**egulated **K**inase
ERK (-1, -2)	**E**xtracellular Signal-**R**egulated **K**inase **(-1, -2)**
F-actin	**F**ilamentous **actin**

FA	**F**ocal **A**dhesion
FAK	**F**ocal **A**dhesion **K**inase
FBS	**F**etal **B**ovine **S**erum
FERM	**F**our (4).1 protein, **E**zrin, **R**adixin, **M**oesin
FN	**F**ibro**n**ectin
FRAP	**F**luorescence **R**ecovery **A**fter **P**hotobleaching
GAP	**G**TPase-**A**ctivating **P**rotein
GFP	**G**reen **F**luorescent **P**rotein
GPI	**G**lycosyl**p**hosphatidyl**i**nositol
GSK-3	**G**lycogen **S**ynthase **K**inase-**3**
GST	**G**lutathione **S**-**T**ransferase
GTP	**G**uanosine **Tri**p**h**osphat
HDL	**H**igh-**D**ensity **L**ipoprotein
HMG-CoA	β-**H**ydroxy-β-**M**ethyl**g**lutaryl-**Co**enzyme **A**
HMGCR	β-**H**ydroxy-β-**M**ethyl**g**lutaryl-**Co**enzyme A **R**eductase
HSL	**H**ormone-**S**ensitive **l**ipase
IDOL	**I**nducible **D**egrader **O**f the **L**DL receptor
iRFP	Near-**i**nfra**r**ed **F**luorescent **P**rotein
LB	**L**ysogeny **B**roth
LC3	Microtubule-associated protein 1 **L**ight **C**hain **3**
LDL	**L**ow-**D**ensity **L**ipoprotein
LDLR	**L**ow-**D**ensity **L**ipoprotein **R**eceptor
LD	**L**ipid **D**roplet
LE	**L**ate **E**ndosome
LIM	**L**in-11, **I**sl-1, **M**EC-3
LKB1	**L**iver **K**inase **B1**
LPDS	**L**ipo**p**rotein-**D**eficient **S**erum
LRP1	**L**DL-**R**elated-**P**rotein **1**
LSB	**L**aemmli **S**ample **B**uffer
LXR	**L**iver **X** **R**eceptor
Lys	**Lys**osome
MAD	**M**ean **A**bsolute **D**eviation
MAPK	**M**itogen-**A**ctivated **P**rotein **K**inase
MβCD	**M**ethyl-β **C**yclo**d**extrin
MCS	**M**embrane **C**ontact **S**ite
MLCK	**M**yosin **L**ight-**C**hain **K**inase
MS	**M**ass **S**pectroscopy

mTOR	**m**ammalian **T**arget **O**f **R**apamycin
mTORC1	**m**ammalian **T**arget **O**f **R**apamycin **C**omplex **1**
MVB	**M**ulti**v**esicular **B**odies
Myo2	**Myo**sin-**2**
Myo5b	**Myo**sin-**5b**
n.d.	**n**ot **d**etected
NPC (-1, -2)	**N**iemann **P**ick type **C** **(-1, -2)**
NSCLC	**N**on-**S**mall **C**ell **L**ung **C**ancer
NSF	**N**-ethylmaleimide-**S**ensitive **F**usion protein
ORP (-1L, -2)	**O**SBP-**R**elated **P**rotein (-1L, -2)
OSBP	**O**xy**s**terol-**B**inding **P**rotein
p130Cas	**p130 C**rk-**a**ssociated **s**ubstrate
PBS	**P**hosphate **B**uffered **S**aline
PCSK9	**P**roprotein **C**onvertase **S**ubtilisin/**K**exin **9**
PDGF	**P**latelet-**D**erived **G**rowth **F**actor
PDGFR	**P**latelet-**D**erived **G**rowth **F**actor **R**eceptor
pEGFP	**p**lasmid **E**nhanced **G**reen **F**luorescent **P**rotein
Pen-Strep	**Pen**icillin-**Strep**tomycin
PFO	**P**er**f**ringolysin **O**
PI3K	**P**hospho**i**nositide **3**-**K**inase
PIP2	**P**hosphatidyl**i**nositol 4,5-bi**p**hosphate
PIP3	**P**hosphatidyl**i**nositol 3,4,5-tri**p**hosphate
PIPKIγ	**P**hosphatidyl**i**nositol **p**hosphate **k**inase type **I** γ
Pax	**Pax**illin
PKB	**P**rotein **K**inase **B**
PKCα	**P**rotein **K**inase **C**α
PM	**P**lasma **M**embrane
PTP	**P**rotein **T**yrosine **P**hosphatase
PVDF	**P**oly**v**inylidene **Dif**luoride
px	**Pix**el
Pyk2	**P**roline-rich t**y**rosine **k**inase **2**
ROI	**R**egion **O**f **I**nterest
RE	**R**ecycling **E**ndosome
RB	**R**etino**b**lastoma protein
RIAM	**R**ap1-**I**nteractive **A**daptor **M**olecule
RM	**R**elative **M**ean
RXR	**R**etinoid **X** **R**eceptor

S6K1	**S6 K**inase **1**
SCAP	**S**REBP-**C**leavage-**A**ctivating-**P**rotein
SD	**S**tandard **D**eviation
SDS	**S**odium **D**odecyl **S**ulfate
SE	**S**tandard **E**rror
SH (-2, -3)	**S**rc **H**omology **(-2, -3)**
SNAP23	**Sn**aptosome-**A**ssociated **P**rotein **23**
SNARE	**S**oluble **N**-ethylmaleimide-sensitive-factor **A**ttachment **Re**ceptor
SOCE	**S**tore-**O**perated **C**a^{2+} **E**ntry
SQLE	**Squal**ene monooxygenase
SRB1	**S**cavenger-**R**eceptor-**B1**
SRE	**S**terol-**R**egulatory-**E**lement
SREBP (-1, -2)	**S**terol-**R**egulatory-**E**lement-**B**inding **P**rotein **(-1, -2)**
StARD (-3)	**St**eroidogenic-**A**cute-**R**egulatory-related lipid tranfer **D**omain **(-3)**
Stx (-4, -6)	**S**yn**tax**in **(-4, -6)**
TAZ	**T**ranscriptional Co**a**ctivator with PD**Z**-binding motif
TBC1D15	**T**re-2/**B**ub2/**C**dc16 **1 D**omain family member **15**
TBS-T	**T**ris-**B**uffered **S**aline-**T**ween
TEMED	**Te**tra**m**ethyl**e**thylene**d**iamine
TGN	**T**rans-**G**olgi-**N**etwork
VAP-A	**V**esicle-**A**ssociated Membrane **P**rotein-**A**
VAMP3	**V**esicle-**A**ssociated **M**embrane **P**rotein **3**
VASP	**Va**sodilator **S**timulated **P**hosphoprotein
VEGF	**V**ascular-**E**ndothelial **G**rowth **F**actor
Vinc	**Vinc**ulin
VLDL	**V**ery **L**ow-**D**ensity **L**ipoprotein
VLDLR	**V**ery **L**ow-**D**ensity **L**ipoprotein **R**eceptor
WB	**W**estern **B**lot
WT	**W**ild **T**ype
YAP	**Y**es-**A**ssociated **P**rotein

List of Figures

1.1 LDL receptor (LDLR)-mediated LDL-cholesterol uptake and intracellular trafficking. 4
1.2 Rab protein-regulated cholesterol transport. 7
1.3 Focal adhesion dynamics in cell migration. 10
1.4 Late endosomal cholesterol transporters and co-proteins associated with cholesterol egress. 16

3.1 Western blot analysis of proteins involved in cholesterol homeostasis and focal adhesion assembly in CHO WT, M12 and M12-A6ko. 31
3.2 Western blot analysis of proteins involved in cholesterol homeostasis and focal adhesion assembly in serum-stimulated CHO WT, M12 and M12-A6ko cells. 33
3.3 Western blot analysis of signalling proteins mediating cell adhesion and migration in CHO WT, M12 and M12-A6ko cells. 35
3.4 Western blot analysis of FAK and Src kinase activation in serum-stimulated CHO WT, M12 and M12-A6ko cells. 36
3.5 Western blot analysis of late endosomal proteins in migrating CHO WT, M12 and M12-A6ko cells. 38
3.6 Western blot analysis of Src and FAK activation in serum-stimulated and multi-scratched CHO WT, M12 and M12-A6ko cells. 41
3.7 Western blot analysis of late endosomal proteins in CHO WT, M12 and M12-A6ko cells after incubation with LPDS-statin media. 42
3.8 Western blot analysis of Src and FAK activation in CHO WT, M12 and M12-A6ko cells after incubation with LPDS-statin media. 44
3.9 Western blot analysis of late endosomal proteins in serum-activated CHO WT, M12 and M12-A6ko cells after incubation with LPDS-statin media. . 46
3.10 Western blot analysis of Src and FAK activation in serum-activated CHO WT, M12 and M12-A6ko cells after with LPDS-statin media. 48
3.11 Focal adhesion distribution and numbers in CHO WT, M12 and M12-A6ko cells at steady state (10% FBS). (A-D) 51

3.11 Focal adhesion distribution and numbers in CHO WT, M12 and M12-A6ko cells at steady state (10% FBS). (E) 52
3.12 Focal adhesion number and distribution in serum-stimulated CHO WT, M12 and M12-A6ko cells. 53
3.13 LDL stimulation of CHO WT, M12 and M12-A6ko cells. 54
3.14 Focal adhesion assembly in LDL-stimulated CHO WT, M12 and M12-A6ko cells. 55
3.15 Spatial distribution and colocalisation of the FA markers vinculin and pY861 FAK in CHO WT, M12 and M12-A6ko cells. 57
3.16 Focal adhesion assembly of GFP-vinculin overexpressing CHO WT, M12 and M12-A6ko cells. 58
3.17 Focal adhesion size in GFP-vinculin overexpressing CHO WT, M12 and M12-A6ko cells. 59
3.18 Spatial distribution and colocalisation of the FA markers paxillin and pY861 FAK in CHO WT, M12 and M12-A6ko. 60
3.19 Focal adhesion assembly in GFP-paxillin-overexpressing CHO WT, M12 and M12-A6ko cells. 61
3.20 Focal adhesion size in GFP-paxillin-overexpressing CHO WT, M12 and M12-A6ko cells. 62
3.21 Spatial association of cholesterol and vinculin in CHO WT, M12 and M12-A6ko cells. 63
3.22 Spatial distribution of cholesterol in CHO WT, M12 and M12-A6ko cells. 64
3.23 Colocalisation of cholesterol and vinculin or paxillin in CHO WT cells. . 65
3.24 Colocalisation of cholesterol and pY861 FAK in CHO M12 and M12-A6ko cells. 66
3.25 Src- and Src Y527F-overexpressing CHO WT, M12 and M12-A6ko cells. 68
3.26 Focal adhesion number and distribution in Src- and Src Y527F-overexpressing CHO WT, M12 and M12-A6ko cells. 69
3.27 Focal adhesion size in Src- and Src Y527F-overexpressing CHO WT, M12 and M12-A6ko. 70
3.28 Cell size of Src- and Src Y527F-overexpressing CHO WT, M12 and M12-A6ko cells. 71

A.1 Characterisation of FAK and pY861 FAK immunostaining. 133
A.2 Focal adhesions at the cell edge and the cell body. 134
A.3 Western blot analysis of late endosomal proteins in LDL-activated CHO WT, M12 and M12-A6ko cells after incubation with LPDS-statin media. . 135

A.4 Western blot analysis of Src and FAK activation in LDL-activated CHO WT, M12, and M12-A6ko cells after incubation with LPDS-statin media. 136
A.5 Western blot analysis of late endosomal proteins in migrating CHO WT, M12 and M12-A6ko cells after incubation with 20%FBS. 137
A.6 Western blot analysis of Src and FAK activation in migrating CHO WT, M12 and M12-A6ko cells after incubation with 20%FBS. 139
A.7 Focal adhesion density in Src- and Src Y527F-overexpressing CHO WT, M12, and M12-A6ko cells. 140

List of Tables

2.1 BSA Standard Curve 23
2.2 Lowry Solution 23
2.3 12% Resolving Gel 24
2.4 4% Stacking Gel 24
2.5 Test Groups 29

B.1 Expendable Materials 141
B.2 Technical Devices 142
B.3 Chemicals and Reagents 142
B.4 Buffer and Solutions 145
B.5 10x Running Buffer 145
B.6 10x Transfer Buffer 145
B.7 1x Transfer Buffer 145
B.8 10x TBS (Tris Buffered Saline) 146
B.9 1x TBS-T (Tris Buffered Saline, with 0.1% Tween-20) 146
B.10 Lowry Solution A 146
B.11 Lowry Solution B 146
B.12 Lowry Solution C 146
B.13 Western Blot Blocking Buffer (5%) 146
B.14 Mild Stripping Buffer 147
B.15 5x Laemmli Sample Buffer 147
B.16 Lysis Buffer (Stock) 147
B.17 Lysis Buffer (Working Solution) 147
B.18 Antibodies 148
B.19 Media 149
B.20 Growth Media 149
B.21 20% FBS Media 149
B.22 Freezing Media 149
B.23 LB Media 149
B.24 LB Agar 150
B.25 LPDS-statin media 150

B.26 Cell lines 150
B.27 Bacteria 151
B.28 Kits 151
B.29 Expression Vectors 151
B.30 Software 152

Bibliography

(*1*) Abe, M., Makino, A., Hullin-Matsuda, F., Kamijo, K., Ohno-Iwashita, Y., Hanada, K., Mizuno, H., Miyawaki, A., and Kobayashi, T., (2012). A role for sphingomyelin-rich lipid domains in the accumulation of phosphatidylinositol-4,5-bisphosphate to the cleavage furrow during cytokinesis. *Molecular and Cellular Biology 32*, 1396–1407.

(*2*) Abu-Ghazaleh, R., Kabir, J., Jia, H., Lobo, M., and Zachary, I., (2001). Src mediates stimulation by vascular endothelial growth factor of the phosphorylation of focal adhesion kinase at tyrosine 861, and migration and anti-apoptosis in endothelial cells. *Biochemical Journal 360*, 255–264.

(*3*) Aebersold, R., Burlingame, A. L., and Bradshaw, R. A., (2013). Western blots versus selected reaction monitoring assays: time to turn the tables? *Molecular & Cellular Proteomics 12*, 2381–2382.

(*4*) Alanko, J., and Ivaska, J., (2016). Endosomes: emerging platforms for inte-grin-mediated FAK signalling. *Trends in Cell Biology 26*, 391–398.

(*5*) Alanko, J., Mai, A., Jacquemet, G., Schauer, K., Kaukonen, R., Saari, M., Goud, B., and Ivaska, J., (2015). Integrin endosomal signalling suppresses anoikis. *Nature Cell Biology 17*, 1412–1421.

(*6*) Ali, Y. B., Carrière, F., Verger, R., Petry, S., Muller, G., and Abousalham, A., (2005). Continuous monitoring of cholesterol oleate hydrolysis by hormone-sensitive lipase and other cholesterol esterases. *Journal of Lipid Research 46*, 994–1000.

(*7*) Alikhani, N., Ferguson, R. D., Novosyadlyy, R., Gallagher, E. J., Scheinman, E. J., Yakar, S., and LeRoith, D., (2013). Mammary tumor growth and pulmonary metastasis are enhanced in a hyperlipidemic mouse model. *Oncogene 32*, 961–967.

(*8*) Angers-Loustau, A., Côté, J.-F., Charest, A., Dowbenko, D., Spencer, S., Lasky, L. A., and Tremblay, M. L., (1999). Protein tyrosine phosphatase-PEST regulates focal adhesion disassembly, migration, and cytokinesis in fibroblasts. *Journal of Cell Biology 144*, 1019–1031.

(*9*) Antalis, C. J., Uchida, A., Buhman, K. K., and Siddiqui, R. A., (2011). Migration of MDA-MB-231 breast cancer cells depends on the availability of exogenous lipids and cholesterol esterification. *Clinical & Experimental Metastasis 28*, 733–741.

(*10*) Arimura, Y., Vang, T., Tautz, L., Williams, S., and Mustelin, T., (2008). TCR-induced downregulation of protein tyrosine phosphatase PEST augments secondary T cell responses. *Molecular Immunology 45*, 3074–3084.

(*11*) Arold, S. T., Hoellerer, M. K., and Noble, M. E., (2002). The structural basis of localization and signaling by the focal adhesion targeting domain. *Structure 10*, 319–327.

(*12*) Arthur, J. R., Heinecke, K. A., and Seyfried, T. N., (2011). Filipin recognizes both GM1 and cholesterol in GM1 gangliosidosis mouse brain. *Journal of Lipid Research 52*, 1345–1351.

(*13*) Atherton, P., Stutchbury, B., Wang, D.-Y., Jethwa, D., Tsang, R., Meiler-Rodriguez, E., Wang, P., Bate, N., Zent, R., Barsukov, I. L., Goult, B. T., Critchley, D. R., and Ballestrem, C., (2015). Vinculin controls talin engagement with the actomyosin machinery. *Nature Communications 6*, 1–12.

(*14*) Babiychuk, E. B., and Draeger, A., (2000). Annexins in cell membrane dynamics: Ca^{2+}-regulated association of lipid microdomains. *Journal of Cell Biology 150*, 1113–1124.

(*15*) Badin, P.-M., Vila, I. K., Louche, K., Mairal, A., Marques, M.-A., Bourlier, V., Tavernier, G., Langin, D., and Moro, C., (2013). High-fat diet-mediated lipotoxicity and insulin resistance is related to impaired lipase expression in mouse skeletal muscle. *Endocrinology 154*, 1444–1453.

(*16*) Baillat, G., Siret, C., Delamarre, E., and Luis, J., (2008). Early adhesion induces interaction of FAK and Fyn in lipid domains and activates raft-dependent Akt signaling in SW480 colon cancer cells. *Biochimica et Biophysica Acta - Molecular Cell Research 1783*, 2323–2331.

(*17*) Boadu, E., Nelson, R. C., and Francis, G. A., (2012). ABCA1-dependent mobilization of lysosomal cholesterol requires functional Niemann–Pick C2 but not Niemann–Pick C1 protein. *Biochimica et Biophysica Acta - Molecular and Cell Biology of Lipids 1821*, 396–404.

(*18*) Brindisi, M., Fiorillo, M., Frattaruolo, L., Sotgia, F., Lisanti, M. P., and Cappello, A. R., (2020). Cholesterol and mevalonate: two metabolites involved in breast cancer progression and drug resistance through the ERRα pathway. *Cells 9*, 1819.

(*19*) Brown, M. C., and Turner, C. E., (2004). Paxillin: adapting to change. *Physiological Reviews 84*, 1315–1339.

(*20*) Brown, M. C., Perrotta, J. A., and Turner, C. E., (1996). Identification of LIM3 as the principal determinant of paxillin focal adhesion localization and characterization of a novel motif on paxillin directing vinculin and focal adhesion kinase binding. *Journal of Cell Biology 135*, 1109–1123.

(*21*) Brown, M. C., Perrotta, J. A., and Turner, C. E., (1998). Serine and threonine phosphorylation of the paxillin LIM domains regulates paxillin focal adhesion localization and cell adhesion to fibronectin. *Molecular Biology of the Cell 9*, 1803–1816.

(*22*) Brown, M. S., and Goldstein, J. L., (1999). A proteolytic pathway that controls the cholesterol content of membranes, cells, and blood. *Proceedings of the National Academy of Sciences 96*, 11041–11048.

(*23*) Bucci, C., Thomsen, P., Nicoziani, P., McCarthy, J., and Van Deurs, B., (2000). Rab7: a key to lysosome biogenesis. *Molecular Biology of the Cell 11*, 467–480.

(*24*) Buckland, G. A., and Wilton, C. D., (1998). Inhibition of human cytosolic phospholipase A2 by human annexin V. *Biochemical Journal 329*, 369–372.

(*25*) Buss, J. E., Kamps, M. P., Gould, K., and Sefton, B. M., (1986). The absence of myristic acid decreases membrane binding of p60Src but does not affect tyrosine protein kinase activity. *Journal of Virology 58*, 468–474.

(*26*) Calalb, M. B., Zhang, X., Polte, T. R., and Hanks, S. K., (1996). Focal adhesion kinase tyrosine-861 is a major site of phosphorylation by Src. *Biochemical and Biophysical Research Communications 228*, 662–668.

(*27*) Calvisi, D. F., Wang, C., Ho, C., Ladu, S., Lee, S. A., Mattu, S., Destefanis, G., Delogu, S., Zimmermann, A., Ericsson, J., Brozzetti, S., Staniscia, T., Chen, X., Dombrowski, F., and Evert, M., (2011). Increased lipogenesis, induced by AKT - mTORC1 - RPS6 signaling, promotes development of human hepatocellular carcinoma. *Gastroenterology 140*, 1071–1083.

(*28*) Caswell, P. T., Vadrevu, S., and Norman, J. C., (2009). Integrins: masters and slaves of endocytic transport. *Nature Reviews Molecular Cell Biology 10*, 843–853.

(*29*) Chakrabarti, P., Kim, J. Y., Singh, M., Shin, Y.-K., Kim, J., Kumbrink, J., Wu, Y., Lee, M.-J., Kirsch, K. H., Fried, S. K., et al. (2013). Insulin inhibits lipolysis in adipocytes via the evolutionarily conserved mTORC1-Egr1-ATGL-mediated pathway. *Molecular and Cellular Biology 33*, 3659–3666.

(*30*) Chen, W., Sun, Y., Welch, C., Gorelik, A., Leventhal, A. R., Tabas, I., and Tall, A. R., (2001). Preferential ATP-binding cassette transporter A1-mediated cholesterol efflux from late endosomes/lysosomes. *Journal of Biological Chemistry 276*, 43564–43569.

(*31*) Chen, Y., and Hughes-Fulford, M., (2001). Human prostate cancer cells lack feedback regulation of low-density lipoprotein receptor and its regulator, SREBP2. *International Journal of Cancer 91*, 41–45.

(*32*) Choudhury, A., Dominguez, M., Puri, V., Sharma, D. K., Narita, K., Wheatley, C. L., Marks, D. L., and Pagano, R. E., (2002). Rab proteins mediate Golgi transport of caveola-internalized glycosphingolipids and correct lipid trafficking in Niemann-Pick C cells. *Journal of Clinical Investigation 109*, 1541–1550.

(*33*) Clarke, P. R., and Hardie, D. G., (1990). Regulation of HMG-CoA reductase: identification of the site phosphorylated by the AMP-activated protein kinase in vitro and in intact rat liver. *The EMBO Journal 9*, 2439–2446.

(*34*) Connell, E., Darios, F., Broersen, K., Gatsby, N., Peak-Chew, S.-Y., Rickman, C., and Davletov, B., (2007). Mechanism of arachidonic acid action on syntaxin–Munc18. *EMBO Reports 8*, 414–419.

(*35*) Cornely, R., Rentero, C., Enrich, C., Grewal, T., and Gaus, K., (2011). Annexin A6 is an organizer of membrane microdomains to regulate receptor localization and signalling. *IUBMB Life 63*, 1009–1017.

(*36*) Costet, P., Luo, Y., Wang, N., and Tall, A. R., (2000). Sterol-dependent transactivation of theABC1 promoter by the liver X receptor/retinoid X receptor. *Journal of Biological Chemistry 275*, 28240–28245.

(*37*) Cruz, P. M., Mo, H., McConathy, W., Sabnis, N. A., and Lacko, A. G., (2013). The role of cholesterol metabolism and cholesterol transport in carcinogenesis: a review of scientific findings, relevant to future cancer therapeutics. *Frontiers in Pharmacology 4*, 119.

(*38*) Cubells, L., Vilà de Muga, S., Tebar, F., Wood, P., Evans, R., Ingelmo-Torres, M., Calvo, M., Gaus, K., Pol, A., Grewal, T., and Enrich, C., (2007). Annexin A6-induced alterations in cholesterol transport and caveolin export from the Golgi complex. *Traffic 8*, 1568–1589.

(*39*) Dahl, N. K., Daunais, M. A., and Liscum, L., (1994). A second complementation class of cholesterol transport mutants with a variant Niemann-Pick type C phenotype. *Journal of Lipid Research 35*, 1839–1849.

(*40*) Danilo, C., Gutierrez-Pajares, J. L., Mainieri, M. A., Mercier, I., Lisanti, M. P., and Frank, P. G., (2013). Scavenger receptor class B type I regulates cellular cholesterol metabolism and cell signaling associated with breast cancer development. *Breast Cancer Research 15*, 1–13.

(*41*) Das, A., Goldstein, J. L., Anderson, D. D., Brown, M. S., and Radhakrishnan, A., (2013). Use of mutant 125I-perfringolysin O to probe transport and organization of cholesterol in membranes of animal cells. *Proceedings of the National Academy of Sciences 110*, 10580–10585.

(*42*) de Diego, I., Schwartz, F., Siegfried, H., Dauterstedt, P., Heeren, J., Beisiegel, U., Enrich, C., and Grewal, T., (2002). Cholesterol modulates the membrane binding and intracellular distribution of annexin 6. *Journal of Biological Chemistry 277*, 32187–32194.

(*43*) De Médina, P., Paillasse, M. R., Segala, G., Voisin, M., Mhamdi, L., Dalenc, F., Lacroix-Triki, M., Filleron, T., Pont, F., Saati, T. A., Morisseau, C., Hammock, B., Silvente-Poirot, S., and Poirot, M., (2013). Dendrogenin A arises from cholesterol and histamine metabolism and shows cell differentiation and anti-tumour properties. *Nature Communications 4*, 1840.

(*44*) Di Paolo, G., and De Camilli, P., (2006). Phosphoinositides in cell regulation and membrane dynamics. *Nature 443*, 651–657.

(*45*) Drees, B., Friederich, E., Fradelizi, J., Louvard, D., Beckerle, M. C., and Golsteyn, R. M., (2000). Characterization of the interaction between zyxin and members of the Ena/vasodilator-stimulated phosphoprotein family of proteins. *Journal of Biological Chemistry 275*, 22503–22511.

(*46*) Drees, B. E., Andrews, K. M., and Beckerle, M. C., (1999). Molecular dissection of zyxin function reveals its involvement in cell motility. *Journal of Cell Biology 147*, 1549–1560.

(*47*) Echarri, A., and Pozo, M. A., (2006). Caveolae internalization regulates integrin-dependent signaling pathways. *Cell Cycle 5*, 2179–2182.

(*48*) Enrich, C., Rentero, C., and Grewal, T., (2017). Annexin A6 in the liver: from the endocytic compartment to cellular physiology. *Biochimica et Biophysica Acta - Molecular Cell Research 1864*, 933–946.

(*49*) Enrich, C., Rentero, C., Vilà de Muga, S., Reverter, M., Mulay, V., Wood, P., Koese, M., and Grewal, T., (2011). Annexin A6-linking Ca^{2+} signaling with cholesterol transport. *Biochimica et Biophysica Acta - Molecular Cell Research 1813*, 935–947.

(*50*) Enrich, C., Rentero, C., Grewal, T., Futter, C. E., and Eden, E. R., (2019). Cholesterol overload: contact sites to the rescue! *Contact 2*, 2515256 419893507.

(*51*) Enrich, C., Rentero, C., Hierro, A., and Grewal, T., (2015). Role of cholesterol in SNARE-mediated trafficking on intracellular membranes. *Journal of Cell Science 128*, 1071–1081.

(*52*) Feldt, M., Menard, J., Rosendahl, A. H., Lettiero, B., Bendahl, P.-O., Belting, M., and Borgquist, S., (2020). The effect of statin treatment on intratumoral cholesterol levels and LDL receptor expression: a window-of-opportunity breast cancer trial. *Cancer & Metabolism 8*, 1–16.

(*53*) Fichter, C. D., Gudernatsch, V., Przypadlo, C. M., Follo, M., Schmidt, G., Werner, M., and Lassmann, S., (2014). ErbB targeting inhibitors repress cell migration of esophageal squamous cell carcinoma and adenocarcinoma cells by distinct signaling pathways. *Journal of Molecular Medicine 92*, 1209–1223.

(*54*) Fincham, V. J., and Frame, M. C., (1998). The catalytic activity of Src is dispensable for translocation to focal adhesions but controls the turnover of these structures during cell motility. *The EMBO Journal 17*, 81–92.

(*55*) Fradelizi, J., Noireaux, V., Plastino, J., Menichi, B., Louvard, D., Sykes, C., Golsteyn, R. M., and Friederich, E., (2001). ActA and human zyxin harbour Arp2/3-independent actin-polymerization activity. *Nature Cell Biology 3*, 699–707.

(*56*) Freed-Pastor, W., Mizuno, H., Zhao, X., Langerød, A., Moon, S.-H., Rodriguez-Barrueco, R., Barsotti, A., Chicas, A., Li, W., Polotskaia, A., Bissell, M., Osborne, T., Tian, B., Lowe, S., Silva, J., Børresen-Dale, A.-L., Levine, A., Bargonetti, J., and Prives, C., (2012). Mutant p53 disrupts mammary tissue architecture via the mevalonate pathway. *Cell 148*, 244–258.

(*57*) Frolov, A., Srivastava, K., Daphna-Iken, D., Traub, L. M., Schaffer, J. E., and Ory, D. S., (2001). Cholesterol overload promotes morphogenesis of a Niemann-Pick C (NPC)-like compartment independent of inhibition of NPC1 or HE1/NPC2 function. *Journal of Biological Chemistry 276*, 46414–46421.

(*58*) Gallagher, E. J., Zelenko, Z., Neel, B., Antoniou, I. M., Rajan, L., Kase, N., and LeRoith, D., (2017). Elevated tumor LDLR expression accelerates LDL cholesterol-mediated breast cancer growth in mouse models of hyperlipidemia. *Oncogene 36*, 6462–6471.

(*59*) García-Melero, A., Reverter, M., Hoque, M., Meneses-Salas, E., Koese, M., Conway, J. R., Johnsen, C. H., Alvarez-Guaita, A., Morales-Paytuvi, F., Elmaghrabi, Y. A., Pol, A., Tebar, F., Murray, R. Z., Timpson, P., Enrich, C., Grewal, T., and Rentero, C., (2016). Annexin A6 and late endosomal cholesterol modulate integrin recycling and cell migration. *Journal of Biological Chemistry 291*, 1320–1335.

(*60*) Gaus, K., Le Lay, S., Balasubramanian, N., and Schwartz, M. A., (2006). Integrin-mediated adhesion regulates membrane order. *Journal of Cell Biology 174*, 725–734.

(*61*) Gay, A., Rye, D., and Radhakrishnan, A., (2015). Switch-like responses of two cholesterol sensors do not require protein oligomerization in membranes. *Biophysical Journal 108*, 1459–1469.

(*62*) Gelissen, I. C., Harris, M., Rye, K.-A., Quinn, C., Brown, A. J., Kockx, M., Cartland, S., Packianathan, M., Kritharides, L., and Jessup, W., (2006). ABCA1 and ABCG1 synergize to mediate cholesterol export to apoA-I. *Arteriosclerosis, Thrombosis, and Vascular Biology 26*, 534–540.

(*63*) George, M., Ying, G., Rainey, M. A., Solomon, A., Parikh, P. T., Gao, Q., Band, V., and Band, H., (2007). Shared as well as distinct roles of EHD proteins revealed by biochemical and functional comparisons in mammalian cells and C. elegans. *BMC Molecular and Cell Biology 8*, 1–22.

(*64*) Gill, S., Stevenson, J., Kristiana, I., and Brown, A. J., (2011). Cholesterol-dependent degradation of squalene monooxygenase, a control point in cholesterol synthesis beyond HMG-CoA reductase. *Cell Metabolism 13*, 260–273.

(*65*) Göbel, A., Rauner, M., Hofbauer, L. C., and Rachner, T. D., (2020). Cholesterol and beyond - The role of the mevalonate pathway in cancer biology. *Biochimica et Biophysica Acta - Reviews on Cancer 1873*, 188351.

(*66*) Goitre, L., Cutano, V., and Retta, S. F., (2014). Fluorescence microscopy study of Rap1 subcellular localization. *Ras Signaling: Methods and Protocols*, 197–205.

(*67*) Goldstein, J. L., and Brown, M. S., (1974). Binding and degradation of low density lipoproteins by cultured human fibroblasts. *Journal of Biological Chemistry 249*, 5153–5162.

(*68*) Goldstein, J. L., Dana, S. E., Faust, J. R., Beaudet, A. L., and Brown, M. S., (1975). Role of lysosomal acid lipase in the metabolism of plasma low density lipoprotein. Observations in cultured fibroblasts from a patient with cholesteryl ester storage disease. *Journal of Biological Chemistry 250*, 8487–8495.

(*69*) Golji, J., Wendorff, T., and Mofrad, M. R., (2012). Phosphorylation primes vinculin for activation. *Biophysical Journal 102*, 2022–2030.

(*70*) Goñi, G. M., Epifano, C., Boskovic, J., Camacho-Artacho, M., Zhou, J., Bronowska, A., Martín, M. T., Eck, M. J., Kremer, L., Gräter, F., Gervasio, F. L., Perez-Moreno, M., and Lietha, D., (2014). Phosphatidylinositol 4, 5-bisphosphate triggers activation of focal adhesion kinase by inducing clustering and conformational changes. *Proceedings of the National Academy of Sciences 111*, E3177–E3186.

(*71*) Green, J. M., Zheleznyak, A., Chung, J., Lindberg, F. P., Sarfati, M., Frazier, W. A., and Brown, E. J., (1999). Role of cholesterol in formation and function of a signaling complex involving $\alpha v\beta 3$, integrin-associated protein (CD47), and heterotrimeric G proteins. *Journal of Cell Biology 146*, 673–682.

(*72*) Grewal, T., and Buechler, C., (2022). Emerging insights on the diverse roles of proprotein convertase subtilisin/kexin type 9 (PCSK9) in chronic liver diseases: cholesterol metabolism and beyond. *International Journal of Molecular Sciences 23*, 1070.

(*73*) Grewal, T., and Enrich, C., (2009). Annexins — modulators of EGF receptor signalling and trafficking. *Cellular Signalling 21*, 847–858.

(*74*) Grewal, T., and Enrich, C., (2006). Molecular mechanisms involved in Ras inactivation: the annexin A6–p120GAP complex. *Bioessays 28*, 1211–1220.

(*75*) Grewal, T., Koese, M., Rentero, C., and Enrich, C., (2010). Annexin A6-regulator of the EGFR/Ras signalling pathway and cholesterol homeostasis. *The International Journal of Biochemistry & Cell Biology 42*, 580–584.

(*76*) Grewal, T., Evans, R., Rentero, C., Tebar, F., Cubells, L., de Diego, I., Kirchhoff, M. F., Hughes, W. E., Heeren, J., Rye, K.-A., Rinninger, F., Daly, R. J., Pol, A., and Enrich, C., (2005). Annexin A6 stimulates the membrane recruitment of p120GAP to modulate Ras and Raf-1 activity. *Oncogene 24*, 5809–5820.

(*77*) Grewal, T., Hoque, M., Conway, J. R., Reverter, M., Wahba, M., Beevi, S. S., Timpson, P., Enrich, C., and Rentero, C., (2017). Annexin A6 — A multifunctional scaffold in cell motility. *Cell Adhesion & Migration 11*, 288–304.

(*78*) Grewal, T., Heeren, J., Mewawala, D., Schnitgerhans, T., Wendt, D., Salomon, G., Enrich, C., Beisiegel, U., and Jackle, S., (2000). Annexin VI stimulates endocytosis and is involved in the trafficking of low density lipoprotein to the prelysosomal compartment. *Journal of Biological Chemistry 275*, 33806–33813.

(*79*) Grewal, T., de Diego, I., Kirchhoff, M. F., Tebar, F., Heeren, J., Rinninger, F., and Enrich, C., (2003). High density lipoprotein-induced signaling of the MAPK pathway involves scavenger receptor type BI-mediated activation of Ras. *Journal of Biological Chemistry 278*, 16478–16481.

(*80*) Guerra, B., Recio, C., Aranda-Tavío, H., Guerra-Rodríguez, M., García-Castellano, J. M., and Fernández-Pérez, L., (2021). The mevalonate pathway, a metabolic target in cancer therapy. *Frontiers in Oncology 11*, 626971.

(*81*) Gunteski-Hamblin, A.-M., Song, G., Walsh, R. A., Frenzke, M., Dorn, G., Kaetzel, M. A., Horseman, N. D., and Dedman, J. R., (1996). Annexin 6 overexpression in transgenic mouse heart alters cardiac myocyte contractile function, calcium dynamics and heart pathology. *American Journal of Physiology 270*, H1091–H1100.

(*82*) Gurgis, F. M., Yeung, Y. T., Tang, M. X., Heng, B., Buckland, M., Ammit, A. J., Haapasalo, J., Haapasalo, H., Guillemin, G. J., Grewal, T., and Munoz, L., (2015). The p38-MK2-HuR pathway potentiates EGFRvIII–IL-1β-driven IL-6 secretion in glioblastoma cells. *Oncogene 34*, 2934–2942.

(*83*) Han, J., Hajjar, D. P., Febbraio, M., and Nicholson, A. C., (1997). Native and modified low density lipoproteins increase the functional expression of the macrophage class B scavenger receptor, CD36. *Journal of Biological Chemistry 272*, 21654–21659.

(*84*) Harder, K. W., Moller, N. P., Peacock, J. W., and Jirik, F. R., (1998). Protein-tyrosine phosphatase α regulates Src family kinases and alters cell-substratum adhesion. *Journal of Biological Chemistry 273*, 31890–31900.

(*85*) Hariharan, N., Maejima, Y., Nakae, J., Paik, J., DePinho, R. A., and Sadoshima, J., (2010). Deacetylation of FoxO by Sirt1 plays an essential role in mediating starvation-induced autophagy in cardiac myocytes. *Circulation Research 107*, 1470–1482.

(*86*) Hildebrand, J. D., Schaller, M. D., and Parsons, J. T., (1993). Identification of sequences required for the efficient localization of the focal adhesion kinase, pp125FAK, to cellular focal adhesions. *Journal of Cell Biology 123*, 993–1005.

(*87*) Hoffmann, P., Roumeguère, T., Schulman, C., and Van Velthoven, R., (2006). Use of statins and outcome of BCG treatment for bladder cancer. *New England Journal of Medicine 355*, 2705–2707.

(*88*) Hoque, M., Rentero, C., Conway, J. R., Murray, R. Z., Timpson, P., Enrich, C., and Grewal, T., (2015). The cross-talk of LDL-cholesterol with cell motility: insights from the Niemann Pick Type C1 mutation and altered integrin trafficking. *Cell Adhesion & Migration 9*, 384–391.

(*89*) Horton, E. R., Byron, A., Askari, J. A., Ng, D., Millon-Frémillon, A., Robertson, J., Koper, E. J., Paul, N. R., Warwood, S., Knight, D., Humphries, J. D., and Humphries, M. J., (2015). Definition of a consensus integrin adhesome and its dynamics during adhesion complex assembly and disassembly. *Nature Cell Biology 17*, 1577–1587.

(*90*) Horton, J. D., Bashmakov, Y., Shimomura, I., and Shimano, H., (1998). Regulation of sterol regulatory element binding proteins in livers of fasted and refed mice. *Proceedings of the National Academy of Sciences 95*, 5987–5992.

(*91*) Horton, J. D., Goldstein, J. L., and Brown, M. S., (2002). SREBPs: activators of the complete program of cholesterol and fatty acid synthesis in the liver. *Journal of Clinical Investigation 109*, 1125–1131.

(*92*) Horzum, U., Ozdil, B., and Pesen-Okvur, D., (2014). Step-by-step quantitative analysis of focal adhesions. *MethodsX 1*, 56–59.

(*93*) Hu, Y.-L., Lu, S., Szeto, K. W., Sun, J., Wang, Y., Lasheras, J. C., and Chien, S., (2014). FAK and paxillin dynamics at focal adhesions in the protrusions of migrating cells. *Scientific Reports 4*, 1–7.

(*94*) Hynes, R. O., (1992). Integrins: versatility, modulation, and signaling in cell adhesion. *Cell 69*, 11–25.

(*95*) Idevall-Hagren, O., Dickson, E. J., Hille, B., Toomre, D. K., and De Camilli, P., (2012). Optogenetic control of phosphoinositide metabolism. *Proceedings of the National Academy of Sciences 109*, E2316–E2323.

(*96*) Ikonen, E., (2008). Cellular cholesterol trafficking and compartmentalization. *Nature Reviews Molecular Cell Biology 9*, 125–138.

(*97*) Ikonen, E., (2018). Mechanisms of cellular cholesterol compartmentalization: recent insights. *Current Opinion in Cell Biology 53*, 77–83.

(*98*) Ilić, D., Genbačev, O., Jin, F., Caceres, E., Almeida, E. A., Bellingard-Dubouchaud, V., Schaefer, E. M., Damsky, C. H., and Fisher, S. J., (2001). Plasma membrane-associated pY397FAK is a marker of cytotrophoblast invasion in vivo and in vitro. *The American Journal of Pathology 159*, 93–108.

(*99*) Ilić, D., Furuta, Y., Kanazawa, S., Takeda, N., Sobue, K., Nakatsuji, N., Nomura, S., Fujimoto, J., Okada, M., Yamamoto, T., and Aizawa, S., (1995). Reduced cell motility and enhanced focal adhesion contact formation in cells from FAK-deficient mice. *Nature 377*, 539–544.

(*100*) Ishibashi, S., Yamazaki, T., and Okamoto, K., (2009). Association of autophagy with cholesterol-accumulated compartments in Niemann-Pick disease type C cells. *Journal of Clinical Neuroscience 16*, 954–959.

(*101*) Jeon, J. H., Kim, S. K., Kim, H. J., Chang, J., Ahn, C. M., and Chang, Y. S., (2010). Lipid raft modulation inhibits NSCLC cell migration through delocalization of the focal adhesion complex. *Lung Cancer 69*, 165–171.

(*102*) Johnson, B. B., Moe, P. C., Wang, D., Rossi, K., Trigatti, B. L., and Heuck, A. P., (2012). Modifications in perfringolysin O domain 4 alter the cholesterol concentration threshold required for binding. *Biochemistry 51*, 3373–3382.

(*103*) Jones, R. B., Gordus, A., Krall, J. A., and MacBeath, G., (2006). A quantitative protein interaction network for the ErbB receptors using protein microarrays. *Nature 439*, 168–174.

(*104*) Jose, J., Hoque, M., Engel, J., Beevi, S. S., Wahba, M., Georgieva, M. I., Murphy, K. J., Hughes, W. E., Cochran, B. J., Lu, A., Tebar, F., Hoy, A. J., Timpson, P., Rye, K.-A., Enrich, C., Rentero, C., and Grewal, T., (2022). Annexin A6 and NPC1 regulate LDL-inducible cell migration and distribution of focal adhesions. *Scientific Reports 12*, 1–17.

(*105*) Joshi, B., Strugnell, S. S., Goetz, J. G., Kojic, L. D., Cox, M. E., Griffith, O. L., Chan, S. K., Jones, S. J., Leung, S.-P., Masoudi, H., Leung, S., Wiseman, S. M., and Nabi, I. R., (2008). Phosphorylated caveolin-1 regulates Rho/ROCK-dependent focal adhesion dynamics and tumor cell migration and invasion. *Cancer Research 68*, 8210–8220.

(*106*) Kabeya, Y., Mizushima, N., Ueno, T., Yamamoto, A., Kirisako, T., Noda, T., Kominami, E., Ohsumi, Y., and Yoshimori, T., (2000). LC3, a mammalian homologue of yeast Apg8p, is localized in autophagosome membranes after processing. *The EMBO Journal 19*, 5720–5728.

(*107*) Kabir, J., Lobo, M., and Zachary, I., (2002). Staurosporine induces endothelial cell apoptosis via focal adhesion kinase dephosphorylation and focal adhesion disassembly independent of focal adhesion kinase proteolysis. *Biochemical Journal 367*, 145–155.

(*108*) Kam, Z., Zamir, E., and Geiger, B., (2001). Probing molecular processes in live cells by quantitative multidimensional microscopy. *Trends in Cell Biology 11*, 329–334.

(*109*) Kanerva, K., Uronen, R.-L., Blom, T., Li, S., Bittman, R., Lappalainen, P., Peränen, J., Raposo, G., and Ikonen, E., (2013). LDL cholesterol recycles to the plasma membrane via a Rab8a-Myosin5b-actin-dependent membrane transport route. *Developmental Cell 27*, 249–262.

(*110*) Katz, B.-Z., Krylov, D, Aota, S.-I., Olive, M, Vinson, C, and Yamada, K., (1998). Green fluorescent protein labeling of cytoskeletal structures—Novel targeting approach based on leucine zippers. *Biotechniques 25*, 298–304.

(*111*) Kean, M. J., Williams, K. C., Skalski, M., Myers, D., Burtnik, A., Foster, D., and Coppolino, M. G., (2009). VAMP3, syntaxin-13 and SNAP23 are involved in secretion of matrix metalloproteinases, degradation of the extracellular matrix and cell invasion. *Journal of Cell Science 122*, 4089–4098.

(*112*) Kenific, C. M., Wittmann, T., and Debnath, J., (2016). Autophagy in adhesion and migration. *Journal of Cell Science 129*, 3685–3693.

(*113*) Kennedy, M. A., Venkateswaran, A., Tarr, P. T., Xenarios, I., Kudoh, J., Shimizu, N., and Edwards, P. A., (2001). Characterization of the human ABCG1 gene: liver X receptor activates an internal promoter that produces a novel transcript encoding an alternative form of the protein. *Journal of Biological Chemistry 276*, 39438–39447.

(*114*) Kim, D.-H., and Wirtz, D., (2013). Predicting how cells spread and migrate: focal adhesion size does matter. *Cell Adhesion & Migration 7*, 293–296.

(*115*) Kim, H. Y., Park, S. J., Joe, E., and Jou, I., (2006). Raft-mediated Src homology 2 domain-containing proteintyrosine phosphatase 2 (SHP-2) regulation in microglia. *Journal of Biological Chemistry 281*, 11872–11878.

(*116*) Kim, J. Y., Jang, M. K., Lee, S.-S., Choi, M.-S., Bok, S.-H., Oh, G. T., and Park, Y. B., (2002). Rab7 gene is up-regulated by cholesterol-rich diet in the liver and artery. *Biochemical and Biophysical Research Communications 293*, 375–382.

(*117*) Kim, S.-W., Rhee, H. J., Ko, J., Kim, Y. J., Kim, H. G., Yang, J. M., Choi, E. C., and Na, D. S., (2001). Inhibition of cytosolic phospholipase A2 by annexin I: specific interaction model and mapping of the interaction site. *Journal of Biological Chemistry 276*, 15712–15719.

(*118*) Kiyoshima, D., Kawakami, K., Hayakawa, K., Tatsumi, H., and Sokabe, M., (2011). Force-and Ca^{2+}-dependent internalization of integrins in cultured endothelial cells. *Journal of Cell Science 124*, 3859–3870.

(*119*) Koese, M., Rentero, C., Kota, B. P., Hoque, M., Cairns, R., Wood, P., Vilà de Muga, S., Reverter, M., Alvarez-Guaita, A., Monastyrskaya, K., Hughes, W. E., Swarbrick, A., Tebar, F., Daly, R. J., Enrich, C., and Grewal, T., (2013). Annexin A6 is a scaffold for PKCα to promote EGFR inactivation. *Oncogene 32*, 2858–2872.

(*120*) Kontos, C. D., Stauffer, T. P., Yang, W.-P., York, J. D., Huang, L., Blanar, M. A., Meyer, T., and Peters, K. G., (1998). Tyrosine 1101 of Tie2 is the major site of association of p85 and is required for activation of phosphatidylinositol 3-kinase and Akt. *Molecular and Cellular Biology 18*, 4131–4140.

(*121*) Kostic, A., and Sheetz, M. P., (2006). Fibronectin rigidity response through Fyn and p130Cas recruitment to the leading edge. *Molecular Biology of the Cell 17*, 2684–2695.

(*122*) Krautbauer, S., Haberl, E. M., Eisinger, K., Pohl, R., Rein-Fischboeck, L., Rentero, C., Alvarez-Guaita, A., Enrich, C., Grewal, T., Buechler, C., et al. (2017). Annexin A6 regulates adipocyte lipid storage and adiponectin release. *Molecular and Cellular Endocrinology 439*, 419–430.

(*123*) Kristiana, I., Yang, H., and Brown, A. J., (2008). Different kinetics of cholesterol delivery to components of the cholesterol homeostatic machinery: implications for cholesterol trafficking to the endoplasmic reticulum. *Biochimica et Biophysica Acta - Molecular and cell biology of lipids 1781*, 724–730.

(*124*) Kruth, H. S., and Fry, D. L., (1984). Histochemical detection and differentiation of free and esterified cholesterol in swine atherosclerosis using filipin. *Experimental and molecular pathology 40*, 288–294.

(*125*) Kuzu, O. F., Noory, M. A., and Robertson, G. P., (2016). The role of cholesterol in cancer. *Cancer Research 76*, 2063–2070.

(*126*) Kwik, J., Boyle, S., Fooksman, D., Margolis, L., Sheetz, M. P., and Edidin, M., (2003). Membrane cholesterol, lateral mobility, and the phosphatidylinositol 4,5-bisphosphate-dependent organization of cell actin. *Proceedings of the National Academy of Sciences 100*, 13964–13969.

(*127*) Kwon, H. J., Abi-Mosleh, L., Wang, M. L., Deisenhofer, J., Goldstein, J. L., Brown, M. S., and Infante, R. E., (2009). Structure of N-terminal domain of NPC1 reveals distinct subdomains for binding and transfer of cholesterol. *Cell 137*, 1213–1224.

(*128*) Lai, I.-R., Chu, P.-Y., Lin, H.-S., Liou, J.-Y., Jan, Y.-J., Lee, J.-C., and Shen, T.-L., (2010). Phosphorylation of focal adhesion kinase at Tyr397 in gastric carcinomas and its clinical significance. *The American Journal of Pathology 177*, 1629–1637.

(*129*) Lawson, M. A., and Maxfield, F. R., (1995). Ca^{2+}-and calcineurin-dependent recycling of an integrin to the front of migrating neutrophils. *Nature 377*, 75–79.

(*130*) Lee, B. Y., Timpson, P., Horvath, L. G., and Daly, R. J., (2015). FAK signaling in human cancer as a target for therapeutics. *Pharmacology & Therapeutics 146*, 132–149.

(*131*) Lele, T. P., Pendse, J., Kumar, S., Salanga, M., Karavitis, J., and Ingber, D. E., (2006). Mechanical forces alter zyxin unbinding kinetics within focal adhesions of living cells. *Journal of Cellular Physiology 207*, 187–194.

(*132*) Lev, S., (2010). Non-vesicular lipid transport by lipid-transfer proteins and beyond. *Nature Reviews Molecular Cell Biology 11*, 739–750.

(*133*) Li, B., and Trueb, B., (2001). Analysis of the α-actinin/zyxin interaction. *Journal of Biological Chemistry 276*, 33328–33335.

(*134*) Li, Y., Wu, S., Zhao, X., Hao, S., Li, F., Wang, Y., Liu, B., Zhang, D., Wang, Y., and Zhou, H., (2023). Key events in cancer: dysregulation of SREBPs. *Frontiers in Pharmacology 14*, 1130747.

(*135*) Lim, Y., Han, I., Jeon, J., Park, H., Bahk, Y.-Y., and Oh, E.-S., (2004). Phosphorylation of focal adhesion kinase at tyrosine 861 is crucial for Ras transformation of fibroblasts. *Journal of Biological Chemistry 279*, 29060–29065.

(*136*) Linder, M. D., Uronen, R.-L., Hölttä-Vuori, M., van der Sluijs, P., Peränen, J., and Ikonen, E., (2007). Rab8-dependent recycling promotes endosomal cholesterol removal in normal and sphingolipidosis cells. *Molecular Biology of the Cell 18*, 47–56.

(*137*) Lingwood, D., and Simons, K., (2010). Lipid rafts as a membrane-organizing principle. *Science 327*, 46–50.

(*138*) Liscum, L., (2000). Niemann–Pick type C mutations cause lipid traffic jam. *Traffic 1*, 218–225.

(*139*) Liscum, L., and Faust, J., (1987). Low density lipoprotein (LDL)-mediated suppression of cholesterol synthesis and LDL uptake is defective in Niemann-Pick type C fibroblasts. *Journal of Biological Chemistry 262*, 17002–17008.

(*140*) Liu, S.-L., Sheng, R., Jung, J. H., Wang, L., Stec, E., O'Connor, M. J., Song, S., Bikkavilli, R. K., Winn, R. A., Lee, D., Baek, K., Ueda, K., Levitan, I., Kim, K.-P., and Cho, W., (2017). Orthogonal lipid sensors identify transbilayer asymmetry of plasma membrane cholesterol. *Nature Chemical Biology 13*, 268–274.

(*141*) Llaverias, G., Danilo, C., Mercier, I., Daumer, K., Capozza, F., Williams, T. M., Sotgia, F., Lisanti, M. P., and Frank, P. G., (2011). Role of cholesterol in the development and progression of breast cancer. *The American Journal of Pathology 178*, 402–412.

(*142*) Loftus, S. K., Morris, J. A., Carstea, E. D., Gu, J. Z., Cummings, C., Brown, A., Ellison, J., Ohno, K., Rosenfeld, M. A., Tagle, D. A., Pentchev, P. G., and Pavan, W. J., (1997). Murine model of Niemann-Pick C disease: mutation in a cholesterol homeostasis gene. *Science 277*, 232–235.

(*143*) Long, T., Qi, X., Hassan, A., Liang, Q., De Brabander, J. K., and Li, X., (2020). Structural basis for itraconazole-mediated NPC1 inhibition. *Nature Communications 11*, 1–11.

(*144*) Lowry, O. H., Rosebrough, N. J., Farr, A. L., and Randall, R. J., (1951). Protein Measurement with the Folin Phenol Reagent. *Journal of Biological Chemistry 193*, 265–275.

(*145*) Lu, F., Liang, Q., Abi-Mosleh, L., Das, A., De Brabander, J. K., Goldstein, J. L., and Brown, M. S., (2015). Identification of NPC1 as the target of U18666A, an inhibitor of lysosomal cholesterol export and Ebola infection. *eLife 4*, e12177.

(*146*) Luo, J., Yang, H., and Song, B.-L., (2020). Mechanisms and regulation of cholesterol homeostasis. *Nature Reviews Molecular Cell Biology 21*, 225–245.

(*147*) Luo, J., Jiang, L., Yang, H., and Song, B.-L., (2017). Routes and mechanisms of post-endosomal cholesterol trafficking: A story that never ends. *Traffic 18*, 209–217.

(*148*) Maekawa, M., and Fairn, G. D., (2015). Complementary probes reveal that phosphatidylserine is required for the proper transbilayer distribution of cholesterol. *Journal of Cell Science 128*, 1422–1433.

(*149*) Mahmood, T., and Yang, P.-C., (2012). Western blot: technique, theory, and trouble shooting. *North American Journal of Medical Sciences 4*, 429.

(*150*) Malaney, S., and Daly, R. J., (2001). The Ras signaling pathway in mammary tumorigenesis and metastasis. *Journal of Mammary Gland Biology and Neoplasia 6*, 101–113.

(*151*) Malumbres, M., and Barbacid, M., (2003). RAS oncogenes: the first 30 years. *Nature Reviews Cancer 3*, 459–465.

(*152*) Mañes, S., and Viola, A., (2006). Lipid rafts in lymphocyte activation and migration. *Molecular Membrane Biology 23*, 59–69.

(*153*) Maslyanko, M., Harris, R. D., and Mu, D., (2021). Connecting cholesterol efflux factors to lung cancer biology and therapeutics. *International Journal of Molecular Sciences 22*, 7209.

(*154*) Maulik, M., Thinakaran, G., and Kar, S., (2013). Alterations in gene expression in mutant amyloid precursor protein transgenic mice lacking Niemann-Pick type C1 protein. *PloS one 8*, e54605.

(*155*) Meneses-Salas, E., García-Melero, A., Kanerva, K., Blanco-Muñoz, P., Morales-Paytuvi, F., Bonjoch, J., Casas, J., Egert, A., Beevi, S. S., Jose, J., Llorente-Cortés, V., Rye, K.-A., Heeren, J., Lu, A., Pol, A., Tebar, F., Ikonen, E., Grewal, T., Enrich, C., and Rentero, C., (2020). Annexin A6 modulates TBC1D15/Rab7/StARD3 axis to control endosomal cholesterol export in NPC1 cells. *Cellular and Molecular Life Sciences 77*, 2839–2857.

(*156*) Millard, E. E., Srivastava, K., Traub, L. M., Schaffer, J. E., and Ory, D. S., (2000). Niemann-pick type C1 (NPC1) overexpression alters cellular cholesterol homeostasis. *Journal of Biological Chemistry 275*, 38445–38451.

(*157*) Mishra, Y. G., and Manavathi, B., (2021). Focal adhesion dynamics in cellular function and disease. *Cellular Signalling 85*, 110046.

(*158*) Mitra, S. K., and Schlaepfer, D. D., (2006). Integrin-regulated FAK–Src signaling in normal and cancer cells. *Current Opinion in Cell Biology 18*, 516–523.

(*159*) Monastyrskaya, K., Babiychuk, E. B., Hostettler, A., Wood, P., Grewal, T., and Draeger, A., (2009). Plasma membrane-associated annexin A6 reduces Ca^{2+} entry by stabilizing the cortical actin cytoskeleton. *Journal of Biological Chemistry 284*, 17227–17242.

(*160*) Moon, H., Ruelcke, J. E., Choi, E., Sharpe, L. J., Nassar, Z. D., Bielefeldt-Ohmann, H., Parat, M.-O., Shah, A., Francois, M., Inder, K. L., Brown, A. J., Russell, P. J., Parton, R. G., and Hill, M. M., (2015). Diet-induced hypercholesterolemia promotes androgen-independent prostate cancer metastasis via IQGAP1 and caveolin-1. *Oncotarget 6*, 7438.

(*161*) Mullen, P. J., Yu, R., Longo, J., Archer, M. C., and Penn, L. Z., (2016). The interplay between cell signalling and the mevalonate pathway in cancer. *Nature Reviews Cancer 16*, 718–731.

(*162*) Murai, T., (2015). Cholesterol lowering: role in cancer prevention and treatment. *Biological Chemistry 396*, 1–11.

(*163*) Murai, T., Maruyama, Y., Mio, K., Nishiyama, H., Suga, M., and Sato, C., (2011). Low cholesterol triggers membrane microdomain-dependent CD44 shedding and suppresses tumor cell migration. *Journal of Biological Chemistry 286*, 1999–2007.

(*164*) Nader, G. P., Ezratty, E. J., and Gundersen, G. G., (2016). FAK, talin and PIPKIγ regulate endocytosed integrin activation to polarize focal adhesion assembly. *Nature Cell Biology 18*, 491–503.

(*165*) Nguyen, M. K., Jose, J., Wahba, M., Bernaus-Esqué, M., Hoy, A. J., Enrich, C., Rentero, C., and Grewal, T., (2022). Linking late endosomal cholesterol with cancer progression and anticancer drug resistance. *International Journal of Molecular Sciences 23*, 7206.

(*166*) Olkkonen, V. M., and Ikonen, E., (2022). Cholesterol transport in the late endocytic pathway: Roles of ORP family proteins. *Journal of Steroid Biochemistry and Molecular Biology 216*, 106040.

(*167*) Oram, J. F., (2002). ATP-binding cassette transporter A1 and cholesterol trafficking. *Current Opinion in Lipidology 13*, 373–381.

(*168*) Pagler, T. A., Neuhofer, A., Laggner, H., Strobl, W., and Stangl, H., (2007). Cholesterol efflux via HDL resecretion occurs when cholesterol transport out of the lysosome is impaired. *Journal of Lipid Research 48*, 2141–2150.

(*169*) Pan, C., Lan, X., Chen, H., and Bishop, C. E., (2010). An economical single-sided antibody incubation method for Western blotting. *Journal of Virological Methods 169*, 409–411.

(*170*) Park, E.-K., Park, M. J., Lee, S.-H., Li, Y. C., Kim, J., Lee, J.-S., Lee, J. W., Ye, S.-K., Park, J.-W., Kim, C.-W., et al. (2009). Cholesterol depletion induces anoikis-like apoptosis via FAK down-regulation and caveolae internalization. *The Journal of Pathology: A Journal of the Pathological Society of Great Britain and Ireland 218*, 337–349.

(*171*) Park, Y. M., (2014). CD36, a scavenger receptor implicated in atherosclerosis. *Experimental & Molecular Medicine 46*, e99.

(*172*) Parsons, J. T., (2003). Focal adhesion kinase: the first ten years. *Journal of Cell Science 116*, 1409–1416.

(*173*) Parton, R. G., and Del Pozo, M. A., (2013). Caveolae as plasma membrane sensors, protectors and organizers. *Nature Reviews Molecular Cell Biology 14*, 98–112.

(*174*) Pasapera, A. M., Schneider, I. C., Rericha, E., Schlaepfer, D. D., and Waterman, C. M., (2010). Myosin II activity regulates vinculin recruitment to focal adhesions through FAK-mediated paxillin phosphorylation. *Journal of Cell Biology 188*, 877–890.

(*175*) Pasello, M., Giudice, A. M., and Scotlandi, K., (2020). The ABC subfamily A transporters: Multifaceted players with incipient potentialities in cancer. *Seminars in Cancer Biology 60*, 57–71.

(*176*) Peterson, C., Vitols, S., Rudling, M., Blomgren, H., Edsmyr, F., and Skoog, L., (1985). Hypocholesterolemia in cancer patients may be caused by elevated LDL receptor activities in malignant cells. *Medical Oncology and Tumor Pharmacotherapy 2*, 143–147.

(*177*) Peterson, T., Sengupta, S., Harris, T., Carmack, A., Kang, S., Balderas, E., Guertin, D., Madden, K., Carpenter, A., Finck, B., and Sabatini, D., (2011). mTOR complex 1 regulates lipin 1 localization to control the SREBP pathway. *Cell 146*, 408–420.

(*178*) Pillai-Kastoori, L., Schutz-Geschwender, A. R., and Harford, J. A., (2020). A systematic approach to quantitative western blot analysis. *Analytical Biochemistry 593*, 113608.

(*179*) Pol, A., Martin, S., Fernández, M. A., Ingelmo-Torres, M., Ferguson, C., Enrich, C., and Parton, R. G., (2005). Cholesterol and fatty acids regulate dynamic caveolin trafficking through the Golgi complex and between the cell surface and lipid bodies. *Molecular Biology of the Cell 16*, 2091–2105.

(*180*) Pons, M., Grewal, T., Rius, E., Schnitgerhans, T., Jäckle, S., and Enrich, C., (2001). Evidence for the involvement of annexin 6 in the trafficking between the endocytic compartment and lysosomes. *Experimental Cell Research 269*, 13–22.

(*181*) Predescu, S. A., Predescu, D. N., Shimizu, K., Klein, I. K., and Malik, A. B., (2005). Cholesterol-dependent syntaxin-4 and SNAP-23 clustering regulates caveolar fusion with the endothelial plasma membrane. *Journal of Biological Chemistry 280*, 37130–37138.

(*182*) Puck, T. T., Cieciura, S. J., and Robinson, A., (1958). Genetics of somatic mammalian cells: III. Long-term cultivation of euploid cells from human and animal subjects. *Journal of Experimental Medicine 108*, 945.

(*183*) Qiagen, (2015). QIAprep Miniprep Handbook., 20–21.

(*184*) Radhakrishnan, A., Goldstein, J. L., McDonald, J. G., and Brown, M. S., (2008). Switch-like control of SREBP-2 transport triggered by small changes in ER cholesterol: a delicate balance. *Cell Metabolism 8*, 512–521.

(*185*) Raftopulos, N. L., Washaya, T. C., Niederprüm, A., Egert, A., Hakeem-Sanni, M.-r. F., Varney, B., Aishah, A., Georgieva, M. L., Olsson, E., Dos Santos, D. Z., Nassar, Z. D., Cochran, B. J., Nagarajan, S. R., Kakani, M. S., Hastings, J. F., Croucher, D. R., Rye, K.-A., Butler, L. M., Grewal, T., and Hoy, A. J., (2022). Prostate cancer cell proliferation is influenced by LDL-cholesterol availability and cholesteryl ester turnover. *Cancer & Metabolism 10*, 1–15.

(*186*) Ramprasad, O. G., Srinivas, G., Rao, K. S., Joshi, P., Thiery, J. P., Dufour, S., and Pande, G., (2007). Changes in cholesterol levels in the plasma membrane modulate cell signaling and regulate cell adhesion and migration on fibronectin. *Cell Motility and the Cytoskeleton 64*, 199–216.

(*187*) Ravnskov, U., Rosch, P. J., and McCully, K. S., (2015). Statins do not protect against cancer: quite the opposite. *Journal of Clinical Oncology 33*, 810–811.

(*188*) Renart, J., Reiser, J., and Stark, G. R., (1979). Transfer of proteins from gels to diazobenzyloxymethyl-paper and detection with antisera: a method for studying antibody specificity and antigen structure. *Proceedings of the National Academy of Sciences 76*, 3116–3120.

(*189*) Reverter, M., Rentero, C., Garcia-Melero, A., Hoque, M., Vilà de Muga, S., Álvarez Guaita, A., Conway, J., Wood, P., Cairns, R., Lykopoulou, L., Grinberg, D., Vilageliu, L., Bosch, M., Heeren, J., Blasi, J., Timpson, P., Pol, A., Tebar, F., Murray, R., Grewal, T., and Enrich, C., (2014). Cholesterol regulates Syntaxin 6 trafficking at trans-Golgi network endosomal boundaries. *Cell Reports 7*, 883–897.

(*190*) Reverter, M., Rentero, C., Vilà de Muga, S., Alvarez-Guaita, A., Mulay, V., Cairns, R., Wood, P., Monastyrskaya, K., Pol, A., Tebar, F., Blasi, J., Grewal, T., and Enrich, C., (2011). Cholesterol transport from late endosomes to the Golgi regulates t-SNARE trafficking, assembly, and function. *Molecular Biology of the Cell 22*, 4108–4123.

(*191*) Rickman, C., and Davletov, B., (2005). Arachidonic acid allows SNARE complex formation in the presence of Munc18. *Chemistry & Biology 12*, 545–553.

(*192*) Ricoult, S. J., Yecies, J. L., Ben-Sahra, I., and Manning, B. D., (2016). Oncogenic PI3K and K-Ras stimulate de novo lipid synthesis through mTORC1 and SREBP. *Oncogene 35*, 1250–1260.

(*193*) Ridley, A. J., (2001). Rho GTPases and cell migration. *Journal of Cell Science 114*, 2713–2722.

(*194*) Ridley, A. J., Schwartz, M. A., Burridge, K., Firtel, R. A., Ginsberg, M. H., Borisy, G., Parsons, J. T., and Horwitz, A. R., (2003). Cell migration: integrating signals from front to back. *Science 302*, 1704–1709.

(*195*) Riggs, K. A., Hasan, N., Humphrey, D., Raleigh, C., Nevitt, C., Corbin, D., and Hu, C., (2012). Regulation of integrin endocytic recycling and chemotactic cell migration by syntaxin 6 and VAMP3 interaction. *Journal of Cell Science 125*, 3827–3839.

(*196*) Riscal, R., Skuli, N., and Simon, M. C., (2019). Even cancer cells watch their cholesterol! *Molecular Cell 76*, 220–231.

(*197*) Robinson, J. M., and Karnovsky, M. J., (1980). Evaluation of the polyene antibiotic filipin as a cytochemical probe for membrane cholesterol. *Journal of Histochemistry & Cytochemistry 28*, 161–168.

(*198*) Roca-Cusachs, P., Del Rio, A., Puklin-Faucher, E., Gauthier, N. C., Biais, N., and Sheetz, M. P., (2013). Integrin-dependent force transmission to the extracellular matrix by α-actinin triggers adhesion maturation. *Proceedings of the National Academy of Sciences 110*, E1361–E1370.

(*199*) Rottner, K., Krause, M., Gimona, M., Small, J. V., and Wehland, J., (2001). Zyxin is not colocalized with vasodilator-stimulated phosphoprotein (VASP) at lamellipodial tips and exhibits different dynamics to vinculin, paxillin, and VASP in focal adhesions. *Molecular Biology of the Cell 12*, 3103–3113.

(*200*) Rye, K.-A., Garrety, K. H., and Barter, P. J., (1993). Preparation and characterization of spheroidal, reconstituted high-density lipoproteins with apolipoprotein AI only or with apolipoprotein AI and A-II. *Biochimica et Biophysica Acta - Lipids and Lipid Metabolism 1167*, 316–325.

(*201*) Sandilands, E., and Frame, M. C., (2008). Endosomal trafficking of Src tyrosine kinase. *Trends in cell biology 18*, 322–329.

(*202*) Sandilands, E., Cans, C., Fincham, V. J., Brunton, V. G., Mellor, H., Prendergast, G. C., Norman, J. C., Superti-Furga, G., and Frame, M. C., (2004). RhoB and actin polymerization coordinate Src activation with endosome-mediated delivery to the membrane. *Developmental Cell 7*, 855–869.

(*203*) Saraste, J., Enyioko, M., Dale, H., Prydz, K., and Machamer, C., (2022). Evidence for the role of Rab11-positive recycling endosomes as intermediates in coronavirus egress from epithelial cells. *Histochemistry and Cell Biology 158*, 241–251.

(*204*) Sathyanarayan, A., Mashek, M. T., and Mashek, D. G., (2017). ATGL promotes autophagy/lipophagy via SIRT1 to control hepatic lipid droplet catabolism. *Cell reports 19*, 1–9.

(*205*) Sato, R., Goldstein, J. L., and Brown, M. S., (1993). Replacement of serine-871 of hamster 3-hydroxy-3-methylglutaryl-CoA reductase prevents phosphorylation by AMP-activated kinase and blocks inhibition of sterol synthesis induced by ATP depletion. *Proceedings of the National Academy of Sciences 90*, 9261–9265.

(*206*) Saunders, R. M., Holt, M. R., Jennings, L., Sutton, D. H., Barsukov, I. L., Bobkov, A., Liddington, R. C., Adamson, E. A., Dunn, G. A., and Critchley, D. R., (2006). Role of vinculin in regulating focal adhesion turnover. *European Journal of Cell Biology 85*, 487–500.

(*207*) Schaller, M. D., Hildebrand, J. D., Shannon, J. D., Fox, J. W., Vines, R. R., and Parsons, J. T., (1994). Autophosphorylation of the focal adhesion kinase, pp125FAK, directs SH2-dependent binding of pp60Src. *Molecular and Cellular Biology 14*, 1680–1688.

(*208*) Schaller, M. D., Hildebrand, J. D., and Parsons, J. T., (1999). Complex formation with focal adhesion kinase: a mechanism to regulate activity and subcellular localization of Src kinases. *Molecular Biology of the Cell 10*, 3489–3505.

(*209*) Schmitz, G., and Grandl, M., (2009). The molecular mechanisms of HDL and associated vesicular trafficking mechanisms to mediate cellular lipid homeostasis. *Arteriosclerosis, Thrombosis, and Vascular Biology 29*, 1718–1722.

(*210*) Schoenherr, C., Byron, A., Sandilands, E., Paliashvili, K., Baillie, G. S., Garcia-Munoz, A., Valacca, C., Cecconi, F., Serrels, B., and Frame, M. C., (2017). Ambra1 spatially regulates Src activity and Src/FAK-mediated cancer cell invasion via trafficking networks. *eLife 6*, e23172.

(*211*) Schoop, V., Martello, A., Eden, E. R., and Höglinger, D., (2021). Cellular cholesterol and how to find it. *Biochimica et Biophysica Acta - Molecular and Cell Biology of Lipids 1866*, 158989.

(*212*) Schreiner, C. L., Bauer, J. S., Danilov, Y. N., Hussein, S., Sczekan, M. M., and Juliano, R., (1989). Isolation and characterization of Chinese hamster ovary cell variants deficient in the expression of fibronectin receptor. *Journal of Cell Biology 109*, 3157–3167.

(*213*) Sever, N., Song, B.-L., Yabe, D., Goldstein, J. L., Brown, M. S., and DeBose-Boyd, R. A., (2003). Insig-dependent ubiquitination and degradation of mammalian 3-hydroxy-3-methylglutaryl-CoA reductase stimulated by sterols and geranylgeraniol. *Journal of Biological Chemistry 278*, 52479–52490.

(*214*) Shackelford, D. B., and Shaw, R. J., (2009). The LKB1–AMPK pathway: metabolism and growth control in tumour suppression. *Nature Reviews Cancer 9*, 563–575.

(*215*) Shaner, N. C., Campbell, R. E., Steinbach, P. A., Giepmans, B., Palmer, A. E., and Tsien, R. Y., (2004). Improved monomeric red, orange and yellow fluorescent proteins derived from Discosoma sp. red fluorescent protein. *Nature Biotechnology 22*, 1567–1572.

(*216*) Shimada, Y., Maruya, M., Iwashita, S., and Ohno-Iwashita, Y., (2002). The C-terminal domain of perfringolysin O is an essential cholesterol-binding unit targeting to cholesterol-rich microdomains. *European Journal of Biochemistry 269*, 6195–6203.

(*217*) Shimomura, O., (2005). The discovery of aequorin and green fluorescent protein. *Journal of Microscopy 217*, 3–15.

(*218*) Silvente-Poirot, S., and Poirot, M., (2014). Cholesterol and cancer, in the balance. *Science 343*, 1445–1446.

(*219*) Simons, K., and Toomre, D., (2000). Lipid rafts and signal transduction. *Nature Reviews Molecular Cell Biology 1*, 31–39.

(*220*) Skalski, M., and Coppolino, M. G., (2005). SNARE-mediated trafficking of $\alpha 5\beta 1$ integrin is required for spreading in CHO cells. *Biochemical and Biophysical Research Communications 335*, 1199–1210.

(*221*) Skalski, M., Sharma, N., Williams, K., Kruspe, A., and Coppolino, M. G., (2011). SNARE-mediated membrane traffic is required for focal adhesion kinase signaling and Src-regulated focal adhesion turnover. *Biochimica et Biophysica Acta - Molecular Cell Research 1813*, 148–158.

(*222*) Slack, J. K., Adams, R. B., Rovin, J. D., Bissonette, E. A., Stoker, C. E., and Parsons, J. T., (2001). Alterations in the focal adhesion kinase/Src signal transduction pathway correlate with increased migratory capacity of prostate carcinoma cells. *Oncogene 20*, 1152–1163.

(*223*) Small, J.-V., Rottner, K., Hahne, P., and Anderson, K. I., (1999). Visualising the actin cytoskeleton. *Microscopy Research and Technique 47*, 3–17.

(*224*) Smith, B. J., (1984). SDS polyacrylamide gel electrophoresis of proteins. *Proteins*, 41–55.

(*225*) Sokolov, A., and Radhakrishnan, A., (2010). Accessibility of cholesterol in endoplasmic reticulum membranes and activation of SREBP-2 switch abruptly at a common cholesterol threshold. *Journal of Biological Chemistry 285*, 29480–29490.

(*226*) Sorrentino, G., Ruggeri, N., Specchia, V., Cordenonsi, M., Mano, M., Dupont, S., Manfrin, A., Ingallina, E., Sommaggio, R., Piazza, S., Rosato, A., Piccolo, S., and Del Sal, G., (2014). Metabolic control of YAP and TAZ by the mevalonate pathway. *Nature Cell Biology 16*, 357–366.

(*227*) Stellaard, F., (2022). From dietary cholesterol to blood cholesterol, physiological lipid fluxes, and cholesterol homeostasis. *Nutrients 14*, 1643.

(*228*) Stolz, A., Ernst, A., and Dikic, I., (2014). Cargo recognition and trafficking in selective autophagy. *Nature Cell Biology 16*, 495–501.

(*229*) Subauste, M. C., Pertz, O., Adamson, E. D., Turner, C. E., Junger, S., and Hahn, K. M., (2004). Vinculin modulation of paxillin–FAK interactions regulates ERK to control survival and motility. *Journal of Cell Biology 165*, 371–381.

(*230*) Sun, X., Shu, Y., Xu, M., Jiang, J., Wang, L., Wang, J., Huang, D., and Zhang, J., (2020). ANXA6 suppresses the tumorigenesis of cervical cancer through autophagy induction. *Clinical and Translational Medicine 10*, e208.

(*231*) Takahashi, K., Kanerva, K., Vanharanta, L., Almeida-Souza, L., Lietha, D., Olkkonen, V. M., and Ikonen, E., (2021). ORP2 couples LDL-cholesterol transport to FAK activation by endosomal cholesterol/PI(4,5)P2 exchange. *The EMBO Journal 40*, e106871.

(*232*) Tao, R., Xiong, X., DePinho, R. A., Deng, C.-X., and Dong, X. C., (2013). Hepatic SREBP-2 and cholesterol biosynthesis are regulated by FoxO3 and Sirt6[S]. *Journal of Lipid Research 54*, 2745–2753.

(*233*) Tayeb, M. A., Skalski, M., Cha, M. C., Kean, M. J., Scaife, M., and Coppolino, M. G., (2005). Inhibition of SNARE-mediated membrane traffic impairs cell migration. *Experimental Cell Research 305*, 63–73.

(*234*) Timpson, P., McGhee, E. J., Morton, J. P., Von Kriegsheim, A., Schwarz, J. P., Karim, S. A., Doyle, B., Quinn, J. A., Carragher, N. O., Edward, M., Olson, M. F., Frame, M. C., Brunton, V. G., Sansom, O. J., and Anderson, K. I., (2011). Spatial regulation of RhoA activity during pancreatic cancer cell invasion driven by mutant p53RhoA activity in vivo. *Cancer Research 71*, 747–757.

(*235*) Tiwari, A., Jung, J.-J., Inamdar, S. M., Brown, C. O., Goel, A., and Choudhury, A., (2011). Endothelial cell migration on fibronectin is regulated by syntaxin 6-mediated $\alpha 5\beta 1$ integrin recycling. *Journal of Biological Chemistry 286*, 36749–36761.

(*236*) Tveten, K., Holla, Ø. L., Cameron, J., Strøm, T. B., Berge, K. E., Laerdahl, J. K., and Leren, T. P., (2012). Interaction between the ligand-binding domain of the LDL receptor and the C-terminal domain of PCSK9 is required for PCSK9 to remain bound to the LDL receptor during endosomal acidification. *Human Molecular Genetics 21*, 1402–1409.

(*237*) Urano, Y., Watanabe, H., Murphy, S. R., Shibuya, Y., Geng, Y., Peden, A. A., Chang, C. C., and Chang, T. Y., (2008). Transport of LDL-derived cholesterol from the NPC1 compartment to the ER involves the trans-Golgi network and the SNARE protein complex. *Proceedings of the National Academy of Sciences 105*, 16513–16518.

(*238*) Vasanji, A., Ghosh, P. K., Graham, L. M., Eppell, S. J., and Fox, P. L., (2004). Polarization of plasma membrane microviscosity during endothelial cell migration. *Developmental Cell 6*, 29–41.

(*239*) Vassilieva, E. V., Gerner-Smidt, K., Ivanov, A. I., and Nusrat, A., (2008). Lipid rafts mediate internalization of $\beta 1$-integrin in migrating intestinal epithelial cells. *American Journal of Physiology-Gastrointestinal and Liver Physiology 295*, G965–G976.

(*240*) Vázquez, M. C., del Pozo, T., Robledo, F. A., Carrasco, G., Pavez, L., Olivares, F., González, M., and Zanlungo, S., (2011). Alteration of gene expression profile in Niemann-Pick type C mice correlates with tissue damage and oxidative stress. *PLoS One 6*, e28777.

(*241*) Vilà de Muga, S., Timpson, P., Cubells, L., Evans, R., Hayes, T. E., Rentero, C., Hegemann, A., Reverter, M., Leschner, J., Pol, A., Tebar, F., Daly, R. J., Enrich, C., and Grewal, T., (2009). Annexin A6 inhibits Ras signalling in breast cancer cells. *Oncogene 28*, 363–377.

(*242*) Villa, G., Hulce, J., Zanca, C., Bi, J., Ikegami, S., Cahill, G., Gu, Y., Lum, K., Masui, K., Yang, H., Rong, X., Hong, C., Turner, K., Liu, F., Hon, G., Jenkins, D., Martini, M., Armando, A., Quehenberger, O., Cloughesy, T., Furnari, F., Cavenee, W., Tontonoz, P., Gahman, T., Shiau, A., Cravatt, B., and Mischel, P., (2016). An LXR-cholesterol axis creates a metabolic co-dependency for brain cancers. *Cancer Cell 30*, 683–693.

(*243*) Vuori, K., Hirai, H., Aizawa, S., and Ruoslahti, E., (1996). Introduction of p130cas signaling complex formation upon integrin-mediated cell adhesion: a role for Src family kinases. *Molecular and Cellular Biology 16*, 2606–2613.

(*244*) Walker, A. K., Yang, F., Jiang, K., Ji, J.-Y., Watts, J. L., Purushotham, A., Boss, O., Hirsch, M. L., Ribich, S., Smith, J. J., Israelian, K., Westphal, C. H., Rodgers, J. T., Shioda, T., Elson, S. L., Mulligan, P., Najafi-Shoushtari, H., Black, J. C., Thakur, J. K., Kadyk, L. C., Whetstine, J. R., Mostoslavsky, R., Puigserver, P., Li, X., Dyson, N. J., Hart, A. C., and Näär, A. M., (2010). Conserved role of SIRT1 orthologs in fasting-dependent inhibition of the lipid/cholesterol regulator SREBP. *Genes & Development 24*, 1403–1417.

(*245*) Wang, B. T., Ducker, G. S., Barczak, A. J., Barbeau, R., Erle, D. J., and Shokat, K. M., (2011). The mammalian target of rapamycin regulates cholesterol biosynthetic gene expression and exhibits a rapamycin-resistant transcriptional profile. *Proceedings of the National Academy of Sciences 108*, 15201–15206.

(*246*) Wang, C., Li, P., Xuan, J., Zhu, C., Liu, J., Shan, L., Du, Q., Ren, Y., and Ye, J., (2017). Cholesterol enhances colorectal cancer progression via ROS elevation and MAPK signaling pathway activation. *Cellular Physiology and Biochemistry 42*, 729–742.

(*247*) Wang, C., Yoo, Y., Fan, H., Kim, E., Guan, K.-L., and Guan, J.-L., (2010). Regulation of Integrin β1 recycling to lipid rafts by Rab1a to promote cell migration. *Journal of Biological Chemistry 285*, 29398–29405.

(*248*) Wang, H., Ma, Q., Qi, Y., Dong, J., Du, X., Rae, J., Wang, J., Wu, W.-F., Brown, A. J., Parton, R. G., Wu, J.-W., and Yang, H.-y., (2019). ORP2 delivers cholesterol to the plasma membrane in exchange for phosphatidylinositol 4,5-bisphosphate (PI(4,5)P2). *Molecular Cell 73*, 458–473.

(*249*) Wang, J., and Richards, D. A., (2012). Segregation of PIP2 and PIP3 into distinct nanoscale regions within the plasma membrane. *Biology Open 1*, 857–862.

(*250*) Wang, M., Pan, M., Li, Y., Lu, T., Wang, Z., Liu, C., and Hu, G., (2023). ANXA6/TRPV2 axis promotes lymphatic metastasis in head and neck squamous cell carcinoma by inducing autophagy. *Experimental Hematology & Oncology 12*, 1–16.

(*251*) Wang, R., Bi, J., Ampah, K. K., Ba, X., Liu, W., and Zeng, X., (2013). Lipid rafts control human melanoma cell migration by regulating focal adhesion disassembly. *Biochimica et Biophysica Acta - Molecular Cell Research 1833*, 3195–3205.

(*252*) Wang, T., and Pattabiraman, P. P., (2022). Cholesterol regulates actin polymerization in trabecular meshwork. *Investigative Ophthalmology & Visual Science 63*, 3292–A0392.

(*253*) Wang, Z., Tung, P. S., and Moran, M. F., (1996). Association of p120 Ras GAP with endocytic components and colocalization with epidermal growth factor (EGF) receptor in response to EGF stimulation. *Cell growth & Differentiation: the Molecular Biology Journal of the American Association for Cancer Research 7*, 123.

(*254*) Webb, D. J., Donais, K., Whitmore, L. A., Thomas, S. M., Turner, C. E., Parsons, J. T., and Horwitz, A. F., (2004). FAK–Src signalling through paxillin, ERK and MLCK regulates adhesion disassembly. *Nature Cell Biology 6*, 154–161.

(*255*) Wehrle-Haller, B., and Imhof, B. A., (2002). The inner lives of focal adhesions. *Trends in Cell Biology 12*, 382–389.

(*256*) Weng, Z., Taylor, J. A., Turner, C. E., Brugge, J. S., and Seidel-Dugan, C., (1993). Detection of Src homology 3-binding proteins, including paxillin, in normal and v-Src-transformed Balb/c 3T3 cells. *Journal of Biological Chemistry 268*, 14956–14963.

(*257*) Whitfield, G. B., Brock, T. D., Ammann, A., Gottlieb, D., and Carter, H. E., (1955). Filipin, an antifungal antibiotic: isolation and properties. *Journal of the American Chemical Society 77*, 4799–4801.

(*258*) Wilhelm, L. P., Wendling, C., Védie, B., Kobayashi, T., Chenard, M.-P., Tomasetto, C., Drin, G., and Alpy, F., (2017). STARD3 mediates endoplasmic reticulum-to-endosome cholesterol transport at membrane contact sites. *The EMBO Journal 36*, 1412–1433.

(*259*) Williams, K. C., and Coppolino, M. G., (2014). SNARE-dependent interaction of Src, EGFR and β1 integrin regulates invadopodia formation and tumor cell invasion. *Journal of Cell Science 127*, 1712–1725.

(*260*) Wüstner, D., Lund, F. W., Röhrl, C., and Stangl, H., (2016). Potential of BODIPY-cholesterol for analysis of cholesterol transport and diffusion in living cells. *Chemistry and Physics of Lipids 194*, 12–28.

(*261*) Xue, L., Qi, H., Zhang, H., Ding, L., Huang, Q., Zhao, D., Wu, B.-y. J., and Li, X., (2020). Targeting SREBP-2-regulated mevalonate metabolism for cancer therapy. *Frontiers in Oncology 10*, 1510.

(*262*) Yanagisawa, M., Nakamura, K., and Taga, T., (2004). Roles of lipid rafts in integrin-dependent adhesion and gp130 signalling pathway in mouse embryonic neural precursor cells. *Genes to Cells 9*, 801–809.

(*263*) Yang, Z., Qin, W., Chen, Y., Yuan, B., Song, X., Wang, B., Shen, F., Fu, J., and Wang, H., (2018). Cholesterol inhibits hepatocellular carcinoma invasion and metastasis by promoting CD44 localization in lipid rafts. *Cancer letters 429*, 66–77.

(*264*) Yu, D.-H., Qu, C.-K., Henegariu, O., Lu, X., and Feng, G.-S., (1998). Protein-tyrosine phosphatase Shp-2 regulates cell spreading, migration, and focal adhesion. *Journal of Biological Chemistry 273*, 21125–21131.

(*265*) Yue, P. Y., Leung, E. P., Mak, N., and Wong, R. N., (2010). A simplified method for quantifying cell migration/wound healing in 96-well plates. *Journal of Biomolecular Screening 15*, 427–433.

(*266*) Zaidel-Bar, R., Ballestrem, C., Kam, Z., and Geiger, B., (2003). Early molecular events in the assembly of matrix adhesions at the leading edge of migrating cells. *Journal of Cell Science 116*, 4605–4613.

(*267*) Zelcer, N., Hong, C., Boyadjian, R., and Tontonoz, P., (2009). LXR regulates cholesterol uptake through Idol-dependent ubiquitination of the LDL receptor. *Science 325*, 100–104.

(*268*) Zhang, J., He, J., Johnson, J. L., Rahman, F., Gavathiotis, E., Cuervo, A. M., and Catz, S. D., (2019). Chaperone-mediated autophagy upregulation rescues megalin expression and localization in cystinotic proximal tubule cells. *Frontiers in Endocrinology 10*, 21.

(*269*) Zhang, X., Jiang, G., Cai, Y., Monkley, S. J., Critchley, D. R., and Sheetz, M. P., (2008). Talin depletion reveals independence of initial cell spreading from integrin activation and traction. *Nature Cell Biology 10*, 1062–1068.

(*270*) Zhang, Z., Izaguirre, G., Lin, S.-Y., Lee, H. Y., Schaefer, E., and Haimovich, B., (2004). The phosphorylation of vinculin on tyrosine residues 100 and 1065, mediated by SRC kinases, affects cell spreading. *Molecular Biology of the Cell 15*, 4234–4247.

(*271*) Zhao, K., and Ridgway, N. D., (2017). Oxysterol-binding protein-related protein 1L regulates cholesterol egress from the endolysosomal system. *Cell Reports 19*, 1807–1818.

(*272*) Zhao, X., and Guan, J.-L., (2011). Focal adhesion kinase and its signaling pathways in cell migration and angiogenesis. *Advanced Drug Delivery Reviews 63*, 610–615.

(*273*) Zhuang, L., Kim, J., Adam, R. M., Solomon, K. R., and Freeman, M. R., (2005). Cholesterol targeting alters lipid raft composition and cell survival in prostate cancer cells and xenografts. *Journal of Clinical Investigation 115*, 959–968.

(*274*) Zidovetzki, R., and Levitan, I., (2007). Use of cyclodextrins to manipulate plasma membrane cholesterol content: evidence, misconceptions and control strategies. *Biochimica et Biophysica Acta - Biomembranes 1768*, 1311–1324.

(*275*) Zimmermann, R., Strauss, J. G., Haemmerle, G., Schoiswohl, G., Birner-Gruenberger, R., Riederer, M., Lass, A., Neuberger, G., Eisenhaber, F., Hermetter, A., and Zechner, R., (2004). Fat mobilization in adipose tissue is promoted by adipose triglyceride lipase. *Science 306*, 1383–1386.

(*276*) Zinchuk, V., and Zinchuk, O., (2008). Quantitative colocalization analysis of confocal fluorescence microscopy images. *Current Protocols in Cell Biology 39*, 4–19.

Appendix A

Supplements

Characterisation of FAK and pY861 FAK immunostaining

In the run-up, immunostaining of focal adhesion (FA) was tested using anti-FAK (BD Transduction Laboratories, Cat. No. 610088, mouse) or anti-pY861 FAK (Abcam, ab4804, rabbit), each in a dilution of 1:200 and 1:500, followed by secondary antibodies coupled to Alexa Fluor® 488 (Thermo Fisher, A11008 anti-rabbit or A11001 anti-mouse, dilution: 1:350). Immunolabelling with anti-pY861 FAK, diluted 1:500, was found to be superior to anti-FAK due to better delineation of FA and less unspecific background staining, particularly in the perinuclear region (FIGURE A.1).

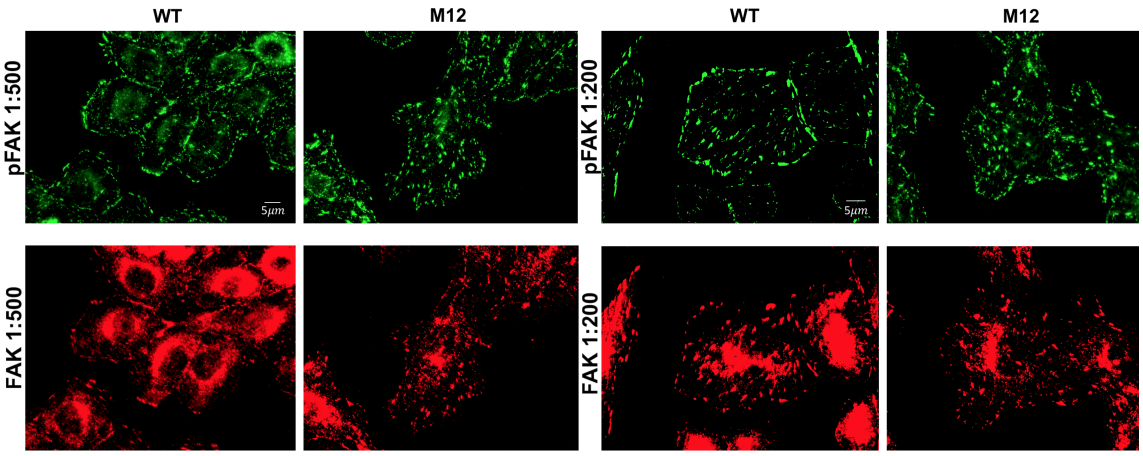

FIGURE A.1: **Characterisation of FAK and pY861 FAK immunostaining.** Shown are CHO WT and M12 cells co-stained with anti-pY861 FAK (green) and anti-FAK (red). For both primary antibodies a dilution of 1:500 and 1:200 was tested, while the secondary antibody dilution remained 1:350. For the experiment, $1.5 * 10^5$ cells/well of a 6-well plate were plated, grown for 48h in growth media (10% FBS), 2h incubated in serum-free medium and subsequently fixed, stained and mounted as described earlier.

Focal adhesions at the cell edge and the cell body

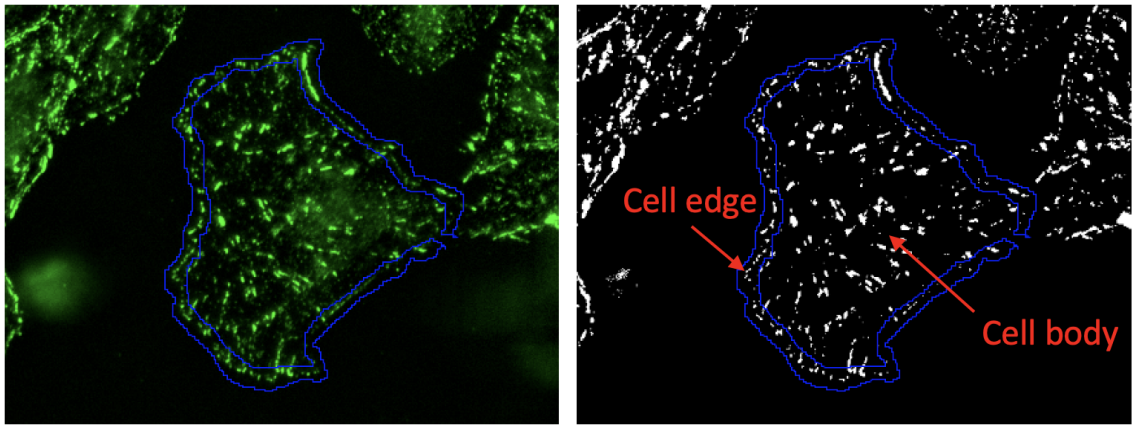

FIGURE A.2: **Focal adhesions at the cell edge and the cell body.** Shown is an anti-pY861 FAK (green) stained CHO wild-type cell in which focal adhesions (FA) at the cell edge were surrounded in blue. FA located towards the centre of the cell were considered to be at the 'cell body'. High brightness was used to delineate the plasma membrane (left), for analysis, unspecific signals were reduced by adaption of the threshold (right).

Expression of late endosomal proteins in LDL-activated cells after incubation with LPDS-statin media

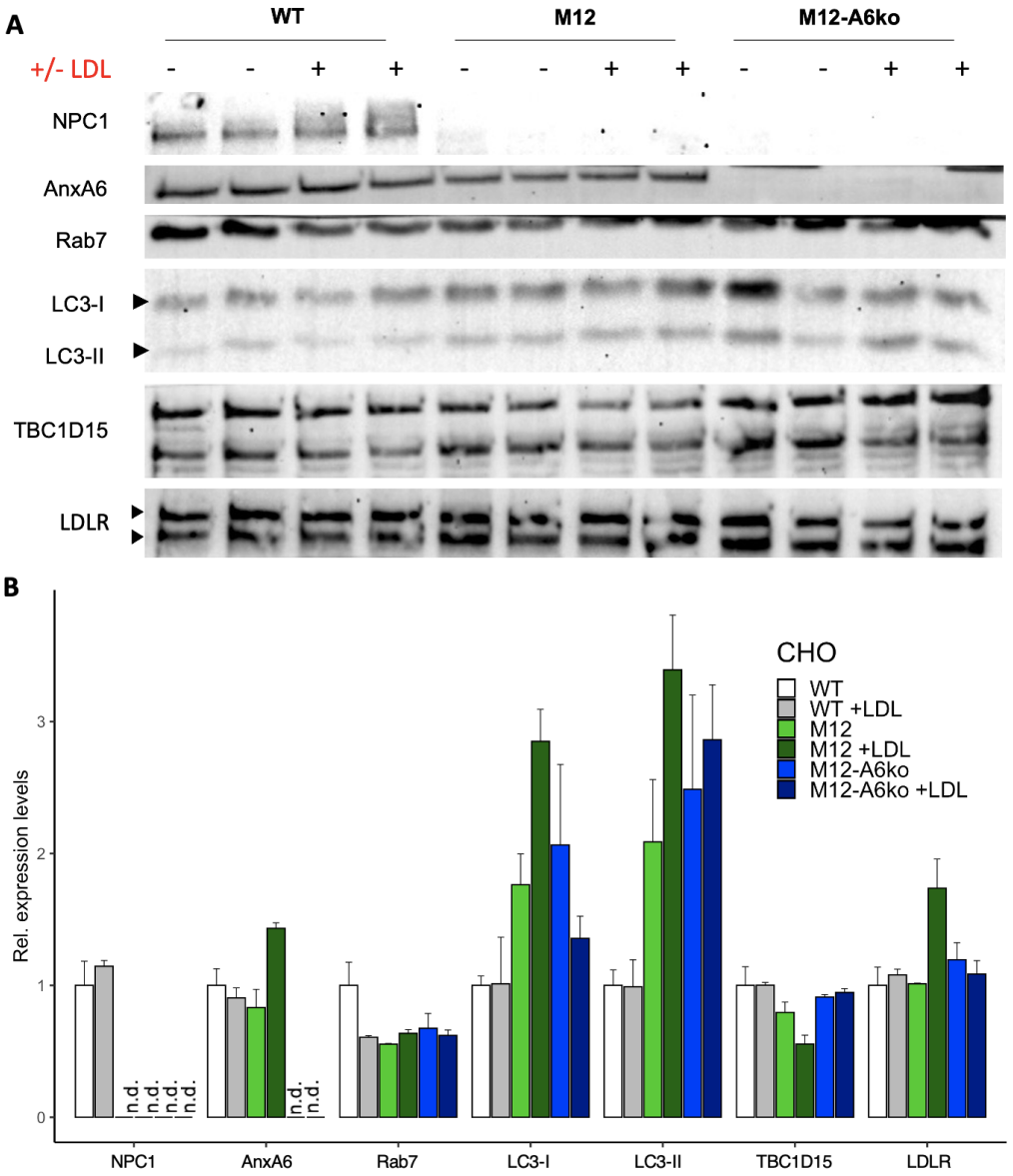

FIGURE A.3: **Western blot analysis of late endosomal proteins in LDL-activated CHO WT, M12 and M12-A6ko cells after incubation with LPDS-statin media.** (A) Cell lysates from CHO WT, CHO M12 and CHO M12-A6ko grown in 10% FBS-containing media were incubated in 10%-LPDS-5mg/ml-mevastatin media (Appendix B.25) for 48h. Then, cells were starved in serum-free media for 2h and activated by LDL for 30min. Subsequently, samples were analysed by western blotting (WB) as described in Methods (Chapter 2.2.2). Shown are the protein levels of Niemann-Pick type C1 (NPC1), annexin A6 (AnxA6), Rab7, light chain 3 (LC3)-I (upper), LC3-II (lower), Tre-2/Bub2/Cdc16 1 domain family member 15 (TBC1D15), and low density lipoprotein receptor (LDLR, upper arrowhead: mature form, lower arrowhead: precursor). (B) The relative expression levels were quantified using ImageJ. The WB signals of NPC1, AnxA6, Rab7, LC3-I/II, and LDLR were normalised to TBC1D15. The mean relative protein level of duplicate samples and median absolute deviation (MAD) is given.

Src and FAK activation in LDL-activated cells after incubation with LPDS-statin-media

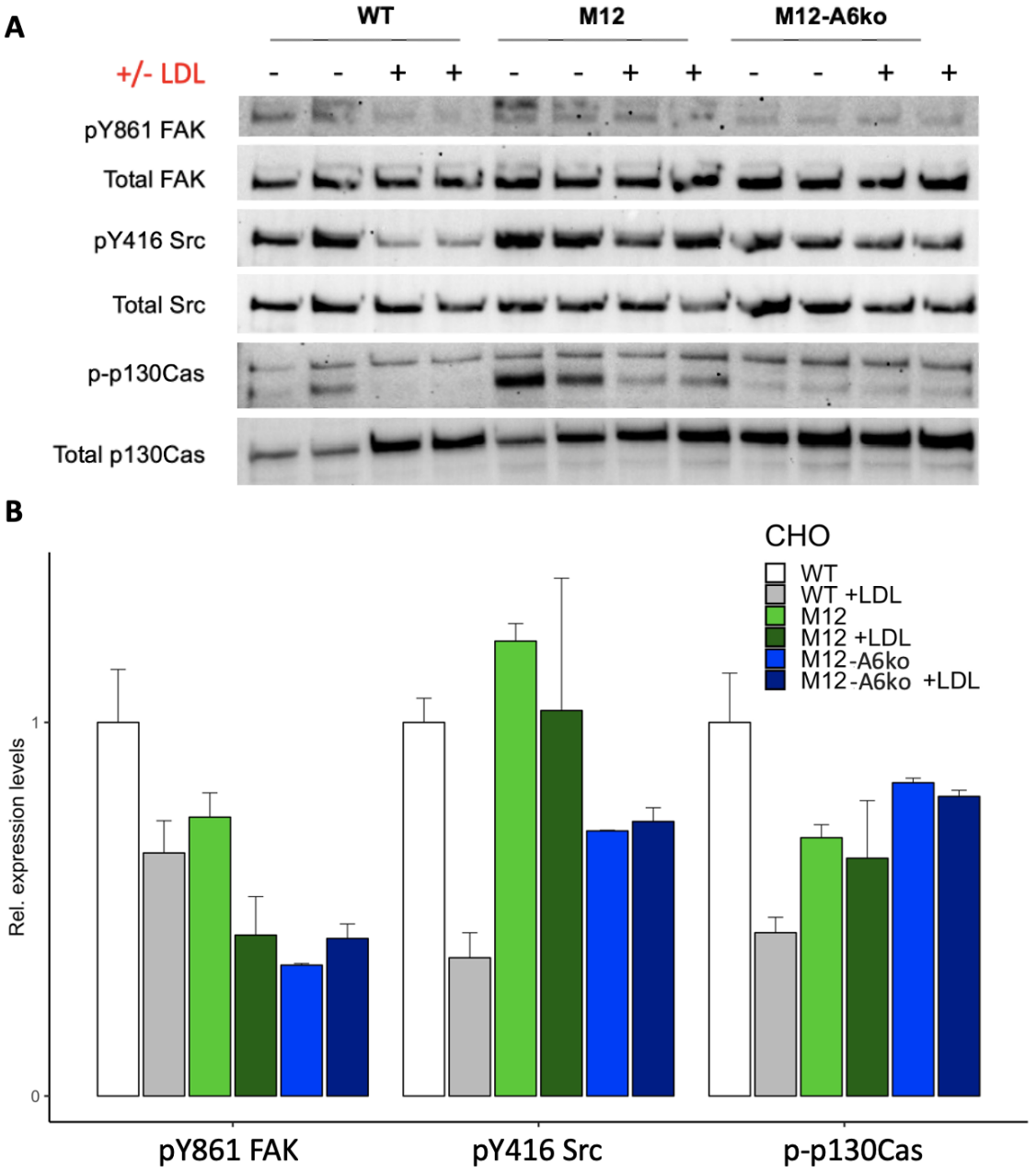

FIGURE A.4: **Western blot analysis of Src and FAK activation in LDL-activated CHO WT, M12, and M12-A6ko cells after incubation with LPDS-statin media.** (A) Cell lysates from CHO WT, CHO M12 and CHO M12-A6ko grown in 10% FBS-containing media were incubated in 10%-LPDS-5mg/ml-mevastatin media (Appendix B.25) for 48h. Then, cells were starved in serum-free media for 2h and activated by LDL for 30min. Subsequently, samples were analysed by western blotting (WB) as described in Methods (Chapter 2.2.2). Shown are the relative protein levels of pY861 focal adhesion kinase (FAK), total FAK, pY416 Src, total Src, p-p130Cas, and p130Cas. (B) The relative protein levels of signals displayed in (A) were quantified using ImageJ and were normalised to the corresponding total protein signal. The mean relative protein level of duplicate samples of the same experiment and median absolute deviation (MAD) are given.

Expression of late endosomal proteins and activation of phosphoproteins in serum-stimulated migrating cells

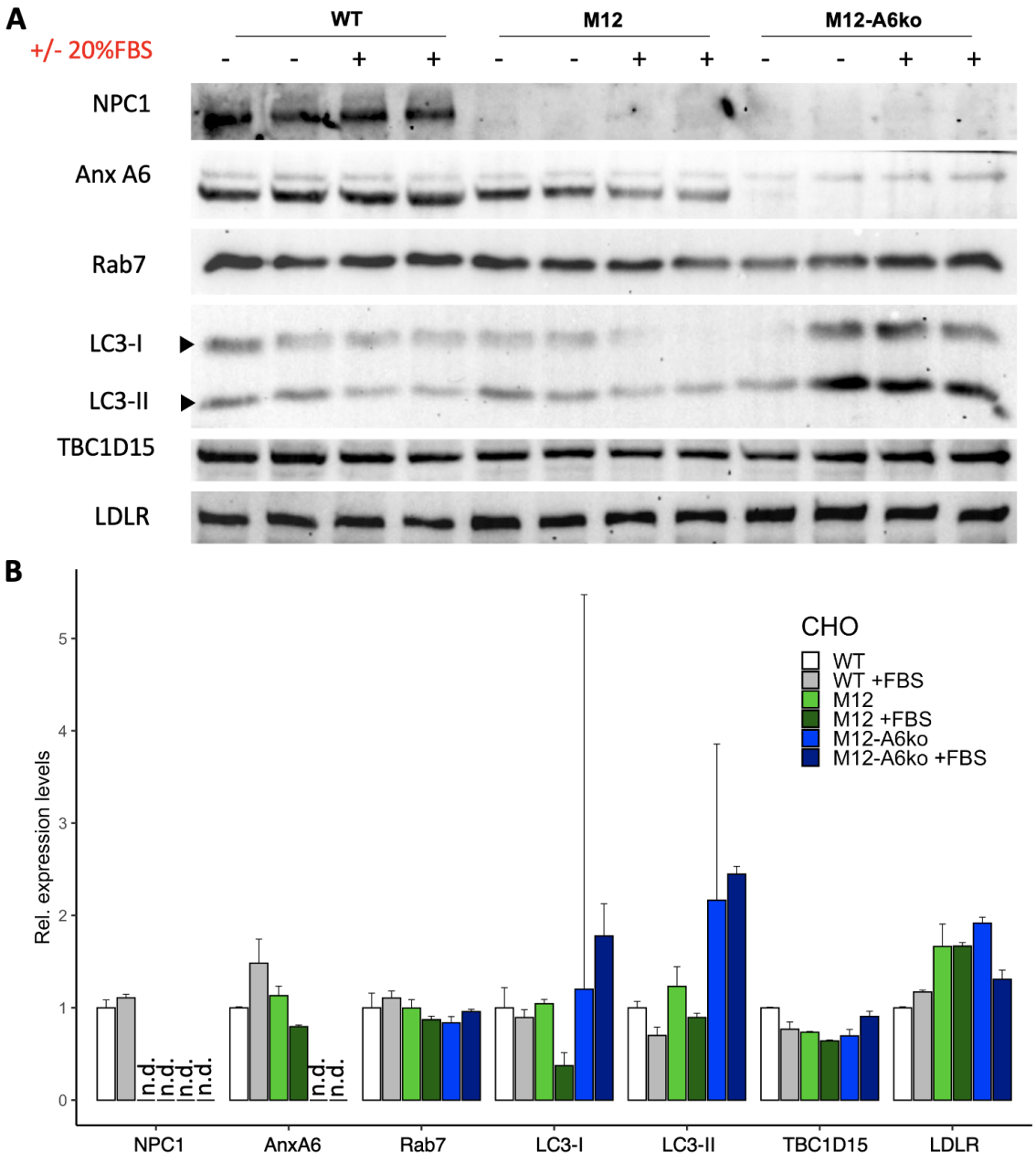

FIGURE A.5: **Western blot analysis of late endosomal proteins in migrating CHO WT, M12 and M12-A6ko cells after incubation with 20%FBS.** (A) CHO WT, CHO M12 and CHO M12-A6ko were starved in serum-free media overnight, scratched and incubated with or without 20% FBS for 30min. Multiple (>5) scratches per 6-well were performed as described (*59*, *234*). Lysates were prepared and analysed by western blotting (WB) as described in Methods (Chapter 2.2.2) for Niemann-Pick type C1 (NPC1), annexin A6 (AnxA6), Rab7, light chain 3 (LC3)-I (upper), LC3-II (lower), Tre-2/Bub2/Cdc16 1 domain family member 15 (TBC1D15), and low density lipoprotein receptor (LDLR). (B) The relative expression levels were quantified using ImageJ. The WB signals of NPC1, AnxA6, Rab7, LC3I/II, and LDLR were normalised to TBC1D15. The mean relative protein level of duplicate samples of the same experiment and median absolute deviation (MAD) are given.

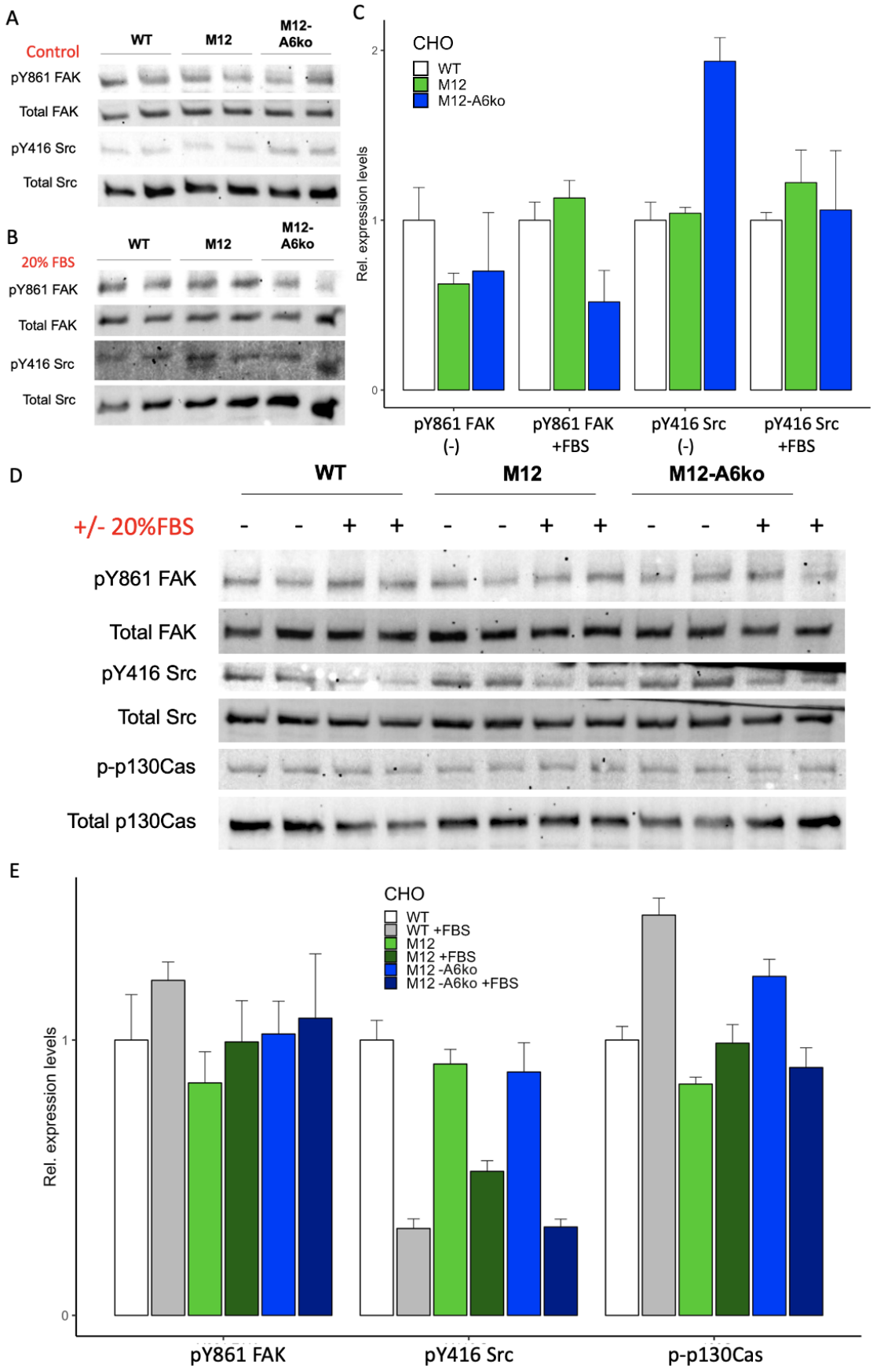
A
Control
WT
M12
M12-A6ko
pY861 FAK
Total FAK
pY416 Src
Total Src
B
20% FBS
C
CHO
WT
M12
M12-A6ko
Rel. expression levels
pY861 FAK (-)
pY861 FAK +FBS
pY416 Src (-)
pY416 Src +FBS
D
+/- 20%FBS
p-p130Cas
Total p130Cas
E
WT +FBS
M12 +FBS
M12 -A6ko
M12 -A6ko +FBS

FIGURE A.6: **Western blot analysis of Src and FAK activation in migrating CHO WT, M12 and M12-A6ko cells after incubation with 20%FBS.** CHO WT, M12 and M12-A6ko were starved in serum-free media overnight, scratched and subsequently incubated with or without 20% FBS for 30min. Multiple (>5) scratches per well were performed as described (*59*, *234*). Lysates were prepared and analysed by western blotting (WB) as described in Methods (Chapter 2.2.2). Panel (A) shows pY861 focal adhesion kinase (FAK), total FAK, pY416 Src, and total Src levels of CHO cells that were not stimulated with 20% FBS. Panel (B) shows pY861 FAK, total FAK, pY416 Src, and total Src levels of CHO cells that were serum-activated (20% FBS) for 30min. (C) The relative protein levels of signals displayed in (A-B) were quantified using ImageJ and were normalised to the corresponding total protein signal. The mean relative protein level of duplicate samples of the same experiment and median absolute deviation (MAD) are given. Panel (D) shows an alternative loading order of the same experiment. The presence or absence of serum is indicated. (E) The relative protein levels of signals displayed in (D) were quantified using ImageJ and were normalised to the corresponding total protein signal. The mean relative protein level of duplicate samples of the same experiment and MAD are given.

Focal adhesion density in Src- and Src Y527F-overexpressing CHO WT, M12, and M12-A6ko cells

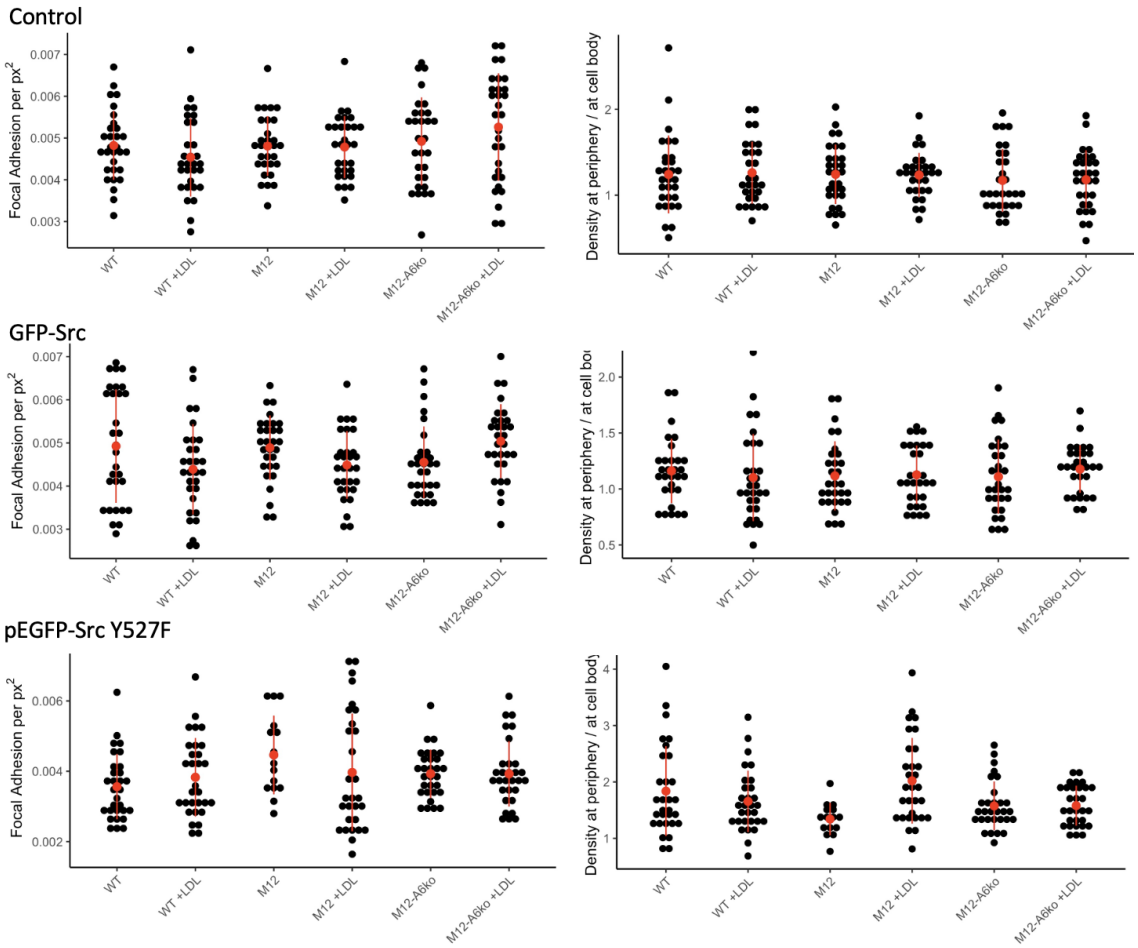

FIGURE A.7: **Focal adhesion density in Src- and Src Y527F-overexpressing CHO WT, M12, and M12-A6ko cells.** The spatial focal adhesion (FA) density and the spatial distribution of FA density, cell edge vs. cell body, of CHO WT, M12 and M12-A6ko cells (n=30 cells, except M12: n=16 cells, per cell line from two independent experiments) were determined using ImageJ. Cells were plated at $1.5 * 10^5$ cells/well of a 6-well plate and transfected with GFP-Src, pEGFP-Src Y527F (Chapter 2.1.1) or remained untransfected (control). Then, cells were grown for 48h in media supplemented with lipoprotein-deficient serum (10% LPDS) and mevastatin (1μM) (see Appendix B.25). Cells were starved for 2h and stimulated with LDL for 4h. Afterwards cells were fixed and stained for pY861 FAK. The mean ± SD is given. *p < 0.05, **p < 0.01, ***p < 0.001; two-way ANOVA with Tukey's post-hoc test.

Appendix B

Material

Expendable Materials

Table B.1: Expendable Materials

Product	**Brand**	**Cat. No.**
6 Well Cell Culture Cluster	Corning Incorporated	3516
Centrifuge Tubes 15ml	Corning Incorporated	430791
Centrifuge Tubes 50ml	Corning Incorporated	430829
Corning® 25cm^2 Flask	Corning Incorporated	430639
Corning® 75cm^2 Flask	Corning Incorporated	430641U
Cover glasses Menzel Gläser 15mm #1	Thermo Scientific	MENZBB0-15015A123
Greiner culture tubes	Sigma-Aldrich	Z617954-800EA
PD-10 Desalting Columns,Sephadex™G-25 M	GE Healthcare	17085101
Premium Glass Plain Slides	Livingstone	7101-BP
Pipette tip 1000μl, blue	Sarstedt	70.762
PowerPac™HC High-Current Power Supply	Bio-Rad Laboratories	1645050
PVDF-Western-Blot-Membrane	Roche	030100400-01
Stripette® 5ml	Corning Incorporated	4487
Stripette® 10ml	Corning Incorporated	4488
Stripette® 25ml	Corning Incorporated	4489

Technical Devices

TABLE B.2: Technical Devices

Device	**Brand**
Autoclave Tangent Tiger	Atherton
Biological Safety Cabinet Class II Ultra Safe® Series 2010	Clyde-Apac
Centrifuge Clements Orbital 310	Clements Medical
Centifuge CR2000 multi purpose	Centurion Scientific
Centrifuge Sigma 2-5	Sigma
DFC395 FX digital camera	Leica
DM5500 microscope	Leica
Dry Block Heater	Thermoline Scientific
Incubator Forma™310 Direct Heat CO_2	Thermo Scientific™
Incubator Shaker ZHWY-200D	Shanghai ZHICHENG Analytical Instruments Manufacturing Co.
Inverted Microscope Eclipse TS100	Nikon®
Laboratory Oven Economy Style, 24L	Thermoline Scientific
Magnetic Stirrer MR Hei-Standard	Heidolph Instruments GmbH
Mini-PROTEAN® Tetra Vertical Electrophoresis Cell	Bio-Rad Laboratories
Pipette Controller PIPETBOY acu 2	Integra Bioscience
PowerPac™HC High-Current Power Supply	Bio-Rad Laboratories
Shaker Duomax 1030	Heidolph Instruments GmbH
Spectrometer Eppendorf BioPhotometer 6131	Eppendorf
Variopipetten 2 μl, 10 μl, 20 μl, 100 μl, 200 μl, 1000 μl	Gilson
Water bath, uncirculated, 24L	Thermoline Scientific

Chemicals and Reagents

TABLE B.3: Chemicals and Reagents

Substance	**Brand**	**Cat. No.**
0.5% Trypsin-EDTA (10X)	Gibco™	15400-054
0.5M Tris-HCL Buffer pH 6.8	Bio-Rad Laboratories	#161-0799
1.5M Tris-HCL Buffer pH 8.8	Bio-Rad Laboratories	#161-0798

2-Mercaptoethanol	Merck	8.05740.0250
Acrylamide/N,N'-Methylenebisacrylamide 37.5:1, 40% mix solution in water (500ml)	Acros Organics	330225000
Agar - High Gel Strength	Sigma Chemical Co	A6924
Aprotinin	Sigma-Aldrich	A1153
Ammonium Persulfate (APS)	Sigma-Aldrich	A3678
Bovine Serum Albumin (BSA)	Sigma-Aldrich	A7906-100G
Bromophenol Blue (1%)	Sigma-Aldrich	B0126
Clarity™Western ECL Substrate	Bio-Rad Laboratories	#170-5061
$CuSO_4$-$5H_2O$	Sigma-Aldrich	C8027
DAPI (4',6-diamidino-2-phenylindole)	Sigma-Aldrich	D9542
Dimethyl sulfoxide (DMSO)	Sigma Chemical Co	D8418-250ml
DL-Dithiothreitol (DTT)	Sigma-Aldrich	D0632
EDTA	Sigma-Aldrich	E9884
Ethanol 80%	POCD Healthcare	ETH80%V/-V2.5P
Fetal Bovine Serum (FBS)	Gibco™	10437-028
Folin-Ciocaulteu's reagent	VWR™	#31360.264
Formalgehyde 4% stabilised	VWR™	#9713.1000
Glycerol	Thermo Fisher Scientific	BSPGL885.500
Glycine	Sigma-Aldrich	G8898-1KG
HCl	Sigma-Aldrich	H9892
Kanamycin	Sigma-Aldrich	K1377
Leupeptin	Sigma-Aldrich	L2884
Lipofectamine™ 2000 reagent	Invitrogen	11668027
Lipoprotein deficient fetal bovine serum (LPDS)	was prepared by preparative ultracentrifugation (FBS from Sigma-Aldrich), LPDS was dialysed extensively against PBS and stored at 4 °C until use (*155*)	

Low-density lipoprotein (LDL)	isolated from donated, pooled blood samples from healthy donors (obtained from Red Cross, Melbourne, Australia; density 1.019–1.055g/ml) by three sequential density gradient ultracentrifugations in KBr gradients (*200*). Protocols for the use of blood products purchased from the Red Cross (Material Supply Agreement no: 19-07NSW-1) for the isolation of plasma lipoproteins were approved by the local ethics committee of the University of New South Wales (HC190432) in accordance with the National Health and Medical Research Council's (NHMRC) National Statement on Ethical Conduct in Human Research (2007) (*104*).	
Methanol	Chem-Supply	MA004-2.5L-J
Mevastatin	Sigma Life Science	M2537-5MG
$MgCl_2$	Sigma-Aldrich	208337
Mowiol	Sigma-Aldrich	81381
N,N,N',N'-Tetramethylethylenediamine (TEMED), 99%	Sigma-Aldrich	T22500-100ml
Na_2CO_3	Sigma-Aldrich	222321
NaF	Sigma-Aldrich	S6776
NaK Tartrate	Sigma-Aldrich	217255
Na_3VO_3	Sigma-Aldrich	S6508
Pen Strep	Gibco™	15140-122
Precision Plus Protein™Dual Color Standards	Bio-Rad	#1610374
SDS	Research Organics	9010L

Sodium chloride (NaCl)	Fisher Scientific UK	S/3160/65
Tris(hydroxymethyl)aminomethane (Tris-Base)	Sigma-Aldrich	T87602-3KG
Triton® X-100	United States Biochemical Corp.	22686
Tryptone	Sigma-Aldrich	T7293
Tween-20	Santa Cruz Biotechnology	sc-29113
Yeast Extract	Sigma-Aldrich	Y1625

Buffers and Solutions

Buffers and Solutions for Tissue Culture

TABLE B.4: Buffer and Solutions

Substance	**Brand**	**Cat. No.**
Phosphate Buffered Saline	Sigma Life Science	806552-500ml

Buffers and Solutions for biochemical Methods

TABLE B.5: 10x Running Buffer

10x Running Buffer	
Tris-Base	30.29g
Glycine	144.13g
SDS	10.00g
dH2O	to 1L

TABLE B.6: 10x Transfer Buffer

10x Transfer Buffer	
Tris-Base	30.26g
Glycine	144.13g
Aqua dest.	to 1L

TABLE B.7: 1x Transfer Buffer

1x Transfer Buffer	
Aqua dest.	700ml
Methanol	200ml

10x Transfer Buffer	100ml

TABLE B.8: 10x TBS (Tris Buffered Saline)

10x TBS (Tris Buffered Saline)	
NaCl	87.7g
1M Tris-Cl (pH7.5)	100ml
Aqua dest.	to 1L

TABLE B.9: 1x TBS-T (Tris Buffered Saline, with 0.1% Tween-20)

1x TBS-T (Tris Buffered Saline, with 0.1% Tween-20)	
10x TBS	100ml
Tween-20	1ml
Aqua dest.	to 1L

TABLE B.10: Lowry Solution A

Lowry Solution A	
Na_2CO_3	30g
NaOH	6g
Aqua dest.	to 1L

TABLE B.11: Lowry Solution B

Lowry Solution B	
NaK Tartrate	2%
Aqua dest.	to 50ml

TABLE B.12: Lowry Solution C

Lowry Solution C	
$CuSO_4$-$5H_2O$	1%
Aqua dest.	to 50ml

TABLE B.13: Western Blot Blocking Buffer (5%)

1x TBST (Tris Buffered Saline, with 0.1% Tween 20)	
Skim Milk or BSA	5g

TBST	100ml

TABLE B.14: Mild Stripping Buffer

Mild Stripping Buffer	
Glycine	15g
SDS	1g
Tween-20	10ml
Aqua dest.	to 1L
HCl	Adjust pH to 2.2

TABLE B.15: 5x Laemmli Sample Buffer

5x Laemmli Sample Buffer	
SDS	2.5g
Glycerol	12.5ml
0.5M Tris-HCl pH 6.8	12.5ml
1% Bromophenol Blue	1ml
DTT	75mg/ml

TABLE B.16: Lysis Buffer (Stock)

Lysis Buffer (Stock)	
1M Tris-HCl (Buffer pH 7.5)	2ml
0.5M EDTA	0.4ml
5M NaCl	2ml
1M $MgCl_2$	0.5ml
Triton X-100	1ml
0.5M NaF	1ml
Glycerol	10ml
Aqua dest.	to 100ml

TABLE B.17: Lysis Buffer (Working Solution)

Lysis Buffer (Working Solution)	
Lysis Buffer Stock	9640μl
10mM Na_3VO_4	100μl
100mM PMSF	100μl

0.5mg/ml Leupeptin	100μl
0.2mg/ml Aprotinin	10μl
Mercaptoethanol	50μl

Antibodies

TABLE B.18: Antibodies

Antibody	**Brand**	**Cat. No.**
β-Actin (13E5), rabbit	Cell Signaling Technology	#4970
ABCA1, rabbit	Novus Biologicals	NB400-105
Alexa Fluor ® 594, goat anti-mouse IgG	Invitrogen	A-11005
Alexa Fluor ® 594, goat anti-rabbit IgG	Invitrogen	A-11012
Alexa Fluor ® 488, goat anti-mouse IgG	Invitrogen	A-11001
Alexa Fluor ® 488, goat anti-rabbit IgG	Invitrogen	A-11008
Annexin VI (H-114), rabbit	Santa Cruz Biotechnology	sc-11388
Anti-rabbit IgG, HRP-linked Antibody	Cell Signaling Technology	#7074
ATGL, rabbit	Cell Signaling Technology	#2138
CD36 (E8B7S), rabbit	Cell Signaling Technology	#28109
FAK (D2R2E), rabbit	Cell Signaling Technology	#13009
FAK, mouse	BD Transduction Laboratories™	610088
Phospho-FAK (Y397), rabbit	Cell Signaling Technology	#3283
Phospho-FAK (Y861), rabbit	Abcam	ab4804
HSL, rabbit	Cell Signaling Technology	#4107
LC3A/B, rabbit	Cell Signaling Technology	#4108
LDL Receptor [EP1553Y], rabbit	Abcam	ab52818
Niemann Pick C1, rabbit	Abcam	ab36983
p130Cas (E1L9H), rabbit	Cell Signaling Technology	#13846
Phospho-p130Cas (Y410), rabbit	Cell Signaling Technology	#4011
Paxillin (D9G12), rabbit	Cell Signaling Technology	#12065
Rab7 (D95F2), rabbit	Cell Signaling Technology	#9367
Src (32G6), rabbit	Cell Signaling Technology	#2123
Phospho-Src Family (Y416), rabbit	Cell Signaling Technology	#2101
Phospho-Src (Y527), rabbit	Cell Signaling Technology	#2105
SREBP2, rabbit	Abcam	ab30682

TBC1D15, rabbit	Abcam	ab121396
Vinculin (E1E9V), rabbit	Cell Signaling Technology	#13901

Media

Table B.19: Media

Media	**Brand**	**Cat. No.**
Ham's Nutrient Mixture F12	Sigma-Aldrich	MFCD00217417
Opti-MEM™	Thermo Fisher Scientific	31985070

Table B.20: Growth Media

Growth Media	
Ham's Nutrient Mixture F12	500ml
FBS	50ml
Pen Strep	5ml

Table B.21: 20% FBS Media

20% FBS Media	
Ham's Nutrient Mixture F12	79ml
FBS	20ml
Pen Strep	1ml

Table B.22: Freezing Media

Freezing Media	
Ham's Nutrient Mixture F12	4ml
FBS	4ml
DMSO	2ml

Table B.23: LB Media

LB Media	
Tryptone	5g
Yeast Extract	2.5g
NaCl	5g

Aqua bidest.	500ml

TABLE B.24: LB Agar

LB Agar	
Tryptone	5g
Yeast Extract	2.5g
NaCl	5g
Bacto Agar	7.5g
Aqua bidest.	500ml
→ autoclaved, cooled down to 60°C	
Kanamycin (50mg/μl)	500μl

TABLE B.25: LPDS-statin media

LPDS-statin media	
Ham's Nutrient Mixture F12	89ml
LPDS	10ml
Pen Strep	1ml
Mevastatin (5mg/ml)	78μl (1μM)

Cell lines

TABLE B.26: Cell lines

Cell line	**Characteristics**	**Origin**
CHO WT	wild type	ATCC (American Type Culture Collection; https://www.atcc.org)
CHO M12	NPC1 lacking	Dr. L. Liscum (Tufts University School of Medicine, USA)
CHO M12-A6ko	NPC1 and AnxA6 lacking	CRISPR generated by Enrich and Grewal Group (*155*)

Bacteria

TABLE B.27: Bacteria

Bacteria	Genotype	Brand	Cat. No.
E. coli HB101	F^-, *thi*-1, *hsd*S20 (r_B^-, m_B^-) *sup*E44, *rec*A13, *ara*-14, *leu*B6, *pro*A2, *lac*Y1, *gal*K2 *rps*L20 (str^r), *xyl*-5, *mtl*-1	Promega Corporation	L2011

Kits

TABLE B.28: Kits

Kit	Brand	Cat. No.
QIAprep® Spin Miniprep Kit	QIAGEN®	27104

Expression Vectors

TABLE B.29: Expression Vectors

Construct	Subject	Origin	Ref.
GFP-Paxillin	EGFP-tagged expression vector encoding paxillin	J. Victor Small (IMBA, Vienna, Austria), Guido Serini (University of Torino, Italy)	(*223*)
GFP-Vinculin	EGFP-tagged expression vector encoding vinculin	J. Victor Small (IMBA, Vienna, Austria), Guido Serini (University of Torino, Italy)	(*110*)
iRFP-PH-PLCδ1	iRFP-tagged expression vector endcoding the PH domain of PLCδ which binds PIP_2	Rob Yang, UNSW, Sydney, Australia	(*95*)
GFP-Akt-PH	GFP-tagged expression vector endcoding the PH domain of Akt which binds PIP_3	Rob Yang, UNSW, Sydney, Australia	(*120*)

mCherry-D4H	mCherry-tagged cholesterol biosensor D4H	Masashi Maekawa and Gregory D. Fairn (University of Toronto, Canada)	(*148*)
GFP-Src	GFP-tagged expression vector endcoding Src	Geraldine M O'Neill, Children's Hospital Westmead, University of Sydney, Australia	(*202*)
pEGFP-Src-Y527F	pEGFP-tagged expression vector endcoding Src Y527F	Geraldine M O'Neill, Children's Hospital Westmead, University of Sydney, Australia	(*202*)

Software

TABLE B.30: Software

Software	**Manufacturer**
Microsoft® Excel for Mac 16.17	Microsoft
RStudio 1.1.453	RStudio, Inc.
Fotos 3.0	Apple Inc.
ImageJ 2.0.0 (FIJI)	National Institute of Health (Bethesda, USA)
Image Lab 5.2	Bio-Rad Laboratories
LAS X v.1.1.0.12420 imaging software	Leica

List of Publications

Jose, Jaimy; Hoque, Monira; Engel, Johanna; Beevi, Syed S; Wahba, Mohamed; Georgieva, Mariya I; Murphy, Kendelle J; Hughes, William E; Cochran, Blake J; Lu, Albert; Tebar, Francesc; Hoy, Andrew J; Timpson, Paul; Rye, Kerry-Anne; Enrich, Carlos; Rentero, Carles and Grewal, Thomas (2022). "Annexin A6 and NPC1 regulate LDL-inducible cell migration and distribution of focal adhesions." *Scientific Reports* 12.1, pp. 1-17.

Eidesstattliche Erklärung

Hiermit erkläre ich, dass ich die vorliegende Arbeit selbständig und ohne unzulässige Hilfe oder Benutzung anderer als der angegebenen Hilfsmittel angefertigt habe. Alle Textstellen, die wörtlich oder sinngemäß aus veröffentlichten oder nichtveröffentlichten Schriften entnommen sind, und alle Angaben, die auf mündlichen Auskünften beruhen, sind als solche kenntlich gemacht. Bei den von mir durchgeführten und in der Dissertation erwähnten Untersuchungen habe ich die Grundsätze guter wissenschaftlicher Praxis, wie sie in der „Satzung der Justus-Liebig-Universität Gießen zur Sicherung guter wissenschaftlicher Praxis“ niedergelegt sind, eingehalten sowie ethische, datenschutzrechtliche und tierschutzrechtliche Grundsätze befolgt. Ich versichere, dass Dritte von mir weder unmittelbar noch mittelbar geldwerte Leistungen für Arbeiten erhalten haben, die im Zusammenhang mit dem Inhalt der vorgelegten Dissertation stehen, oder habe diese nachstehend spezifiziert. Die vorgelegte Arbeit wurde weder im Inland noch im Ausland in gleicher oder ähnlicher Form einer anderen Prüfungsbehörde zum Zweck einer Promotion oder eines anderen Prüfungsverfahrens vorgelegt. Alles aus anderen Quellen und von anderen Personen übernommene Material, das in der Arbeit verwendet wurde oder auf das direkt Bezug genommen wird, wurde als solches kenntlich gemacht. Insbesondere wurden alle Personen genannt, die direkt und indirekt an der Entstehung der vorliegenden Arbeit beteiligt waren. Mit der Überprüfung meiner Arbeit durch eine Plagiatserkennungssoftware bzw. ein internetbasiertes Softwareprogramm erkläre ich mich einverstanden.

_____ _____

Ort, Datum Unterschrift

Danksagung

An dieser Stelle möchte ich allen Personen, die mich bei der Anfertigung meiner Doktorarbeit mit Rat und Tat unterstützt haben, ein herzliches Dankeschön aussprechen.

Mein besonderer Dank gilt Prof. Thomas Grewal, University of Sydney, für die ausgezeichnete Betreuung und enorme Unterstützung bei der Durchführung der gesamten Arbeit. Zudem möchte ich Monira Hoque, Yasmin Ahmed Elmaghrabi sowie William E. Hughes für die tolle Unterstützung im Labor und am Mikroskop danken. Mein Dank gilt auch Andreas Niederprüm, der immer ein offenes Ohr und Ideen für Aktivitäten außerhalb des Labors hatte. Die Zeit im Labor der Faculty of Pharmacy der Sydney University wird mir stets in guter Erinnerung bleiben.

Außerdem möchte ich Prof. Andre Menke, Universität Gießen, ganz herzlich für die nicht-selbstverständliche Bereitschaft der Betreuung einer Doktorarbeit im Ausland danken.

Ein ganz großes Danke geht an meine Eltern, ohne deren Unterstützung das Jahr Australien und meine gesamte universitäre Ausbildung nicht möglich gewesen wäre. Nicht zuletzt möchte ich mich bei Olli bedanken, all die Abende und Wochenenden des gemeinsamen Arbeitens an unseren Dissertationen hat gemeinsam sehr viel mehr Spaß gemacht.

Für die finanzielle Unterstützung möchte ich mich herzlich bei der Studienstiftung des deutschen Volks bedanken.